Inhibition Studies of the Tubulin Detyrosination/Tyrosination Cycle

by

Jennifer Kristine Griffith

B.Sc., Western Washington University, 2005
M.Sc., Western Washington University, 2007

A THESIS SUBMITTED IN PARTIAL FULFILLMENT OF THE REQUIREMENTS FOR THE DEGREE OF

DOCTOR OF PHILOSOPHY

in

The Faculty of Graduate and Postdoctoral Studies
(Chemistry)

The University of British Columbia
(Vancouver)

August 2014

Abstract

Microtubules are a highly dynamic component of the cytoskeleton, which are crucial for many cellular processes. Microtubules are comprised of α/β-tubulin heterodimers, which are subject to multiple post-translational modifications including the detyrosination/tyrosination cycle. This cycle involves the removal of an RNA-encoded C-terminal α-tubulin tyrosine residue by tubulin carboxypeptidase, followed by the reattachment of the tyrosine residue by tubulin tyrosine ligase. This research project is focused on the development of an inhibitor against tubulin tyrosine ligase and tubulin carboxypeptidase. The precise function of this cycle has yet to be determined; an inhibitor could function as a chemical biology tool that could be used to study the physiological effects of the detyrosination/tyrosination cycle.

This thesis details the design and synthesis of phosphinic acid and phosphonic acid peptide analogue inhibitors. Progress towards the synthesis of a dipeptide phosphinic acid is reported; due to complications in phosphorus-carbon bond forming reactions the total synthesis was not completed. The focus of the research project changed to the synthesis of phosphonic acid peptide analogue inhibitors. A dipeptide phosphonic acid inhibitor was successfully synthesized, but was inactive against tubulin tyrosine ligase. Progress towards the synthesis of a tripeptide phosphonic acid inhibitor is reported; due to complications in the final deprotection steps the total synthesis was not completed. A pentapeptide phosphonic acid inhibitor was successfully synthesized, and it showed moderate inhibitor activity against tubulin tyrosine ligase.

Preface

This dissertation is original unpublished work. All the synthetic experiments were completed by the author of this thesis, under the supervision of Professor Martin Tanner. All the inhibition experiments were completed by our collaborators in the Roll-Mecak lab at the Cell Biology and Biophysics Unit, National Institute of Neurological Disorders in Maryland, USA.

Table of Contents

List of Tables

List of Figures

List of Symbols and Abbreviations

+TIP	plus-end tracking protein
ACE	angiotensin-converting enzyme
ADP	adenosine diphosphate
AIBN	azobisisobutyronitrile
AMP	adenosine monophosphate
ATP	adenosine triphosphate
BOC	*tert*-butyloxycarbonyl
BOP	(benzotriazol-1-yloxy)tris(dimethylamino)phosphonium hexafluorophosphate
BSA	bis(trimethylsilyl)acetamide
CAP-Gly	cytoskeleton-associated protein glycine rich
Cbz	benzyloxycarbonyl
CCP	cytosolic carboxypeptidases
CPA	carboxypeptidase A
CPM	counts per minute
DABCO	1,4-diazabicyclo[2.2.2]ocatane
DBU	1,8-diazabicycloundec-7-ene
DCC	*N,N'*-dicyclohexylcarbodiimide
DCM	dichloromethane
DEAE	diethylaminoethanol
DIAD	diisopropyl azodicarboxylate
DIBAL-H	diisobutylaluminium hydride

DMF	dimethylformamide
DPPA	diphenylphosphoryl azide
DTT	dithiothreitol
E. coli.	*Escherichia coli*
EB1	end-binding protein 1
EDTA	ethylenediaminetetraacetic acid
EGTA	ethylene glycol tetraacetic acid
ESI-MS	electrospray ionization mass spectrometry
EtOAc	ethyl acetate
FMOC	fluorenylmethyloxycarbonyl
FPGS	folylpoly-γ-glutamyl synthetase
GDP	guanosine diphosphate
GST	glutathione *S*-transferases
GTP	guanosine triphosphate
HBTU	*N,N,N′,N′*-tetramethyl-*O*-(1*H*-benzotriazol-1-yl)uronium hexafluorophosphate
HMDS	hexamethyldisilazane
HMPA	hexamethylphosphoramide
HPLC	high-performance liquid chromatography
IC_{50}	half maximal inhibitory concentration
IPTG	isopropyl β-D-galactopyranoside
K_D	dissociation constant
kDa	kilodalton

K_i	inhibition constant
K_M	Michaelis Constant
LDA	lithium diisopropylamide
LiHMDS	lithium hexamethyldisilazide
M	molar
MAP	microtubule-associated protein
MCAK	mitotic centromere-associated kinesin
MCF	Michigan Cancer Foundation
MES	2-(*N*-morpholino)ethanesulfonic acid
MHz	megahertz
MTOC	microtubule organizing centers
Mur	muramic acid
MurNAc	*N*-acetylmuramic acid
NMR	nuclear magnetic resonance
PCC	pyridinium chlorochromate
ppm	parts per million
SPPS	solid phase peptide synthesis
TCP	tubulin carboxypeptidase
THF	tetrahydrofuran
TLC	thin layer chromatography
TMSCl	trimethylsilyl chloride
TTL	tubulin tyrosine ligase
TTLL	tubulin tyrosine ligase-like

UDP	uridine diphosphate
γ-TuRC	tubulin ring complex
γ-TuSC	tubulin heterotetramer
δ	chemical shift (ppm)

Common Amino Acid Abbreviations:

A	Ala	alanine
C	Cys	cysteine
D	Asp	aspartic acid
E	Glu	glutamic acid
F	Phe	phenylalanine
G	Gly	glycine
H	His	histidine
I	Ile	isoleucine
K	Lys	lysine
L	Leu	leucine
M	Met	methionine
N	Asn	asparagine
P	Pro	proline
Q	Gln	glutamine
R	Arg	arginine
S	Ser	serine
T	Thr	threonine
V	Val	valine

W	Trp	tryptophan
Y	Tyr	tyrosine

Acknowledgements

Above all, I would like to thank my research supervisor Martin Tanner for his continued patience and support. I appreciate his guidance through the many challenges and frustrations presented by this project. I would like to thank past and present members of the Tanner lab for their encouragement and support in both lab and life. All the laughs and good times made my experience at UBC unforgettable. In particular, I would like to thank Timin Hadi for being my life coach and Niusha Mahmoodi for being my dear friend. I could not have finished this adventure without the two of you. I would also like to thank the dedicated staff in the Department of Chemistry at UBC for all their assistance and expertise. In particular I would like to thank the Biological Services Laboratory, the Mass Spectrometry facility, and the NMR facility for all of their help.

I would like to thank my parents Dave and Kathy for their unwavering belief in me and in my abilities. Thank you to Christina for being my most entertaining distraction. Finally, thank you to my husband Mike for being my rock. Words cannot express how much you mean to me and how much you have done for me.

Dedicated to

Gracelyn Louise

Chapter 1: The Detyrosination/Tyrosination Cycle

1.1 Microtubule Formation and Function

1.1.1 Microtubule Structure

Microtubules are an essential component of the cytoskeleton found in eukaryotic cells. Microtubules play a key role in a variety of cellular functions. During interphase, microtubules extend throughout the cell defining its shape and resisting deforming forces. With the help of motor proteins, microtubules transport organelles and vesicles throughout the cell, which defines cell polarity. During cellular division, microtubules constitute the mitotic spindle, which functions to align and separate sister chromatids. Together with centrosomes, microtubules form the core of flagella and cilia, which contribute to cell motility.

Microtubules are the largest component of the cytoskeleton; the rigid hollow tubes are about 25 nM in diameter, and built from heterodimers of the globular protein, α/β-tubulin. The α- and β-tubulin monomers have similar masses of about 55 kDa and have about 40% sequence identity (Wade, 2009). Both α- and β-tubulin exist as various isotypes. In humans six different genes encode for α-tubulin and seven different genes encode for β-tubulin. Most tissues express several isotypes; therefore the resulting microtubules are composed of a mixture of isotypes. The most sequence variation between isotypes is seen in the last 15 residues of the α- and β-tubulin C-terminus (Garnham, 2012). The α-tubulin end of one heterodimer is non-covalently bound to the β-tubulin end of another heterodimer in a head-to-tail fashion, forming a protofilament

(Figure 1.1). The α- and β-tubulin monomers are each bound to a molecule of GTP. The α-tubulin bound GTP is non-exchangeable, while the β-tubulin bound GTP is hydrolyzed to GDP during polymerization (Desai, 1997).

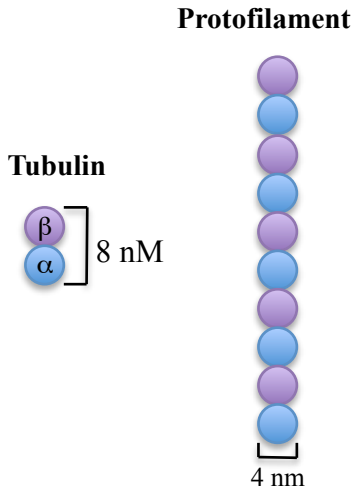

Figure 1.1 α/β-Tubulin heterodimer and assembled protofilament.

Protofilaments, consisting of six to twelve tubulin dimers, associate laterally to form sheets, which then becomes the hollow cylindrical microtubule (Figure 1.2). The primary lateral contacts linking protofilaments are between subunits of the same type (α-α or β-β). However when the sheet closes to form the tube, the lateral contacts are reversed (α-β) forming a seam down the length of the microtubule (Figure 1.2). The number of protofilaments in the microtubule can vary between nine and sixteen, with the most common being thirteen (Dráber, 2012). The protofilaments in the microtubule are arranged in parallel, resulting in a polar structure; the exposed α-subunits of the microtubule creates the minus end and the exposed β-subunits of the microtubule creates the plus end (Figure 1.2) (Downing, 2000).

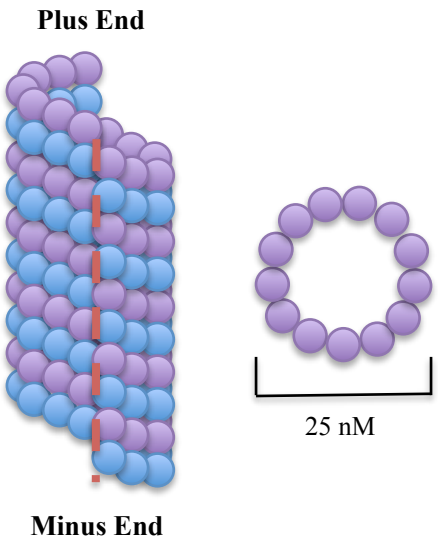

Figure 1.2 Assembled microtubule and cross section.

Microtubules can self-assemble *in vitro* at high concentrations. In the cell cytoplasm α/β-tubulin is widely dispersed and at a lower concentration. Therefore, spontaneous polymerization is kinetically limited; to overcome this barrier, nucleation occurs at microtubule organizing centers (MTOC). These nucleation sites vary in size, shape and occurrence within a cell and between organisms. However, they all have one protein in common, γ-tubulin. This highly conserved member of the tubulin superfamily is present in MTOCs either as a monomer or as a heterotetramer (γ-TuSC). A larger a γ-tubulin ring complex (γ-TuRC) is formed when several γ-TuSCs associate with three or more accessory proteins (Job, 2003). In animal cells nucleation of the microtubule occurs on γ-TuRCs (shown in black) located in the pericentriolar material (shown in blue) of centrosomes (Figure 1.3). A centrosome consists of two arrays of nine triplet microtubules oriented at right angles to each other called centrioles (shown in red). The γ-TuRC remains associated with the minus end of the microtubule during polymerization, therefore functioning as a nucleator and a minus-end cap (Wiese, 2006).

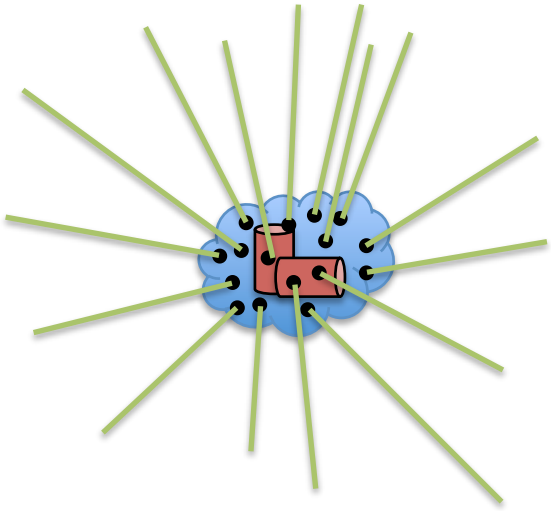

Figure 1.3 Microtubule-organizing center in animal cells.

1.1.2 Microtubule Dynamics

Microtubules exhibit dynamic instability, meaning that a microtubule polymer never reaches a steady state length, but instead continually polymerizes and depolymerizes (Figure 1.4). Microtubule dynamic instability allows for the rapid reorganization and restructure of the cytoskeleton. Polymerization is dependent on the energy provided by the hydrolysis of a GTP molecule bound to the β-tubulin. During polymerization a GTP-bound tubulin binds to the end of microtubule. Quickly after, the β-tubulin GTP molecule is hydrolyzed to GDP. The hydrolysis of GTP changes the conformation of the protofilament from straight to curved, and the GDP-tubulin is locked into the microtubule core in a strained conformation. The GDP-tubulin subunit is very unstable and microtubule will depolymerize quickly unless there is a cap of GTP bound tubulin at both ends (Desai, 1997).

At this point the microtubule might pause at this length, undergo further polymerization or switch to the depolymerization phase. During depolymerization, the

GTP-bound tubulin cap is hydrolyzed to GDP and the protofilaments dissociate into α/β-tubulin subunits. The GDP is exchanged to GTP and the cycle begins again (Desai, 1997). The two ends of the microtubule have distinct polymerization rates; the plus end with the exposed β-subunit grows ten times faster than the minus end with the exposed α-tubulin.

In some cells the microtubule is not anchored to a MTOC, and in that case they undergo a different type of dynamic behavior called treadmilling. Treadmilling is a constant assembly of subunits at one end of the microtubule, with a balanced loss of subunits at the other end of the microtubule (Chen, 2004).

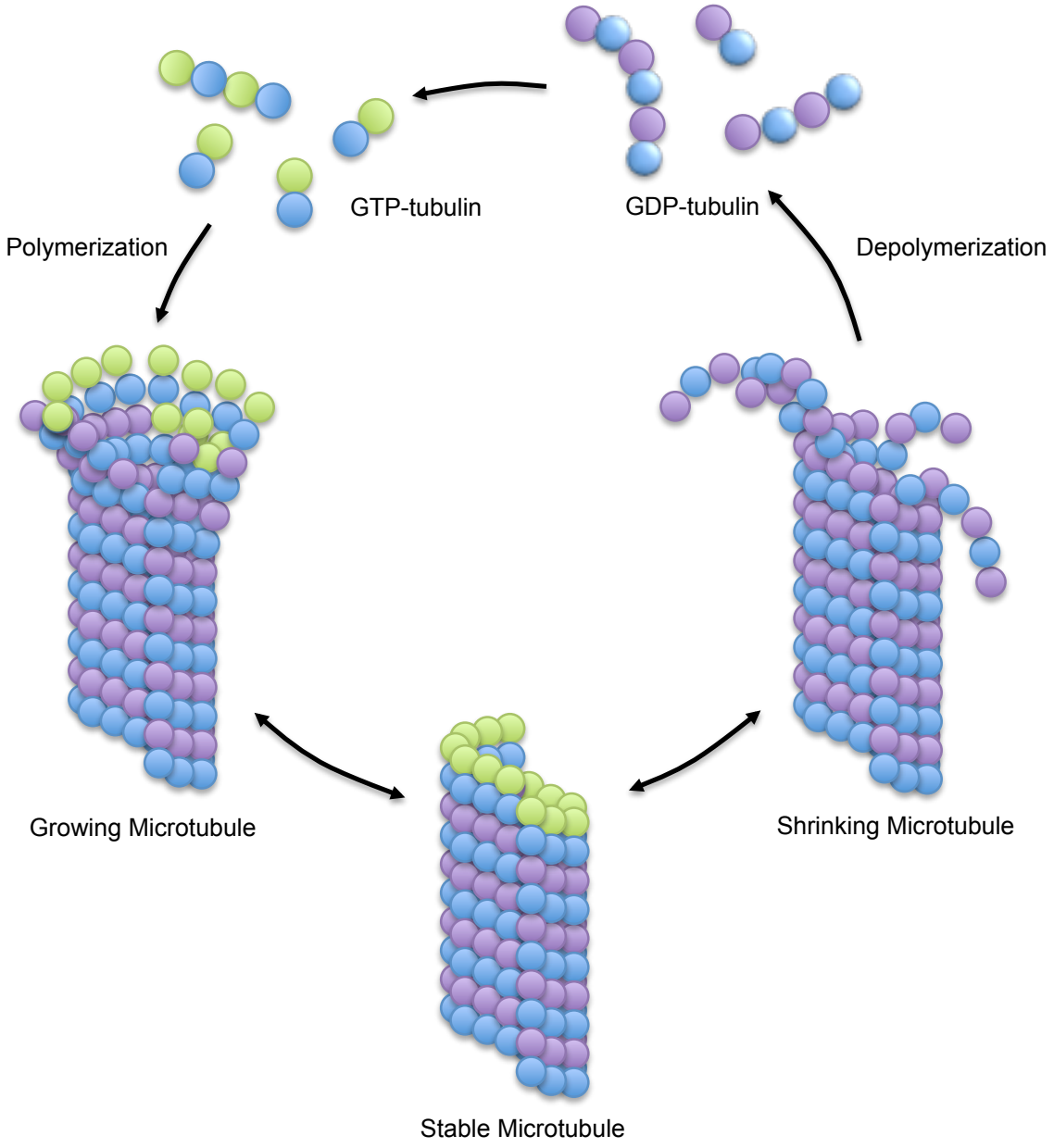

Figure 1.4 Polymerization and depolymerization cycle of the microtubule.

Control of microtubule assembly has been a popular target for the development of anticancer drugs due do to the importance of microtubules in regulating cytoskeletal structure, cell mobility, cell division, and cell differentiation. Two of the earliest developed anticancer drugs that targeted microtubule assembly were vincristine and vinblastine (Figure 1.5).

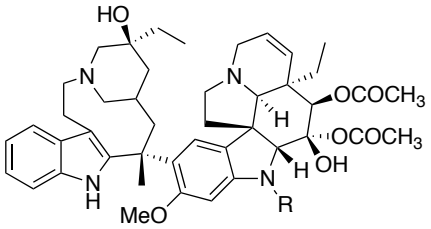

R = CHO Vincristine

R = CH_3 Vinblastine

Figure 1.5 Structure of vinblastine and vincristine.

Both are vinca alkaloids, which were isolated from periwinkle leaves. This class of microtubule-targeted antimitotic drug binds to β-tubulin at the plus end of the microtubule. At low concentrations it blocks new dimers from polymerizing, therefore suspending the microtubule in a paused state, neither growing nor shortening (Jordan, 2004). At higher concentrations the vincas cause incorrect binding of the new dimer, which causes the protofilament to kink or spiral, impairing microtubule formation.

Paclitaxel (Taxol) is another microtubule-targeted antimitotic drug that was isolated from the pacific yew tree (Figure 1.6). This anticancer drug stimulates microtubule polymerization by stabilizing the lateral interactions between protofilaments. It binds to the β-subunit on the inside of the microtubule. It keeps GTP-bound tubulin from hydrolyzing to GDP, therefore stabilizing the microtubule and affecting depolymerization (Downing, 2000).

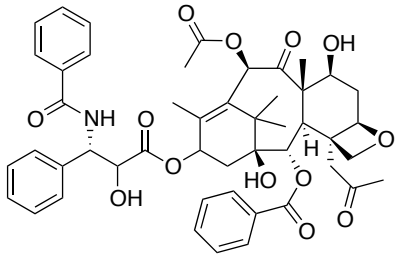

Figure 1.6 Structure of Taxol.

Suppression of dynamics by these microtubule-targeting antimitotic drugs prevents the mitotic spindle from assembling normally. This prevents mitosis from progressing past metaphase into anaphase. With the chromosomes stuck at the spindle poles, the cell exits mitosis and eventually undergoes apoptosis. Cancer cells are more sensitive to antimitotic drugs because cancer cells go through mitosis more frequently (Jordan, 2004).

1.1.3 Microtubule-Regulatory Proteins

A large number of proteins interact with microtubules. These interactions affect microtubule dynamics by stabilizing the microtubule, promoting microtubule disassembly and regulating growth. Microtubule-associated proteins (MAPs) bind to microtubules in order to stabilize and to promote the assembly of microtubules. MAP2, MAP4 and tau stabilize microtubules by binding to the highly acidic C-terminal end of tubulin and shielding this charged region (Downing, 2000). MAP2 and tau are found in neurons, while MAP4 is found in other tissues. The binding of these MAPs to microtubules is regulated by phosphorylation (Desai, 1997).

Microtubule destabilizing factors include the microtubule-severing proteins katanin and spastin and the tubulin-sequestering protein stathmin. Katanin releases microtubules from γ-TuRC and spastin generates internal breaks in the microtubule by

binding to the C-terminus of tubulin and destabilizing tubulin-tubulin interactions (Wasteneys, 2011). Stathmin binds to α/β-tubulin dimers, removing them from the pool of free tubulin available for polymerization. It has also been reported to enhance GTP hydrolysis, which initiates microtubule disassembly (Downing, 2000).

Microtubule plus end-binding proteins called plus-end tracking protein (+TIPs) regulate the dynamics of the microtubule plus end. The first +TIP to be described was CLIP-170, which is a linker between the plus end of microtubules and cell membranes. Microtubules close to cell membranes show frequent fluctuations in growing and shrinking, which is thought to allow microtubules to adapt to changes in cell shape. CLIP-170 rescues depolymerizing microtubules near the cell membrane. When CLIP-170 is removed from cells, the microtubule depolymerization rate increases and fewer microtubules reach the ends of the cell. Another +TIP is end-binding protein 1 (EB1), which binds and stabilizes microtubules during mitosis by keeping the microtubule from bending (Howard, 2003).

Microtubules also serve as tracks for the intracellular transport of organelles, chromosomes and protein complexes. Motor proteins such as kinesin and dynein drive this transport. Each harnesses the chemical energy released by the hydrolysis of ATP and convert it into mechanical work. Kinesins move cellular cargo toward the plus end of the microtubule while dyneins move cellular cargo towards the minus end of the microtubule (Wasteneys, 2011). Mitotic centromere-associated kinesins (MCAKs) also associate at the plus end of the microtubule, however MCAKs use ATP hydrolysis to remove tubulin subunits and trigger depolymerization. They preferentially bind to bent microtubules,

which may be the way that they discriminate between the microtubule ends and lattice (Howard, 2003).

1.1.4 Post-Translational Modifications of Tubulin and Microtubules

Microtubules are involved in a variety of cellular processes; these various functions require variable structures. Because microtubules are composed of a single building block, structural diversity in the microtubule is obtained by incorporating the different α- and β-tubulin isotypes into the polymer and by post-translational modifications of both tubulin and microtubules. These post-translational modifications include acetylation/deacetylation, detyrosination/tyrosination, polyglycylation and polyglutamylation (Figure 1.7). The highest density of these post-translational modifications is found on stable and complex microtubule arrays, such as those of cilia or neurons.

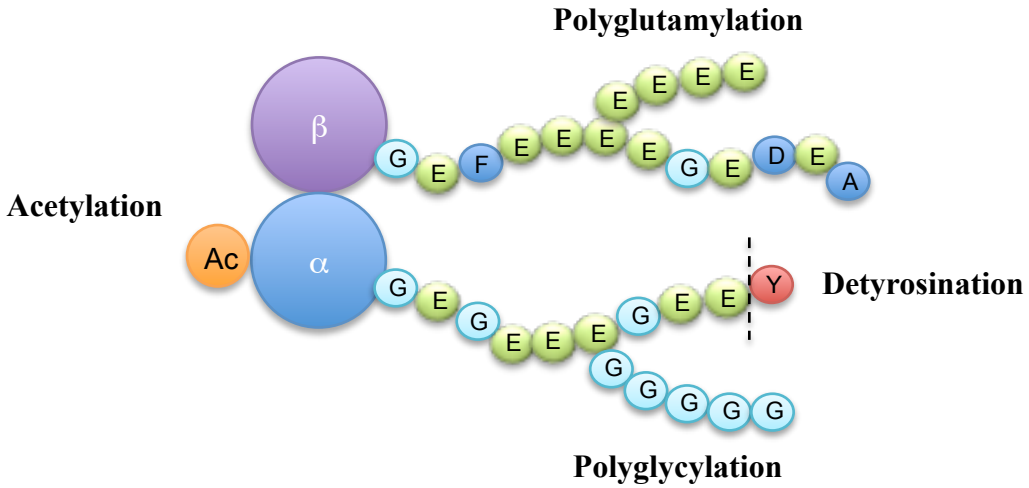

Figure 1.7 Post-translational modifications of α- and β-tubulin.

Most post-translational modifications occur on the surface exposed C-terminus of α- and β-tubulin. The acylation of α-tubulin occurs primarily at the ε-amino group of

Lys_{40}, which is located on the inside surface of the microtubule. Acetylation has also been shown to occur at Lys_{252} on β-tubulin of soluble tubulin heterodimers (Chu, 2001). The α-tubulin acetyltransferases (ARD1-NAT1, ELP, and MEC-17/αTAT1), the β-tubulin acetyltransferase (SAN) and the deacetylases (HDAC6 and SirT2) have been identified and shown to also modify other proteins unrelated to tubulin (Valenzuela-Fernandez, 2008) (Chu, 2011). The physiological importance of microtubule acetylation has yet to be completely resolved. Elimination of the tubulin acetylation site by site directed mutagenesis of the lysine residue to an arginine residue resulted in no observable cell abnormalities indicating acetylation is nonessential (Gaertig, 1995). Recent studies have shown that acetylation is associated with stable microtubules and that kinesin-1 shows a preference for acetylated microtubules (Garnham, 2012).

Detyrosination of the RNA-encoded C-terminal tyrosine on α-tubulin is removed by an unidentified tubulin carboxypeptidase. This modification is reversible in that tyrosine may be replaced by tubulin tyrosine ligase. Tubulin carboxypeptidase favors polymerized tubulin, while tubulin tyrosine ligase exclusively tyrosinates the α/β-tubulin dimer. Detyrosinated tubulin can be further modified by removal of its C-terminal glutamic acid, resulting in Δ2-tubulin. The detyrosination/tyrosination cycle will be discussed in greater detail in Section 1.2.

Both polyglycylation and polyglutamylation involve the sequential addition of glycine and glutamic acid residues, respectively, to the γ-carboxylate of a C-terminal glutamic acid residue on either α- or β-tubulin. These post-translational modifications occur preferentially on polymerized microtubules. Polyglycylation was first detected on

the axoneme microtubules from *Paramecium* (Redeker, 1994), and polyglutamylation was first detected in cultured mouse brain neurons (Edde, 1990).

Because the glutamylases and glycylases responsible for these modifications show homology to tubulin tyrosine ligase they have been grouped in the tubulin tyrosine ligase-like (TTLL) family. Certain TTLL enzymes are specific for catalyzing the addition of the first branched amino acid (termed initiases), while other TTLL enzymes are specific for catalyzing the elongation of the branched amino acid chain (termed elongases) (Garnham, 2012). Tubulin glutamylation is also a reversible process as deglutamylating enzymes have also been identified and grouped in a family of cytosolic carboxypeptidases (CCP). Deglutamylating enzymes in the CCP family are also responsible for the generation of Δ2-tubulin.

The length of the added chain is highly variable; glutamic acid and glycine chains of 20 and 34 residues, respectively, have been reported (Garnham, 2012). This variability significantly increases the heterogeneity of the microtubule. Usually the length of the polyglutamic acid side chain is between one and six residues, with the longest chains found in cilia. The length and location of the polyglutamic acid chain has been shown to influence the binding and activity of MAPs, motor proteins and microtubule severing enzymes. For example, kinesin-1, MAP2, and tau bind to microtubules with chains consisting of three glutamic acids while MAP1A binds to microtubules with longer chains (six residues). Also, spastin and katatin prefer binding to polyglutamylated microtubules (Garnham, 2012).

Polyglutamylation of α-tubulin, in both axonal and dendritic neurites, is crucial for normal neuronal development and function. Microtubules isolated from the brains of

mice lacking PGs1 (a subunit of an enzyme complex with polyglutamylase activity) displayed weaker binding affinity to microtubule motor proteins such as kinesin and dynein. This disruption in motor protein binding led to a decrease in the density of synaptic vesicles, which resulted in reduced synaptic transmission. The results of this study implicate that disruptions in tubulin polyglutamylation might be associated with neurological disorders such as schizophrenia or Alzheimer's disease (Ikegami, 2007).

Polyglycylated microtubules are primarily found on the axoneme of cilia and flagella. Gene knockdown experiments involve reducing the expression of an organism's genes either through genetic modification or by treatment with a reagent. Knockdown experiments of the polyglycylase gene TTLL3 only mildly affected cilia structure and motility. Similarly, knockdown experiments of the polyglutamylase gene TTLL6 only mildly affected cilia structure and motility. A double knockdown experiment of TTLL3 and TTLL6 resulted in the complete loss of cilia structure and mobility. These results indicate that microtubule glycylation and glutamylation have overlapping functions (Pathak, 2011).

Pancreatic cancer cells express a higher level of the polyglutamylation enzyme TTLL4. Knockdown experiments of TTLL4 reduced pancreatic cancer cell growth, while the introduction of TTLL4 increased cell growth (Kashiwaya, 2010). An increase in polyglutamylation of α-tubulin was also seen in prostate cancer cell lines (Souček, 2006). These two results indicate that TTLL polyglutamylating enzymes are potential therapeutic targets for novel cancer therapies.

Post-translationally modified tubulins are not uniformly distributed along the microtubule. This resulting complexity marks distinct populations of microtubules for

specific functions and interactions. It has been proposed that these post-translational modifications function to create a "tubulin code" that is read by proteins that interact with microtubules (Verhey, 2007). Interfering with the proper reading of this code could be detrimental to the growth of cells and therefore, post-translational modification enzymes are potential targets for anticancer development.

1.2 The Detyrosination/Tyrosination Cycle

The post-translational modification of interest to this project is the detyrosination/tyrosination cycle (Figure 1.8). In this cycle, an RNA encoded C-terminal tyrosine on the α-tubulin subunit (Tyr-tubulin) is removed from the peptide chain by tubulin carboxypeptidase (TCP) resulting in Glu-tubulin. The tyrosine is reattached to the peptide chain in an ATP-dependent reaction catalyzed by tubulin tyrosine ligase (TTL), resulting in the original Tyr-tubulin. If the penultimate glutamic acid is removed before the tyrosine residue is replaced, Δ2-tubulin is formed. This form of tubulin cannot be reconverted to Glu-tubulin, and is therefore no longer a substrate for TTL (Westermann, 2003). Deglutamylase enzymes belonging to the family of cytosolic carboxypeptidases catalyze the formation of Δ2-tubulin. Δ2-Tubulin is abundant in the brain and accounts for about 35% of the tubulin present in these tissues.

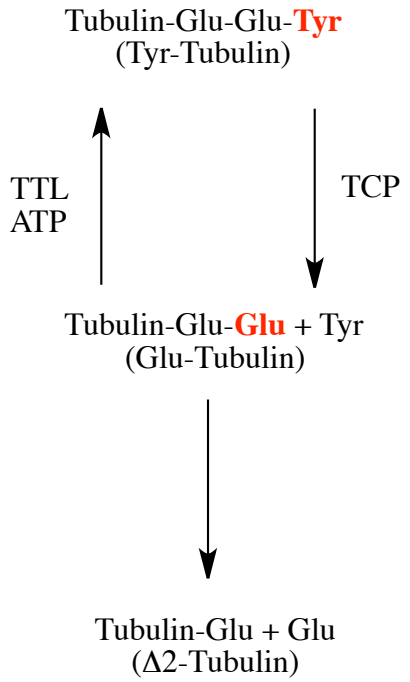

Figure 1.8 The detyrosination/tyrosination cycle.

1.2.1 Discovery of the Detyrosination/Tyrosination Cycle

The action of protein tyrosination was first described in 1973. It was shown that tyrosine was incorporated into a protein present in rat brain extracts by a ribosome-free process. Brain preparations were tyrosinated more than kidney, liver or thyroid extracts and the reaction required ATP, Mg^{2+}, and K^{+} (Barra, 1973).

Tyrosine was incorporated into a protein that displayed characteristics similar to tubulin; it had a molecular weight of 54 kDa, and was found in different states of aggregation (Barra, 1974). To confirm that the acceptor protein was tubulin, a [^{3}H] colchicine-binding method was employed. In this method rat brain extracts were simultaneously incubated with ^{14}C-tyrosine and ^{3}H-colchicine. Colchicine is a natural product that binds to tubulin and prevents polymerization. Formation and isolation of ^{3}H-colchicine bound tubulin is a sensitive assay in the detection and purification of tubulin

(Weisenberg, 1968). The incubated mixture was purified by ion exchange chromatography; column fractions were assayed for radioactivity. ^{14}C and ^{3}H labels were found in the same column fractions, providing evidence that the acceptor protein is tubulin (Figure 1.9) (Barra, 1974) (Arce, 1975).

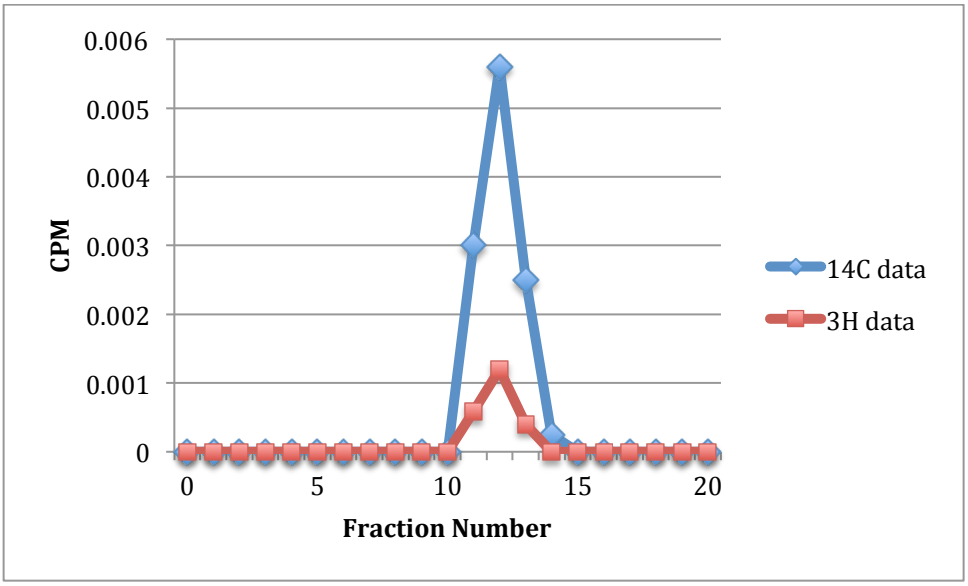

Figure 1.9 Plot of CPM vs column fraction (figure adapted from Arce, 1975).

Rat brain extracts were also incubated with only ^{14}C-tyrosine and purified by ion exchange chromatography. Dodecylsulfate-polyacrylamide gel electrophoresis of the radioactive fraction produced two bands, which corresponded to α- and β-tubulin. The entire ^{14}C radioactivity was found in the band corresponding to the α-tubulin subunit (Arce, 1975).

1.2.2 Isolation, Purification and Characterization of Tubulin Tyrosine Ligase

The ligase responsible for tyrosinating α-tubulin, tubulin tyrosine ligase (TTL), was first identified and partially purified from bovine brain extracts in 1977 (Raybin, 1977a). TTL was shown to tyrosinate purified Glu-tubulin in the presence of ATP (K_M =

0.75 mM), Mg^{2+} (optimal concentration 8-16 mM), and K^{+} (optimal concentration >30 mM) (Raybin, 1975). Along with tyrosine (K_M of 0.043 mM), TTL can also accept phenylalanine (K_M of 1.2 mM) and dihydroxyphenylalanine (K_M of 0.16-1.2 mM) as substrates (Deanin, 1976). The majority of brain α-tubulin is in the Glu-tubulin form, so this is the source of substrate for studies with TTL.

Initial TTL studies were carried out on various mammalian and avian tissues, in particular the brain and other nervous tissues (Deanin, 1976). In 1979 a study was undertaken to determine the phylogenic distribution of TTL. Nervous tissue from various vertebrates and invertebrates were assayed for ^{3}H-tyrosine incorporation into α-tubulin. All vertebrates tested (dogfish, shark, carp, newt, frog and chameleon) were able to incorporate tyrosine into endogenous brain α-tubulin. The amount of tyrosine incorporated was increased with the addition of rat brain tubulin or TTL, indicating compatibility between mammalian TTL and other vertebrate forms. This compatibility indicates a functional evolutionary conservation. All invertebrate nervous tissues studied (sea squirt, beetle, lobster, and squid) were unable to incorporate tyrosine into tubulin. The absence of tyrosine incorporation indicates an evolutionary divergence in the post-translational modification of the tubulin protein (Preston, 1979).

The TTL enzyme was first purified to homogeneity using DEAE-cellulose chromatography, followed by sepharose-sebacic acid hydrazide-ATP affinity chromatography, and finally by sepharose-tubulin affinity chromatography. The molecular weight of TTL was determined to be 37,000. Conditions for optimal activity were found to be a pH of 8, a KCl concentration of 0.15-0.3 M and a $MgCl_2$ concentration of 5-30 mM (Murofushi, 1980). This method of purification is difficult

because of enzyme instability and the tendency for TTL to form a stable complex with tubulin that results in co-purification of the enzyme and protein. An improved method of purification was published in 1986 that omits the sepharose-tubulin affinity chromatography and replaces it with immunoaffinity chromatography using mouse monoclonal antibodies. This improvement allowed for a more rapid purification with improved enzyme stability (Wehland, 1986).

Depolymerized tubulin is the preferred substrate of TTL. To show that TTL acts on depolymerized or non-assembled tubulin, the enzyme was incubated with purified rat brain tubulin in the presence of colchicine. Colchicine inhibits the polymerization of microtubules, leaving only α/β-tubulin subunits available as substrate. The presence of colchicine did not affect the incorporation of tyrosine indicating that depolymerized tubulin is a substrate for TTL (Arce, 1975). To show that assembled microtubules were not a substrate for TTL, rat brain extracts containing tubulin were allowed to assemble for 30 minutes. At that time, ^{14}C-labeled tyrosine, ATP, $MgCl_2$, KCl and TTL were added. Aliquots were taken at various times, and assembled and non-assembled tubulin were separated and assayed for ^{14}C-labeled tyrosine incorporation (Figure 1.10). Incorporation of the ^{14}C-labeled tyrosine on non-assembled tubulin was 10 fold higher than on assembled tubulin (Arce, 1978).

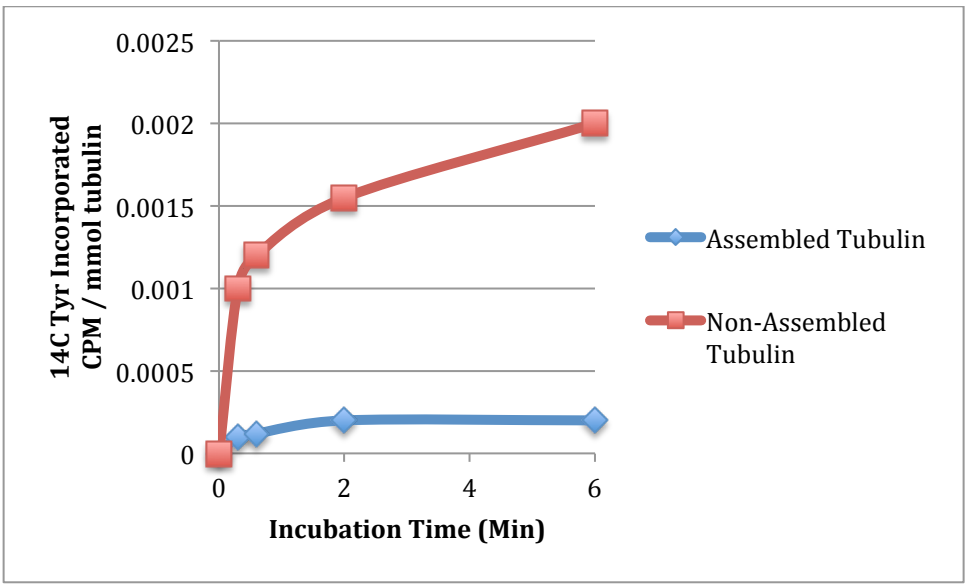

Figure 1.10 Incorporation of ^{14}C-tyrosine into assembled and non-assembled tubulin (figure adapted from Arce, 1978).

Peptide chains mimicking the C-terminal sequence of α-tubulin (VDSVEGEGEEEGEE) can also serve as a substrate for TTL (Rüdiger, 1994). A series of peptide substrates were synthesized to analyze the substrate specificity of TTL; point mutations and variations in length were examined. Point mutations introducing alternative amino acids eliminated TTL activity. Even substituting aspartic acid for glutamic acid resulted in no activity. Peptide length also strongly influenced TTL activity. A very low level of activity was seen with a hexapeptide substrate (EEEGEE). TTL activity increased with each additional amino acid. Any increase in length beyond the tetradecapeptide (VDSVEGEGEEEGEE) provided no further activity enhancement. Even though TTL recognizes the tetradecapeptide as a substrate, its activity is 50 fold lower than the activity of TTL against α/β-tubulin.

1.2.2.1 Crystal Structure Analysis of Tubulin Tyrosine Ligase

Once recombinant TTL became available, larger quantities of the protein could be purified and it became possible to carry out structural studies. The crystal structure of TTL from *Xenopus tropicalis*, which has 81% sequence identity to humans, was determined in its apo, ATP- and ADP-bound states (Figure 1.11) (Szyk, 2011). There were no major conformational changes found between the apo and nucleotide bound crystal structures. TTL is an elongated molecule consisting of an N-terminal, a central and a C-terminal domain, with the active site lying at the interface between the C-terminal and central domain (Szyk, 2011).

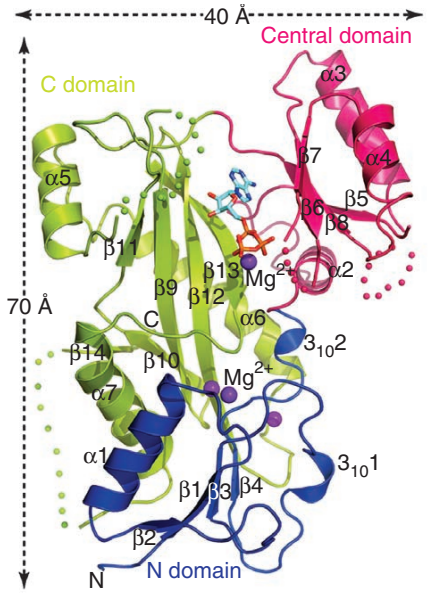

Figure 1.11 Ribbon representation of the crystal structure of TTL bound to the ATP analogue AMPPNP (Szyk, 2011).

The fold of TTL resembles a family of enzymes called the ATP grasp enzymes. Enzymes in this family include D-alanine:D-alanine ligase, biotin carboxylase, and glutathione synthetase. ATP grasp enzymes catalyze either the ATP dependent ligation of a carboxylic acid with a nucleophile via the formation of an acylphosphate

intermediate, or they act as a kinase and catalyze only a phosphoryl transfer (Fawaz, 2011). Unique to this superfamily is the ATP binding site; ATP is grasped between two domains. In the case of TTL, the ATP is grasped between the central and C-terminal domain.

Based on sequence comparison between TTL and members of the TTLL family, the secondary structure of TTL is predicted to be similar to the TTLL enzymes tubulin polyglutamylase and tubulin polyglycylase. The residues involved in ATP binding are invariant between the TTL and TTLL enzymes, while surface residues vary to accommodate a variety of recognition specificities between the different types of enzymes.

Mutagenesis of surface and active site residues indicate binding interactions that are crucial for tubulin tyrosination. ATP is wedged against a loop located between the central and C-domain. Mutation of residues on this loop that facilitate ATP binding abolished activity of the enzyme, confirming that ATP is crucial for enzyme catalysis. The surface of TTL has a conserved positively charged strip of residues that extends from the ATP binding site to the N-terminal domain (shown in red, Figure 1.12). These residues interact with the negatively charged α-tubulin tail. Mutagenesis of these conserved residues impaired catalytic activity.

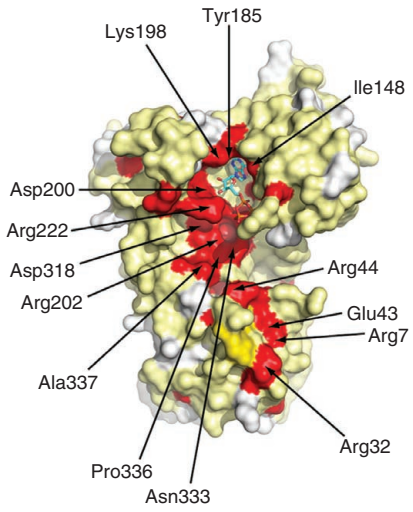

Figure 1.12 Molecular surface of TTL (Szyk, 2011).

Mutated TTL was assayed with both the α-tubulin tail peptide (VDSVEGEGEEEGEE) and tubulin. Mutations that impaired TTL activity when the α-tubulin tail peptide was the substrate also impaired activity when tubulin was the substrate. Mutagenesis of residues at the junction between the central and N-terminal domains had a greater decrease in activity when tubulin was the substrate. This indicated that TTL is interacting with the tubulin dimer, not just the tail of the α-tubulin subunit.

1.2.3 Isolation, Purification and Characterization of Tubulin Carboxypeptidase

The carboxypeptidase responsible for detyrosinating the α-tubulin subunit, tubulin carboxypeptidase (TCP), was first isolated and partially purified from rat brains. Rat brain extracts were incubated with ^{14}C-labeled tyrosine-tubulin, and the ^{14}C-tyrosine released was measured by counting in a scintillation spectrometer (Hallak, 1977). The TCP was separated from the TTL in crude rat brain extracts through ammonium sulfate precipitations and partially purified by DEAE-Sephadex chromatography (Argaraña, 1978). The partially purified TCP is very unstable, and activity is lost after 24 hours

(Argaraña, 1980). Because of this instability, attempts at purifying TCP to homogeneity have been unsuccessful. No cofactor is required for TCP activity, but it has been found that TCP has an optimal activity with 1-4 mM of $MgCl_2$ and 15-30 mM of KCl (Argaraña, 1978). The molecular weight of TCP is estimated to be 90,000 (Argaraña, 1980).

Polymerized tubulin is slightly preferred as a substrate of TCP. To test this, two types of ^{14}C-labeled tyrosine tubulin were prepared. The first one, called tubulin-PC, is a phosphocellulose-purified tubulin that is unable to self-assemble. The second one, called tubulin-5xP, is an assembly competent form of tubulin purified with co-assembling MAPs. The TCP reaction was assayed by incubating the ^{14}C-labeled tyrosine tubulin-PC or -5xP with TCP. The reaction was stopped by the addition of trichloroacetic acid and the released ^{14}C-labeled tyrosine was measured on a scintillation counter (Figure 1.13). It was shown that TCP could catalyze complete detyrosination of both types of tubulin after 2 hours, but the assembly competent tubulin-5xP was detyrosinated 2-3 times faster (Kumar, 1981).

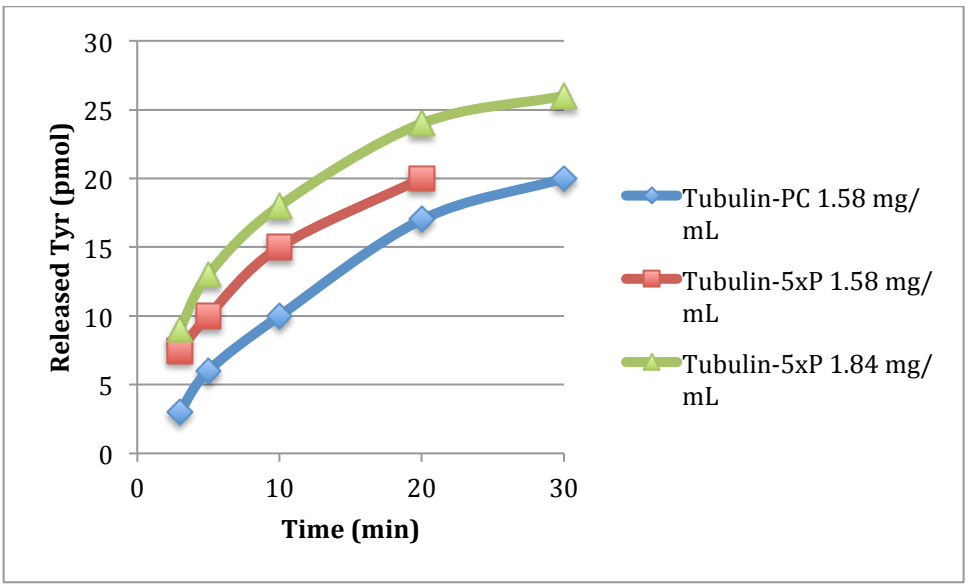

Figure 1.13 Release of tyrosine from ^{14}C-tyrosinated tubulin-PC and -5xP (figure adapted from Kumar, 1981).

Because of the increased rate of detyrosination on assembly competent tubulin-5xP, further studies were undertaken to show that polymerized tubulin was the preferred substrate for TCP. Assembly competent tubulin-5xP was incubated with an increasing concentration of podophyllotoxin followed by incubation with TCP. Podophyllotoxin is a non-alkaloid toxin lignin from *Podophyllum* that binds to tubulin and prevents MT assembly. The rate of tyrosine release decreased proportionally to the increase in podophyllotoxin concentration. This trend was also seen when podophyllotoxin was replaced with colchicine. When tubulin-5xP was incubated with taxol, a natural product that promotes microtubule polymerization by stabilizing the microtubule, an increase in TCP activity was seen (Kumar, 1981).

1.3 Role of the Detyrosination/Tyrosination Cycle

There are have been numerous studies, in vivo and in vitro, to determine the specific role tubulin detyrosination and tyrosination has in regulating microtubule function, but the precise function of this cycle is still unclear. Biochemical studies have examined the kinetic effect of Glu-tubulin and Tyr-tubulin in tubulin polymerization. The assembly properties of Glu-tubulin and Tyr-tubulin into the microtubule were found to be the same (Arce, 1978 and Raybin, 1977b).

Peptide antibodies specific for both Tyr-tubulin and Glu-tubulin were prepared and used to image microtubules in vivo. Imaging results revealed that microtubules consist of both Glu-tubulin and Tyr-tubulin. The Tyr-tubulin extends from the center of the microtubule to the periphery of the cell, while the Glu-tubulin, also found in the cell center, did not reach the periphery of the cell. Interphase microtubules and the metaphase spindle were found to contain primarily Tyr-tubulin, while older more stable microtubules were found to contain primarily Glu-tubulin. This result confirmed that Glu-tubulin and Tyr-tubulin are predominantly present in different populations of microtubules and supports the idea that the role of the cycle is to generate functionally distinct microtubules (Gunderson, 1984).

Studies on the dynamics of Glu-tubulin microtubules and Tyr-tubulin microtubules have shown that Tyr-tubulin microtubules are more dynamic and Glu-tubulin microtubules are more stable (Kreis, 1987). Because TTL works on depolymerized tubulin, the pool of α/β tubulin dimers available for polymerization is completely tyrosinated. Initially, the newly formed microtubule is completely composed of Tyr-tubulin. Dynamic microtubules turn over so quickly that detyrosination does not

happen. If the microtubule becomes stabilized, the tubulin composing them is detyrosinated by TCP, resulting in a Glu-tubulin microtubule. Even though Glu-tubulin is found on more stable microtubules, the detyrosination is a consequence of, rather than a cause of, microtubule stability (Bulinski, 1991). In vivo studies where TTL was inhibited resulted in Glu-tubulin microtubules that did not differ in their dynamics compared to the analogous Tyr-tubulin microtubule (Webster, 1990). It has been suggested that the stable Glu-tubulin microtubules are important for the generation of cell polarity because the Glu-tubulin microtubules are more pronounced along the axis (Bulinski, 1991).

One approach to understanding the function of the detyrosination/tyrosination cycle was to look at MAPs that exhibit differences in binding to Glu-tubulin microtubules over Tyr-tubulin microtubules. In vitro studies showed that MAP2 and MAP4 do not prefer binding to one form over the other. However, Tyr-tubulin microtubules are associated with plus-end tracking proteins (+TIPs). These proteins bind to the plus-end of the microtubule and effect dynamic instability of the microtubule. Many of these +TIPs have a cytoskeleton-associated protein glycine rich (CAP-Gly) domain, such as CLIP-170. The presence of Tyr-tubulin at the plus end of the microtubule is crucial for binding of the +TIPs with a CAP-Gly domain. In TTL-null cells, where the population of Tyr-tubulin is greatly reduced, the +TIPs with a CAP-Gly domain are unable to associate with the microtubule. This causes abnormalities in mitotic spindle positioning and irregularities in cell shape and morphology (Peris, 2006).

The microtubule motor protein kinesin preferentially binds to Glu-tubulin microtubules over Tyr-tubulin microtubules with a 2.8-fold higher affinity (Liao, 1998).

The tightly bound kinesin-1 moves slower along the Glu-tubulin enriched microtubules, ensuring a uniform delivery of cargo throughout the cell (Dunn, 2008).

The first incidence of TTL's involvement in the growth of cancer cells was reported in 1998 (Lafanechère, 1998). Subclonal lines of mouse cells, devoid of TTL through spontaneous mutation (NH-3T3), were introduced into nude mice and resulted in the production of sarcomas. The resulting tumors predominantly contained Glu-tubulin and Δ2-tubulin microtubules. The presence of Δ2-tubulin is unique to tumor cells; normal tissue samples are completely devoid of Δ2-tubulin, with the exception of the brain. The loss of TTL activity during tumor growth is also seen in several human cancer cells, including breast tumor biopsies. TTL suppression is an important factor of tumor growth (Lafanechère, 1998).

Breast cancer cells were further examined to determine if TTL suppression was linked to tumor severity. Glu-tubulin microtubules were absent in normal breast tissue epithelial cells, but were found in over 50% of carcinomatous tumor cells. The tubulin detyrosination occurred more frequently in tumors of high severity. These studies indicate that the suppression of TTL favors tumor growth and that it defines high-risk tumors (Mialhe, 2001).

Gene knockout experiments invole making an organism's genes inoperative. TTL knockout experiments in mice were conducted to test the importance of TTL in the whole animal. The TTL-null mice were born, but they displayed defective breathing and ataxia, and they died after a few days. This indicates that TTL plays a vital role in the control of neuronal organization. The tubulin composition was probed using antibodies for Tyr-, Glu- and Δ2-tubulin. Glu- and Δ2-tubulin were detected in all tissues analyzed. No

obvious malformations of any organs were detected, but analysis of the TTL-null brain organization and neurons showed a disruption in the cortico-thalamic loop, causing abnormalities in the organization of neuronal networks and ultimately, death of the TTL-null mice (Erck, 2005). The disruption of the detyrosination/tyrosination cycle in tumor cells makes this post-translational modification a novel target in cancer research and therapies.

1.4 Proposed Mechanism of Tubulin Tyrosine Ligase

TTL has been extensively studied, but the detailed molecular mechanism remains unresolved. Because of its structural similarities to the ATP-grasp ligases, it can be concluded that TTL has a similar mechanism. The mechanism of ATP-grasp enzymes can be described by two half reactions (Figure 1.14). In the first part of the reaction, the substrate carboxylic acid reacts with ATP to produce an activated acylphosphate intermediate. In the second part of the reaction the substrate nucleophile attacks the carbonyl carbon of the acylphosphate intermediate to yield a tetrahedral intermediate. Decomposition of this tetrahedral intermediate results in the final product and inorganic phosphate. The second half reaction requires an active site base for removal of a proton from the thiol or amine substrate nucleophile (Fawaz, 2011).

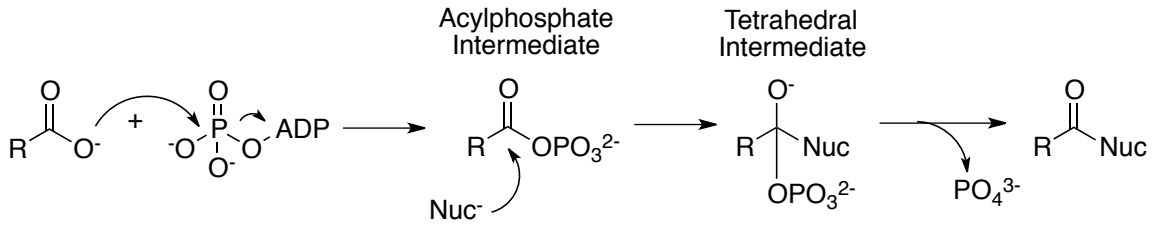

Figure 1.14 General mechanism of ATP-grasp enzymes.

One example of an ATP-grasp ligase is D-alanine:D-alanine ligase, which catalyzes the ligation of two D-alanines. The D-alanine dipeptide is an important constituent of peptidoglycan, which is an essential component of the bacteria cell wall. Failure to assemble the dipeptide and incorporate it into the peptidoglycan layer would result in bacterial lysis, therefore making this enzyme a popular target for antibiotic design. The mechanism of D-alanine:D-alanine ligase involves the carboxylic acid on the first alanine reacting with ATP to form an activated acylphosphate intermediate, followed by nucleophilic attack of the amino group of the second D-alanine forming a tetrahedral intermediate. Collapse of the tetrahedral intermediate releases inorganic phosphate to give the D-alanine-D-alanine dipeptide (Figure 1.15) (Fan 1994).

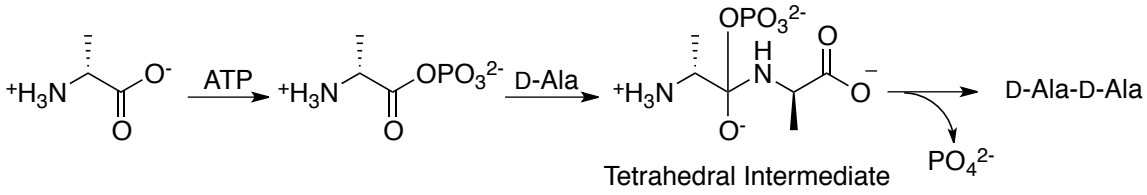

Figure 1.15 Reaction mechanism of D-alanine:D-alanine ligase.

The formation of the D-alanylphosphate intermediate has been proven through positional isotope exchange studies (Figure 1.16). D-Alanine:D-alanine ligase catalyzed the positional exchange of the β,γ-bridge oxygen in [γ-$^{18}O_4$]-ATP to a β-non-bridge position (Mullins, 1990).

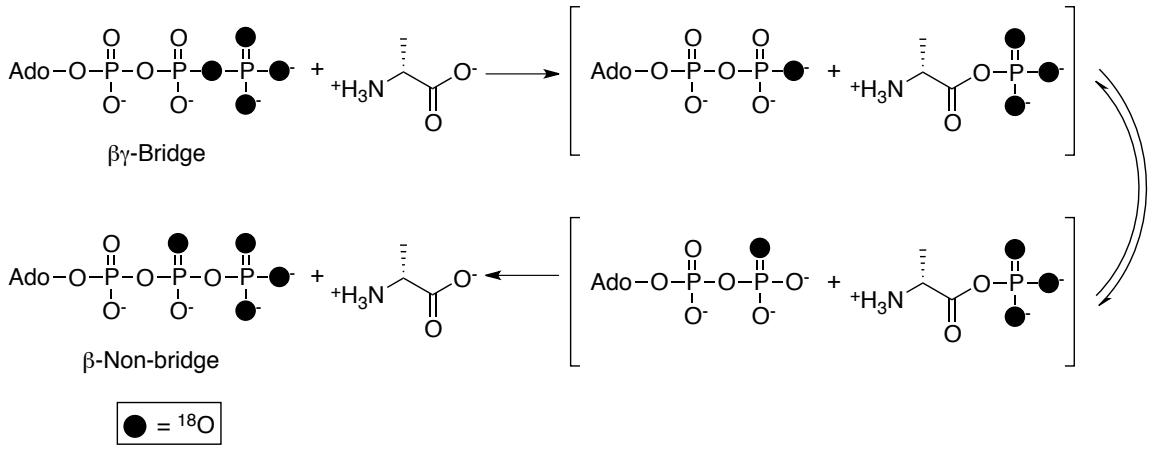

Figure 1.16 Positional isotope exchange studies.

The proposed mechanism of TTL, based on mechanistic studies of ATP-grasp enzymes, involves activation of the terminal Glu residue of the α-tail with ATP to form an acylphosphate intermediate. Nucleophilic attack on the phosphorylated carboxylate by the amine from a tyrosine residue would forms the tetrahedral intermediate, which collapses to give Tyr-tubulin and inorganic phosphate (Figure 1.17).

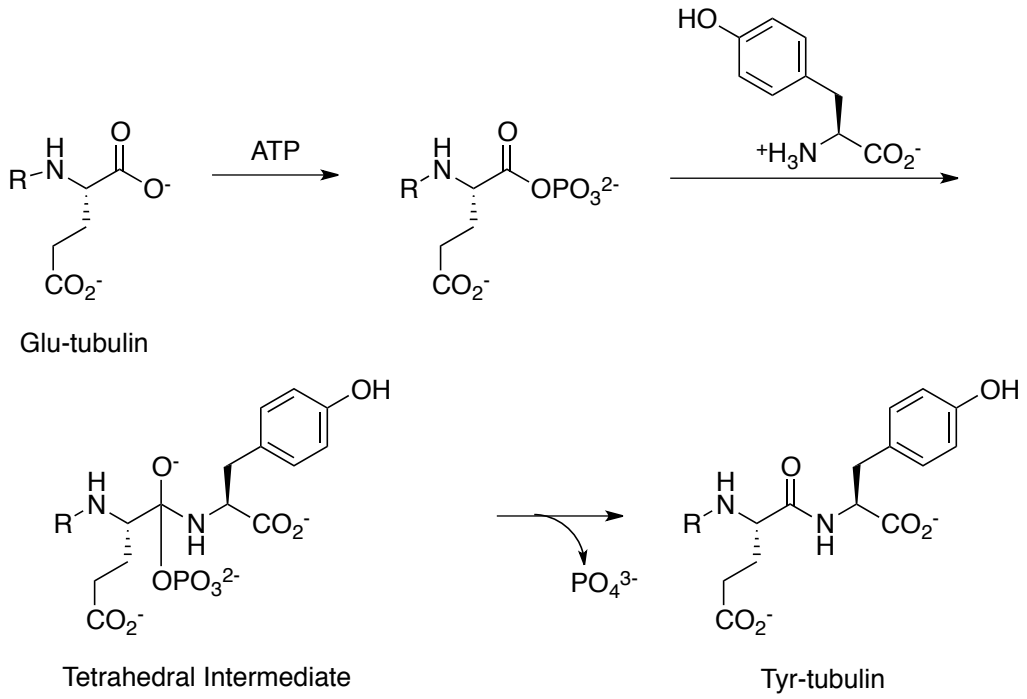

Figure 1.17 Proposed reaction mechanism of TTL.

Work towards further characterization of the ligase and elucidation of the mechanism has included kinetic experiments and inhibitor studies. Using initial rate experiments to determine the kinetic mechanism of multi-substrate single enzyme reactions is complicated when three substrates are involved. Deans *et. al.* used a procedure (Frieden, 1959) that involved holding one substrate at a constant high concentration, while the other substrate levels were varied. This was repeated in three sets of experiments, holding a substrate constant in each set: tubulin, tyrosine or ATP. A double reciprocal plot of the initial rate data for each set resulted in non-parallel lines, indicating a sequential mechanism instead of a ping-pong (or non-sequential) mechanism (Deans, 1992).

The initial rate data was supplemented with experiments involving competitive and product inhibitors. This was done by holding two substrates at a high concentration

while varying the concentration of the third substrate and inhibitor. The first inhibitor that was evaluated was AMP. The double reciprocal plot of initial rate data showed that AMP acts as a competitive inhibitor of ATP, a non-competitive inhibitor of tyrosine and a non-linear inhibitor of tubulin. Inhibitors ADP and 3,4-dihydroxyphenylalanine were also evaluated. ADP demonstrated competitive inhibition to ATP and non-competitive inhibition to tyrosine and tubulin. 3,4-Dihydroxyphenylalanine demonstrated competitive inhibition to tyrosine and non-competitive inhibition to ATP and tubulin. This data eliminated the possibility of an ordered substrate addition mechanism, and instead pointed to a random substrate addition mechanism. The combined results indicate that TTL operates by a random sequential pathway (Deans, 1992).

1.5 Proposed Mechanism of Tubulin Carboxypeptidase

Proteases (also known as peptidases) catalyze the breakdown of proteins by hydrolysis of peptide bonds. Proteases can cleave the terminal amino acid (termed exopeptidase) from the N-terminus (aminopeptidase) or from the C-terminus (carboxypeptidase). Alternatively, proteases can hydrolyze internal peptide bonds (termed endopeptidase). The mechanism of action involves either nucleophilic catalysis (serine, cysteine or threonine proteases) or general acid-base catalysis involving an activated water molecule (aspartic, glutamic or metalloproteases) (Turk, 2006).

Serine, cysteine and threonine proteases contain catalytic active site residues consisting of a nucleophile, base and acid (Figure 1.18). The adjacent basic resude (histidine) activates the nucleophilic residue (Ser, Cys or Thr). In serine proteases, an acidic residue such as aspartic acid stabilizes the resulting imidazolium cation of histidine. The activated nucleophile attacks the amide carbonyl of the peptide chain

forming a tetrahedral oxyanion intermediate. This tetrahedral intermediate resembles the tetrahedral intermediate formed in ATP-grasp ligase reactions. This high-energy intermediate is stabilized by hydrogen bonding between the oxyanion and main chain amide N-H bonds. The leaving-group nitrogen is protonated by the catalytic histidine and the tetrahedral intermediate collapses, which results in the amine product and a covalent acyl-enzyme intermediate. Histidine deprotonates a water molecule, which attacks the acyl-enzyme intermediate, forming another tetrahedral oxyanion intermediate. This intermediate collapses to release the carboxylic acid product (Frey, 2007).

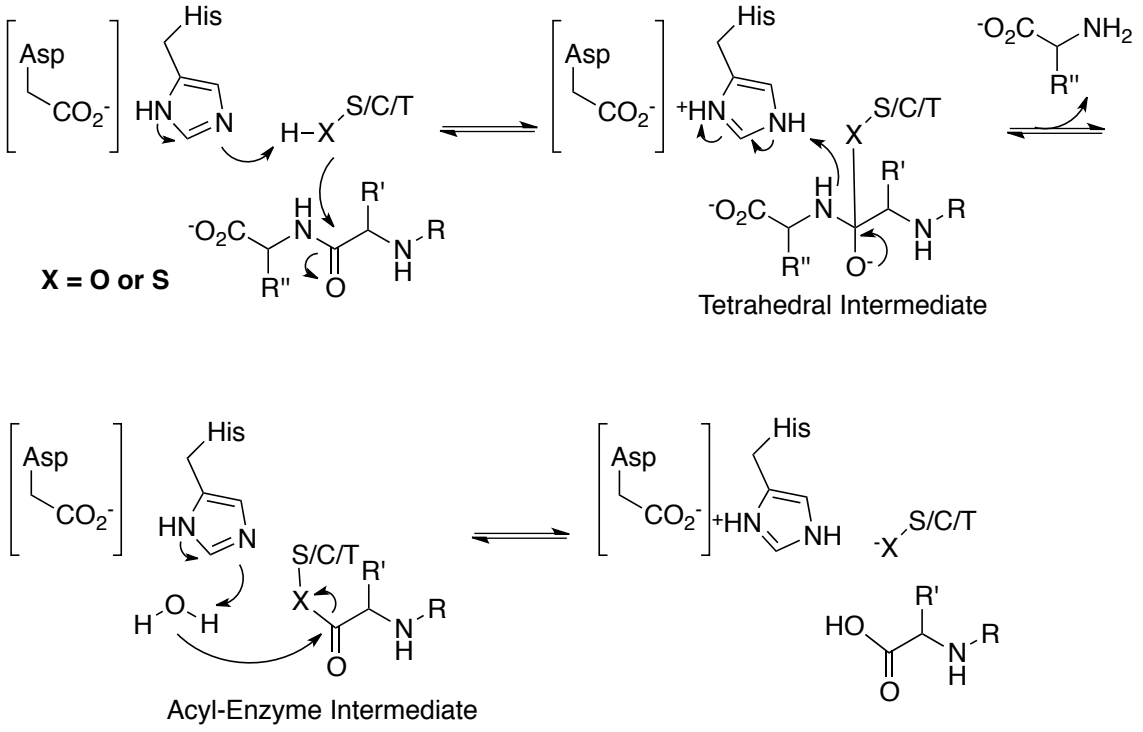

Figure 1.18 Reaction mechanism of proteases that utilize nucleophilic catalysis.

In aspartic and metalloproteases the nucleophile is an activated water molecule that is generated by an acid/base reaction between itself and either an aspartic acid (aspartic protease) or an active site metal ion (metalloprotease) (Turk, 2006). Metalloproteases are the largest family of proteolytic enzymes. The metal ion in the

active site (usually a zinc cation) coordinates to a water molecule, reducing the pKa from 15.5 to 9.6. Abstraction of a water molecule proton by a weak base in the active site generates a hydroxide ion that attacks the amide bond of the peptide chain (Figure 1.19). The resulting oxyanion tetrahedral intermediate is stabilized through interactions with the metal ion. The tetrahedral intermediate collapses and the hydrolysis products are released (Frey, 2007).

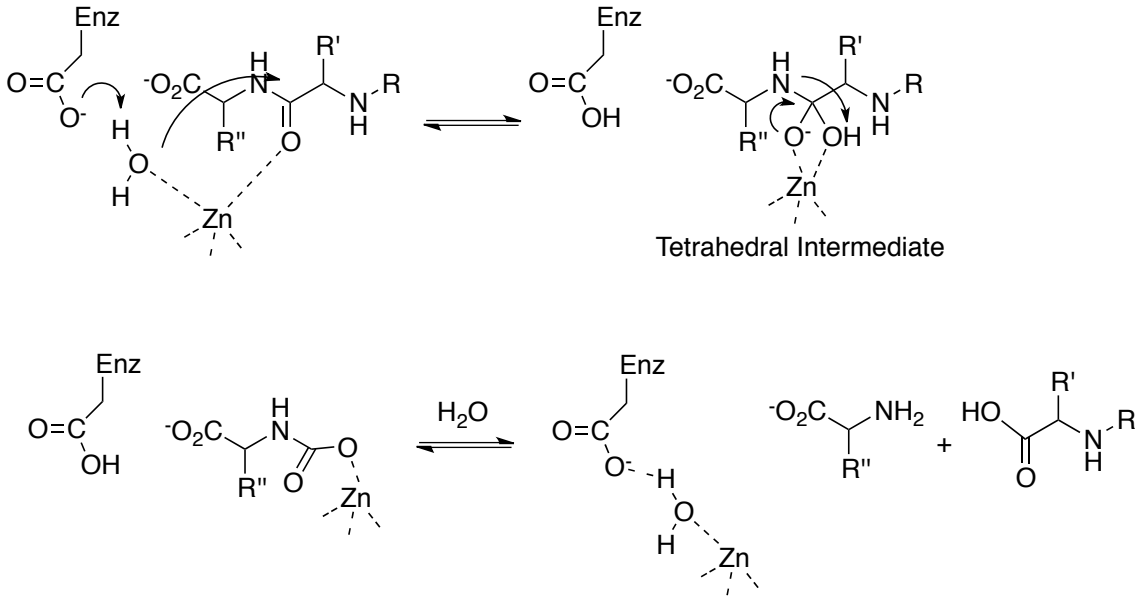

Figure 1.19 Reaction mechanism of metalloproteases.

Because TCP has not been purified to homogeneity little is known about its structure or reaction mechanism. Carboxypeptidase A (CPA) is a pancreatic zinc-metalloprotease with a high selectivity for hydrophobic C-terminal amino acids, in particular those with aromatic side chains. Because α-tubulin is also a substrate for CPA, comparisons between CPA and TCP have been used to infer details about TCP. The presence of EDTA (5 mM) strongly inhibits CPA activity, but one report suggests that it increases the activity of TCP (Argaraña, 1980). This result would imply that TCP is not a

metalloprotease, but it is also possible that the metal cofactor could be buried in the active site and unaffected by the presence of EDTA. Often, metalloprotease activity is lost after dialysis, but is regenerated by the addition of metal ions. TCP activity is unaffected after dialysis and is inhibited by the addition of zinc and copper ions (Webster, 1996).

It has been suggested that TCP belongs to a family of cytosolic carboxypeptidases (CCPs). CCP enzymes are metalloproteases that modify cytosolic proteins, including tubulin. The deglutamylase enzymes involved in the polyglutamylation post-translational modification also belong to this family. Analysis of α-tubulin in mice lacking the gene for the CCP Nna1 revealed a lack of Glu-tubulin suggesting that this enzyme in the metalloprotease family may be TCP (Kalinina, 2007).

1.6 Mechanism-Based Inhibitors

An effective approach to the synthesis of selective, potent enzyme inhibitors has been to design mechanism-based, or transition state analogue inhibitors. These inhibitors are stable compounds that mimic the structural and electronic features of the intermediate or transition state formed during the enzymatic reaction. As enzymes must bind tightly to these high-energy structures, they will also bind tightly to close analogues. For enzymatic reactions that involve a nucleophilic substitution on a carbonyl carbon, phosphorus- and sulfur-containing peptide analogues are commonly used as the structural unit to mimic the negatively charged tetrahedral intermediate or the transition state leading to it. Phosphorus derivatives posses a stable tetrahedral geometry in combination with carbon, nitrogen or oxygen (Figure 1.20). The substituents have reasonable hydrolytic stability in water, and the bonds to phosphorus are only 10-15% longer than

the bonds to carbon, so the inhibitors are not significantly bulkier than the actual intermediate (Bartlett, 1978). These compounds are acidic and will bear a negative charge at physiological pH. This charge mimics the oxyanion formed during catalysis. Glutamine synthetase, D-alanine:D-alanine ligase, MurE and MurD will be examined in the following sections as examples of ATP-dependent ligases that were inhibited by a phosphorus-containing mechanism-based inhibitor.

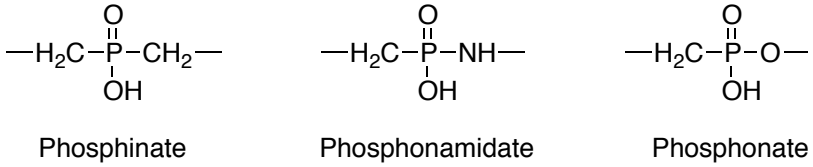

Figure 1.20 Phosphorus based transition state analogue inhibitors.

1.6.1 Inhibition Studies of Glutamine Synthetase

Glutamine synthetase catalyzes the ATP-dependent synthesis of glutamine from glutamic acid and ammonia (Figure 1.21). It is an important enzyme in nitrogen assimilation, photorespiration, and maintaining carbon balance in plants. The mechanism of glutamine synthetase proceeds by the initial formation of a γ-glutamyl phosphate intermediate. Proceeding though a tetrahedral intermediate, phosphate is displaced by ammonia to give inorganic phosphate and glutamine (Meek, 1980).

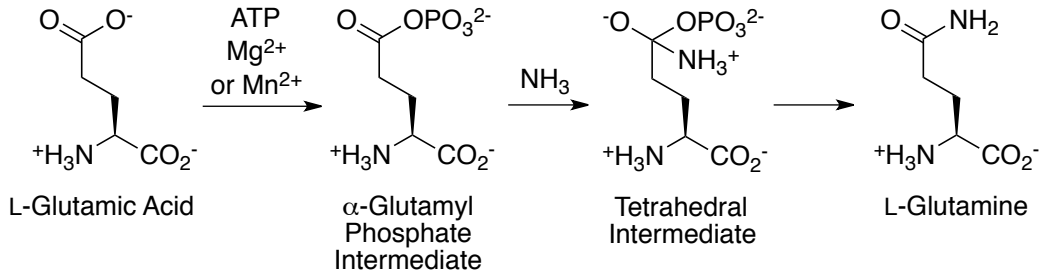

Figure 1.21 Reaction mechanism of glutamine synthetase.

Methionine sulfoxide (Elliot, 1948) and L-methionine sulfoximine (Pace, 1952) were the first competitive inhibitors reported to inhibit the synthesis of glutamine from glutamic acid (Figure 1.22).

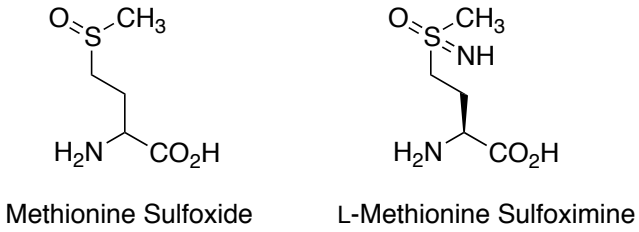

Figure 1.22 Chemical structures of methionine sulfoxide and methionine sulfoximine.

L-Methionine sulfoximine, a tight-binding irreversible inhibitor, mimics the transition state in the glutamine synthetase reaction. It binds to the enzyme by occupying both the glutamic acid and ammonia binding sites (Ronzio, 1968). A ^{14}C-methyl-methionine sulfoximine and ^{32}P-(β,γ)-ATP were used to show that in the presence of glutamine synthetase, Mg^{2+}, and ATP, L-methionine sulfoximine is phosphorylated (Figure 1.23). This derivative forms the tight-binding irreversible inhibitor. This derivative can be released from the enzyme and isolated by heating or by treatment with perchloric acid, indicating that it is not covalently bound (Ronzio, 1969).

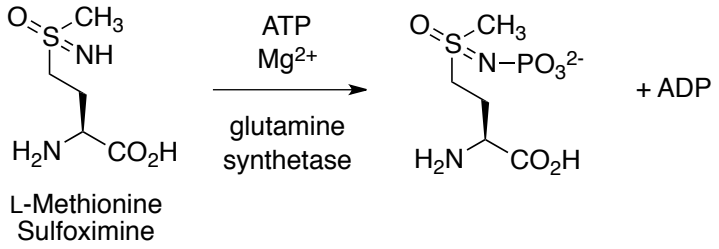

Figure 1.23 Phosphorylation methionine sulfoximine.

DL-Phosphinothricin, or glufosinate, is also another potent competitive inhibitor (Figure 1.24). It is derived from the tripeptide bialophos, which is produced by

Streptomyces viridochromogenes and *Streptomyces hygroscopicus*. Biolophos is metabolized to phosphinothricin in plants and microorganisms. DL-Phosphinothricin competitively inhibits glutamine synthetase, with respect to glutamate, in pea leaf with a K_i of 0.073 nM (Leason, 1982).

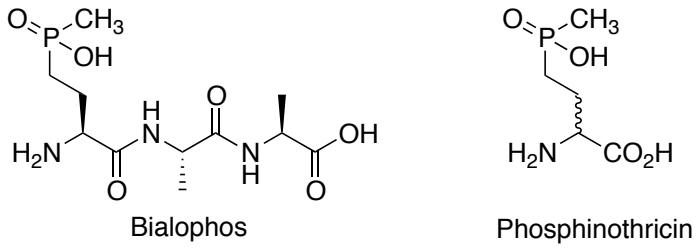

Figure 1.24 Chemical structures of bialophos and DL-phosphinothricin.

DL-Phosphinothricin inactivates glutamine synthetase by a mechanism similar to L-methionine sulfoximine; the tetrahedral phosphorus atom at the γ position mimics the transition state in the glutamine synthetase reaction and binds tightly to the enzyme. It was inferred that phosphinothricin was also phosphorylated, because in the absence of glutamic acid and when enzyme was pre-incubated with a low concentrations of ATP, it became an irreversible inhibitor (Colanduoni, 1986). First attempts at isolating the phosphorylated inhibitor under acidic conditions were unsuccessful, but switching to a base allowed for the isolation and characterization of the phosphorylated DL-phosphinothricin (Abell, 1991).

1.6.2 Inhibition Studies of D-Alanine:D-Alanine Ligase

As discussed previously, D-alanine:D-alanine ligase is an ATP-grasp enzyme that catalyzes the ATP-dependent ligation of two alanine residues. The products of the reaction are ADP, inorganic phosphate, and D-alanine:D-alanine (Figure 1.25).

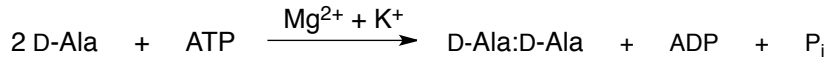

Figure 1.25 Reaction catalyzed by D-alanine:D-alanine ligase.

D-Alanine:D-alanine ligase has two binding sites for D-alanine. The binding site for the N-terminal alanine is highly specific for D-alanine, while the binding site for the C-terminal alanine accepts a variety of D-amino acids. Therefore, the enzyme is able to synthesize a variety of mixed dipeptides such as D-alanine:D-serine (Parsons, 1988). The D-alanine:D-alanine dipeptide is added to a uridine-5′-diphosphate-*N*-acetylmuramyl tripeptide, which is a constituent of the bacteria cell wall peptidoglycan layer. Because the failure to assemble and incorporate D-alanine:D-alanine into the peptidoglycan layer results in bacterial lysis, this enzyme has been a popular target for antibiotic development (Healy, 2000).

A successful approach to inhibiting D-alanine:D-alanine ligase was to design a mechanism-based inhibitor that used phosphorus to mimic the tetrahedral intermediate formed in the ligase reaction pathway (Figure 1.26).

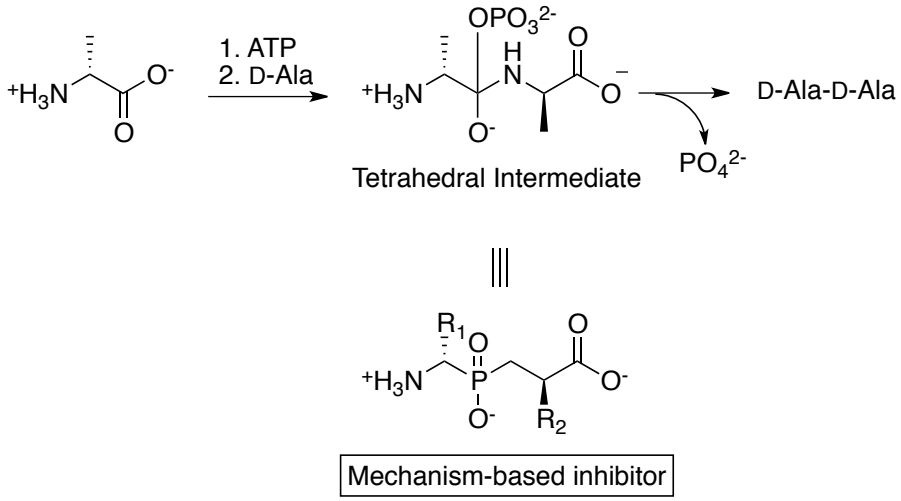

Figure 1.26 Rationale behind mechanism-based inhibitor design.

A series of phosphinic acid dipeptide analogues were synthesized and tested for D-alanine:D-alanine ligase inhibition and antibacterial activity. Enzyme inhibition data showed that R_1 (Figure 1.26) is optimally a methyl group with a D configuration and that R_2 (Figure 1.26) is optimally a larger group (*n*-heptyl or methylthio) with a D configuration (Parsons, 1988). The analogue R_1 = methyl and R_2 = heptyl was shown to be a high affinity, time-depended inhibitor of *Salmonella* D-alanine:D-alanine ligase with a K_i of 1.2 μM. This tight-binding inhibition requires the presence of ATP (Duncan, 1988). Based on analogy with glutamine synthetase, this result implied that the inhibitor is being phosphorylated. Despite the potent inhibition, the phosphinic acid dipeptide analogues exhibited poor to moderate antibacterial activity. The suspected reason for this was poor transport of the analogue into the bacteria (Parsons, 1988).

Solid-state ^{31}P NMR techniques were used to confirm phosphorylation of the phosphinic acid analogue inhibitor (R_1 = methyl and R_2 = heptyl) (Figure 1.27). ADP (-8 and -14 ppm), the phosphinic acid inhibitor (53 ppm) and the phosphorylated inhibitor (-3 ppm) all exhibited diagnostic isotropic chemical shifts and shift anisotropies

(McDermott, 1990). A K_i of 33 nM was measured for the phosphorylated inhibitor (Shi, 1995).

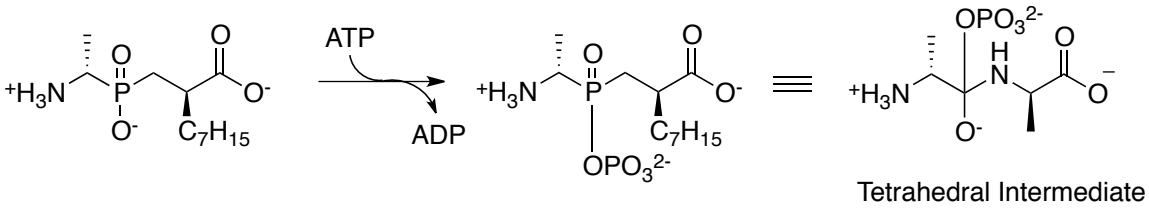

Figure 1.27 Phosphorylation of D-alanine:D-alanine ligase inhibitor.

D-Alanine:D-alanine ligase from *E. coli* was co-crystalized with an S,R-methylphosphinic acid (R_1 = methyl and R_2 = methyl, Figure 1.26) and ATP (Figure 1.28) (Fan, 1994).

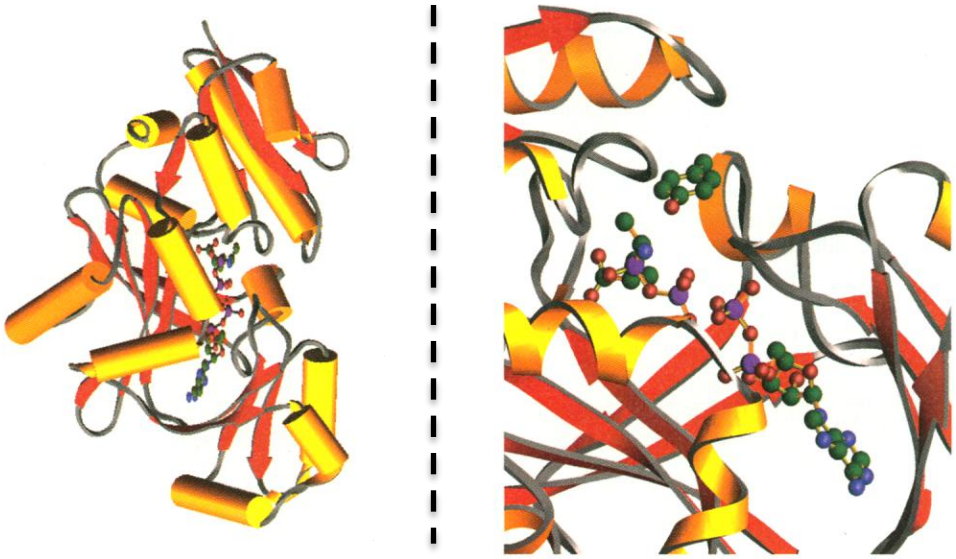

Figure 1.28 Crystal structure of D-alanine:D-alanine ligase with ADP and the phosphinophosphate transition state analogue (Fan, 1994).

Based on x-ray crystal structure analysis, D-alanine:D-alanine ligase consists of an N-terminal, central and C-terminal domain. ATP is grasped between the central and C-terminal domain. A catalytic triad of tyrosine, serine and glutamic acid assists in binding and deprotonation steps in the enzymatic reaction (Figure 1.29). The phosphinic acid

inhibitor is observed, bound to the active site, as a phosphorylated phosphinate. The observation of the phosphorylated inhibitor is consistent with a mechanism in which phosphorylation of the first D-alanine by ATP forms the activated acylphosphate. Attack from the amine on the second D-alanine results in a tetrahedral intermediate. This collapses, resulting in the D-alanine: D-alanine dipeptide (Fan, 1994).

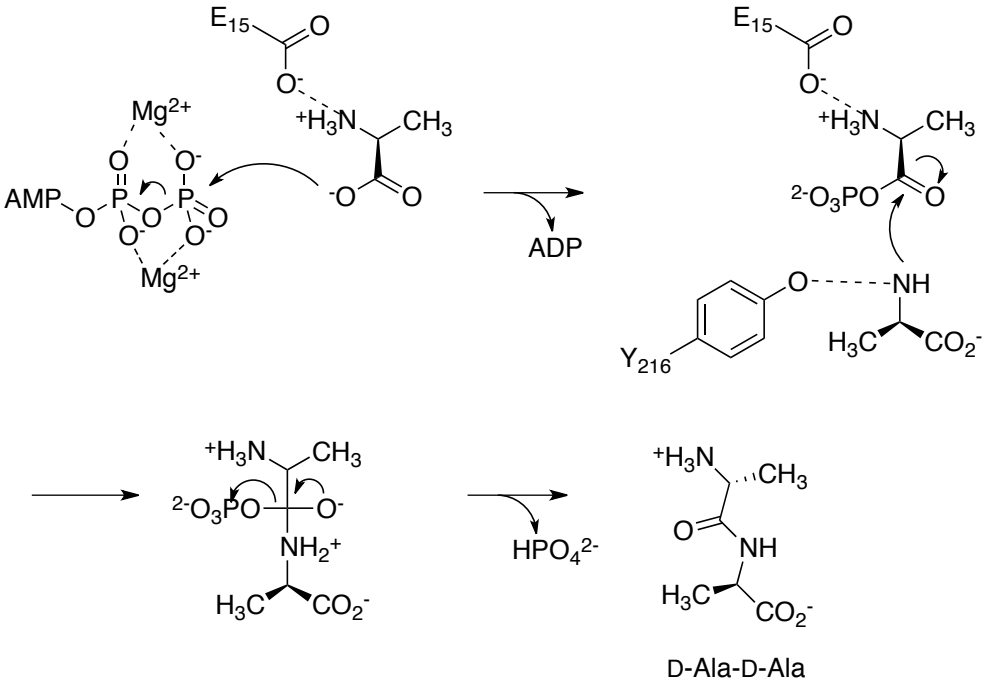

Figure 1.29 Mechanism of D-alanine:D-alanine ligase (Fan, 1994).

1.6.3 Inhibition Studies of MurD and MurE

MurD and MurE are two enzymes involved in the biosynthesis of the UDP-*N*-acetylmuramic acid (UDP-MurNAc) pentapeptide (Figure 1.30). UDP-MurNAc pentapeptide is a precursor in the biosynthesis of peptidoglycan, which is a component of the bacterial cell wall. The biosynthesis of UDP-MurNAc pentapeptide involves the sequential ATP-dependent addition of L-Ala, D-Glu, *meso*-Dap and D-Ala-D-Ala to UDP-MurNAc. The enzymes MurC, MurD, MurE and MurF respectively catalyze these

addition reactions (Götz, 2006). Similar to the D-alanine:D-alanine ligase discussed previously, the enzymes involved in the biosynthesis of UDP-MurNAc pentapeptide are attractive targets for the design of antibiotics.

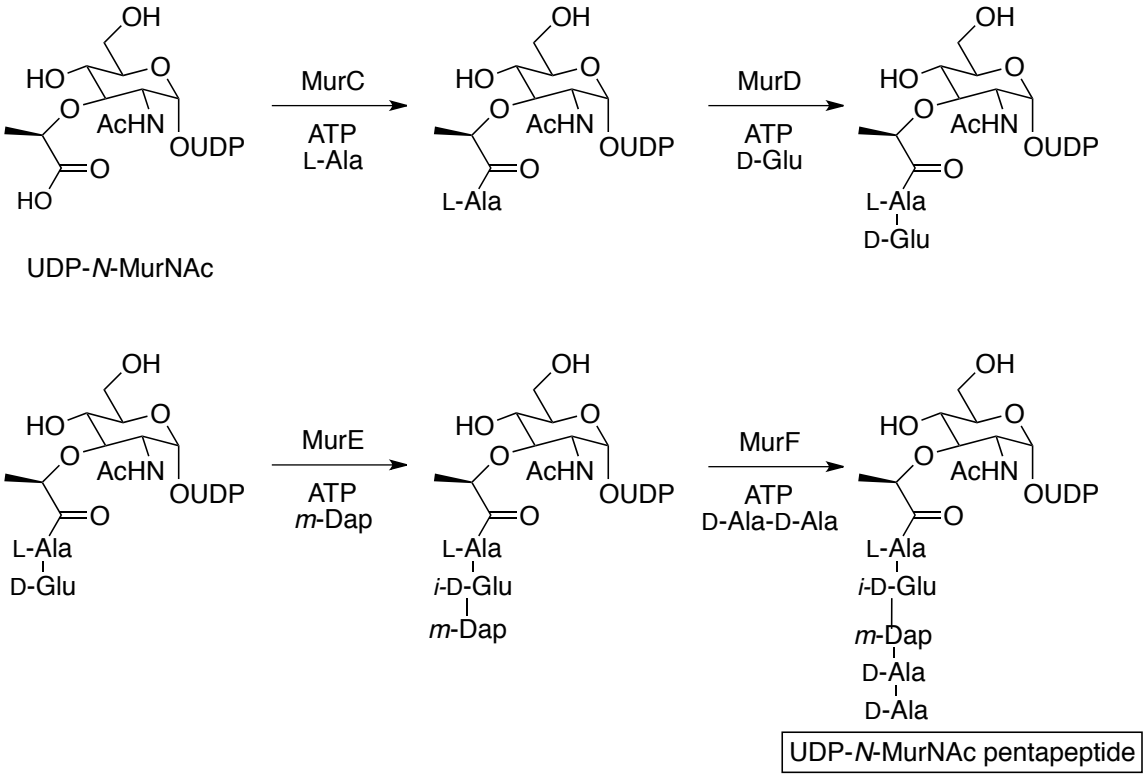

Figure 1.30 Biosynthesis of the UDP-*N*-MurNAc pentapeptide (Götz, 2006).

The reaction mechanisms employed by MurC, MurD, MurE and MurF are similar to those of other ATP-dependent ligases, such as D-alanine: D-alanine ligase. A phosphinic acid mechanism-based inhibitor was extremely effective at inhibiting D-alanine: D-alanine ligase, so a similar design was employed for MurD and MurE.

In the MurD catalyzed reaction, a tetrahedral intermediate is formed when the amine of D-glutamic acid attacks the phosphorylated carboxy of L-alanine (Figure 1.31). A phosphinic acid-containing analogue of this tetrahedral intermediate was found be a good inhibitor of MurD with an IC_{50} value of 0.68 μM (Tanner, 1996). When the

inhibitor was pre-incubated with inhibitor and ATP irreversible inhibition was not observed. This indicates that the phosphinic acid is not phosphorylated in the active site. The inhibitor was designed to include the charged UDP moiety, but replace the muramoyl residue with an aliphatic linker. The hydrocarbon chain mimicked the length of the muramoyl residue, while simplifying the synthesis.

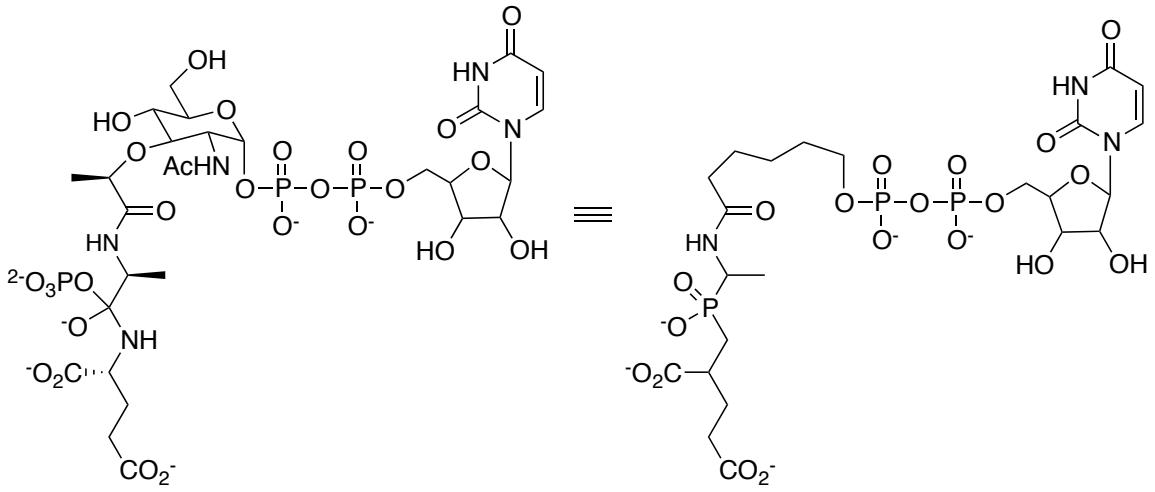

Figure 1.31 Phosphinic acid-based MurD inhibitor (Tanner, 1996).

In an effort to prepare a more potent MurD inhibitor, the stereochemistry of the α-amino phosphinate was resolved and the complete muramic acid moiety was included (Figure 1.32). A significant increase in potency was achieved; an IC_{50} value of less than 1 nM was measured (Gegnas, 1998).

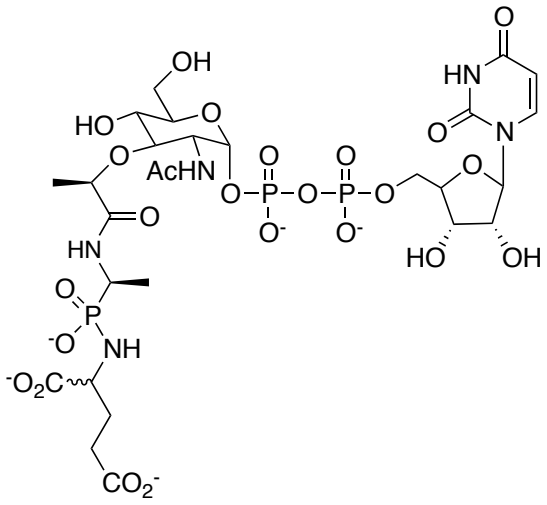

Figure 1.32 Structure of improved MurD inhibitor (Gegnas, 1998).

Similarly in the MurE catalyzed reaction, a tetrahedral intermediate is formed when the amine of *meso*-diaminopimelic acid attacks the phosphorylated γ-carboxylate of D-glutamic acid (Figure 1.33). A phosphinic acid containing analogue of this transition state was found be a good inhibitor of MurE with an IC_{50} value of 1.1 μM (Zeng, 1998).

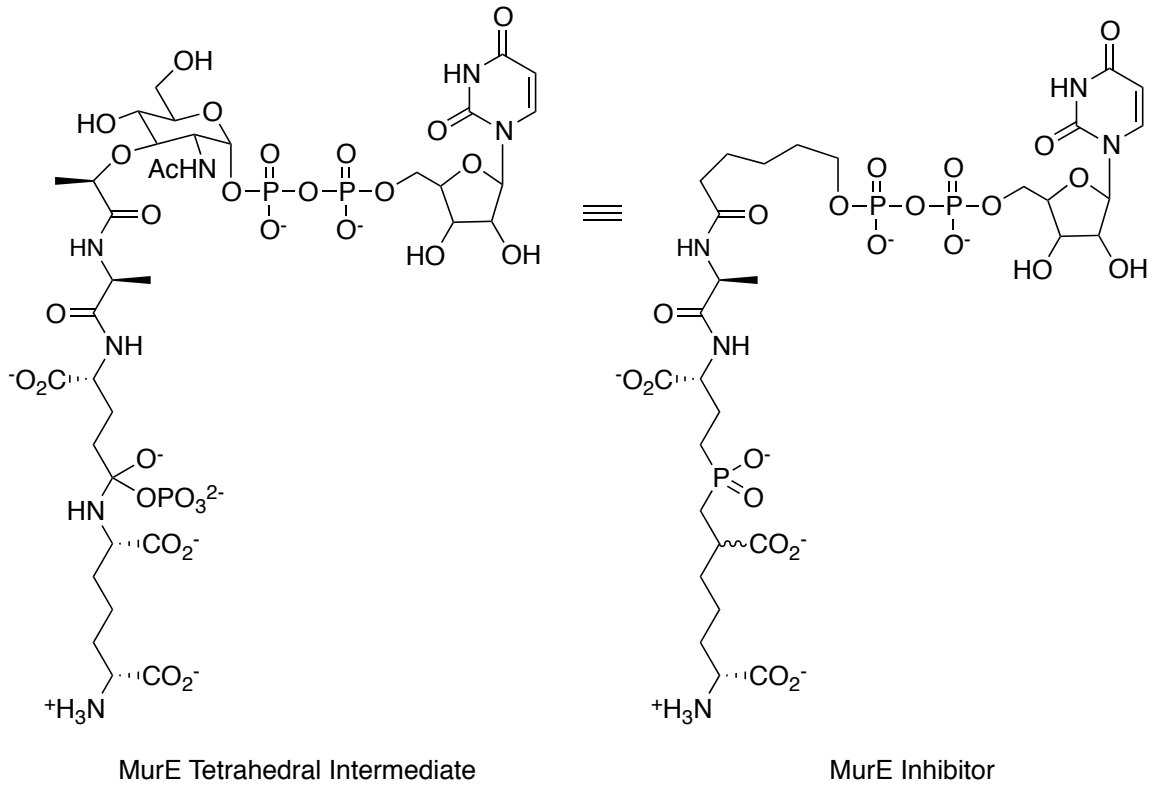

Figure 1.33 Phosphinic acid-based MurE inhibitor (Zeng, 1998).

1.7 Project Goals

This research project represents the first steps towards the development of inhibitors that target tubulin post-translation modifying enzymes. TTL was chosen as the first target as it is the best characterized of these enzymes from both a structural and functional point of view. The same inhibitors that were designed to target TTL could also target TCP thereby shutting down the detyrosination/tyrosination cycle completely. As discussed previously, TTL activity is suppressed during cancer progression and is associated with more aggressive tumors. A TTL inhibitor could function as a chemical biology tool that could be used to further study the physiological effects of TTL suppression in cancer cells. The crystal structure of TTL has been determined but

without a bound peptide. A crystal structure of TTL with a tight binding inhibitor would be useful in determining mechanistic details of the enzyme.

Previous research has shown a group of sesterterpenes, isolated from *Salvia dominica,* interacts and inhibits TTL in cancer cells (Dal Piaz, 2009). MCF-7 breast cancer cell lysate was screened for potential interactions with the isolated sesterterpenes using compound-immobilized affinity chromatography. Sensitive and high-throughput mass spectrometry analysis identified TTL as one of the proteins that interact with the sesterterpenes. Surface Plasmon resonance was used to investigate the interactions and measure the kinetic parameter K_D between TTL and the isolated sesterterpenes. The sesterterpene with the best K_D (K_D = 7 nM) is shown in Figure 1.34.

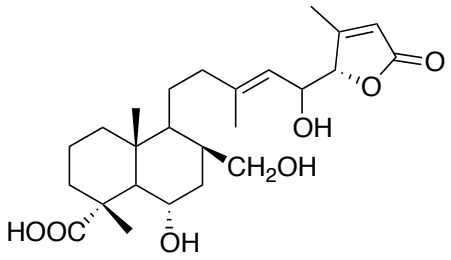

Figure 1.34 Chemical structure of the most interactive sesterterpene.

MCF-7 cells were incubated with the most interactive sesterterpene for 24 and 48 hours, followed by western blot analysis of Δ2-tubulin levels. Increased levels of Δ2-tubulin, characterized by a multiband signal given by Δ2-antibody in the western blot, were observed in cell extracts incubated with the sesterterpene. This result indicates that the sesterterpene is able to penetrate the cell membrane and act as a TTL inhibitor in cancer cells.

In order to probe the inhibition of TTL further, the design, synthesis and testing of phosphorus-based transition state analogue inhibitors will be undertaken (Figure 1.35).

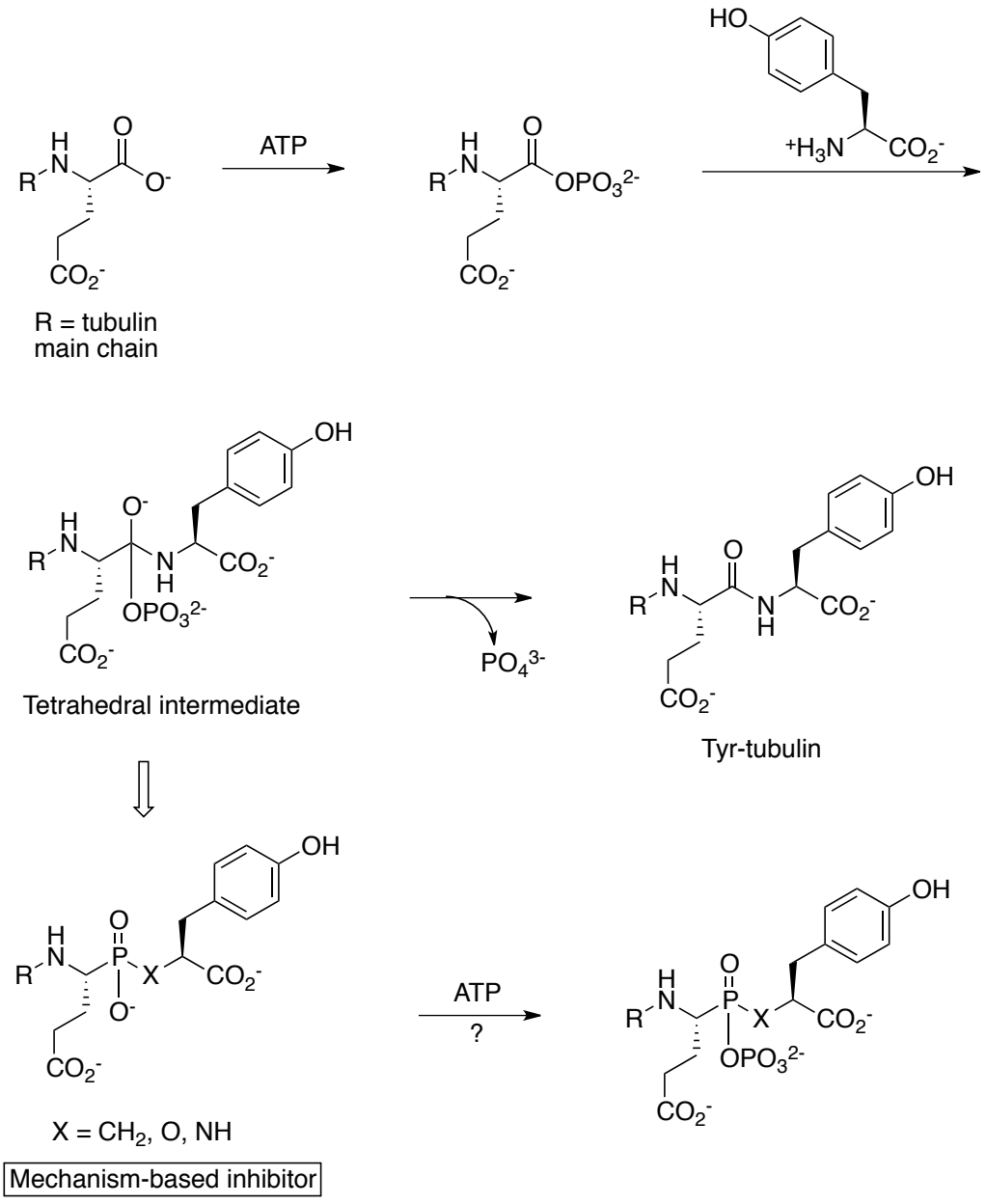

Figure 1.35 Design of mechanism-based inhibitor for TTL.

Because TTL and TCP share a similar reaction transition state (Figure 1.36), the synthesized inhibitors could also be used to study the inhibition of TCP.

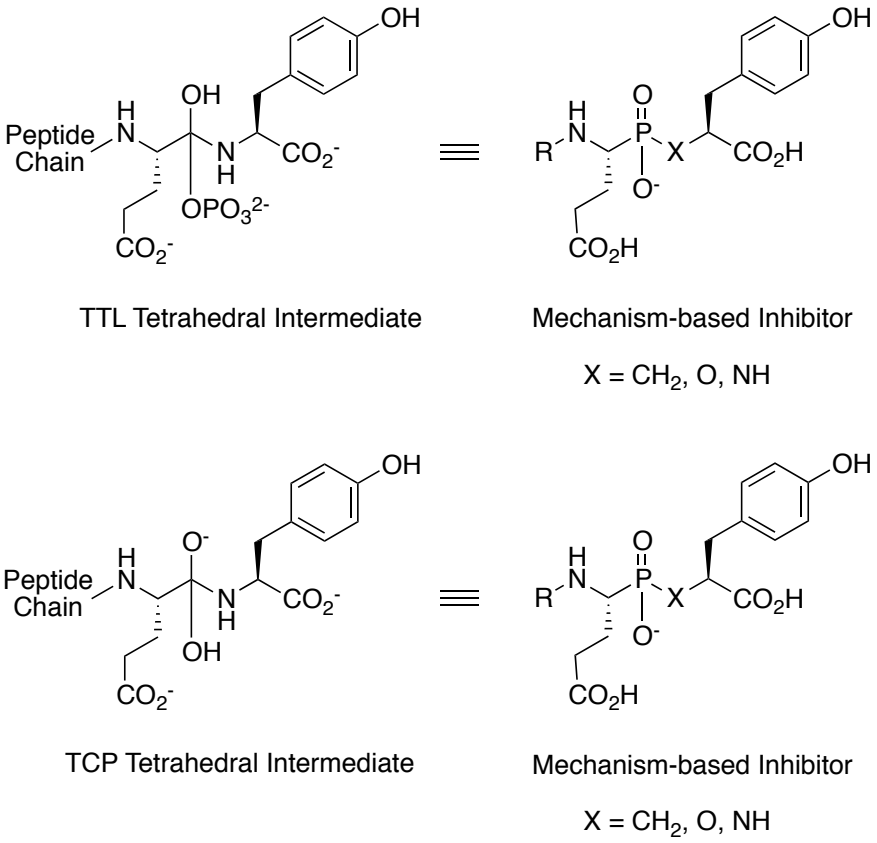

Figure 1.36 Similarities between TTL and TCP tetrahedral intermediate.

Chapter 2 details research performed on the design and synthesis of a phosphinic acid containing dimer pseudopeptide inhibitor (inhibitor **1**) and the design, synthesis and inhibition of a phosphonic acid containing dimer pseudopeptide inhibitor (inhibitor **2**) (Figure 1.37).

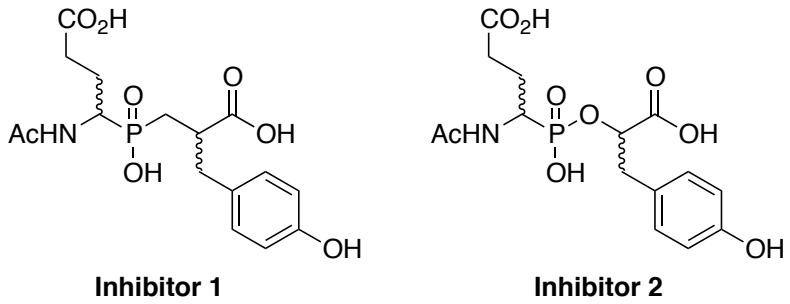

Figure 1.37 Chemical structures of Inhibitors 1 and 2.

Chapter 3 details the research performed on the design and synthesis of a phosphonic acid containing trimer pseudopeptide inhibitor (inhibitor **3**) and the design, synthesis and inhibition of a phosphonic acid containing pentamer pseudopeptide inhibitor (inhibitor **4**) (Figure 1.38).

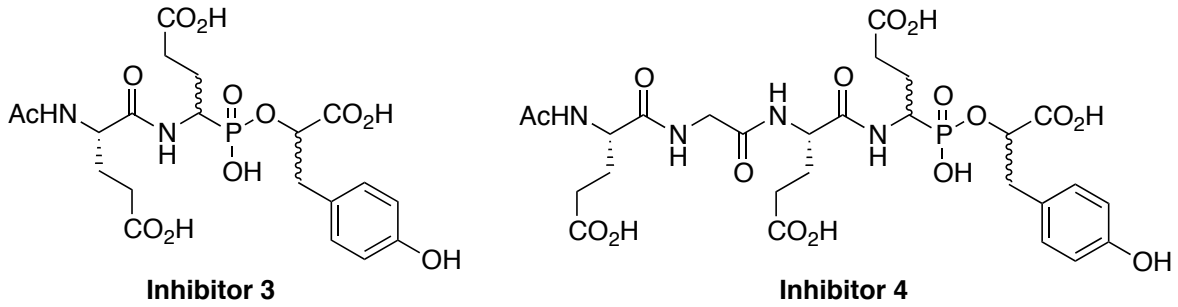

Figure 1.38 Chemical structures of Inhibitors 3 and 4.

All inhibition studies with TTL were completed by our collaborators in the Roll-Mecak lab at the Cell Biology and Biophysics Unit, National Institute of Neurological Disorders in Maryland, USA.

Chapter 2: Design and Synthesis of a Phosphinic and a Phosphonic Acid Dipeptide Inhibitor for the Inhibition of TTL

This chapter details the design and synthesis of inhibitors **1** and **2** for the inhibition of TTL. Previous research done on phosphorus-carbon bond formation and H-phosphinic acid synthesis are examined and applied towards the synthetic design of inhibitor **1**. Research completed towards the synthesis of inhibitor **1** is then reported. Due to complications in this synthesis, the focus of the research project changed to the synthesis of a phosphonic acid containing inhibitor, inhibitor **2**. General phosphonic acid synthetic strategies are discussed, followed by the completed synthesis of inhibitor **2**. Finally, inhibition studies of TTL with inhibitor **2** are presented.

2.1 Strategies for Inhibitor 1 Synthesis

The idea to synthesize a phosphinic acid containing inhibitor to study TTL inhibition came from work previously done in the Tanner research group on the inhibition of MurD and MurE (see Chapter 1). In the proposed reaction mechanism of TTL, a tetrahedral intermediate is formed when the amine of tyrosine attacks the phosphorylated glutamic acid of Glu-tubulin (Figure 2.1). Like the MurD and MurE inhibitors, inhibitor **1** was designed to mimic the tetrahedral intermediate formed in TTL-catalyzed reaction with a phosphinic acid. Inhibitor **1** is a glutamic acid-tyrosine dipeptide analogue, where the amide bond linkage is replaced with a methylenephosphinic acid and the N-terminus is capped with an acetyl group to mimic the continuation of the peptide chain.

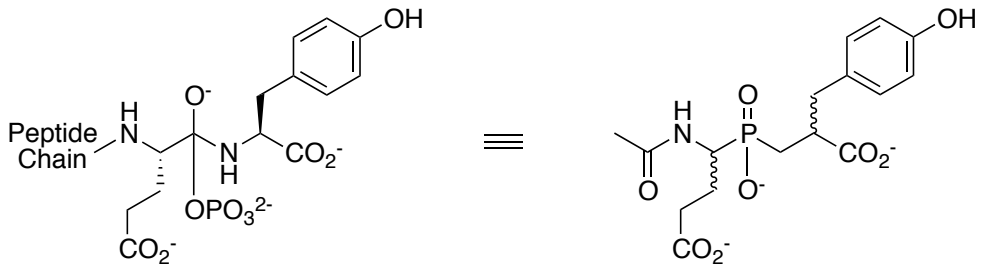

TTL Tetrahedral Intermediate

Inhibitor **1**

Figure 2.1 Phosphinic acid-based TTL inhibitor.

2.1.1 Methods in Phosphorus-Carbon Bond Formation

When designing the synthesis of inhibitor **1**, the most obvious disconnection for a convergent synthesis was the phosphorus-carbon (P-C) bond between the glutamic acid and tyrosine analogues. Various approaches exist for the preparation of α-aminophosphinic acid derivatives including radical-based coupling, alkylation, and conjugate addition.

A radical-based approach to the preparation of phosphinic acid derivatives involves the addition of an H-phosphinate across an olefin bond at high temperature and pressure. Using this method for the synthesis of the P-C bond in inhibitor **1** would involve generating a phosphorus-based radical with peroxyester or AIBN, and then reacting it with a protected 2-(4-hydroxybenzyl) acrylate at high temperature (Figure 2.2).

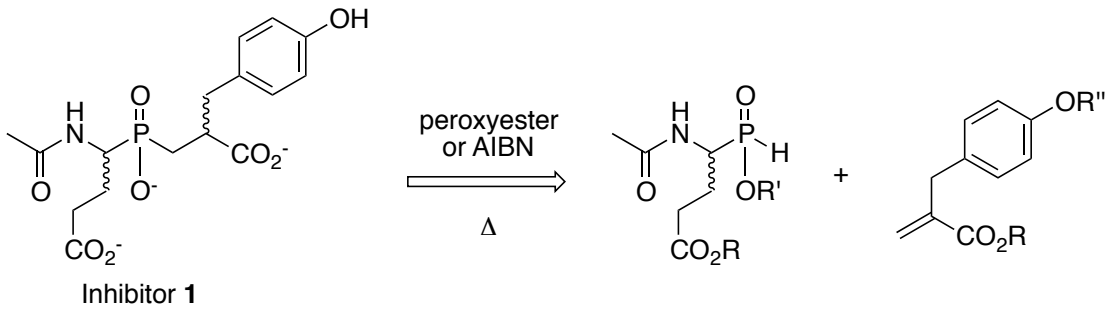

Inhibitor **1**

Figure 2.2 Application of a radical-based approach in the synthesis of inhibitor 1.

The radical-based methodology was successfully used to synthesize L-phosphinothricin (Zeiss, 1992). A temperature of 120 °C and *tert*-butyl peroxy-2-ethylhexanoate were used to generate an ethyl methylphosphinate radical, which was added to a L-vinylglycine derivative (Figure 2.3).

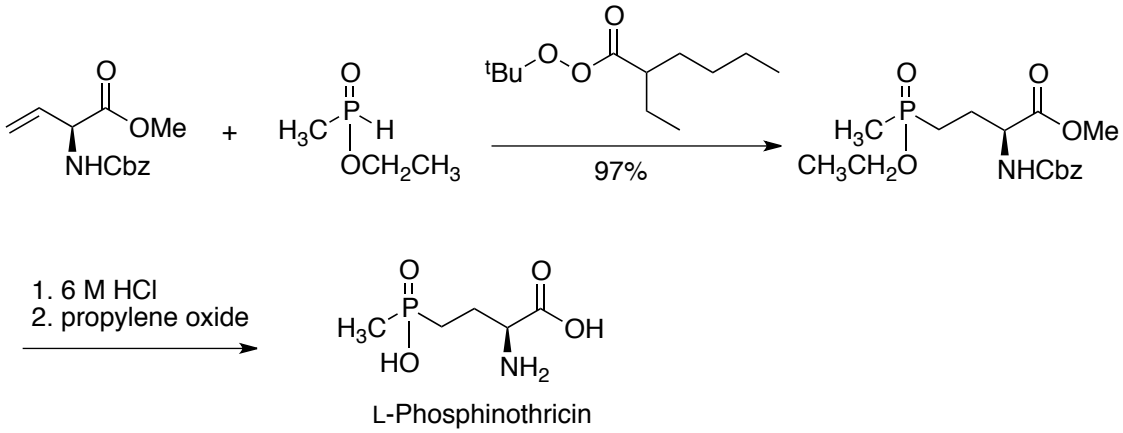

L-Phosphinothricin

Figure 2.3 Radical-based synthesis of L-phosphinothricin (Zeiss, 1992).

The radical-based approach was attempted in the synthesis of a phosphinic acid pseudopeptide inhibitor for folylpoly-γ-glutamyl synthetase (FPGS). However, this approach was unsuccessful due to the instability of the carboalkoxy-substituted phosphinic acid esters at high temperature and pressure (Figure 2.4) (Valiaeva, 2001).

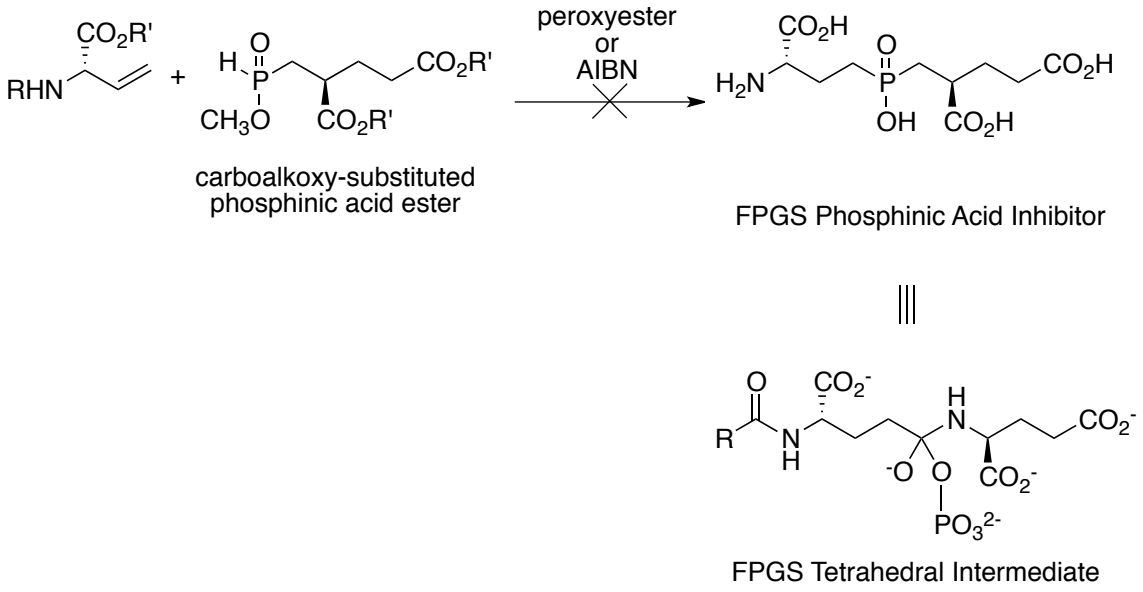

Figure 2.4 Attempted application of a radical-based approach in the synthesis of an FPGS inhibitor (Valiaeva, 2001).

As with the FPGS inhibitor, an H-phosphinic acid analogue of glutamic acid will be utilized in the synthesis of inhibitor **1**. Because carboalkoxy substituted phosphonates are not stable at elevated temperatures, using the radical-based approach in the synthesis of inhibitor **1** is impractical.

The alkylation and conjugate addition methods of phosphinic acid synthesis involve the *in situ* generation of a nucleophilic trivalent phosphorus ester followed by reaction with an electrophile: an alkyl halide or Michael acceptor (Figure 2.25). The nucleophilic phosphorus (III) species is generated from the phosphorus (V) tautomer either by a silylating agent or a strong base. In the synthesis of inhibitor **1**, alkylation or conjugate addition methods would involve the activation of an H-phosphinate glutamic acid analogue by a silylating agent or strong base, followed by reaction with either a protected halogen-substituted tyrosine analogue or a protected 2-(4-hydroxybenzyl) acrylate, respectively.

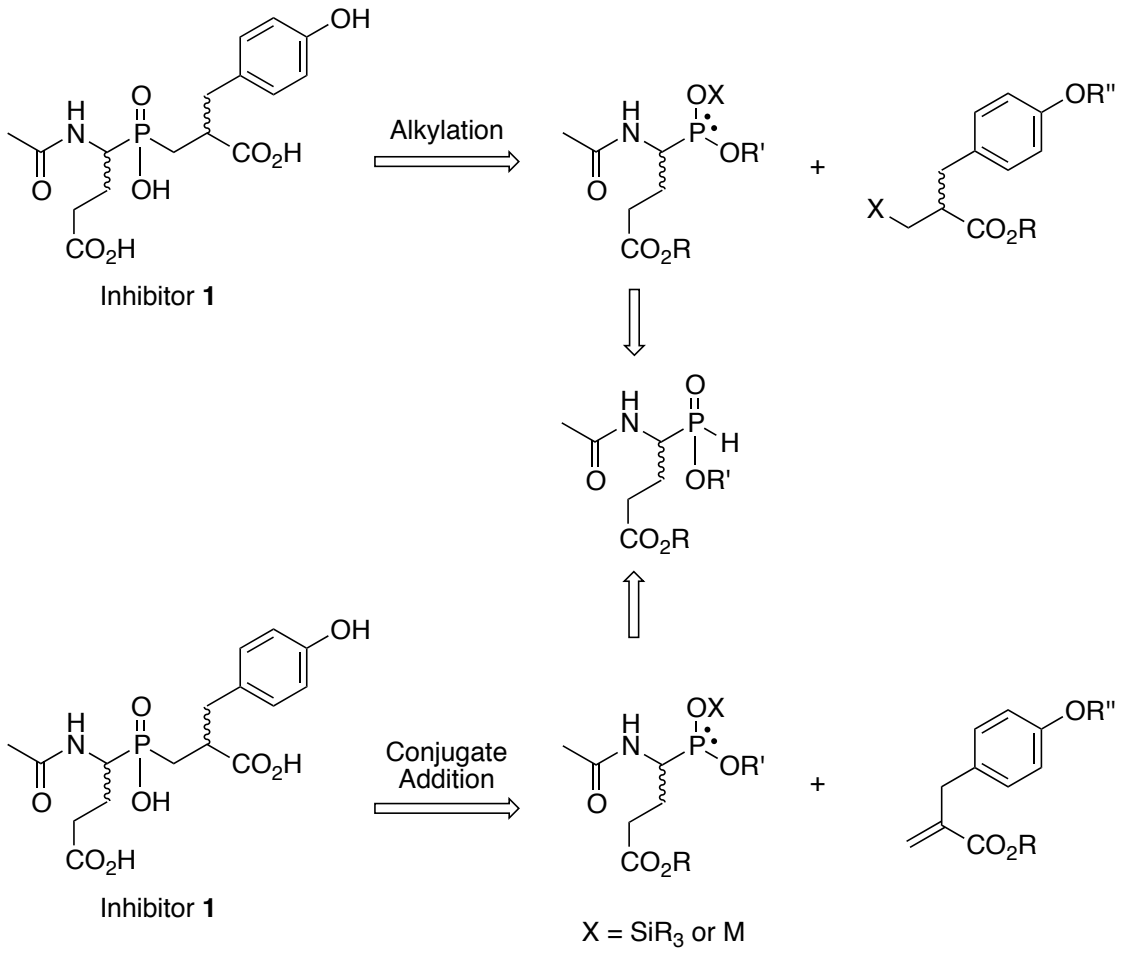

Figure 2.5 Application of alkylation or conjugate addition in the synthesis of inhibitor 1.

The most investigated and widely employed phosphorus alkylation reaction is the Michaelis-Arbuzov rearrangement, or simply the Arbuzov rearrangement. Discovered in 1898 by Michaelis (Michaelis, 1898) and further explored by Arbuzov, the arrangement involves the reaction of a trivalent phosphorus ester with an alkyl halide. It has been used in the synthesis of phosphonates, phosphinates and phosphine oxides (Figure 2.6).

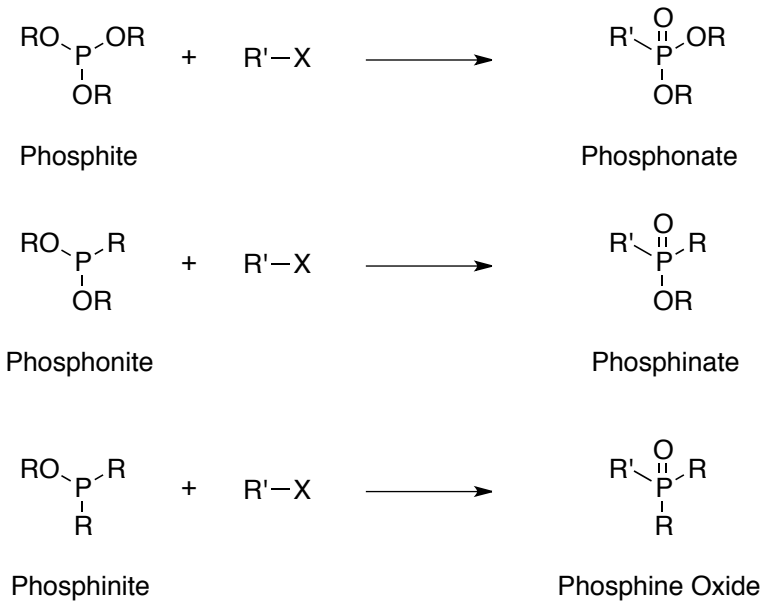

Figure 2.6 Organophosphorus compounds synthesized via the Arbuzov rearrangement.

The classical Arbuzov rearrangement can require high temperatures (120-160 °C), neat reaction mixtures and reaction times of several hours. This can lead to decomposition of phosphonites and isomerization of phosphinites to undesired phosphine oxides (Bhattacharya, 1981). A milder version of the Arbuzov rearrangment was developed for the synthesis of phosphinates from H-phosphinic acids, termed an Arbuzov-like rearrangement (Thottathil, 1984a). In the modified reaction, either an H-phosphinic acid or an H-phosphinate was activated with trimethylsilyl chloride (TMSCl) followed by alkylation with a highly reactive alkyl halide (Figure 2.7).

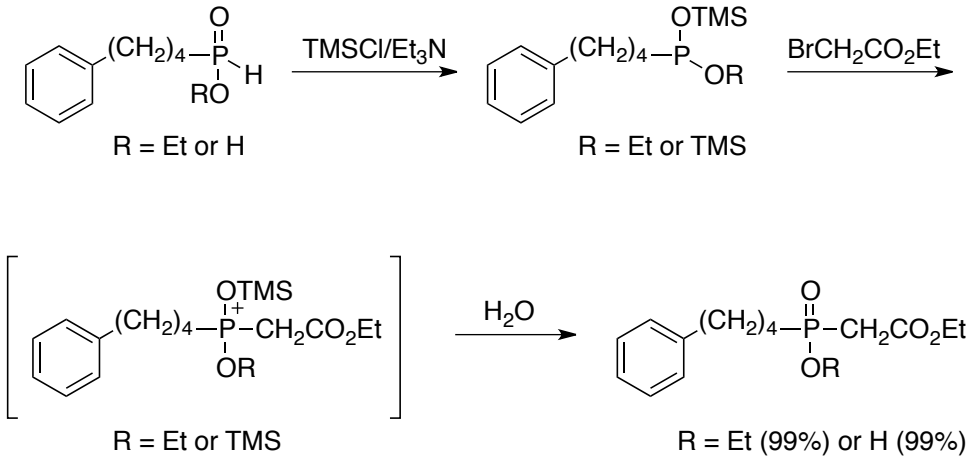

Figure 2.7 Arbuzov-like rearrangements of H-phosphinate and H-phosphinic acids (Thottathil, 1984a).

The method of Arubzov-like alkylation of H-phosphinates was applied to the synthesis of a FPGS inhibitor. Initially, TMSCl was used to silylate an alkyl H-phosphinate, followed by reaction with an alkyl halide. However, due to low yields, N,O-bis(trimethylsilyl)acetamide (BSA) was used instead of TMSCl to silylate the H-phosphinic acid (Figure 2.8) (Valiaeva, 2001).

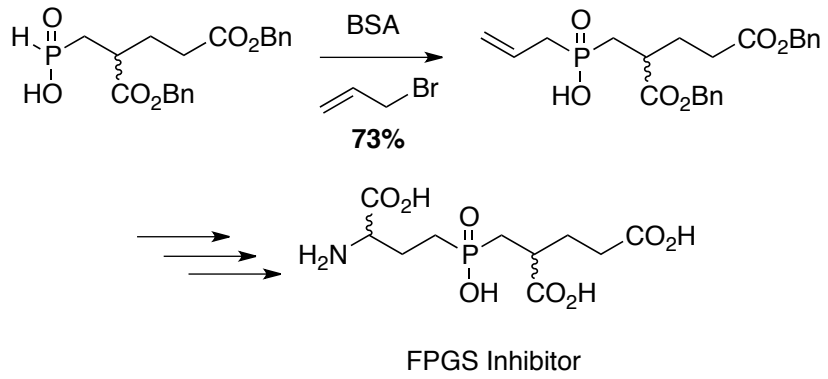

Figure 2.8 Arbuzov-like alkylation in the synthesis of a FPGS inhibitor (Valiaeva, 2001).

This revised Arbuzov-like alkylation method was not completely ideal though. Only activated alkyl halides produced the desired product unless long reaction times and

harsh reaction conditions were used; product isomerization was also seen (Bartley, 2005). An alternative method for the preparation of phosphinic acids was developed, which involved the Michael addition of either an H-phosphinic acid or ester to an activated conjugated system (Thottathil, 1984b). This alternative method was successful in the synthesis of a phosphinic acid-based inhibitor of MurE (Figure 2.9). Silylation of the H-phosphinic acid was accomplished by reaction with BSA (Zeng, 1998).

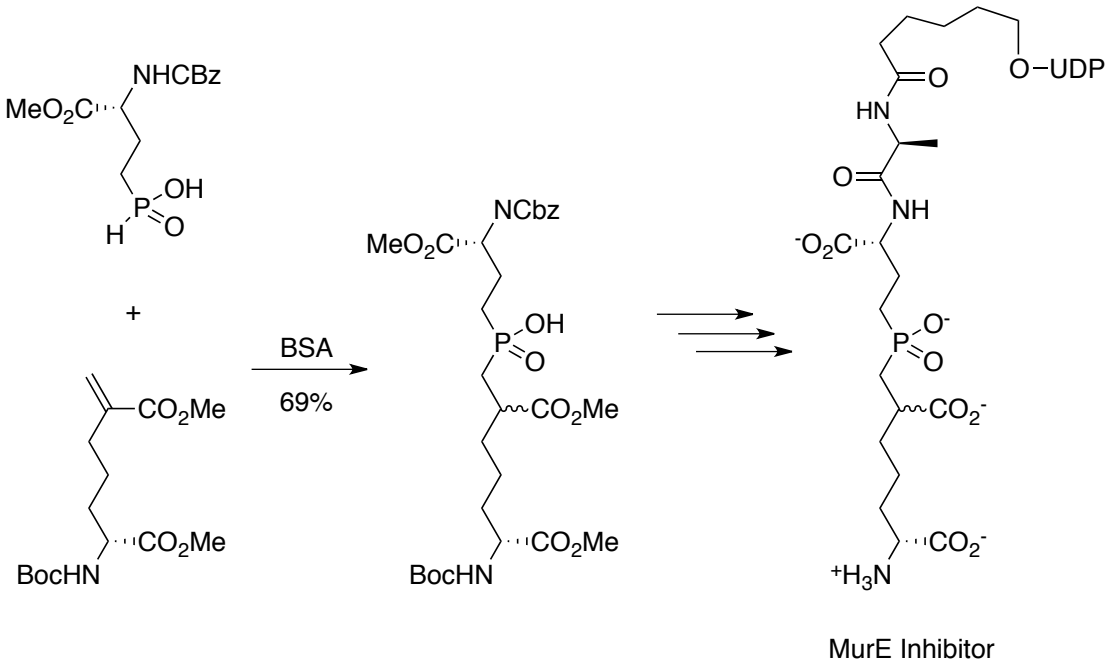

Figure 2.9 Conjugate addition in the synthesis of a phosphinic acid-based MurE inhibitor (Zeng, 1998).

The use of conjugate addition was also investigated in the synthesis of the FPGS inhibitor (Figure 2.10). With this modification, the synthesis of the phosphinic acid was less sensitive to the nature of the H-phosphinate and more sensitive to the electron density of the olefin, which permitted the use of a greater variety of functionalized P(III) nucleophiles (Bartley, 2005).

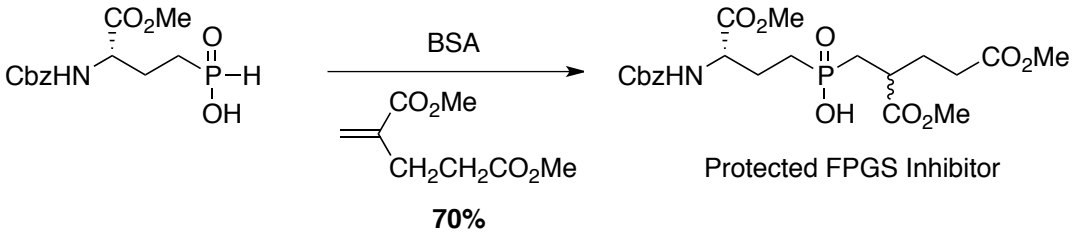

Figure 2.10 Conjugate addition in the synthesis of a FPGS inhibitor (Bartley, 2005).

Because of its widespread use, allowance for functionalized H-phosphinates and mild reaction conditions, the method of silylation followed by conjugate addition is a viable option in the synthesis of inhibitor **1**.

The *in situ* generation of a nucleophilic P(III) ester can also occur by reaction with a strong base. Base-promoted alkylation of H-phosphinates was initially thought to be impossible because of base-promoted decomposition of the phosphinate anion in the presence of less reactive reagents, such as alkyl halides (Fookes, 1978). However it was later shown that hypophosphite esters could be alkylated using sodium *iso*-propoxide as the base (Figure 2.11) (Gallagher, 1996).

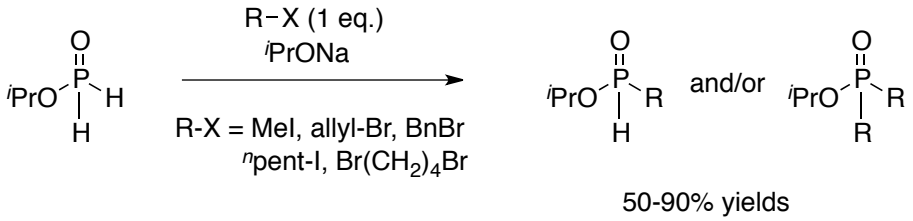

Figure 2.11 Base-promoted alkylation of a hypophosphite ester (Gallagher, 1996).

The base-promoted alkylation method was extended to an H-phosphinate using lithium hexamethyldisilazide **(**LiHMDS) and a reactive electrophile (Figure 2.12) (Abrunhosa-Thomas, 2007).

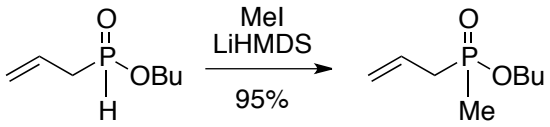

Figure 2.12 Base-promoted alkylation of H-phosphinates (Abrunhosa-Thomas, 2007).

Base-promoted alkylation has also been applied to the synthesis of biologically active targets, including a phosphinothricin precursor (Figure 2.13) (Abrunhosa-Thomas, 2007).

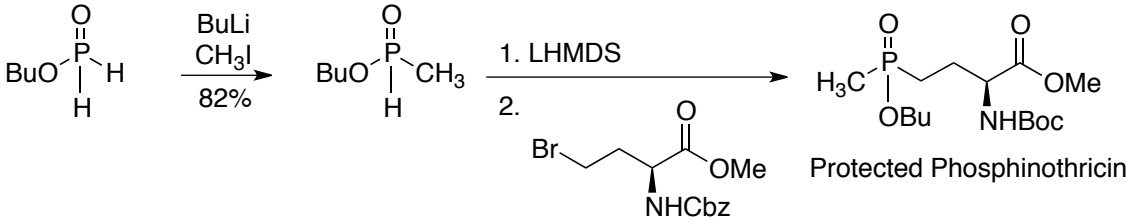

Figure 2.13 Base-promoted alkylation in the synthesis of a phosphinothricin precursor (Abrunhosa-Thomas, 2007).

Base-promoted alkylation is a straightforward reaction, but the scope of this method in P-C bond formation is very limited, prone to generate complex product mixtures and is at risk for decomposition of the phosphinate nucleophile. Because of this, base-catalyzed conjugate addition to a Michael acceptor was developed in the synthesis of tetrahedral intermediate analogue inhibitors for D-alanine:D-alanine ligase (Parsons, 1988). Sodium methoxide was used to activate the methyl-protected α-amino-H-phosphinate, followed by Michael addition to a series of methyl acrylates (Figure 2.14).

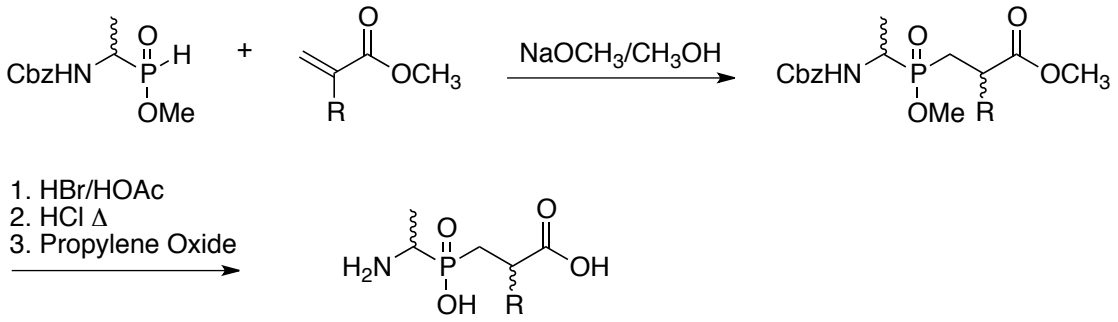

Figure 2.14 Base-catalyzed conjugate addition in the synthesis of D-alanine:D-alanine ligase inhibitors (Parsons, 1988).

Sodium methoxide-catalyzed conjugate addition was also used in the Tanner research group for the synthesis of a phosphinic acid-based inhibitor for MurD (Figure 2.15) (Tanner, 1996).

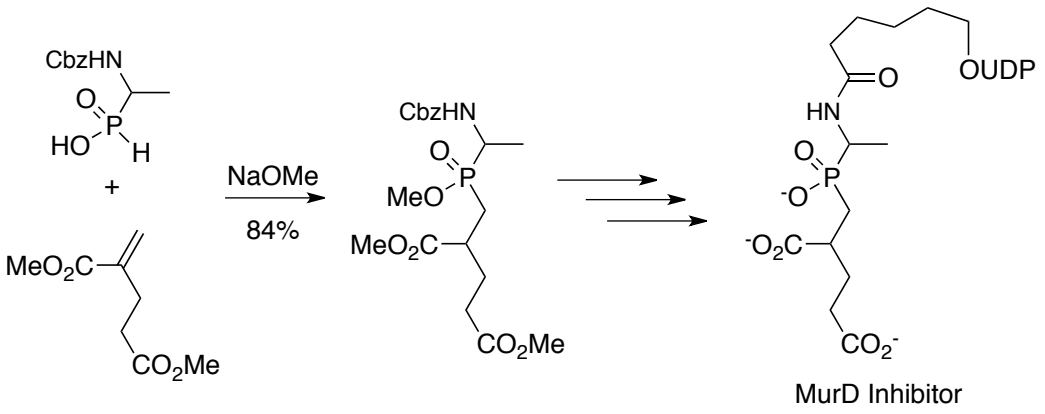

Figure 2.15 Base-catalyzed conjugate addition in the synthesis of a MurD inhibitor (Tanner, 1996).

A variety of bases have been used with this method, including potassium *tert*-butoxide (*t*-BuOK), sodium hydride (NaH), and lithium diisopropylamide (LDA). The bulky *t*-BuOK was used to avoid dealkylation of the H-phosphinate by methoxide. This unwanted side reaction was more prominent with H-phosphinates that were unsubstituted at the α position (Figure 2.16) (Cristau, 2002). NaH and LDA promoted the reaction at low temperatures, but at a reduced yield (Liu, 2002).

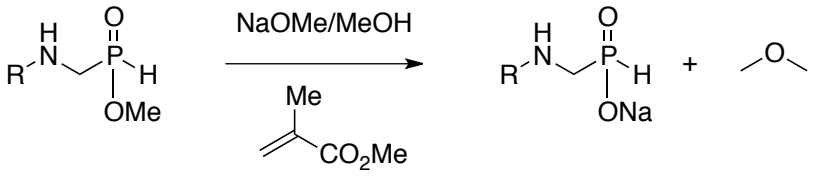

Figure 2.16 Nucleophilic-substitution reaction of unsubstituted H-phosphinates (Cristau, 2002).

Because of its success in the synthesis of phosphinic acid-based inhibitors with functionalized H-phosphinates and mild reaction conditions, a base-catalyzed conjugate addition method is a viable option in the synthesis of inhibitor **1**.

2.1.2 Methods for α-Amino-H-Phosphinic Acid Synthesis

The two viable methods for phosphinic acid preparation in the synthesis of inhibitor **1**, silylation or base-catalyzed conjugate addition, both require an H-phosphinic acid analogue of glutamic acid (Figure 2.17).

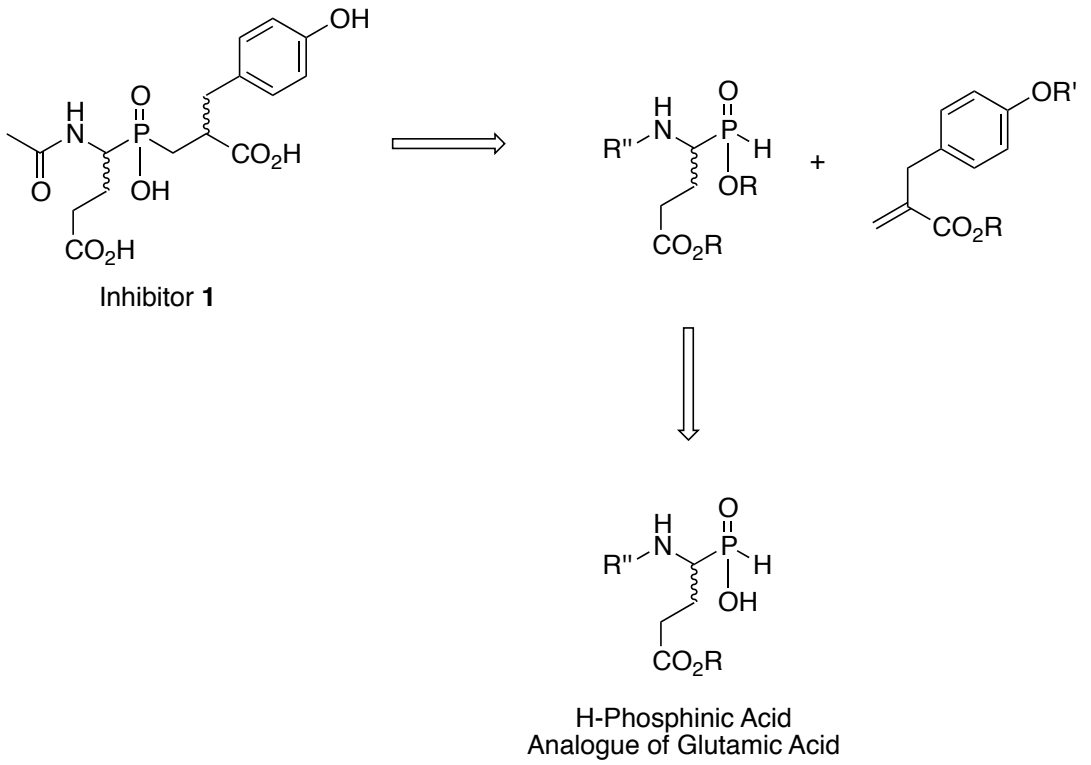

Figure 2.17 H-Phosphinic acid analogue of glutamic acid in the synthesis of inhibitor 1.

Early research on the synthesis of H-phosphinic acids includes the preparation of *p-N,N*-dimethylaminophenyl phosphinic acid by the reaction of dimethylaniline with phosphorus trichloride followed by hydrolysis (Figure 2.18) (Raudnitz, 1927).

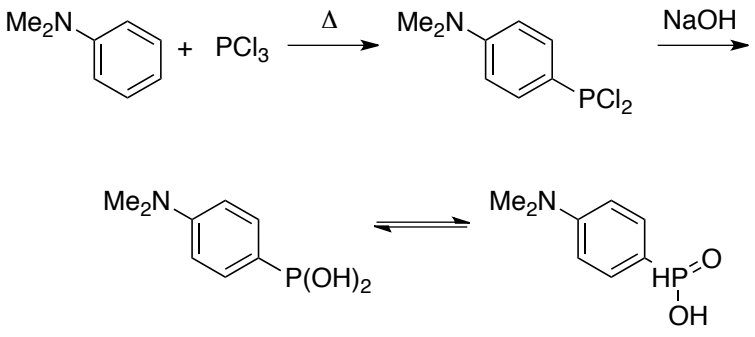

Figure 2.18 Synthesis of *p-N,N*-dimethylaminophenylphoshinic acid (Raudnitz, 1927).

It also included the preparation of *p*-aminophenylphosphinic acid by the reaction of *p*-bromophenylphosphinic acid with ammonia in the presence of cuprous oxide (Figure 2.19) (Klotz, 1947).

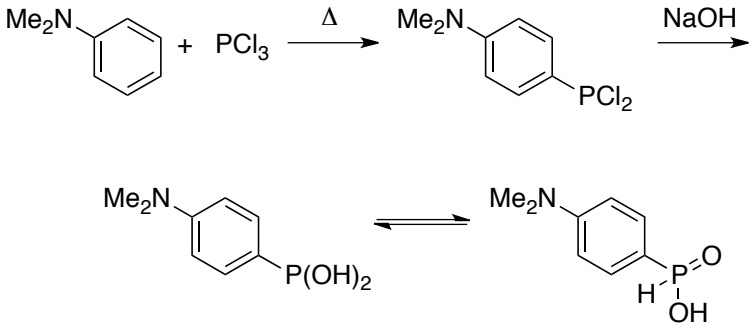

Figure 2.19 Synthesis of *p*-aminophenylphosphinic acid (Klotz, 1947).

In 1948, a method for the synthesis of simple low molecular weight α-alkyl-α-(arylamino)alkylphosphinic acids was developed (Schmidt, 1948). Two variations on the proposed method included condensation of a hypophosphite salt of a primary amine with an aldehyde or ketone in a Kabachnik-Fields reaction (Method A), and adding hypophosphorus acid to an imine in a phospha-Mannich reaction (Method B) (Figure 2.20).

Method A:

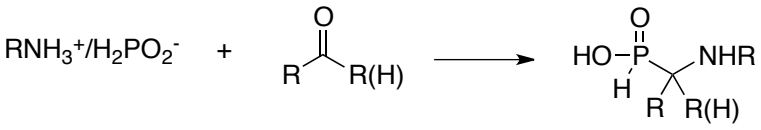

Method B:

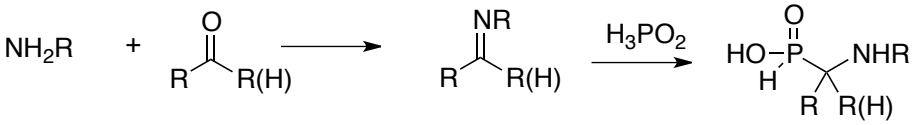

Figure 2.20 Two methods for the synthesis of H-phosphinic acids.

Methods A and B were applied to the synthesis of various aryl and long chain alkyl α-amino-H-phosphinic acids. It was found that when the hypophosphite amino salt was formed first, followed by the addition of the aldehyde (Method A), the reaction yields were lower and the reaction products were less pure (Linfield, 1961).

H-Phosphinic acid analogues of alanine, valine, methionine and glutamic acid were the first to be synthesized in a modified version of Method B; the imine is replaced with an oxime (Figure 2.21) (Khomutov, 1978). The resulting hydroxylamine is presumably reduced by excess H_3PO_2.

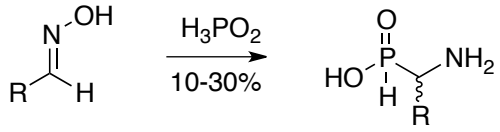

Figure 2.21 Oxime method in the synthesis of H-phosphinic acids (Khomutov, 1979).

Because of the low yields using the oxime procedure, Methods A and B were used by Baylis in the synthesis of H-phosphinic acid analogues of glycine, alanine, valine, leucine, isoleucine, phenylalanine, tyrosine, tryptophan, serine, threonine, methionine, cysteine, glutamic acid, lysine, arginine, and proline (Baylis, 1984). Either hypophosphorus acid was added to the corresponding diphenylmethylimine in ethanol or the diphenylmethylamine salt of hypophosphorus acid was heated to reflux with the corresponding aldehyde in ethanol or dioxane (Baylis, 1984). Diphenylmethylamine was chosen as the protecting group for the amine in the synthesis because its bulk led to improved crystallization of products and it can be cleaved under a variety of conditions including acidic treatment or hydrogenolysis. Ultimately, acidic treatment was used because of catalyst poisoning by the H-phosphinic acid and P-C bond cleavage under higher catalyst loadings.

The H-phosphinic acid analogue of glutamic acid was synthesized by refluxing the hypophosphite salt of the diphenylmethylamine with methyl 4-oxobutanoate in dioxane (Figure 2.22). The diphenylmethyl protecting group was removed by reflux in 48% HBr, with an overall synthetic yield of 29%.

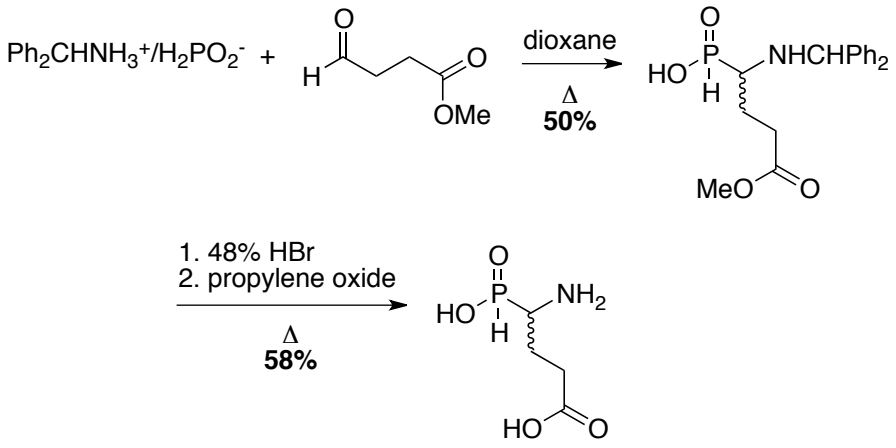

Figure 2.22 Synthesis of an H-phosphinic acid analogue of glutamic acid using Method A (Baylis, 1984).

Even though the method by Baylis (1984) is simple and economical, the preparative yields are low and the suitable precursor aldehyde is not always easily prepared or available. An alternative synthetic strategy involved the conjugate addition of a glycine H-phosphinic acid analogue anion to ethyl acrylate. However, synthesizing the H-phosphinic acid analogue of glutamic acid by this method required five steps with only an overall synthetic yield of 18% (Figure 2.23) (McCleery, 1989).

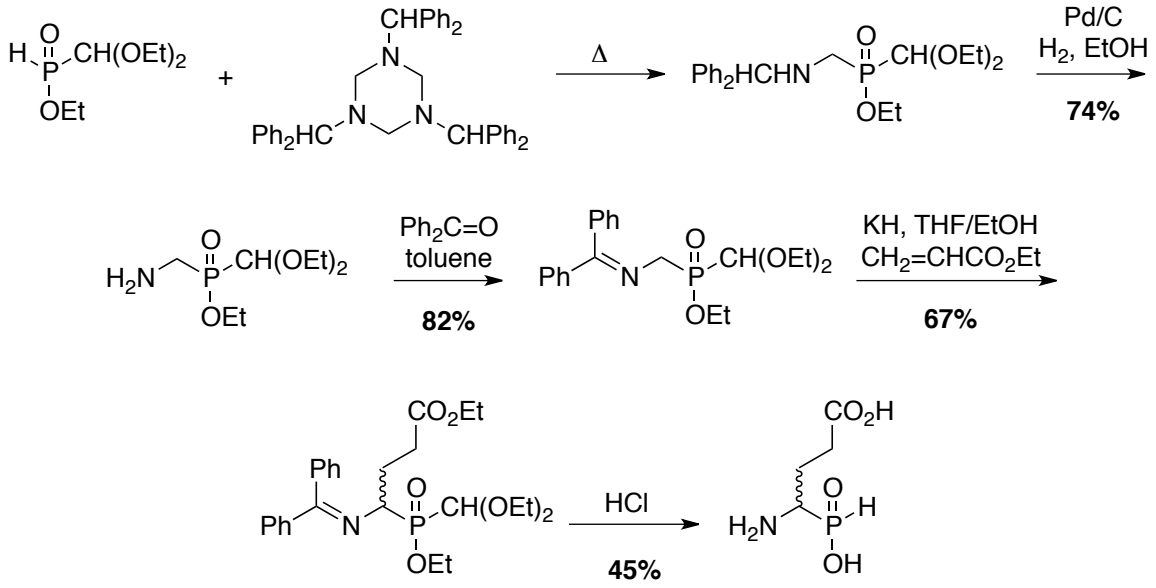

Figure 2.23 Synthesis of an H-phosphinic acid analogue of glutamic acid by a conjugate addition method (McCleery, 1989).

Formation of the hypophosphite salt of the diphenylmethylamine followed by reflux with methyl 4-oxobutanoate in dioxane has been shown to be the best method for the synthesis of the H-phosphinic acid analogue of glutamic acid.

2.2 Progress Towards the Synthesis of Inhibitor 1

The synthetic approach towards inhibitor **1** can be divided into three sections: synthesis of an H-phosphinic acid analogue of glutamic acid (**Section 2.2.1**), synthesis of a protected 2-(4-hydroxybenzyl) acrylate (**Section 2.2.2)** and P-C bond formation (**Section 2.2.3**) (Figure 2.24).

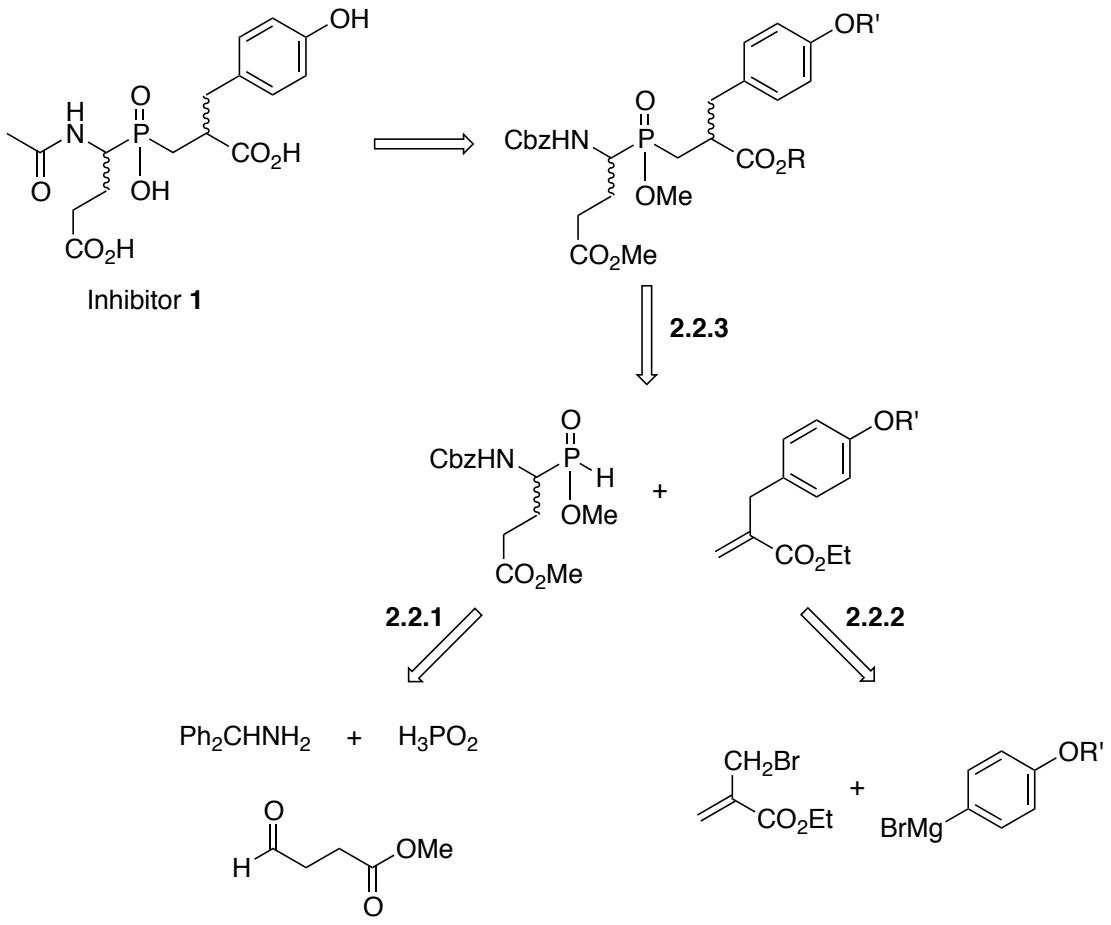

Figure 2.24 Retrosynthesis of inhibitor 1

Generally, the biological activity of α-amino H-phosphinic acids depends on the stereochemistry of the carbon center α to the phosphorus atom. Inhibitor **1** has two stereogenic centers that are set during P-C bond forming steps. Because of the increased difficulty in an enantioselective synthesis, inhibitor **1** will be synthesized and tested as a mixture of four diastereomers. If potent inhibition is observed, further research will focus on preparing the individual stereoisomers.

2.2.1 Synthesis of an H-Phosphinic Acid Analogue of Glutamic Acid

We decided to follow the procedure outlined by Baylis (1984) in the synthesis of an H-phosphinic acid analogue of glutamic acid. The primary reaction in the synthesis of

an H-phosphinic acid analogue of glutamic acid is a Kabachnik-Fields reaction involving a hypophosphite salt of a primary amine and an aldehyde. The synthesis of the corresponding aldehyde began with base-catalyzed methanolysis of γ-butyrolactone (**5**) to methyl 4-hydroxybutanoate (**6**) (Figure 2.25). The crude alcohol was oxidized to methyl-4-oxobutanoate (**7**) using pyridinium chlorochromate (PCC) (Gannett, 1988). The aldehyde proved to be difficult to purify due to co-distillation of methyl-4-oxobutanoate and γ-butyrolactone. The collected Kugelrohr distillate contained 70% aldehyde and 30% γ-butyrolactone. The methyl 4-hydroxybutanoate and γ-butyrolactone mixture was then condensed with diphenylmethylamine hypophosphite in dioxane. Initial attempts at this Kabachnik-Fields reaction resulted in low yields (less than 5%) and low-purity products. The reaction yield and product purity were improved by adding an excess of aldehyde to the diphenylmethylamine hypophosphite at 100 °C. The dioxane/water azeotrope was distilled off under vacuum, while the reaction remained at 100 °C. These adjustments resulted in the formation of the diphenylmethylaminophosphinic acid (**8**) in 39% yield.

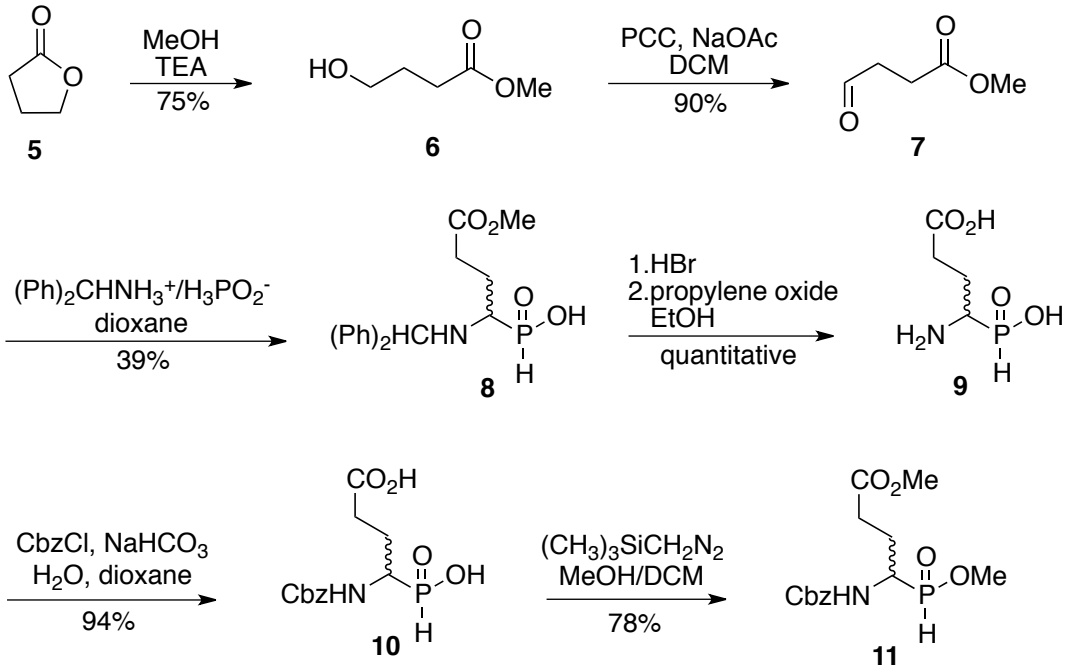

Figure 2.25 Synthesis of an H-phosphinic acid analogue of glutamic acid.

Refluxing in 48% hydrobromic acid not only cleaved the diphenylmethyl group, but it also hydrolyzed the methyl ester to a carboxylic acid. The free α-amino-H-phosphinic acid (**9**) was obtained by treatment with propylene oxide in ethanol. Temperature control and the method of propylene oxide addition were significant in the optimization of this reaction. In order to avoid ethyl esterification of the free carboxylic acid, the crude bromide salt was kept at 0 °C during ethanol addition. In order for product precipitation to occur, the propylene oxide needed to be layered on top of the ethanol solution and allowed to slowly diffuse through the ethanol solution overnight at 4 °C.

The α-amine was protected as a benzyloxycarbamate by reaction with benzyl chloroformate. The protected product (**10**) was very water-soluble, so an overnight continuous liquid extractor was utilized to obtain maximum product. The carboxylic acid

and phosphinic acid were protected as a methyl ester by treatment with trimethylsilyldiazomethane. The fully protected H-phosphinic acid analogue of glutamic acid (**11**) was unstable on silica gel. To avoid decomposition during purification, the compound was only exposed to silica gel for fifteen minutes. The H-phosphinic acid analogue of glutamic acid was synthesized in six steps with an overall yield of 19%.

2.2.2 Synthesis of a Protected 2-(4-Hydroxybenzyl) Acrylate

The synthesis of a protected 2-(4-hydroxybenzyl)acrylate involves the coupling of a cuprate generated from a protected 4-bromophenol with an ethyl 2-(bromomethyl)acrylate (**14**) (Figure 2.24, step 2.2.2). One approach to the synthesis of **14** is based on the Wittig-Horner reaction of triethyl phosphonoacetate with formaldehyde followed by treatment of the ethyl 2-(hydroxymethyl)acrylate with phosphorus tribromide (Figure 2.26) (Villieras, 1988).

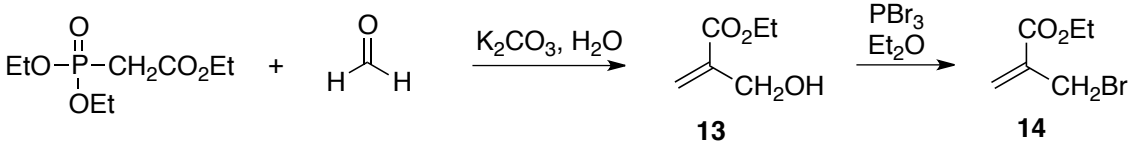

Figure 2.26 Wittig-Horner Synthesis of Compound 14.

An improved preparation was based on the Baylis-Hillman reaction of an acrylic ester with paraformaldehyde and 1,4-diazabicyclo[2.2.2]ocatane (DABCO) (Figure 2.27) (Byun, 1994). This method is advantageous over the Wittig-Horner approach because it is more economical, it has a simplified procedure, and no byproducts are formed.

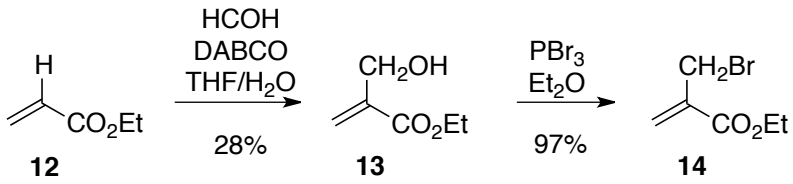

Figure 2.27 Baylis-Hilman synthesis of Compound 14.

A methoxymethyl protected 4-bromophenol (**16)** and a benzyl protected 4-bromophenol (**18)** were both synthesized and utilized in a copper-catalyzed substitution reaction with ethyl 2-(bromomethyl)acrylate (**14**) (Figure 2.28 and 2.29) (Zhu, 2008). Compound **16** was prepared by reaction of 4-bromophenol (**15**) with dimethoxymethane and phosphorus pentoxide in dichloromethane (Diemer, 2006). Compound **18** was prepared by nucleophilic substitution of benzyl bromide with **15** in DMF (Figure 2.29).

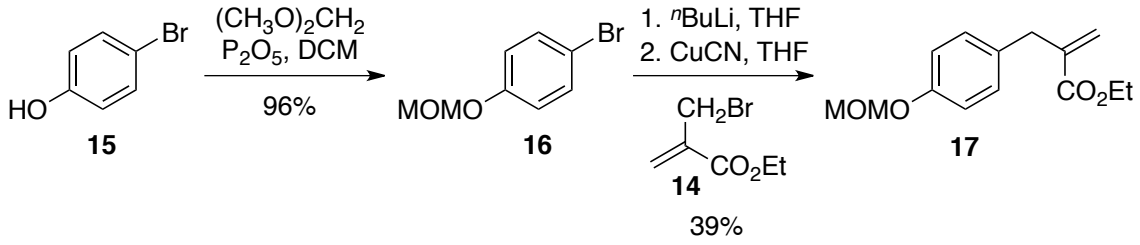

Figure 2.28 Synthesis of methoxymethyl protected acrylate 17.

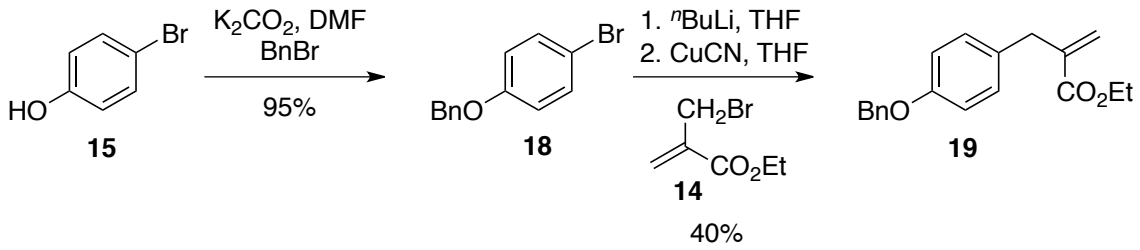

Figure 2.29 Synthesis of the benzyl protected acrylate 19.

The protected phenols each underwent metal-halogen exchange by reaction with ^{n}BuLi. Copper cyanide was added to the organolithium species to form a lithium

organocuprate, R-$C_6H_5Cu(CN)Li$. Reaction of these species with compound **14** resulted in the ethyl 2-(protected phenyl)acrylate compounds **17** and **19**.

2.2.3 Conjugate Addition in the Synthesis of Inhibitor 1

Conjugate addition, or phospha-Michael addition, between the ethyl 2-(protected phenyl)acrylate compounds and the H-phosphinic acid analogue of glutamic acid was attempted as the method for P-C bond formation in the synthesis of inhibitor **1**. Activation by strong base and activation by a silylating agent were both tried. For the base-promoted phospha-Michael addition method, sodium methoxide, which was prepared by treating dry methanol with sodium metal, was added to a solution of the H-phosphinic acid analogue of glutamic acid (**11**) in methanol at -78 °C. Either compound **17** or **19** was slowly added and four hours later, only hydrolyzed H-phosphinic acid (compound **10**) and the acrylate were present (Figure 2.30). The presence of hydrolyzed starting material indicates that water must have been present in the reaction vessel. This could have come from starting material, glassware or solvent. Due to the low overall yield in the synthesis of compound **11** only a small quantity was available for coupling reaction trials. Despite the best efforts to eliminate water from all components this reaction was unsuccessful on a small scale.

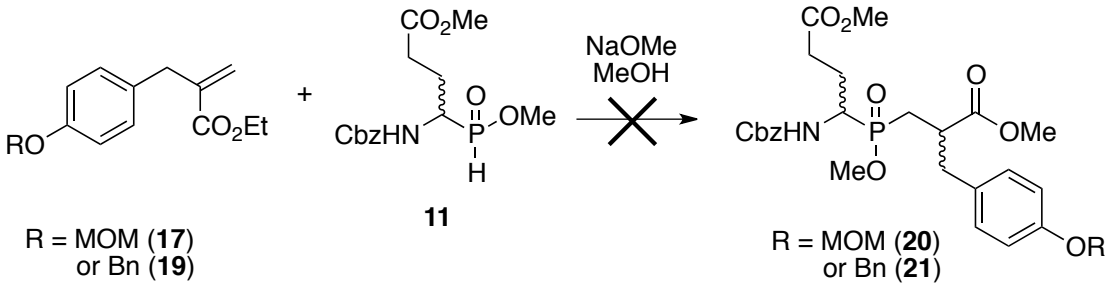

Figure 2.30 Attempted base-promoted coupling reaction.

The phospha-Michael addition method was also attempted using the silylating agent BSA. The H-phosphinic acid **11** and acrylate (**17** or **19)** were heated to reflux in the presence of BSA, but after 24 hours analysis by ESI-MS revealed only starting materials were present (Figure 2.31). The BSA-promoted phospha-Michael addition was also attempted using the unprotected H-phosphinic acid **10**. After refluxing for 24 hours analysis by ESI-MS revealed only starting materials were present.

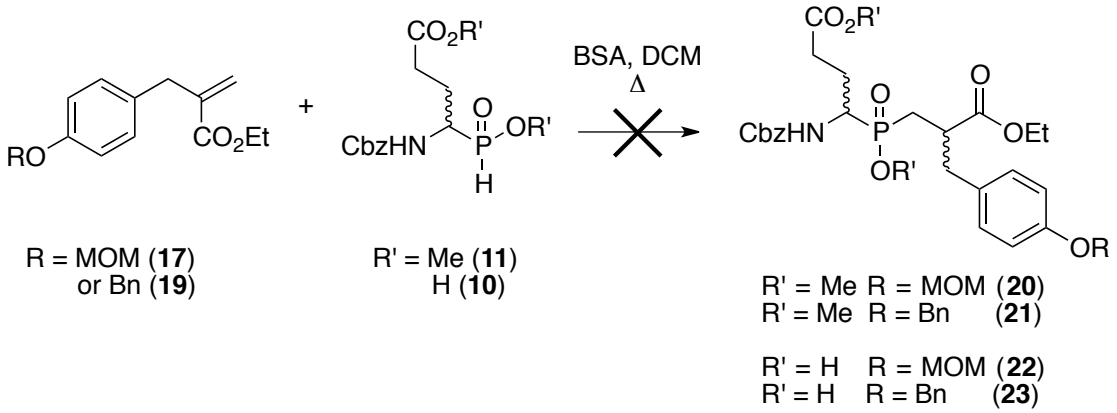

Figure 2.31 Attempted BSA-promoted coupling reactions.

It is not immediately apparent why the BSA-promoted coupling reactions failed, but because the analysis by ESI-MS revealed starting materials one possibility is that the H-phosphinic acid analogue of glutamic acid was never successfully activated to the P(III) nucleophile. Another possibility is that after activation the trivalent phosphorus reacted with the adjacent methyl ester forming a cyclized product (Figure 2.31). This species was not observed by mass spectrometry, but is a viable side reaction.

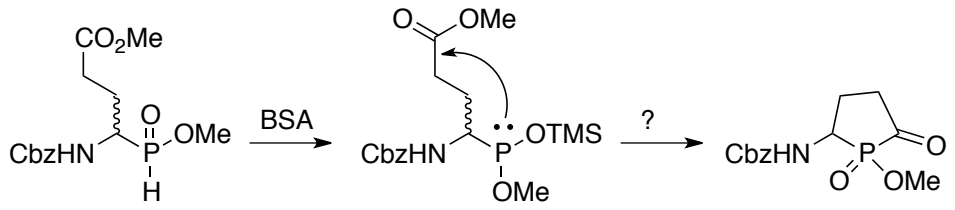

Figure 2.32 Possible side reaction in the BSA-promoted coupling reaction.

Georgiadis (1999) reported a similar result; conjugate addition of an H-phosphinic acid analogue of glutamic acid and an acrylate failed to form a P-C bond (Figure 2.33).

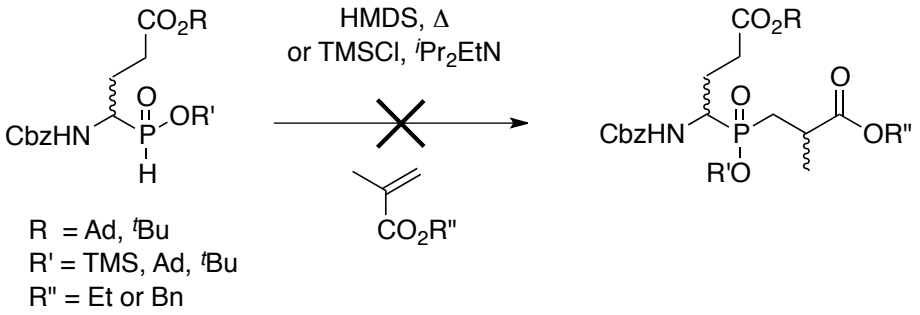

Figure 2.33 Attempted P-C bond formation reaction (Georgiadis, 1999).

Attempts at coupling various protected H-phosphinic acid analogues of glutamic acid with ethyl and benzymethylacrylate were unsuccessful. HMDS and TMSCl reagents were both used to form the trivalent phosphorus nucleophile; both methods were unsuccessful. Georgiadis (1999) hypothesized that the presence of an adjacent carboxylate group from the glutamic acid side chain was the reason for the unsuccessful coupling attempts; an explanation for this hypothesis was not reported. To circumvent this problem, the glutamic acid carboxylate side chain was masked with a phenyl group and was oxidized to the carboxylic acid after coupling (Figure 2.34). Georgiadis (1999) also reported a similar result with protected aspartic acid H-phosphinic acid analogues.

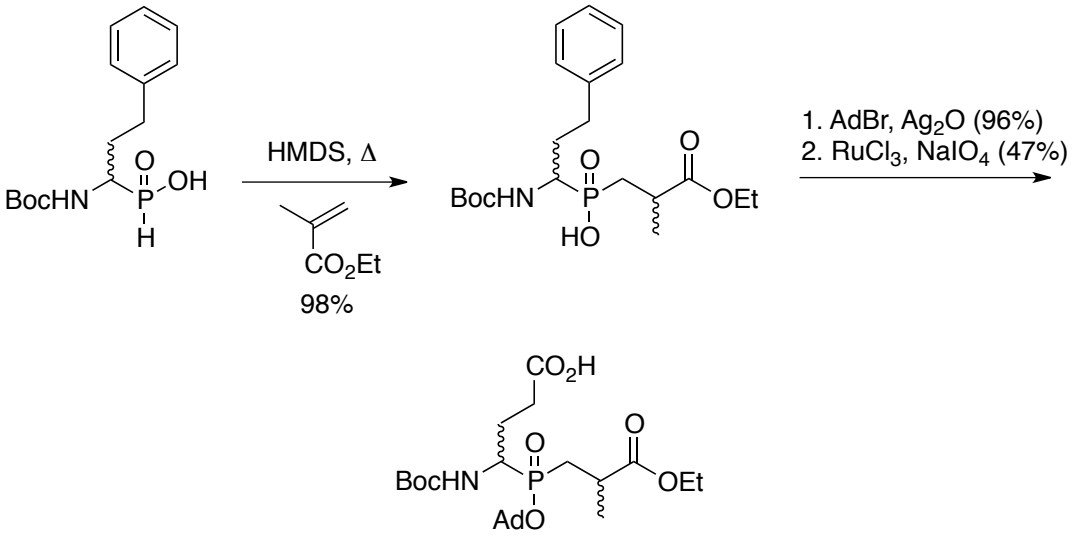

Figure 2.34 Glutamic acid carboxylate masking method (Georgiadis, 1999).

Masking the glutamic acid carboxylic acid with a phenyl group is not feasible in the synthesis of inhibitor **1**; the adjacent tyrosine residue would also be oxidized. Two other methods of making the carboxylic acid were examined: replacing the functionality with an amide and with an alkene.

The idea to mask the carboxylic acid/ester as an amide, involved reacting compound **10** with thionyl chloride to form the acyl chloride (Figure 2.35). This would be followed by reaction with dimethyl amine, which would result in the desired glutamine H-phosphinic acid analogue. After BSA-promoted coupling of this analogue to an ethyl 2-(protected phenyl)acrylate, the amide would be hydrolyzed to the desired carboxylic acid containing product.

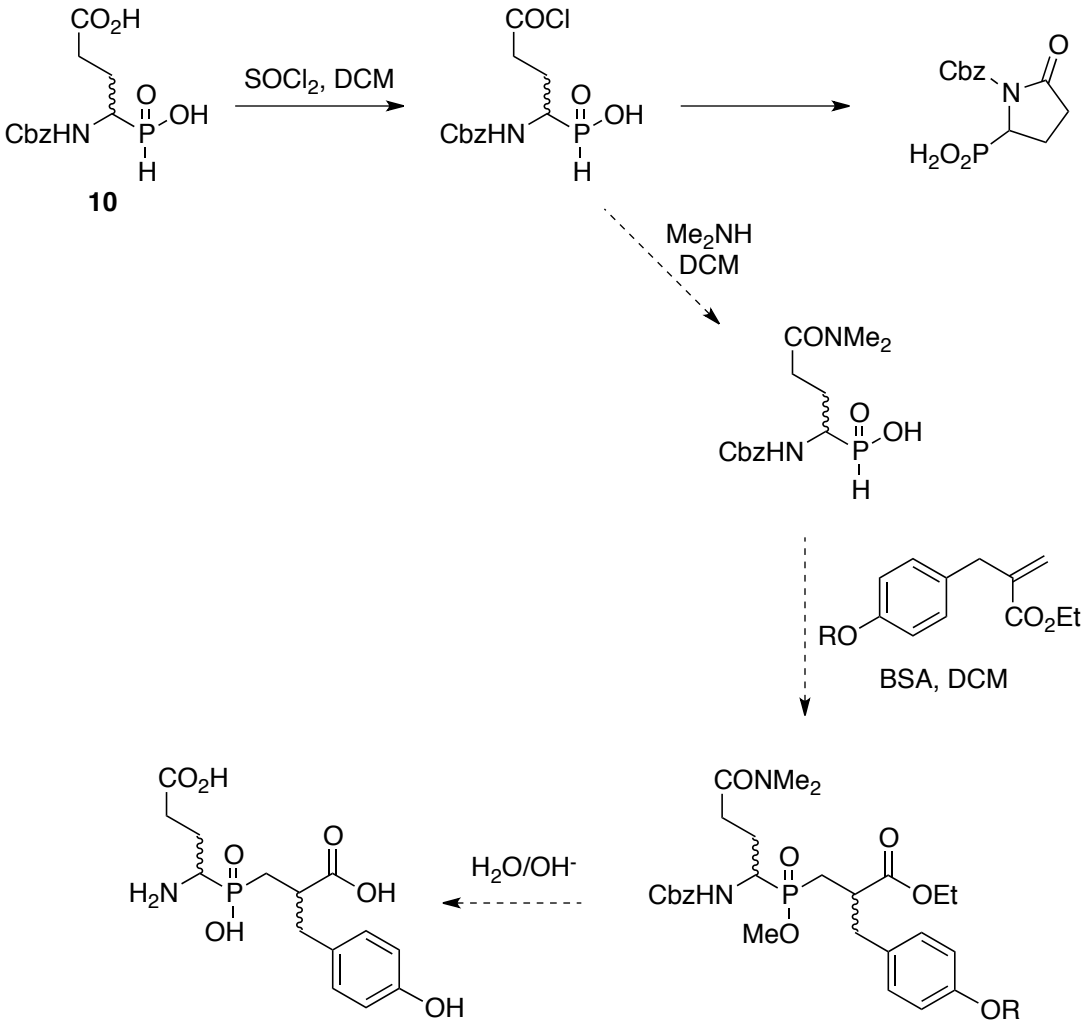

Figure 2.35 Masking the glutamic acid carboxylate with as an amide.

Unfortunately there were two problems with this revised synthesis. First, a phosphinic chloride was also formed during treatment with thionyl chloride. Second, the highly reactive acyl chloride underwent intramolecular nucleophilic attack from the amine forming a five membered ring (Figure 2.35). The presence of the cyclized product was confirmed by ESI mass spectrometry.

The idea to mask the carboxylic acid as an alkene involved synthesizing an α-amino-5-hydroxypentyl phosphinic acid **27** (Figure 2.36). Elimination of the alcohol to the alkene, before or after coupling, followed by oxidation, would result in the desired

carboxylic acid compound (**34**). First, δ-valerolactone (**24**) was reduced with DIBAL-H in 71% yield with no further purification needed. The aldehyde (**25**) underwent a Kabachnik-Fields reaction with diphenylaminomethane and hypophosphorus acid to form the α-amino phosphinic acid **26** in 50% yield. The diphenylmethane protecting group was removed by refluxing in trifluoroacetic acid and anisole, followed by the addition of ethanol to give compound **27**. The free amine was protected as a benzyl carbamate using benzyl chloroformate and the free phosphinic acid was protected as the methyl ester using TMS-diazomethane to give compound **28** and **29**, respectively. Attempts at purifying compound **29** were unsuccessful, so the crude product was carried on without further purification.

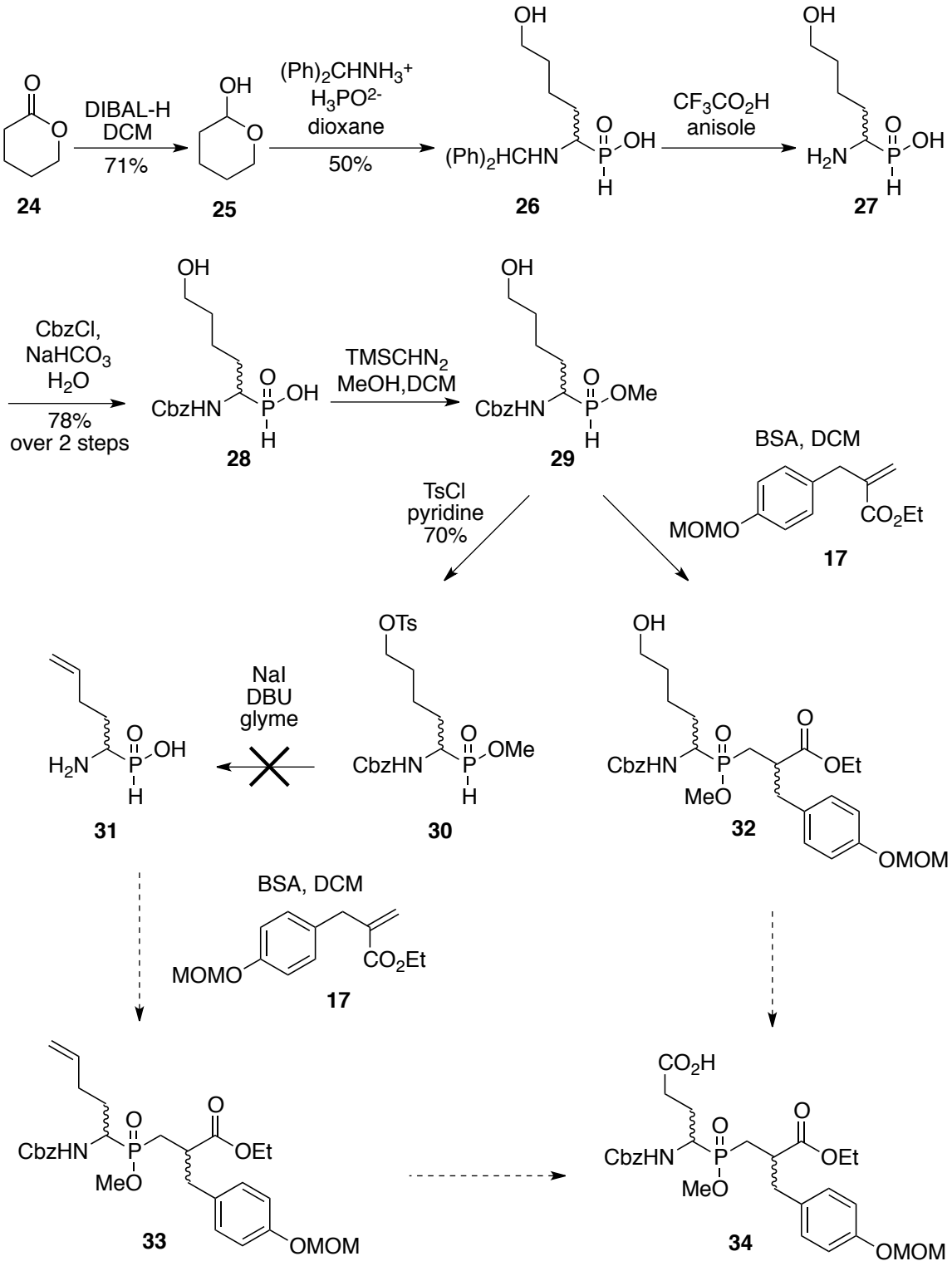

Figure 2.36 Masking the glutamic acid carboxylate with an alkene.

The alcohol of compound **29** was tosylated to give compound **30** and elimination reactions were attempted with 1,8-diazabicycloundec-7-ene (DBU). Because all attempts at base-catalyzed elimination of the alcohol to the alkene were unsuccessful, we decided to try coupling the acrylate and phosphinic acid first to form compound **32**, and if that was successful, focus on troubleshooting the elimination reaction. The first attempt at a BSA-promoted phospha-Michael addition between compounds **29** and **17** was successful. Analysis by ESI-MS revealed compound **32** had formed after 24 hours at room temperature. After an acidic workup (1 M HCl), analysis by ESI-MS indicated that the MOM protecting group had been cleaved and the coupled product remained in the aqueous layer and was never isolated. All subsequent attempts at this coupling reaction failed to produce coupled product (**32**). This result is possibly due to the presence of impurities in compound **29**.

Due to difficulties in the P-C bond formation reaction, we decided to divert our efforts towards the synthesis a phosphonic acid-containing dipeptide inhibitor, inhibitor **2**.

2.3 Strategies for Inhibitor 2 Synthesis

Inhibitor **2**, a phosphonic acid, differs from inhibitor **1**, a phosphinic acid, by the replacement of the carbon linkage between phosphorus and the tyrosine moiety with an oxygen atom (Figure 2.37). The structural consequences of this substitution are minimal, however the effect on inhibitor potency has been shown to be substantial in some cases.

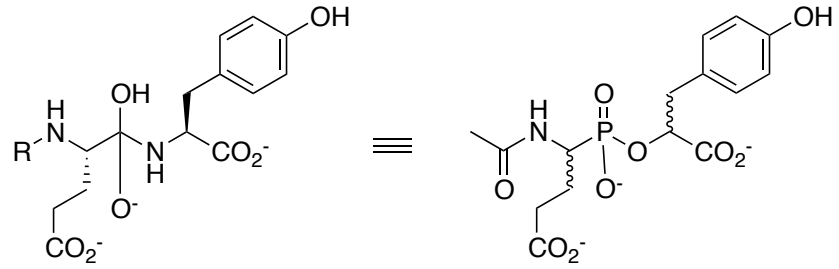

Figure 2.37 Structure of inhibitor 2.

The matrix metalloproteinase, stromelysin-1, is more strongly inhibited by a phosphinic acid than by the corresponding phosphonamidate and phosphonic acid analoges (Figure 2.38) (Caldwell, 1996).

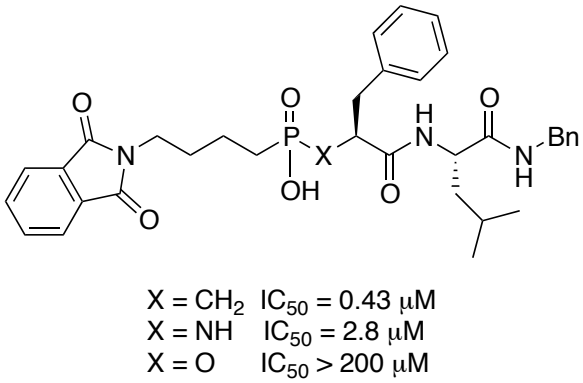

Figure 2.38 Structures of stromelysin-1 inhibitors (Caldwell, 1996).

D-Alanine:D-alanine ligase is also more strongly inhibited by a phosphinic aid than by the corresponding phosphonic acid (Ellsworth, 1996) and the phosphonamidate (Lacoste, 1991).

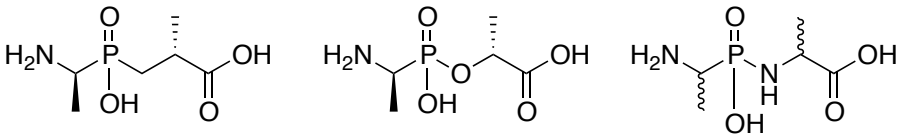

Figure 2.39 Structures of D-alanine:D-alanine ligase inhibitors (Ellsworth, 1996) (Lacoste, 1991).

Alternatively, the angiotensin-converting enzyme (ACE) is more strongly inhibited by the phosphonamidate and phosphonic acid than the phosphinic acid (Figure 2.40) (Karanewsky, 1988).

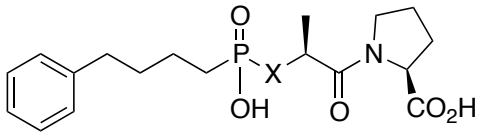

Figure 2.40 Structures of ACE inhibitors (Karanewsky, 1988).

The small 5-fold difference between the phosphonamidate and phosphonic acid IC_{50} values was unexpected because of a previous study on thermolysin inhibition. A large 800-fold average difference in binding affinity between a series of phophonamides and phosphonates was observed in that study (Figure 2.41). This dramatic difference in binding affinity was initially thought to be due to the presence of a hydrogen bond between the phosphonamidate and the enzyme active site (Bartlett, 1987). However, the affinity of a phosphinic acid containing inhibitor was shown to be only slightly weaker (20-fold difference) than the phosphonamidate isostere (Grobelny, 1989); a hydrogen bond interaction is impossible with the phosphinate isostere.

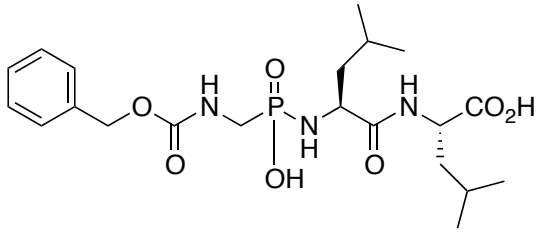

X = NH K_i = 0.0091 μM
X = CH_2 K_i = 0.180 μM
X = O K_i = 9.00 μM

Figure 2.41 Structures of thermolysin inhibitors (Bartlett, 1987).

A stronger inhibition by a phosphonic acid is seen when comparing isosteres of CPA inhibitors (Figure 2.42). While the phosphonic acid is only slightly more potent than the phosphinic acid, a substantial increase in inhibition (35-fold difference) is seen between the phosphonic acid and phosphonamidate (Kaplan, 1991).

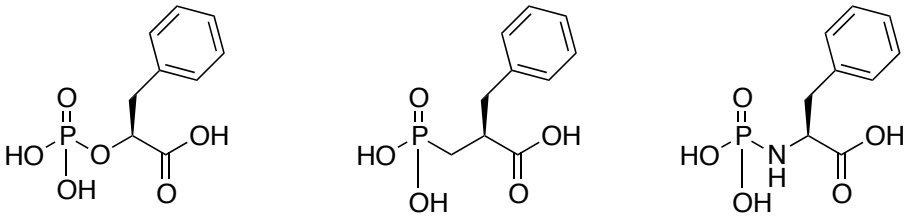

K_i = 0.140 μM K_i = 0.220 μM K_i = 5.00 μM

Figure 2.42 Structures of CPA inhibitors (Kaplan, 1991).

While the phosphinic acid is the most stable isostere, it is not necessarily the most potent inhibitor; strong inhibition and binding affinity depends on specific interactions between the inhibitor and enzyme.

2.3.1 Methods in Phosphorus-Oxygen Bond Formation

Phosphonic acid peptide analogues are prepared by the reaction of a hydroxy ester with an activated phosphonate. The phosphonate can be activated with a coupling reagent such as DCC, BOP, BOP-Cl, PyBOP or TPP/DIAD, or it can be activated as a

phosphonochloridate by reaction with thionyl chloride, oxalyl chloride or carbon tetrachloride/triethylamine (Figure 2.43). The most common method is activation of a phosphonic acid with thionyl chloride followed by reaction with a hydroxy ester. Phosphonamidate peptide analogues are synthesized in a similar manner, except the hydroxy ester is replaced with an amino acid ester.

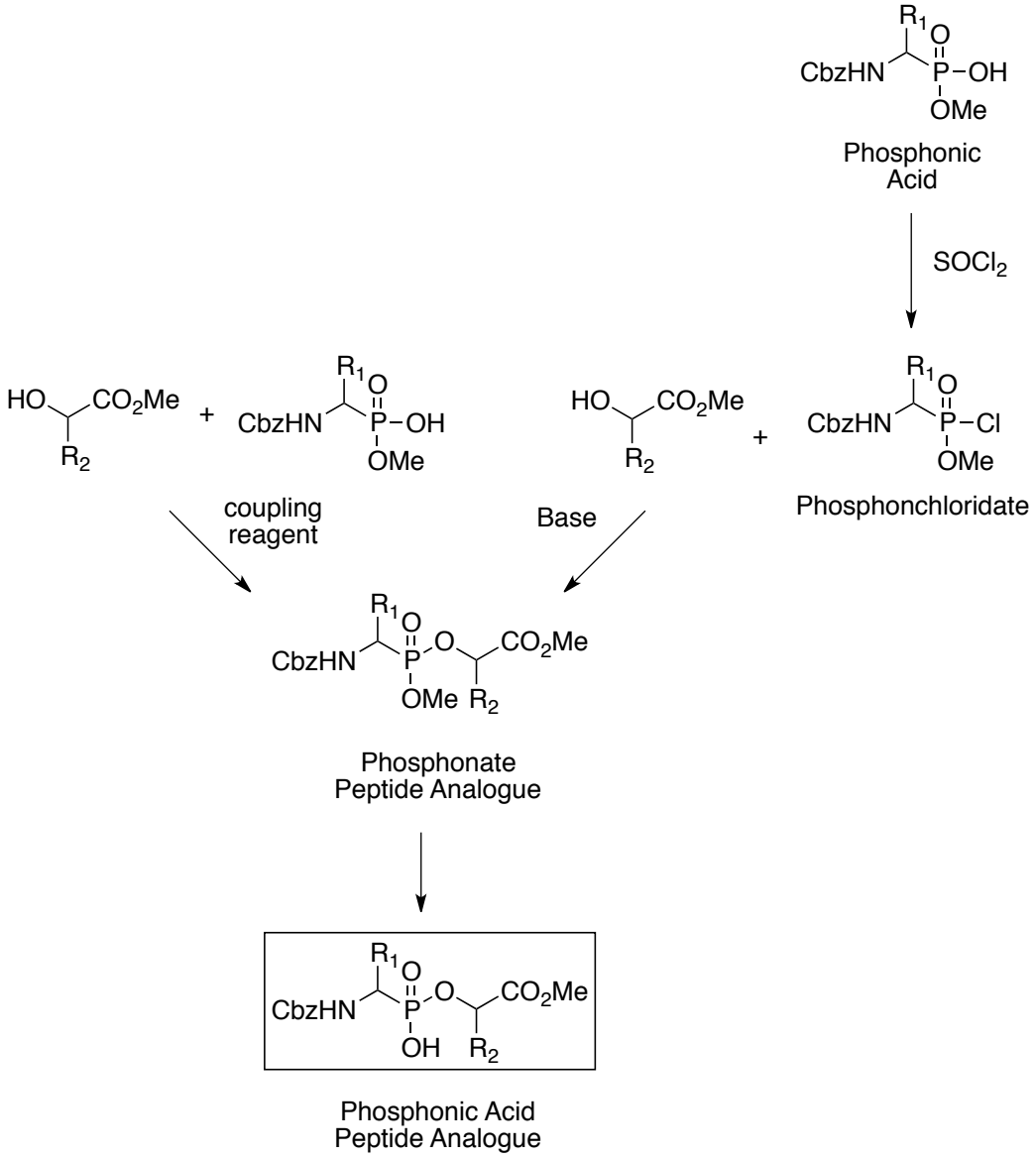

Figure 2.43 Methods in phosphonic acid peptide analogue synthesis.

2.3.1.1 Phosphonic Acid Synthesis

One method in the preparation of phosphonic acids involves the base hydrolysis of either a symmetrical phosphonate or a phosphonochloridate (Figure 2.44). While the reactions proceed in good yield without significant hydrolysis of the ester product (Rabinowitz, 1960), the variety and complexity of the prepared phosphonic acid is limited.

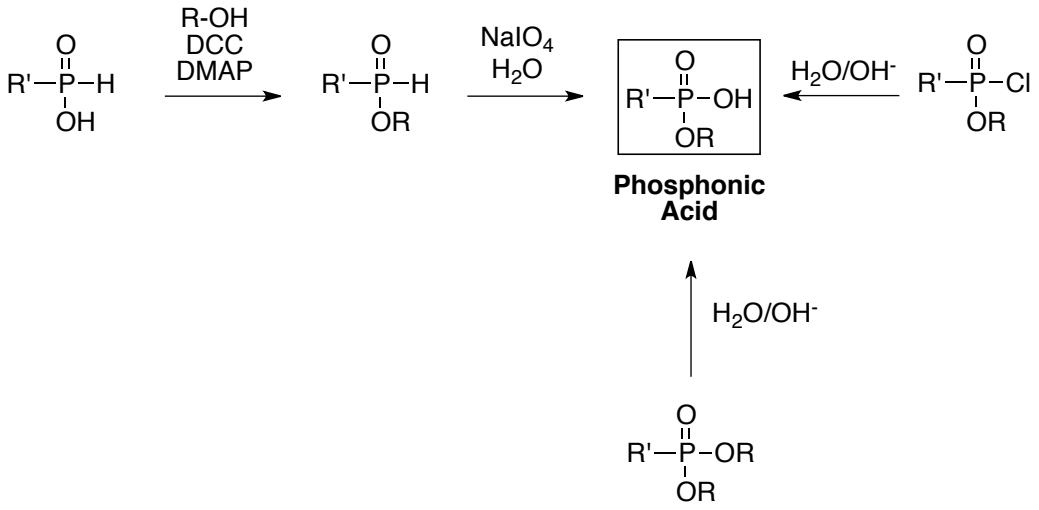

Figure 2.44 Methods in phosphonate monoester synthesis.

Karanewsky (1986) developed an improved method which involved the direct esterification of an H-phosphinic acid followed by oxidation to the phosphonic acid with sodium periodate (Figure 2.44). The esterification of an H-phosphinic acid proceeds rapidly at room temperature and with only a slight excess of the alcohol component. This method has been applied to a variety of alcohols and H-phosphinic acids with moderate to high yields.

2.3.1.2 Phosphonochloridate Synthesis

Activation of the phosphonic acid to the phosphonochloridates is commonly achieved by reaction with thionyl chloride. Alternatively, phosphonochloridates are prepared by the reaction of phosphonates with phosphorus pentachloride (Thorsett, 1982), by the treatment of phosphinic acids with oxalyl chloride (Jacobsen, 1981), or by the oxidative chlorination of silyl-activated H-phosphinic acids with carbon tetrachloride (Sampson, 1988) (Figure 2.45).

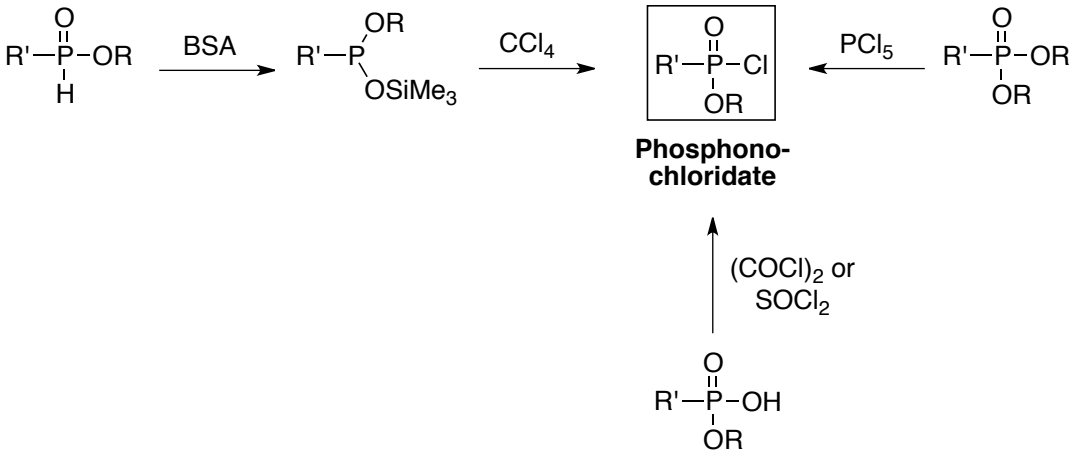

Figure 2.45 Methods in phosphonochloridate synthesis.

Difficulties in the formation of phosphonochloridates by reaction with thionyl chloride are enhanced when highly functionalized phosphonates are utilized. Often the phosphonochloridate decomposes when the reaction solution is concentrated or stored for extended periods of time; it should be used immediately after synthesis (Malachowski, 1994).

One side product in the phosphonochloridate synthesis is a phosphonic acid anhydride (Figure 2.46). Addition of the phosphonate monoester to a solution of thionyl

chloride suppresses the formation of the anhydride by keeping the chlorinating agent in excess (Hirschmann, 1997).

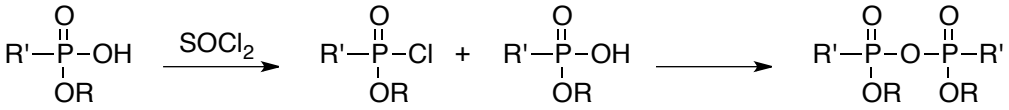

Figure 2.46 Side product formed in phosphonochloridate synthesis.

Low yields are common in the synthesis of phosphonate peptide analogues from a phosphonochloridate and an alcohol. Some improvement in the yields and reaction time is seen when triethylamine is added to the reaction mixture. It was initially added along with the nucleophile as an acid scavenger. However, it has been postulated that when a carbamate-protecting group is present, the triethylamine catalyzes the intramolecular cyclization to a more reactive oxazaphospholine (Figure 2.47). However, this reactive intermediate has never been isolated (Cullis, 2002).

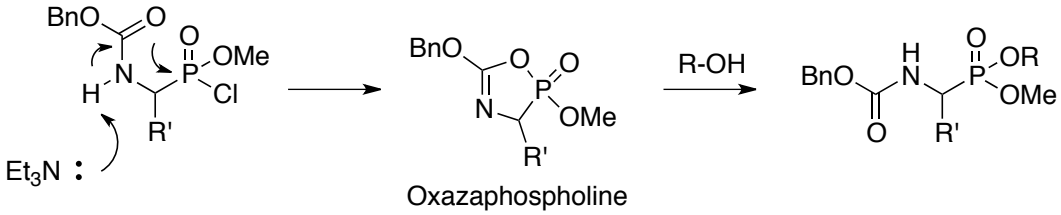

Figure 2.47 Formation of an oxazaphospholine.

It is more likely that the triethylamine is generating a highly reactive phosphonylammonium salt (Figure 2.48). To form the phosphonylammonium salt, and improve the reaction yield, the triethylamine must be added as a deliberate step, not just in conjunction with the nucleophile to neutralize acid (Hirschmann, 1997).

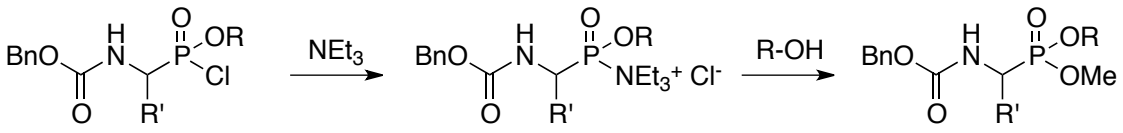

Figure 2.48 Formation of phosphonylammonium salt.

2.4 Synthesis of Inhibitor 2

The synthesis of inhibitor **2** can be divided into three sections: synthesis of a glutamic acid phosphonochloridate analogue (**Section 2.4.1**), synthesis of a protected 4-hydroxyphenyllactic acid (**Section 2.4.2)** and P-O bond formation and deprotection steps (**Section 2.4.3**) (Figure 2.49). Inhibitor **2** has two stereogenic centers, but because of the increased difficulty in an enantioselective synthesis inhibitor **2** will be synthesized and tested as a mixture of four diastereomers. If potent inhibition is observed, further research will focus on preparing the individual stereoisomers.

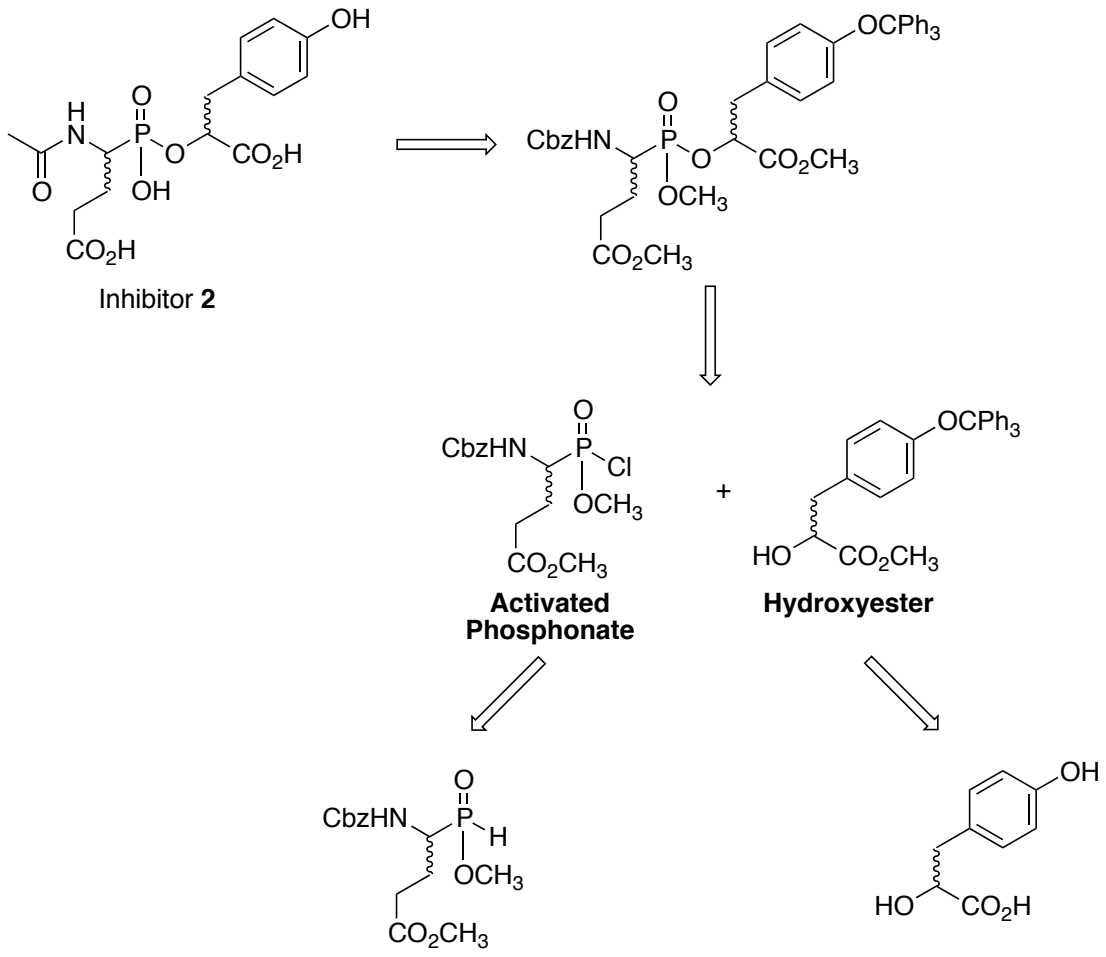

Figure 2.49 Retrosynthesis of inhibitor 2.

2.4.1 Synthesis of a Glutamic Acid Phosphonochloridate Analogue

The glutamic acid phosphonochloridate was synthesized from a glutamic acid phosphonic acid analogue, which in turn was synthesized from the H-phosphinic acid analogue of glutamic acid (compound **11)** previously prepared during the synthesis of inhibitor **1**. Compound **11** was oxidized to the phosphonic acid **35** in a procedure reported by Karanewsky (1986) that employs sodium periodate in aqueous dioxane (Figure 2.50). The work up involved multiple aqueous washes, including 2% $KHSO_4$, water, dilute $NaHSO_3$ and saturated NaCl. Because simple aliphatic and aromatic H-phosphinic acids

were used in the literature example, the phosphinic acids were easily extracted from the aqueous washes. The glutamic acid phosphinic acid analogue is much more polar, therefore the work-up procedure had to be adjusted. After treatment with sodium periodate and filtration, the reaction mixture was acidified to pH = 1 and then extracted multiple times with ethyl acetate to yield the phosphinic acid in 86% yield.

The phosphonochloridate **36** was formed from the reaction of the glutamic acid phosphinic acid analogue **35** with thionyl chloride. Because compound **35** is highly functionalized, the phosphonochloridate **36** is prone to decomposition. To avoid this, the thionyl chloride was freshly distilled before each use and the phosphonochloridate was used immediately after formation.

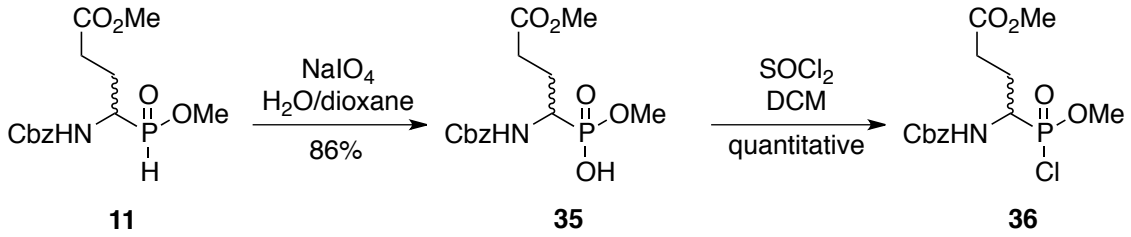

Figure 2.50 Synthesis of the glutamic acid phosphonochloridate analogue.

2.4.2 Synthesis of a Protected 4-Hydroxyphenyllactic Acid

4-Hydroxyphenyllactic acid (compound **37**) contains two functional groups that require protection: the phenol and the carboxylic acid (Figure 2.51). The protection of the carboxylic acid is straightforward; reaction with trimethylsilyldiazomethane protects the carboxylic acid as a methyl ester to give compound **38** in quantitative yield. Selective protection of the phenol is complicated by the presence of a secondary alcohol, which must remain unprotected in order to form the P-O bond in inhibitor **2**. Most phenol protecting groups also protect secondary alcohols. It was reported by Sefkow (1999) that

in the presence of a secondary alcohol, a phenol could be selectively protected as a triphenylmethyl ether. This method was applied in the protection of 4-hydroxyphenyllactic acid. Compound **38** was treated with triethylamine and triphenylmethyl chloride producing compound **39** in 96% yield.

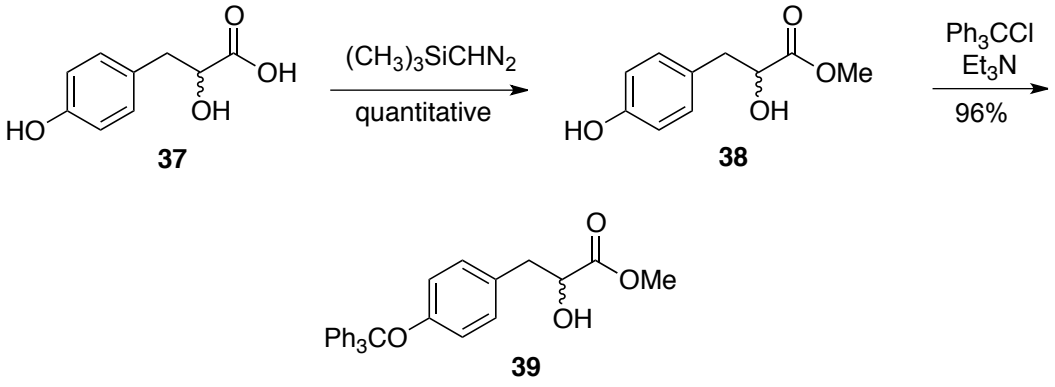

Figure 2.51 Synthesis of protected 4-hydroxyphenyllactic acid.

2.4.3 Formation of the Phosphorus-Oxygen Bond and Deprotections

Reaction of the phosphonochloridate **36** and triethylamine generated the highly reactive phosphonylammonium salt. This reactive species has been shown to improve reaction times and yields over the phosphonochloridate alone (Hirschmann, 1997). The phosphonylammonium salt was then coupled to the protected 4-hydroxyphenyllactic acid **39** to form the fully protected phosphonate peptide analogue (**40**) (Figure 2.52). Purification by silica gel flash column chromatography produced compound **40** in 57% yield.

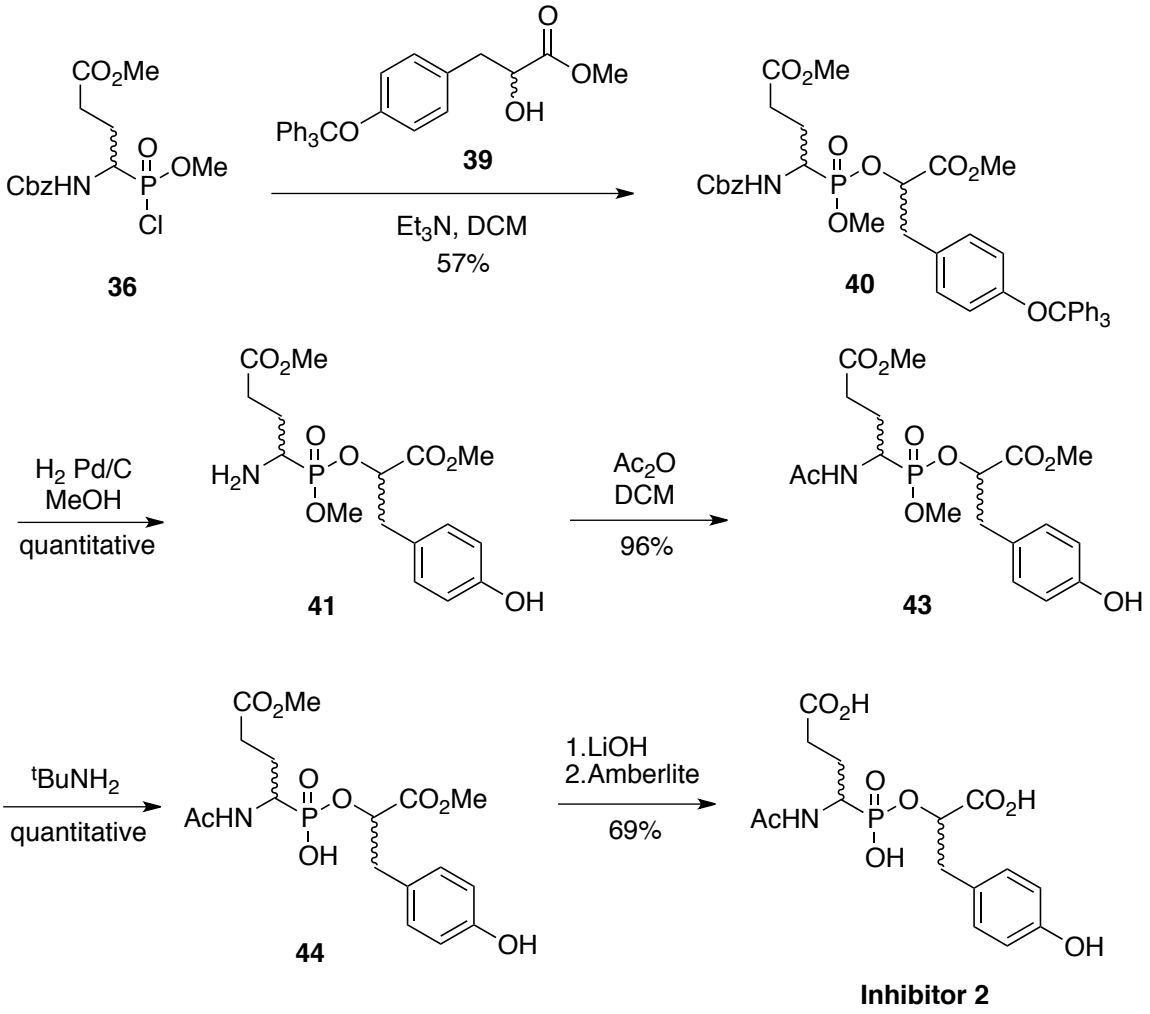

Figure 2.52 Coupling and deprotection steps in the synthesis of inhibitor 2.

The remaining reactions in the synthesis of inhibitor **2** involved the subsequent removal of the four protecting groups, with the benzyloxycarbamate being the first protecting group removed. The benzyloxycarbamate was removed by palladium-catalyzed hydrogenolysis. The triphenylmethyl protecting group was also removed under the palladium-catalyzed hydrogenolysis conditions to give compound **41**. Removal of the benzyloxycarbamate-protecting group leaves a primary amine that is proximal to a methyl ester. Because intramolecular cyclization is a concern, compound **41** was immediately acetylated with acetic anhydride to avoid this side reaction. Initially the free

amine was acetylated under basic conditions, but cyclized product **42** formed (Figure 2.53).

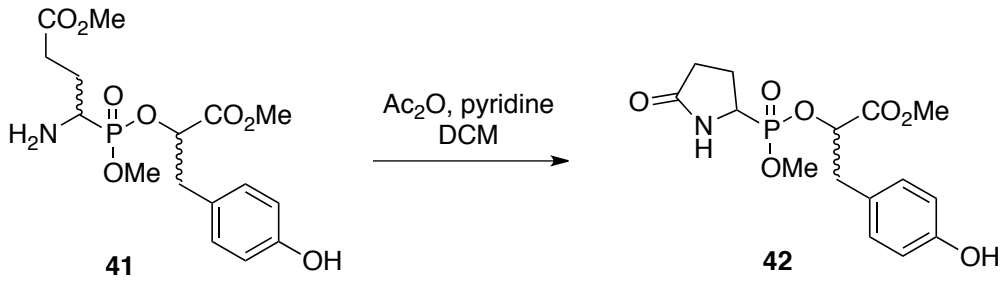

Figure 2.53 Intramolecular cyclization side product.

It was found that if a large excess of acetic anhydride was used (80 equivalents), acetylation of the primary amine proceeded in the absence of base to give **43**, and formation of the cyclized side product was avoided. Impurities remained even after Compound **43** was purified by silica gel flash column chromatography. We estimate compound **43** is only 80% pure by the presence of unidentified peaks in the ^{1}H NMR spectrum.

Conversion of the phosphonate peptide analogue to the phosphonic acid peptide analogue was a complicated deprotection. Because the phosphonate contains two P-O bonds, base hydrolysis can cleave either bond resulting in two products (Figure 2.54).

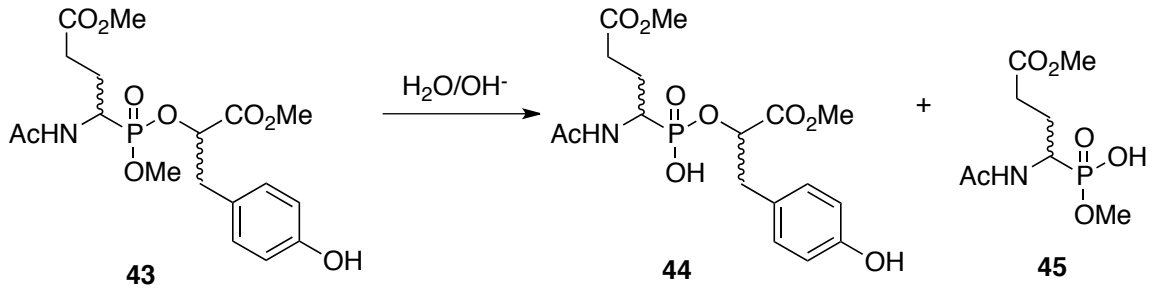

Figure 2.54 Expected base hydrolysis products.

Cleavage of the alkyl oxygen bond of the phosphonate methyl ester by nucleophilic displacement of the phosphonate anion from the methyl group would result in complete formation of the phosphonic acid **44** (Figure 2.55).

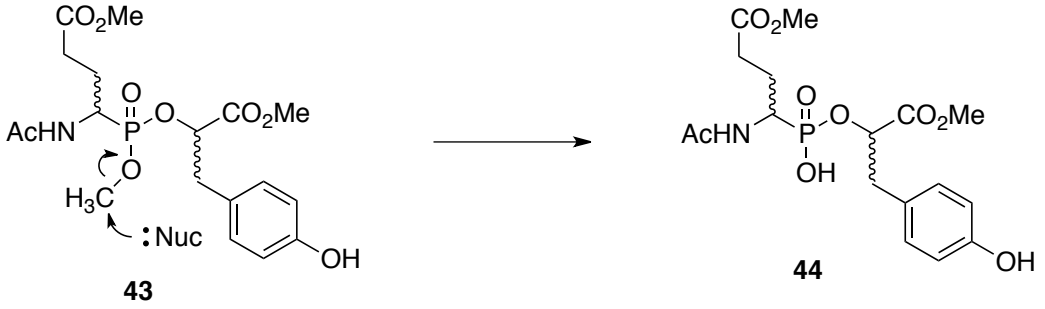

Figure 2.55 Nucleophilic deprotection of the phosphonate methyl ester.

The first method investigated for the nucleophilic deprotection of compound **43** was developed for the deprotection of methyl esters with steric hinderance or other acid- or base-sensititve group present (Bartlett, 1970). Lithium *n*-propyl mercaptide in hexamethylphosphoramide (HMPA) was found to be an effective reagent for the cleavage of methyl esters under mild conditions. This method was successfully applied in the total synthesis of a phosphonic acid-containing inhibitor for CPA (Figure 2.56) (Hanson, 1989).

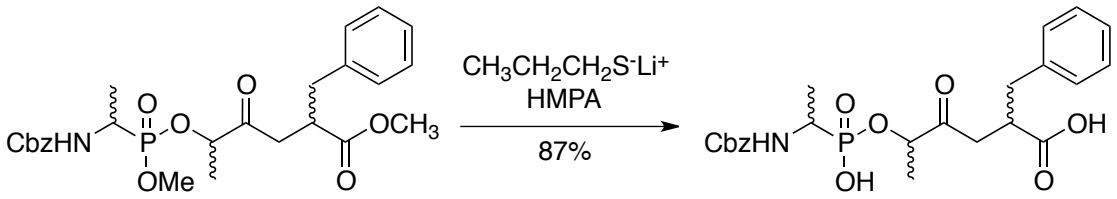

Figure 2.56 Nucleophilic deprotection of CPA inhibitor (Hanson, 1989).

This method was attempted in the deprotection of compound **43**. The reagent, lithium *n*-propyl mecaptide, was prepared by the addition of *n*-propyl mercaptan to a suspension of lithium hydroxide in dry, oxygen-free HMPA. After 1 hour, the remaining

lithium hydroxide was filtered off without contact with air. The freshly prepared lithium *n*-propyl mecaptide was added to a solution of compound **43** in HMPA. After 2 hours the reaction was quenched by the addition of water, acidified, and purified by ion exchange chromatography. After analyzing the column fractions by ESI-mass spectrometry and NMR spectroscopy, it was concluded that a 50:50 mixture of compounds **44** and **45** had been formed (Figure 2.54). The failure of this reaction to selectively produce **44** indicates that water must have been present in the reaction vessel. This could have come from starting material, reagents, or glassware, but despite multiple efforts to dry all components, this was unsuccessful on a small-scale reaction.

The next method investigated for the nucleophilic deprotection of compound **43** was the selective cleavage of phosphonate methyl esters by *tert*-butylamine (Gray, 1980). *tert*-Butylamine was found to be effective in solution or when the amine itself was used as the solvent. For simple phosphonate esters the transformation was complete in minutes at room temperature, but for more sterically hindered phosphonate esters the transformation required days at an elevated temperature (Malachowski, 1994).

This procedure was applied in the synthesis of inhibitor **2**. Compound **43** was heated to reflux in *tert*-butylamine and the reaction was monitored by ESI-mass spectrometry. After 12 hours the transformation was complete with the only product being compound **44**.

The final deprotection involved reaction in aqueous lithium hydroxide to hydrolyze the two remaining methyl esters. This reaction was complete in 1 hour and the final product, inhibitor **2**, was isolated and purified using ion-exchange chromatography. Inhibitor **2** was synthesized in 15 synthetic steps with a longest linear sequence of 13

steps and an overall yield of 6%. While the mass spectrum and ^{1}H NMR spectrum confirmed that inhibitor **2** had been formed and was reasonably pure, the ^{31}P NMR spectrum was extremely broad indicating that metal ions may be present in the sample. This material was used in inhibition studies without further purification. The final NMR spectra of inhibitor **2** can be found in the Appendix, Figures A.17 and A.18.

2.5 Inhibition Studies with Inhibitor 2

Inhibition studies with inhibitor **2** were completed by our collaborators in the Roll-Mecak lab at the Cell Biology and Biophysics Unit, National Institute of Neurological Disorders in Maryland, USA. *Xenopus tropicalis* tubulin tyrosine ligase was overproduced in *E. coli* as a glutathione S-transferase (GST)-fusion protein. The protein was purified by affinity chromatograpy, followed by proteolytic removal of the GST tag. The TTL protein was further purified by ion exchange chromatography, hydrophobic interaction chromatography and size exclusion chromatography. The purity and integrity of the TTL protein was verified by mass spectrometry.

The potency of inhibitor **2** was assayed with bovine brain tubulin as the substrate. Reactions were assembled at room temperature in MES buffer at pH 6.9 containing KCl, $MgCl_2$, DTT, ATP, Tyr (2% [^{3}H]-Tyr) and tubulin. The reactions were initiated by the addition of TTL and a variable concentration of inhibitor **2** (5, 50, 500, and 1000 μM), and reactions were incubated for 0-120 minutes. The tyrosinated tubulin was separated from free tyrosine and measured by scintillation counting (counts per minute, CPM).

The following data was obtained after 0, 1 and 2 hours at inhibitor **2** concentrations of 0, 5, 50, 500 and 1000 μM. The scintillation counting was plotted vs. time (Figure 2.57).

[Inhibitor 2]	Time = 0 h	Time = 1 h	Time = 2 h
0 μM	41.0 CPM	6449.5 CPM	7025.0 CPM
5 μM	54.0 CPM	6775.5 CPM	6851.0 CPM
50 μM	39.0 CPM	7500.5 CPM	7857.5 CPM
500 μM	-15.0 CPM	7105.5 CPM	7762.5 CPM
1000 μM	107.5 CPM	6285.0 CPM	6574.0 CPM

Table 2.1 Scintillation-counting data for various concentrations of inhibitor 2 at 0, 1 and 2 h with tubulin as substrate.

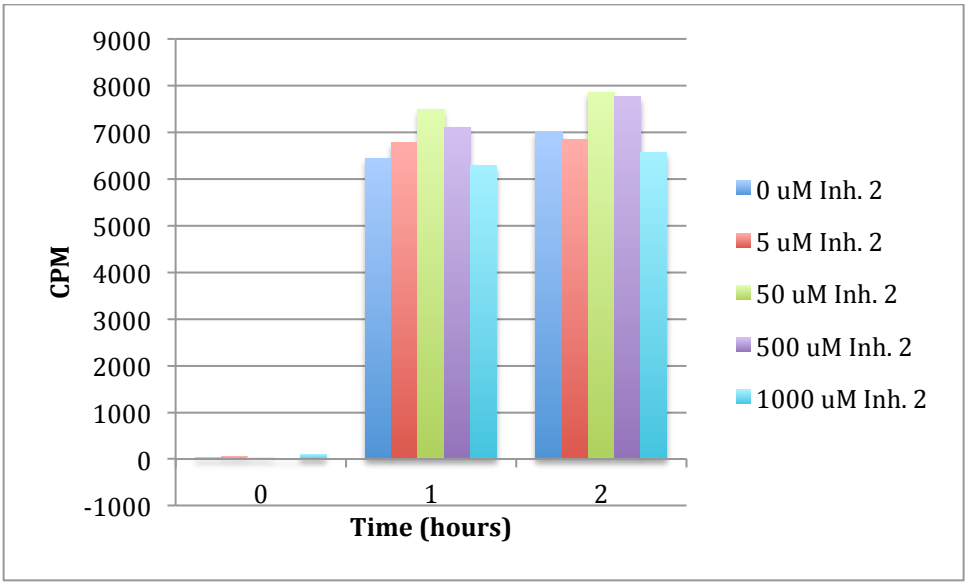

Figure 2.57 CPM vs time for various inhibitor 2 concentrations with tubulin as substrate.

After 1 hour, the amount of α-Tyr-tubulin detected when inhibitor **2** was not present (6449.5 CPM) was similar to the amount of α-Tyr-tubulin detected at various concentrations of inhibitor **2**. Even a concentration of 1000 μM of inhibitor **2** failed to substantially decrease the amount of α-Tyr-tubulin formed. A similar result was seen

after 2 hours; scintillation-counting data when inhibitor **2** was not present (7025 CPM) was similar to data when 1000 μM of inhibitor **2** was present (6574 CPM).

The activity of inhibitor **2** against tubulin was repeated using a similar assay method. However, this time inhibitor **2** was pre-incubated with TTL and ATP at 4 °C overnight followed by addition to the reaction mixture at room temperature. After 30 min, inhibitor **2** failed to substantially decrease the tyrosination of α-tubulin at 0.1 mM or 1 mM.

The activity of inhibitor **2** was also assayed with the C-terminal α-tubulin tail peptide as substrate. The 14-mer synthetic peptide (VDSVEGEGEEEGEE) was dissolved in MES buffer at pH 6.9 containing KCl, $MgCl_2$, DTT, ATP, and Tyr. The reaction was initiated by the addition of TTL and a variable concentration of inhibitor **2** (0.0, 0.1, 0.5, 1.0 mM). After 0-120 minutes at room temperature, aliquots were subjected to high-performance liquid chromatography (HPLC) using a reversed phase analytical column. The more hydrophobic product (VDSVEGEGEEEGEEY) is separated from the starting material peptide substrate and the quantities of both substrate and product peptides were estimated form the areas of the corresponding peaks on the UV detection absorbance spectrum.

The activity of TTL on the 14-mer synthetic peptide at various concentrations of inhibitor **2** was determined by comparison of product peak area when no inhibitor was present (0.0 mM) to the product peak area when inhibitor **2** was present. These activities were plotted against inhibitor **2** concentration (Figure 2.58).

[Inh. **2**]	0.0 mM	0.1 mM	0.5 mM	1.0 mM
Activity (%)	100	92	94	100

Table 2.2 Activity of TTL at various concentrations of inhibitor 2 with peptide as substrate.

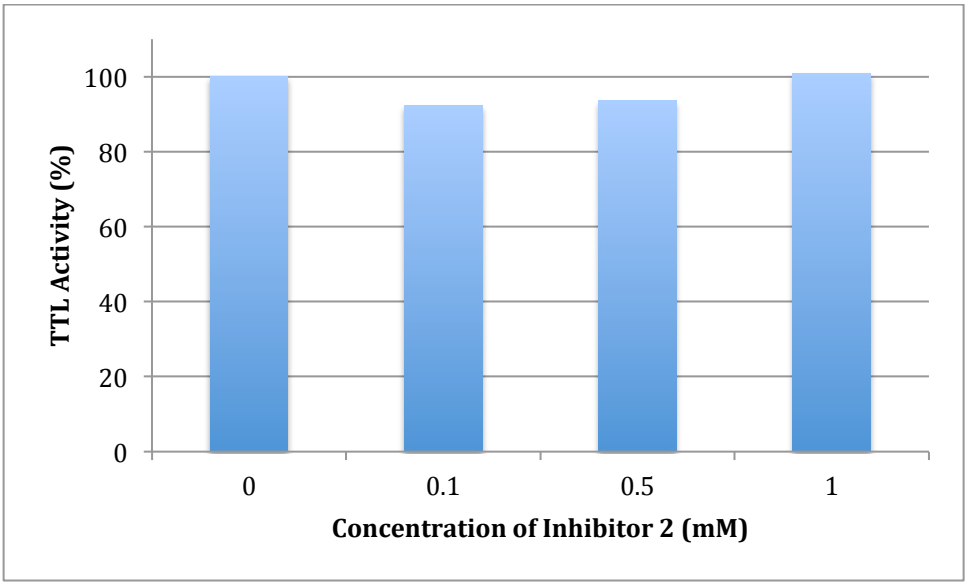

Figure 2.58 TTL activity vs. concentration of inhibitor 2 with peptide as substrate.

The activity of TTL on the C-terminal α-tubulin peptide tail was only marginally reduced to 92 % and 94 % in the presence of 0.1 mM and 0.5 mM of inhibitor **2**, respectively. A slight increase in TTL activity was seen in the presence of 1.0 mM of inhibitor **2**, but this is likely due to experimental error.

The ability of inhibitor **2** to inhibit the tyrosination of both tubulin and the C-terminal α-tubulin peptide tail was evaluated. No inhibition of TTL activity against tubulin was seen up to 1 mM of inhibitor **2**. Also, no substantial inhibition of TTL activity against the C-terminal α-tubulin peptide tail was seen up to 1 mM of inhibitor **2**. It can be concluded that inhibitor **2** does not inhibit the activity of TTL. A possible explanation for this result is that inhibitor **2** is too short to make important interactions

with the TTL enzyme. In particular, interaction with the positive strip of conserved TTL surface residues. Because of the higher flexibility in short peptides, inhibitor **2** might not adopt the correct conformation for sufficient interaction with the TTL enzyme. In a peptide substrate study by Rüdiger (1994) it was shown that the most important residues for TTL substrate activity were the three or four C-terminal residues of detyrosinated α-tubulin, (Glu)-Gly-Glu-Glu. Based on this study the next step for this research project is to synthesis longer inhibitors.

2.6 Summary and Conclusions

This chapter details the design and synthesis of inhibitor **1** and inhibitor **2**. After the evaluation of previously reported methods on phosphorus-carbon bond formation, the synthesis of inhibitor **1** was designed to include the synthesis of an H-phosphinic acid analogue of glutamic acid and the coupling of this analogue to an ethyl 2-(protected phenyl)acrylate. The H-phosphinic acid analogue of glutamic acid was synthesized by a method reported by Baylis (1984) and functional groups were protected by standard protecting group procedures. Starting from γ-butyrolactone, the protected H-phosphinic acid analogue of glutamic acid (**11**) was synthesized in 6 steps in 19% overall yield.

The ethyl 2-(protected phenyl)acrylate was synthesized by the copper mediated 1,4-conjugate addition of ethyl 2-(bromomethyl)acrylate (**14**) to a protected bromo-phenol. Ethyl 2-(4-(methoxymethoxy)benzyl)acrylate (**17**) was synthesized from ethyl acrylate in 3 steps in 10% overall yield. Ethyl 2-(4-(benzyloxy)benzyl)acrylate (**19**) was synthesized from ethyl acrylate in 3 steps in 11% overall yield.

Coupling between the protected H-phosphinic acid analogue of glutamic acid and the ethyl 2-(protected phenyl)acrylate was attempted in the presence of base and in the presence of a silyl-activating compound; neither method were successful.

It was hypothesized that the failure to couple was due to the presence of the glutamic acid side chain carboxylate. Attempts were made to mask the carboxylate with an amide and with an alkene, which would be converted back to the carboxylate after coupling. These modified methods also failed to produce inhibitor **1**.

At this point, the focus of the research project changed to the synthesis of a phosphonic acid containing inhibitor, inhibitor **2**. After the evaluation of previously reported methods on phosphorus-oxygen bond formation, the synthesis of inhibitor **2** was designed to include the oxidation of a glutamic acid H-phosphinic acid to a glutamic acid phosphonic acid analogue (**35**). This analogue was activated to a phosphonochloridate and coupled to a protected 4-hydroxyphenyllactic acid. The coupled product was deprotected to give inhibitor **2** starting from compound **11** in 7 steps in 32% overall yield.

Inhibitor **2** was sent to our collaborators and inhibition studies were completed. It was determined that inhibitor **2** had no activity, up to a 1 mM concentration, in inhibiting the tyrosination of α-tubulin or a C-terminal α-tubulin peptide tail. We postulate that as in the peptide substrate studies, a minimal peptide length is required for inhibition.

Future work in the study of the inhibition of tubulin tyrosine ligase will involve the synthesis of phosphonic acid containing inhibitors with an increased number of amino acid residues. The details of this work will be presented in Chapter 3.

2.7 Experimental Procedures

2.7.1 Materials and General Methods

All reagents were purchased from Alfa Aesar or Aldrich and were used without further purification unless otherwise noted. Silica gel chromatography was performed using Silica Gel SiliaFlash (230-400 mesh, Silicycle). The solvents triethylamine, dichloromethane and methanol were distilled over CaH_2 under inert atmosphere.

^{1}H NMR spectra were recorded on either a Bruker AV300 or Bruker AV400 spectrometer at field strengths of 300 or 400 MHz. Proton-decoupled ^{31}P NMR spectra were recorded on either a Bruker AV300 or Bruker AV400 spectrometer at field strengths of 121.5 or 162 MHz. Mass spectrometry was performed by electrospray ionization (ESI-MS) using an Esquire LC mass spectrometer. Neutral compounds were detected as positive ions, and negatively charged compounds were detected as negative ions.

2.7.2 Experimental Procedures in the Synthesis of Inhibitor 1

2.7.2.1 Methyl 4-Hydroxybutanoate (6)

A solution of triethylamine (120 mL, 1.2 mol) in methanol (300 mL) was charged with γ-butyrolactone **5** (15.2 mL, 0.2 mol), and the reaction mixture was stirred under an argon atmosphere for 12 h at rt. Triethylamine and methanol were removed under vacuum to yield a mixture of γ-butyrolactone and compound **6** (total 17.8 g molar ratio 3:1 product:starting material determined by ^{1}H NMR). The mixture was directly used in the next step without purification. ^{1}H NMR data was identical to that previously reported in the literature (Ohashi, 2004).

2.7.2.2 Methyl 4-Oxobutanoate (7)

A solution of methyl 4-hydroxybutanoate **6** (17.8 g, 0.15 mol) in dichloromethane (500 mL) was charged with pyridinium chlorochromate (45.0 g, 0.21 mol) and sodium acetate (2.0 g, 25 mmol) under an argon atmosphere. After stirring at rt for 1.5 h, the heterogenous reaction mixture was diluted with ether (300 mL) and filtered through Florisil. The filtrate was concentrated and Kugelrohr distilled (0.03 mmHg, 65 °C) to yield **7** (13.9 g, 90%) as a colorless oil. ^{1}H NMR data was identical to that previously reported in the literature (Gannett, 1988).

2.7.2.3 1-(Benzhydrylamino)-4-methoxy-4-oxobutylphosphinic Acid (8)

A 50% aqueous solution of hypophosphorous acid (10.2 mL) was concentrated to 100% hypophosphorus acid under vacuum at 50 °C. The concentrated acid was added to benzhydrylamine (17.2 mL, 100 mmol) in dioxane (600 mL) to form the diphenylmethylamine hypophosphite salt. The suspension was heated to 100 °C and compound **7** (10.9 g, 106 mmol) was added. The solution was heated to reflux under reduced pressure and water was removed azeotropically with dioxane. When 400 mL of the solvent volume had been removed, the reaction was cooled and ethanol (300 mL) was added. The diphenylmethylaminophosphinic acid slowly crystallized out of solution, was filtered off, washed with ethanol and then ether, and dried to yield **8** (13.8 g, 39%) as a white solid. ^{1}H and ^{31}P NMR data were identical to that previously reported in the literature (Baylis, 1984).

2.7.2.4 4-Amino-4-(hydroxyhydrophosphoryl)butanoic Acid (9)

Compound **8** (1.25 g, 3.5 mmol) was dissolved in an excess of 48% hydrobromic acid (15 mL) and heated to 100 °C until two distinct layers had formed (2 h). The

reaction mixture was evaportated to dryness and the resulting residue was taken up in water (15 mL) and washed with petroleum ether (3 × 15 mL). The aqueous layer was evaporated to dryness, cooled to 0 °C and taken up in ethanol (10 mL). Propylene oxide (20 mL) was layered on top and allowed to slowly diffuse through the solution at 4 °C. The mother liquor was decanted off and the resulting precipitate was rinsed with diethylether and dried under high vacuum to yield **9** in quantitative yield as a white solid, which was used without further purification. ^{1}H and ^{31}P NMR data were identical to that previously reported in the literature (Baylis, 1984).

2.7.2.5 4-(Benzyloxycarbonylamino)-4-(hydroxyhydrophosphoryl)butanoic Acid (10)

Compound **9** (3.5 mmol) was dissolved in water:dioxane (20 mL, 3:1) and cooled in an ice bath. Sodium bicarbonate (0.88 g, 10.5 mmol) was slowly added with stirring. Benzylchloroformate (0.75 mL, 5.3 mmol) was added dropwise via syringe over 10min, and the reaction was stirred for an additional 2 h at rt. The reaction was transferred to a separatory funnel and extracted with diethyl ether (3 × 20 mL). The aqueous layer was acidified to pH = 1 with 2 M HCl, transferred to a continuous liquid extractor and extracted for 12 h with ethyl acetate. The organic layer was dried with Na_2SO_4, filtered and concentrated under vacuum to yield **10** (0.99 g, 94%) as a colorless oil, which was used without further purification. ^{1}H NMR (300 MHz, CD_3OD) δ 7.37-7.30 (m, 5H), 6.9 (d, 2H, J = 539.9 Hz), 5.12 (s, 2H), 3.85-3.75 (m, 1H), 2.52-2.36 (m, 2H), 2.22-2.06 (m, 1H), 1.92-1.75 (m, 1H); ^{31}P NMR (121.5 MHz, CD_3OD) δ 30.36; ESI-MS *m/z* 300.3 $[M - H]^-$.

2.7.2.6 Cbz-Glu(OMe)PO(OMe)H (11)

Compound **10** (0.63 g, 2.1 mmol) was dissolved in dry methanol:dichloromethane (25 mL, 1:4) and put under an argon atmosphere. A 2 M solution of trimethylsilyldiazomethane in hexanes (2.7 mL) was added via syringe until a yellow color persisted. The reaction was stirred for an additional 20 min and concentrated under vacuum to yield crude **11** (two diastereomeric sets of enantiomers) as a colorless oil. Crude **11** was either carried on without further purification or purified by flash column chromatography (4:1 DCM/^{i}PrOH) to yield **11** (0.54 g, 78%) as a colorless oil. ^{1}H NMR (300 MHz, $CDCl_3$) δ 7.35 (s, 5H), 7.04 and 7.01 (dd, 1H, $J_{P\text{-}H}$ = 555.8 Hz), 5.43 and 5.20 (2d, 1H, J = 9.7 Hz), 5.12 (s, 2H), 4.13-3.99 (m, 1H), 3.82 and 3.80 (2d, 3H, J =11.1 Hz), 3.66 (s, 3H), 2.54-2.46 (m, 2H), 2.30-2.12 (m, 1H), 2.03-1.91 (m, 1H); ^{31}P NMR (121.5 MHz, $CDCl_3$) δ 35.74, 34.68; ESI-MS *m/z* 352.2 $[M\text{-}Na]^{+}$.

2.7.2.7 Ethyl 2-(Hydroxymethyl)acrylate (13)

Paraformaldehyde (24.7 g, 0.83 mol), 0.5 M phosphoric acid (3 mL), and water (80 mL) were heated at 90 °C for 1.5 h. The clear homogenous solution was cooled to rt and THF (80 mL), ethyl acrylate (**12**, 82 mL) and DABCO (8.4 g, 0.075 mol) were added. The reaction mixture was stirred for an additional 36 h at rt. The reaction was quenched with NaCl (30 g) and ether (80 mL). The aqueous layer was extracted with ether and the combined organic layers were washed with brine, dried over $MgSO_4$, filtered and concentrated under vacuum. The crude oil was purified by fractional distillation under reduced pressure (23 mmHg, 90 °C) to yield **13** (27.3 g, 28%) as a colorless oil. ^{1}H NMR data was identical to that previously reported in the literature (Byun, 1994 and Villieras, 1988).

2.7.2.8 Ethyl 2-(Bromomethyl)acrylate (14)

A solution of **13** (27.3 g, 0.21 mol) in anhydrous ether (250 mL) under an argon atmosphere was cooled to -5 °C. PBr_3 (9.2 mL, 0.10 mol) was slowly added via syringe and the reaction was stirred at rt for 3 h. The reaction was cooled to 0 °C and quenched with 150 mL of cold water. The aqueous layer was extracted with hexane and the combined organic layers were washed with brine, dried with Na_2SO_4, filtered and concentrated under vacuum. The crude yellow oil was distilled under reduced pressure (23 mmHg, 93 °C) to yield **14** (28.6 g, 70%) as a colorless oil. ^{1}H NMR data was identical to that previously reported in the literature (Villieras, 1988).

2.7.2.9 1-Bromo-4-(methoxymethoxy)benzene (16)

A solution of 4-bromophenol **15** (4.3 g, 25 mmol) in dichloromethane (200 mL) was charged with dimethoxymethane (19.0 g, 250 mmol) and phosphorus pentoxide (12.5 g, 88 mmol). The reaction mixture was stirred under an argon atmosphere at rt for 12 h. The reaction solution was decanted and quenched by the addition of saturated aqueous Na_2CO_3. The aqueous later was extracted with DCM (3 × 50 mL) and the combined organic extracts were washed with brine, dried over Na_2SO_4, filtered and concentrated under vacuum. The resulting crude oil was purified by flash column chromatography (6:1 hexanes/EtOAc) to yield **16** (4.81 g, 88%). ^{1}H NMR data was identical to that previously reported in the literature (Diemer, 2006 and Kubo, 2003).

2.7.2.10 Ethyl 2-(4-(Methoxymethoxy)benzyl)acrylate (17)

A solution of **16** (5.2 g, 24 mmol) in anhydrous THF (200 mL) under an argon atmosphere at -78 °C was charged with a solution of ^{n}BuLi in hexanes (1.5 M, 24 mL). After stirring at -78 °C for 1 h, the reaction mixture warmed to 0 °C and CuCN (2.4 g,

26.4 mmol) was added. After 30 min at 0 °C, the reaction was cooled to -78 °C and **14** (3.4 mL, 21.6 mmol) was added via syringe. After 30 min at -78 °C, the reaction was warmed to -10 °C for 10 min. The reaction was quenched with NH_4Cl and ice, followed by extraction with DCM. The combined organic extracts were washed with water, dried with Na_2SO_4, filtered and concentrated under vacuum. The resulting crude oil was purified by flash column chromatography (9:1 hexanes/EtOAc) to yield **17** (2.1 g, 39%). ^{1}H NMR (300 MHz, $CDCl_3$) δ 7.12 (d, 2H, *J* = 8.5 Hz), 6.97 (d, 2H, *J* = 8.5 Hz), 6.21 (s, 1H), 5.45 (s, 1H), 5.16 (s, 2H), 4.19 (d, 2H, *J* = 7.2 Hz), 3.58 (s, 2H), 3.49 (s, 3H), 1.28 (t, 3H, *J* = 7.0 Hz).

2.7.2.11 1-(Benzyloxy)-4-bromobenzene (18)

A solution of 4-bromophenol **15** (4.3 g, 25 mmol) in anhydrous DMF (100 mL) under an argon atmosphere was charged with K_2CO_3 (10.0 g, 75 mmol). Benzyl bromide (12.5 g, 88 mmol) was added and the reaction was stirred at rt for 12 h. The reaction solution quenched by water (100 mL) and extracted with EtOAc (3 × 50 mL) and the combined organic extracts were washed with brine, dried over Na_2SO_4, filtered and concentrated under vacuum to yield **18** (6.25 g, 95%) as a white solid, which was used without further purification. ^{1}H NMR data was identical to that previously reported in the literature (Sueki, 2013).

2.7.2.12 Ethyl 2-(4-(Benzyloxy)benzyl)acrylate (19)

A solution of **18** (3.0 g, 11.5 mmol) in anhydrous THF (100 mL) under an argon atmosphere at -78 °C was charged with a solution of ^{n}BuLi in hexanes (1.5 M, 9.2 mL). After stirring at -78 °C for 1 h, the reaction mixture warmed to 0 °C and CuCN (1.13 g, 12.7 mmol) was added. After 30 min at 0 °C, the reaction was cooled to -78 °C and **14**

(1.45 mL, 9.2 mmol) was added via syringe. After 30 min at -78 °C, the reaction was warmed to -10 °C for 10 min. The reaction was quenched with NH_4Cl and ice, followed by extraction with DCM. The combined organic extracts were washed with water, dried with Na_2SO_4, filtered and concentrated under vacuum. The resulting crude oil was purified by flash column chromatography (9:1 hexanes/EtOAc) to yield **19** (1.03 g, 40%). ^1H NMR data was identical to that previously reported in the literature (Yang, 2010).

2.7.2.13 Tetrahydro-2*H*-pyran-2-ol (25)

A solution of δ-valerolactone **24** (6.6 mL, 70 mmol) in dry dichloromethane at -78 °C was slowly charged with a solution of DIBAL-H in hexanes (1 M, 100 mL). After stirring at -78 °C for 3 h, the reaction was warmed to 0 °C and diluted with diethyl ether (100 mL). The reaction was quenched by the successive addition of water (4 mL), 15% NaOH (4 mL), and water (15 mL). The mixture as warmed to rt, dried with $MgSO_4$, filtered and concentrated under vacuum to yield **25** (5.1 g, 71%) as a yellow oil, which was used without further purification. ^1H NMR data was identical to that previously reported in the literature (Vinczer, 1990).

2.7.2.14 1-(Benzhydrylamino)-5-hydroxypentyl Phosphinic Acid (26)

A 50% aqueous solution of hypophosphorous acid (3.9 mL) was concentrated under vacuum to 100% hypophosphorus acid under vacuum at 50 °C. This was mixed with benzhydrylamine (6.6 mL, 100 mmol) in dioxane (150 mL) to form the diphenylmethylamine hypophosphite salt. The suspension was heated to 100 °C and **25** (4.3 g, 40.5 mmol) was added. The solution was heated to reflux under reduced pressure and water was removed azeotropically with dioxane. When 70 mL of the solvent volume had been removed, the reaction was cooled and ethanol (75 mL) was added. The

diphenylmethylaminophosphinic acid slowly crystallized out of solution, was filtered off washed with ethanol and then ether and dried to yield **26** (6.7 g, 50%) as a white solid. ^{1}H and ^{31}P NMR data were identical to that previously reported in the literature (Baylis, 1984).

2.7.2.15 1-Amino-5-hydroxypentylphosphinic Acid (27)

Compound **26** (1 g, 3.2 mmol) was dissolved in an excess of trifluoroacetic acid (7 mL) and heated to 100 °C until two distinct layers had formed (2 h). The reaction mixture was evaportated to dryness and the resulting residue was taken up in water (10 mL) and washed with petroleum ether (3 × 10 mL). The aqueous layer was evaporated to dryness. The resulting residue was taken up in hot ethanol (10 mL) and reconcentrated under vacuum until a precipate formed, yielding **27** (0.53 g, 98%) as a white solid, which was used without further purification. ^{1}H and ^{31}P NMR data were identical to that previously reported in the literature (Baylis, 1984).

2.7.2.16 1-(Benzyloxycarbonylamino)-5-hydroxypentylphosphinic Acid (28)

Compound **27** (1.65 g, 9.8 mmol) was dissolved in water:dioxane (50 mL, 5:1) and cooled in an ice bath. Sodium bicarbonate (2.5 g, 29.4 mmol) was slowly added while stirring. Benzylchloroformate (2.1 mL, 14.7 mmol) was added dropwise via syringe over 10 min, and the reaction was stirred for an additional 2 h at rt. The reaction was transferred to a separatory funnel and extracted with diethyl ether (3 × 20 mL). The aqueous layer was acidified to pH = 1 with 2 M HCl and transferred to a continuous liquid extractor and extracted for 12 h with ethyl acetate. The organic layer was dried with Na_2SO_4, filtered and concentrated under vacuum to yield **28** (2.3 g, 78%) as a colorless oil, which was used without further purification. ^{1}H NMR (400 MHz, CD_3OD)

δ 7.40-6.26 (m, 5H), 6.89 (d, 1H, J = 548.6 Hz), 5.10 (s, 2H), 4.04 (t, 2H, J = 6.6 Hz), 3.83-3.75 (m, 1H), 1.86-1.37 (m, 6H); ^{31}P NMR (162 MHz, CD_3OD) δ 31.68; ESI-MS *m/z* 300 $[M - H]^-$.

2.7.2.17 1-(Benzyloxycarbonylamino)-5-hydroxypentyl-methoxyphosphinic Acid (29)

Compound **28** (0.53 g, 1.7 mmol) was dissolved in anhydrous methanol:dichloromethane (25 mL, 1:4) and put under an argon atmosphere. A 2 M solution of trimethylsilyldiazomethane in hexanes (1.2 mL) was added via syringe until a yellow color persisted. The reaction was stirred for an additional 20 min and the reaction was quenched by the addition of acetic acid until a colorless solution persisted. The reaction was concentrated under vacuum to yield compound **29** in quantitative yield (two diastereomeric sets of enantiomers), which was carried on without further purification. ^{1}H NMR (400 MHz, $CDCl_3$) δ 7.36 (s, 5H), 7.01 and 6.99 (2d, 1H, J = 552.2 Hz), 5.48 and 5.32 (2d, 1H, J = 10.0 Hz), 5.14 (s, 2H), 4.10-3.97 (m, 1H), 3.85-3.76 (m, 3H), 3.68-3.63 (m, 2H), 1.87-1.40 (m, 6H); ^{31}P NMR (162 MHz, $CDCl_3$) δ 37.84, 36.99; ESI-MS *m/z* 338.4 $[M\text{-}Na]^+$.

2.7.2.18 1-(Benzyloxycarbonyamino)-5-(tosyloxy)pentyl-methoxyphosphnic Acid (30)

A solution of **29** (2.39 g, 7.6 mmol) in dry pyridine under argon atmosphere was charged with 4-toluenesulfonyl chloride (1.74 g, 9.12 mmol) at 0 °C. The reaction mixture was warmed to rt and stirred for 2.5 h. The reaction mixture was quenched by the addition of water (40 mL) and extractd with dichloromethane (3 × 30 mL). The combined extracts were washed with 1M HCl, saturated $NaHCO_3$ and brine, dried with

Na_2SO_4, filtered and concentrated to yield **30** (2.46 g, 70%) as a yellow oil. The compound was not pure by NMR. ESI-MS m/z 470.4 $[M - H]^+$.

2.7.3 Experimental Procedures in the Synthesis of Inhibitor 2

2.7.3.1 Methyl 4-((Benzyloxycarbonyl)amino))-4-(hydroxymethoxyphosphoryl)-butanoate (35)

A solution of **11** (4.2 g, 12.8 mmol) in dioxane:water (60 mL, 1:1) was treated with $NaIO_4$ (3.15 g, 14.7 mmol) and stirred at rt for 16 h. The red-orange heterogenous solution was filtered, and the filtrate was concentrated under vacuum. The resulting crude oil was redissolved in water (25 mL) and acidified with 2 M HCl until the pH reached 1. The aqueous solution was extracted with ethyl acetate (5 × 50 mL) and the combined extracts were dried with Na_2SO_4, filtered and concentrated under vacuum to yield **35** (3.83 g, 86%) as a white solid, which was used without further purification. ^{1}H NMR (300 MHz, CD_3OD) δ 7.39-7.27 (m, 5H), 5.10 (2, 2H), 4.14-3.97 (m, 1H), 3.70 (d, 3H, J = 10.6 Hz), 3.63 (s, 3H), 2.47-2.40 (m, 2H), 2.23-2.09 (m, 1H), 1.94-1.77 (m, 1H); ^{31}P NMR (121.5 MHz, CD_3OD) δ 25.94; ESI-MS *m/z* 344.2 $[M - H]^-$.

2.7.3.2 Methyl 4-((Benzyloxycarbonyl)amino))-4-(chloromethoxy-phosphoryl)-butanoate (36)

The phosphonate monoester **35** (1.2 g, 3.5 mmol) was dissolved in dichloromethane (30 mL) under an argon atmosphere and cooled to 0 °C. Freshly distilled thionyl chloride (0.5 mL, 7 mmol) was added to the solution dropwise via syringe over 10 min and after stirring at 0 °C for 1 h, was warmed to rt and stirred for an

additional 3 h. The reaction mixture was concentrated and dried under high vacuum for 1 h. The crude phosphonochloridate **36** was used immediately without further purification.

2.7.3.3 Methyl 2-Hydroxy-3-(4-hydroxyphenyl)propanoate (38)

A solution of 4-hydroxyphenyllactic acid (**37**, 1.0 g, 5.4 mmol) in anhydrous methanol:dichloromethane (120 mL, 1:5) under an argon atmosphere was charged with a 2 M solution of trimethylsilyldiazomethane in hexanes (3 mL). The reaction was stirred for 20 min and concentrated under vacuum to yield compound **38** in quantitative yield, which was carried on without further purification. ^{1}H NMR (300 MHz, CD_3OD) δ 6.65 (d, 2H, J = 8.4 Hz), 6.32 (d, 2H, J = 8.5 Hz), 3.92 (dd, 1H, J = 5.1, 7.4 Hz), 2.94 (s, 3H), 2.57 (dd, 1H, J = 5.1, 13.8 Hz), 2.46 (dd, 1H, J = 7.5, 13.8 Hz) ; ESI-MS *m/z* 195.3 $[M - H]^-$.

2.7.3.4 Methyl 2-Hydroxy-3-(4-(trityloxy)phenyl)propanoate (39)

A solution of **38** (1.05 g, 5.4 mmol) in anhydrous dichloromethane under an argon atmosphere was cooled to 0 °C and charged with triethylamine (1.2 mL, 8.1 mmol). After 10 min triphenylmethyl chloride (1.60 g, 5.9 mmol) was slowly added and the reaction was warmed to rt. After 2 h, the reaction mixture was concentrated under vacuum and the resulting crude solid was purified by flash column chromatography (4:1 hexanes/EtOAc) to yield **39** (2.28 g, 96%) as a white solid. ^{1}H NMR (400 MHz, $CDCl_3$) δ 7.39-7.28 (m, 15H), 7.08 (d, 2H, J = 8.5 Hz), 6.76 (d, 2H, J = 8.7 Hz), 4.43 (s, 1H), 3.81 (s, 3H), 3.07 (dd, 1H, J = 4.3, 13.9 Hz), 2.92 (dd, 1H, J = 6.4, 14.2 Hz).

2.7.3.5 Cbz-Glu(CO_2Me)-PO(OMe)-O-Tyr(OTr)-CO_2Me (40)

Compound **36** (1.2 g, 3.5 mmol) was dissolved in anhydrous dichloromethane under an argon atmosphere (30 mL) and cooled to 0 °C. Triethylamine (0.53 mL, 3.85) was slowly added to the solution and stirred for 10 min. A solution of **39** (1.54 g, 3.5 mmol) in dichloromethane (10 mL) was added and the reaction mixture was warmed to rt and stirred for 18 h. The reaction mixture was concentrated under vacuum and the resulting crude solid was purified by flash column chromatography (1:1 hexanes/EtOAc) to yield **40** (1.52 g, 57% over 2 steps) as a white solid (four diastereotopic sets of enantiomers). ^{1}H NMR (400 MHz, CD_2Cl_2) δ 7.48-7.42 (m, 5H), 7.37-7.21 (m, 15H), 6.90-6.81 (m, 2H), 6.61-6.60 (m, 2H), 5.08 (s, 2H), 5.03-4.86 (m, 1H), 4.18-3.95 (m, 1H), 3.70 (m, 3H), 3.67-3.60 (m, 6H), 3.15-2.96 (m, 2H), 2.44-2.27 (m, 2H), 2.17-1.61 (m, 2H); ^{31}P NMR (162 MHz, CD_2Cl_2) δ 26.16, 25.96, 25.43, 25.09; ESI-MS *m/z* 788 $[M - Na]^+$.

2.7.3.6 NH_2-Glu(CO_2Me)-PO(OMe)-O-Tyr(OH)-CO_2Me (41)

Compound **40** (0.22 g, 0.29 mmol) was dissolved in 20 mL of anhydrous MeOH and 10% Pd/C (31 mg) was added. The reaction mixture was placed under vacuum and then blanketed with H_2 (760 mmHg). This sequence was repeated twice to ensure a complete hydrogen atmosphere. The reaction mixture was stirred for 12 h; reaction progress was monitored by ESI-MS. The reaction mixture was filtered through Celite and the filtrate was and dried under high vacuum for 1 h. Crude **41** was used immediately without further purification.

2.7.3.7 AcNH-Glu(CO_2Me)-PO(OMe)-O-Tyr(OH)-CO_2Me (43)

A solution of compound **41** (0.1 g, 0.29 mmol) in anhydrous dichloromethane under an argon atmosphere was charged with acetic anhydride (2 mL, 21 mmol). After 5 h at rt, the reaction was quenched by the addition of water (15 mL). The aqueous layer was extracted with dichloromethane (5 × 15 mL) and the combined organic layers were dried with Na_2SO_4, filtered and concentrated under vacuum. The resulting crude residue was purified by flash column chromatography (9:1 DCM/^{i}PrOH) to yield **43** (four diastereotopic sets of enantiomers) (0.12 g, 96% over two steps) as a white solid. We estimate the compound is only 80% pure by the presence of unidentified peaks in the ^{1}H NMR spectrum. ^{1}H NMR (400 MHz, $CDCl_3$) δ 7.29-7.24 (m, 2H), 7.09-7.02 (m, 2H), 5.32-5.01 (m, 1H), 4.62-4.29 (m, 1H), 3.85-3.80 (m, 3H), 3.78 (s, 3H), 3.67 (s, 3H), 3.21-3.01 (m, 2H), 2.45-2.31 (m, 2H), 2.29 (s, 3H), 1.77-1.63 (m, 2H); ^{31}P NMR (162 MHz, $CDCl_3$) δ 25.75, 24.69, 24.31; ESI-MS *m/z* 454.2 $[M - Na]^+$.

2.7.3.8 AcNH-Glu(CO_2Me)-PO(OH)-O-Tyr(OH)-CO_2Me (44)

Compound **43** (0.08 g, 0.18 mmol) was dissolved in freshly distilled *tert*-butylamine (5 mL). A flame-dried condenser was attached and the reaction mixture was heated to reflux for 14 h. The reaction mixture was concentrated and dried under high vacuum to yield **44** in quantitative yield (two diastereotopic sets of enantiomers), which was used without further purification. ESI-MS *m/z* 416.2 $[M - Na]^-$.

2.7.3.9 AcNH-Glu(CO_2H)-PO(OH)-O-Tyr(OH)-CO_2H (Inhibitor 2)

Compound **44** (0.024 g, 0.057 mmol) was dissolved in water:dioxane (10 mL 1:1). A 0.5 M solution of $LiOH_{aq}$ was added until the pH of the solution reached 13 (≈1 mL). After 2 h the reaction mixture was acidified to pH = 6 with Amberlite 120-H (H^+

form) resin. The mixture was filtered and concentrated under vacuum. The crude product was dissolved in H_2O (0.5 mL) and loaded onto a 1 mL column of AG-1X8 resin (formate form). The column was washed successively with H_2O (10 mL), 1 M formic acid (20 mL), and 5 M formic acid (20 mL). The fractions that eluted using 5 M formic acid were reduced under vacuum and dissolved in water and evaporated to dryness to remove any residual formic acid in the mixture. The product was dissolved in H_2O (3 mL) and stirred with Amberlite DP-1 (sodium form) resin until the pH of the solution reached 7.0. The solution was then filtered, frozen, and lyophilized to give inhibitor **2** as the trisodium salt (15.3 mg, 69%) (two diastereotopic sets of enantiomers). The compound appeared pure by ^{1}H NMR spectroscopy, however the very broad ^{31}P NMR spectrum indicated that metal impurities may be present. ^{1}H NMR (400 MHz, D_2O) δ 7.14 (d, 2H *J* = 8.0), 6.81 (d, 2H *J* = 8.0), 4.18 (s, 1H), 3.99-3.82 (m, 1H), 3.06-2.91 (m, 1H), 2.89-2.72 (m, 1H), 2.25-2.12 (m, 2H), 2.12-2.03 (m, 1H), 2.00 (s, 3H), 1.82-1.65 (m, 1H); ^{31}P NMR (162 MHz, D_2O) δ 17.70; ESI-MS *m/z* 388.2 $[M - Na]^-$.

2.7.4 Experimental Procedures in the Inhibition Studies of Inhibitor 2

The following experimental procedures were completed by our collaborators in the Roll-Mecak lab at the Cell Biology and Biophysics unit, National Institute of Neurological Disorders in Maryland, USA.

2.7.4.1 Protein Expression and Purification

X. tropicalis tubulin tyrosine ligase was transformed into BL21 Rosetta (DE3) pLysS *E. coli.* as a GST-fusion protein. Protein expression wa induced with 0.5 mM isopropyl β-D-galactopyranoside (IPTG) for 16 h at 16 °C. The cells were lysed using a microfluidizer, and the cellular debris was removed by centrifugation at 100,000 xg for 1

h. The protein was purified by a GST resin column (GE Healthcare), followed by proteolytic removal of the GST tag with TEV protease. The TTL protein was further purified by ion exchange chromatography, hydrophobic interaction chromatography and size exclusion chromatography. The structure and integrity of the TTL protein was verifed by mass spectrometry (Szyk, 2011).

2.7.4.2 TTL Activity Assay Against Inhibitor 2 with Tubulin as Substrate

Tyrosination of bovine brain tubulin (Cytoskeleton) by TTL was assayed against variable concentrations of inhibitor **2**. Reactions were assembled in MES buffer (50 mM, pH = 6.9) containing KCl (100 mM), $MgCl_2$ (10 mM), DTT (1 mM), ATP (2.0 mM), tyrosine (0.3 mM, 2% [^{3}H]-Tyr) and tubulin (10 μM). The reaction was initiated by the addition of TTL (1 μM) and a variable concentration of inhibitor **2** (5, 50, 500, and 1000 μM), and it was incubated for 0-120 minutes. The tyrosinated tubulin was separated from free tyrosine on a filter that binds tubulin with high affinity and the excess tyrosine was washed away. Filter-bound radioactive Tyr-tubulin was measured by scintillation counting (CPM) (Kormendi, 2012).

2.7.4.3 TTL Activity Assay Against Inhibitor 2 with Peptide as Substrate

Tyrosination of a C-terminal α-tubulin tail peptide (VDSVEGEGEEEGEE) was assayed against variable concentrations of inhibitor **2**. Reactions were assembled in MES buffer (50 mM, pH = 6.9) containing KCl (100 mM), $MgCl_2$ (10 mM), DTT (1 mM), ATP (2.5 mM), tyrosine (0.3 mM) and synthetic peptide. The reaction was initiated by the addition of TTL (1 μM) and a variable concentration of inhibitor **2** (0.0, 0.1, 0.5, 1.0 mM). After 0-120 minutes at room temperature, 25 μL of reaction mixture was mixed with an equal volume of 0.1% trifluoroacetic acid and subjected to high-resolution liquid

chromatography (HPLC) using a reversed phase (RP) analytical column. The more hydrophobic product (VDSVEGEGEEEGEEY) was separated from the starting material peptide substrate using an acetonitrile gradient (5-35% in 30 minutes) in 0.05% trifluoroacetic acid as an eluent. Quantities of both substrate and product peptides were estimated from the areas of the corresponding peaks on the UV detection absorbance spectrum (Szyk, 2011).

Chapter 3: Design and Synthesis of a Phosphonic Acid Tripeptide and Pentapeptide Inhibitor for the Inhibition of TTL

This chapter details the synthesis of inhibitors **3** and **4** for the inhibition of TTL. Literature examples of improving inhibition by elongating the amino acid chain of the phosphorous- containing inhibitors are reviewed and applied towards the synthesis of extended inhibitors. Research completed towards the synthesis of the tripeptide phosphonic acid analogue inhibitor, inhibitor **3**, is reported. Due to complications in the final deprotection step and the final purification, the synthesis of inhibitor **3** was not completed. Research efforts were directed towards the synthesis of the pentapeptide phosphonic acid inhibitor, inhibitor **4**. The completed synthesis of inhibitor **4** is reported, followed by a discussion on the inhibition studies of inhibitor **4** with TTL. Finally, the future of this research project is discussed.

3.1 Improving Inhibitor Activity by Extending Inhibitor Length

Thermolysin, a zinc-containing metalloendoprotease, specifically cleaves the N-terminal side of larger hydrophobic residues such as leucine, phenylalanine, isoleucine and valine. Phosphoramidon was the first phosphorus-based compound that demonstrated potent inhibition of thermolysin (Figure 3.1). Phosphoramidon is a phosphonic acid-containing chemical compound isolated from a culture filtrate of *Streptomyces tanashiensis* (Umezawa, 1972). It was shown to be a potent inhibitor of thermolysin with a K_i of 0.034 μM (Kam, 1979).

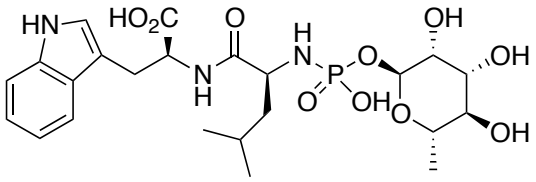

Figure 3.1 Structure of Phosphoramidon.

Phosphoramidon did not inhibit other proteases such as trypsin, papain, α-chymotrypsin or pepsin (Suda, 1973). A crystallographic study of the thermolysin-phosphoramidon complex confirmed that phosphoramidon was binding to the active site and resembled the tetrahedral intermediate of the thermolysin-catalyzed peptide bond hydrolysis (Weaver, 1977).

These results prompted the exploration of various *N*-phosphorylated amino acids and peptides. Phosphorylated amino acids showed moderate inhibition; a K_i of 1.3 μM and a K_i of 73 μM were reported for phosphorylated leucine and phenylalanine, respectively (Figure 3.2) (Kam, 1979).

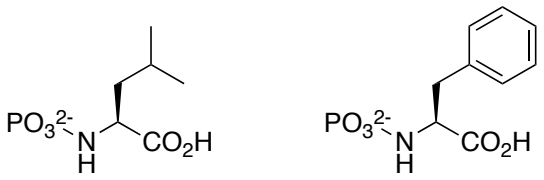

Figure 3.2 Phosphorylated amino acid inhibitors of thermolysin (Kam, 1979).

Increasing the inhibitor length to an *N*-phosphorylated dipeptide resulted in a dramatic increase in inhibition; a K_i of 0.019 μM and a K_i of 0.015 μM were reported for phosphorylated leucine-phenylalanine and phosphorylated leucine-tryptophan, respectively (Figure 3.3) (Kam, 1979).

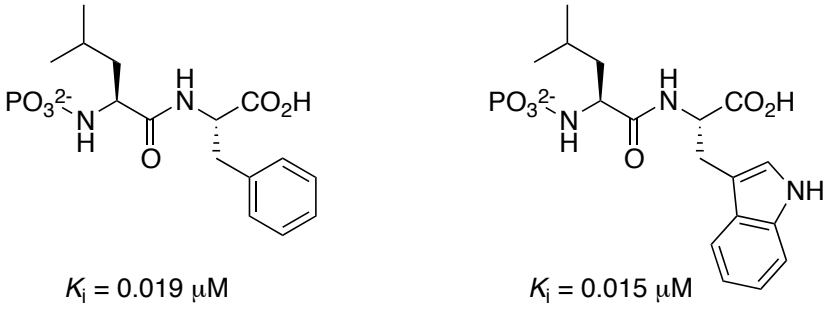

Figure 3.3 Phosphorylated dipeptide inhibitors of thermolysin (Kam, 1979).

This was carried a step further by the synthesis of phophoramidate tripeptide analogues. In these compounds the phosphorus moiety was placed between two amino acid residues, therefore even more closely resembling the reaction intermediate. The K_i for the tripeptide phosphonamidate Cbz-Gly-P-Leu-Leu was determined to be 9.1 nM (Figure 3.4) (Bartlett, 1987).

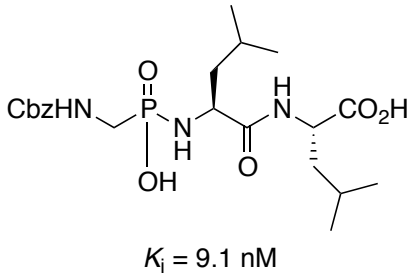

Figure 3.4 Tripeptide Cbz-Gly-P-Leu-Leu inhibitor of thermolysin (Bartlett, 1987).

By increasing the length of the enzyme amino acid recognition sequence, the level of inhibitor potency drastically increased. This is due to increased interactions between the enzyme active site and inhibitor.

This strategy was applied to the synthesis of phosphorylated inhibitors of carboxypeptidase A (CPA). CPA, a zinc-containing metalloprotease, cleaves C-terminal amino acids with a preference for the aromatic residues phenylalanine and tyrosine.

Starting with a phosphorylated amino acid, phosphorylated phenylalanine showed moderate inhibition with a K_i of 5.0 μM (Figure 3.5) (Kam, 1979). Increasing the size of the inhibitor to a dipeptide phosphonamide resulted in a dramatic increase in inhibition. A K_i of 90 nM was measured for the Cbz-protected dipeptide glycine-phenylalanine (Jacobsen, 1981). Synthesis of the tripeptide phosphonic acid inhibitor resulted in a further dramatic increase in inhibition; a K_i of 3 pM was measured for the Cbz-protected tripeptide Ala-Ala-P(O)-Phe (Figure 3.5) (Hanson, 1989).

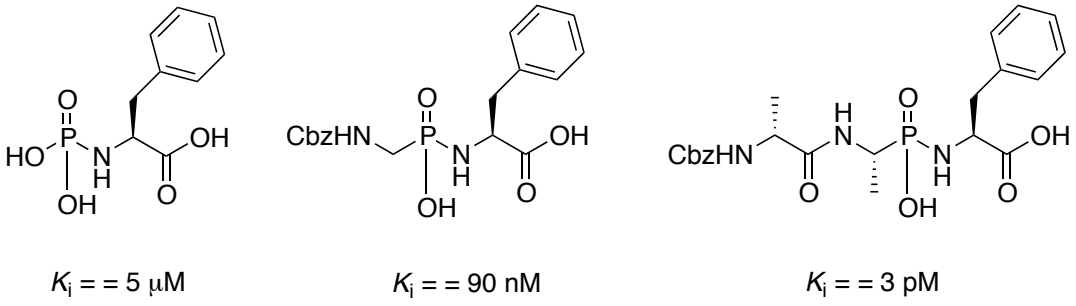

Figure 3.5 Phosphorylated amino acid, dipeptide and tripeptide inhibitors of CPA.

Inhibition of both thermolysin and CPA by phosphorus-based amino acid analogue inhibitors improved as the length of the inhibitor was increased. This clearly demonstrates that "remote" interactions can be crucially important in obtaining potent inhibition in peptide-bond inhibitors.

3.2 Strategies for Inhibitor 3 Synthesis

The dipeptide phosphonic acid analogue inhibitor, inhibitor **2**, failed to inhibit TTL activity, therefore the next logical step was to synthesize the tripeptide phosphonic acid analogue inhibitor, inhibitor **3**. The structure of inhibitor **3** differs from the structure of inhibitor **2** by the addition of a glutamic acid residue (Figure 3.6). This residue was added with the aim of increasing inhibitor activity by increasing the interactions between

enzyme and inhibitor. The N-terminus of inhibitor **3** is acetylated in order to remove the positive charge that would not be present at the C-terminus of tubulin. The second glutamic acid could be added to inhibitor **2** using standard peptide coupling procedures.

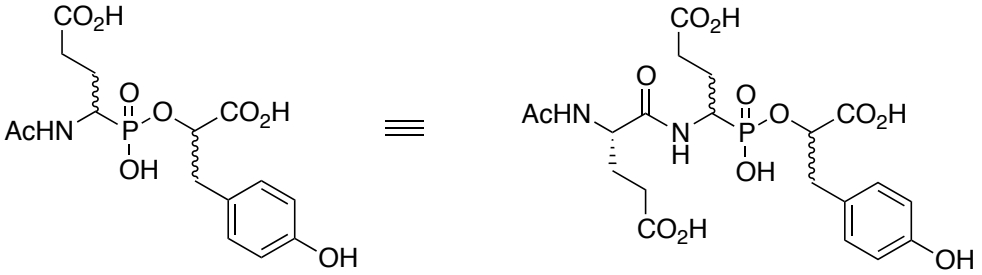

Inhibitor **2** - Glu-P-Tyr Inhibitor **3** - **Glu**-Glu-P-Tyr

Figure 3.6 Structure of inhibitor 3.

3.2.1 Methods in Peptide Bond Formation

In a typical peptide bond formation reaction, the carboxylic acid of one amino acid is activated by a peptide-coupling reagent and then reacted with an amine of another amino acid (Figure 3.7).

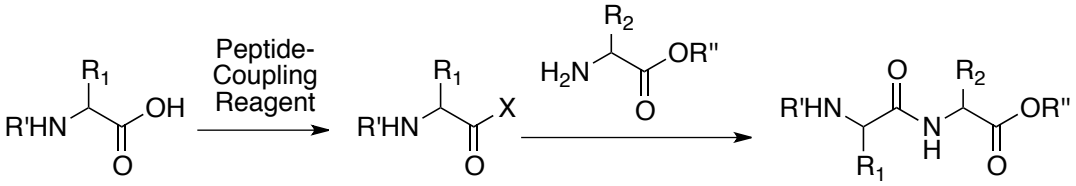

Figure 3.7 Typical peptide bond formation reaction.

The controlled formation of a peptide bond requires the use of protecting groups. To avoid undesired coupling products and side reactions, appropriate protecting groups for the C-terminus, N-terminus and side chains are required. The carboxylic acid is commonly protected as an alkyl or aryl ester. A methyl ester is stable under most coupling conditions and is easily removed by base hydrolysis, however, selectivity can be

problematic and the basic conditions can lead to substrate epimerization. A benzyl ester is easily prepared and can be removed either by treatment with strong acid or by the milder alternative, hydrogenolysis. A *tert*-butyl ester is a useful C-terminal protecting group because it is stable to base-catalyzed hydrolysis, hydrogenolysis and weak acids. The *tert*-butyl ester is selectively removed by treatment with trifluoroacetic acid or treatment with dilute hydrochloric acid. These three protecting groups offer different carboxylated deprotection methods.

The N-terminal amine is most commonly protected with a carbamate, such as benzyloxycarbonyl (Cbz or Z), 9-fluorenylmethyloxycarbonyl (Fmoc), or *tert*-butyloxycarbonyl (Boc). The use of these protecting groups also avoids racemization. To prepare the Cbz protected amine, benzyloxycarbonyl chloride is allowed to react with the amino acid under basic conditions. This protecting group is removed by catalytic hydrogenolysis of the benzylic C-O bond, followed by decarboxylation of the carbamic acid. The Fmoc is prepared by reaction of the free amine with Fmoc-Cl, but cleavage is performed under mild base conditions. Because *tert*-butyl chlorofomate is unstable, the Boc protected amine is prepared by reaction with *tert*-butyl dicarbonate. Instead of hydrogenolysis or base, the protecting group is removed by treatment with trifluroacetic acid at room temperature. These three protecting groups offer different methods of amine deprotection, which is beneficial when side chain functional groups are present.

Amino acid side chain functional groups are protected to avoid side reactions and incorrect coupling products. The side chain protecting groups must be stable under conditions employed to remove N- and C-terminal protecting groups. Side chain functionalities that require protection include the ε-amino group of Lys, the β-mercapto

group of Cys, the β- and γ-carboxyl group of Asp and Glu, the aliphatic hydroxyl group of Ser and Thr, the phenolic hydroxyl group of Tyr, the δ-guanidine group of Arg and the imidazole nitrogen of His, and the indole nitrogen of Trp (Okada, 2001).

The stepwise elongation from the C-terminus by one amino acid is an effective method for the synthesis of small peptides. Avoiding racemization is a main concern in the stepwise elongation procedure. Activating the carboxylic acid with a peptide-coupling reagent and using an appropriate racemization-suppressing agent (HOBt) is helpful in avoiding racemization. The racemization suppressor can also play a role in enhancing reaction rate (Han, 2004). There are numerous coupling reagents available; the most common are phosphonium reagents (BOP), uronium reagents (HBTU), carbodiimide reagents (DCC), and organophosphorus reagents (DPPA) (Han, 2004). The carbodiimide reagent DCC is the most widely used coupling reagent in peptide synthesis for both solid phase and solution methods.

3.3 Synthesis of Inhibitor 3

The synthesis of inhibitor **3** can be divided into two sections: peptide bond formation (**Section 3.3.1**), and the deprotection and purification of inhibitor **3** (**Section 3.3.2**) (Figure 3.8). As with inhibitors **1** and **2**, it will initially be prepared as a mixture of diastereomers about the "Phe" and "Glu" centers. If potent inhibition is observed further studies will focus on isolating/synthesizing individual stereoisomers.

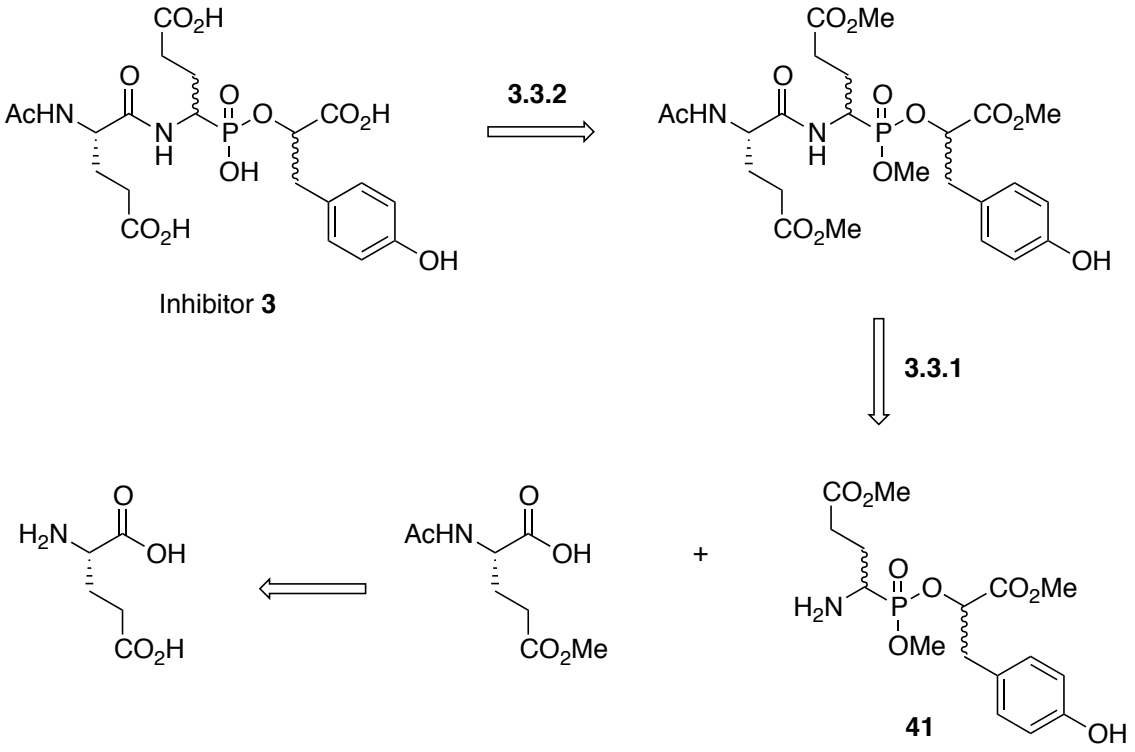

Figure 3.8 Retrosynthesis of inhibitor 3.

3.3.1 Peptide Bond Formation

Elongation of the dipeptide inhibitor to a tripeptide inhibitor involved coupling a protected glutamic acid residue to the dipeptide phosphonate (compound **41**). Ideally, the glutamic acid amine would be protected with an acetyl group and the carboxylic acid side chain would be protected as a methyl ester. Keeping consistent with inhibitor **2**, the acetyl cap functions to mimic the continuation of the α-tubulin peptide sequence. Use of a methyl ester keeps the carboxylic acid protecting groups consistent and simplifies the final deprotection. The glutamic acid mono-methyl ester was prepared by first mixing thionyl chloride with methanol to generate HCl *in situ*. Addition of glutamic acid resulted in Fischer esterification of the γ-carboxylate (Cox, 2001). The hydrochloride salt was isolated in 82% yield. An aqueous solution of the glutamic acid methyl ester

hydrochloride (**47**) was treated with acetic anhydride and base to yield the acetylated glutamic acid methyl ester in 83% yield (Figure 3.9).

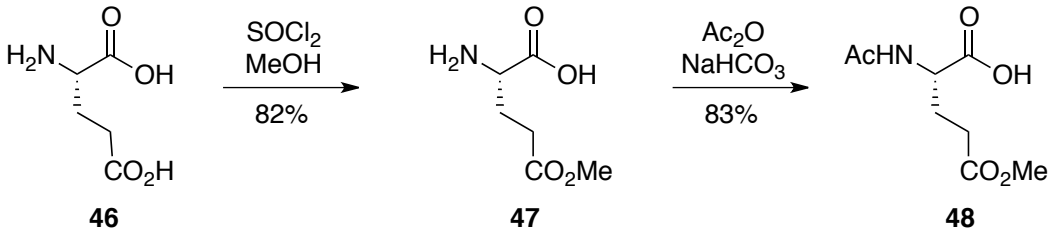

Figure 3.9 Synthesis of the acetylated glutamic acid methyl ester 48.

In the first coupling attempt, compound **48** was activated with DCC and then reacted with compound **41**. After three hours at room temperature mass spectrometry and TLC analysis revealed that only intramolecular cyclized product had formed (Figure 3.10).

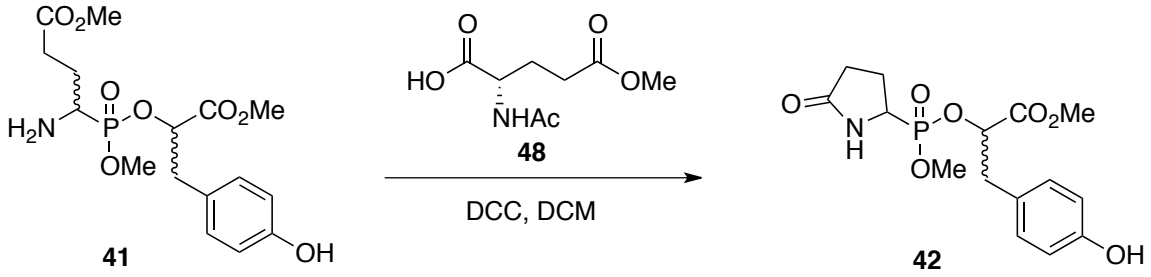

Figure 3.10 DCC mediated coupling reaction.

The competing intramolecular cyclization reaction is kinetically more favorable than the coupling reaction between the dipeptide phosphonate analogue and the protected glutamic acid. In order to reduce the amount of cyclized product formed, we needed to minimize the amount of time compound **41** was in solution and maximize the reactivity of the activated carboxylic acid.

Carboxylate groups activated as an N-hydroxysuccinimide (NHS) ester are highly reactive towards amine nucleophiles. A common method for synthesizing an NHS ester involves mixing NHS with a carboxylic acid in the presence of a carbodiimide-coupling reagent such as DCC or EDC (Figure 3.11). NHS derivatives are relatively stable and can be isolated, purified and stored at low temperatures. Reaction of the NHS ester with an amine releases NHS as the leaving group and forms an amide bond (Hermanson, 2013).

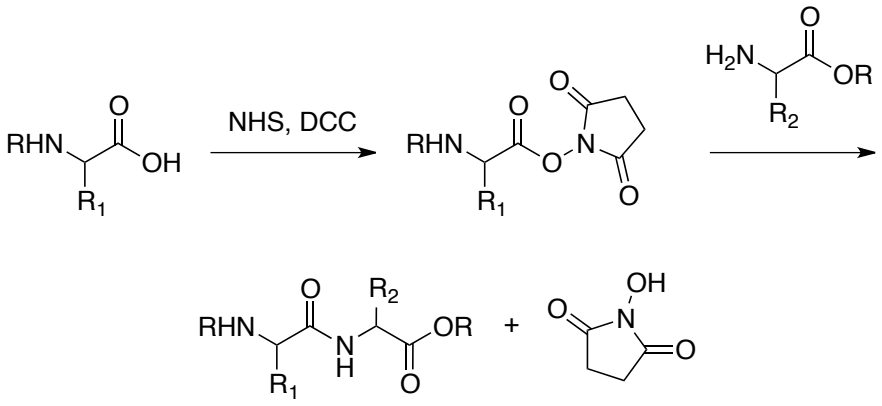

Figure 3.11 NHS-activated peptide coupling.

NHS activated amino acids are commercially available. While the acetylated analogue of glutamic acid was not commercially available, the Cbz and methyl ester protected NHS ester (Z-Glu(OMe)-OSu **49**) was. A base-catalyzed coupling between compound **49** and **41** was attempted; after 3 hours at room temperature TLC and mass spectrometry analysis revealed that only intramolecular cyclized product had formed (Figure 3.12).

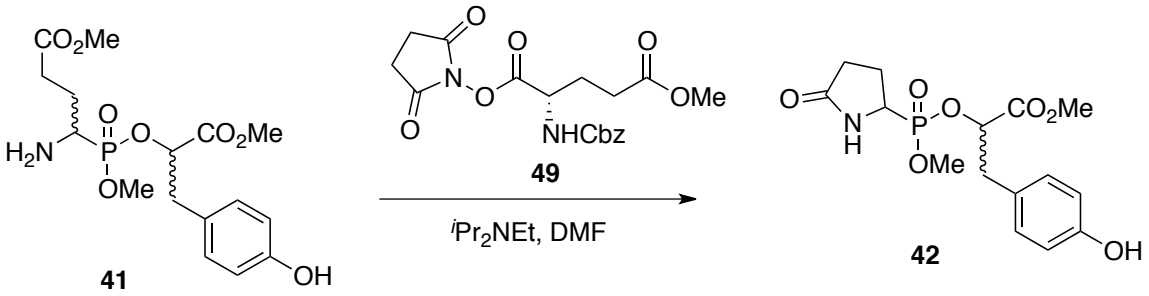

Figure 3.12 Base-catalyzed NHS-activated coupling.

In the synthesis of inhibitor **2**, base-catalyzed acetylation of **41** with acetic anhydride in pyridine also resulted in cyclized product **42**. To avoid the formation of this cyclized side product, the base was omitted and an excess of acetic anhydride was used. This revised procedure was applied to the coupling reaction between compounds **41** and **49**; the *N*,*N*-diisopropylethylamine was omitted and a large excess of Z-Glu(OMe)-OSu was used (10 equivalents). After 12 hours at room temperature, formation of the fully protected tripeptide phosphonate analogue **50** was verified by TLC and mass spectrometry (Figure 3.13).

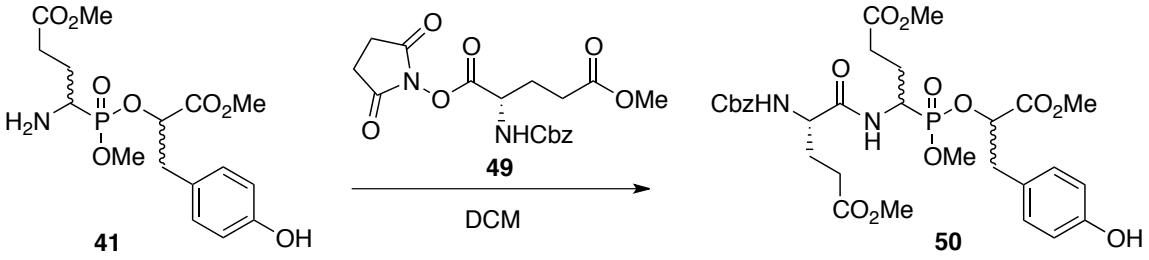

Figure 3.13 Synthesis of compound 50.

The crude reaction mixture was difficult to purify because of the large excess of Z-Glu(OMe)-OSu. With the aim of simplifying the purification, the coupling reaction was repeated using a reduced amount of **49** (5 equivalents). After three purifications by silica gel flash column chromatography, a mixture of **50** and **49** remained. In an effort to

make the fully protected tripeptide phosphonate analogue more non-polar and easier to purify by silica gel flash column chromatography, the methyl ester of **49** was substituted with a *tert*-butyl ester. Using 2 equivalents of Z-Glu(O^{t}Bu)-OSu (**51**), the tripeptide phosphonate analogue **52** was formed after 12 hours at room temperature. Compound **52** was successfully isolated and purified by silica gel flash column chromatography in 43% yield (Figure 3.14).

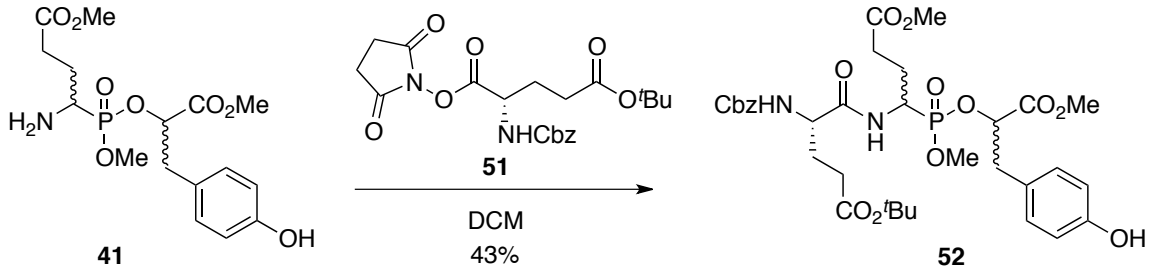

Figure 3.14 Synthesis of compound 52.

3.3.2 Deprotection and Purification of Inhibitor 3

The deprotection of **52** was approached in a similar manner to the deprotection of **40** in the synthesis of inhibitor **2**. The first step was the removal of the benzyloxy carbamate group by treatment with palladium on carbon under hydrogen atmosphere (Figure 3.15).

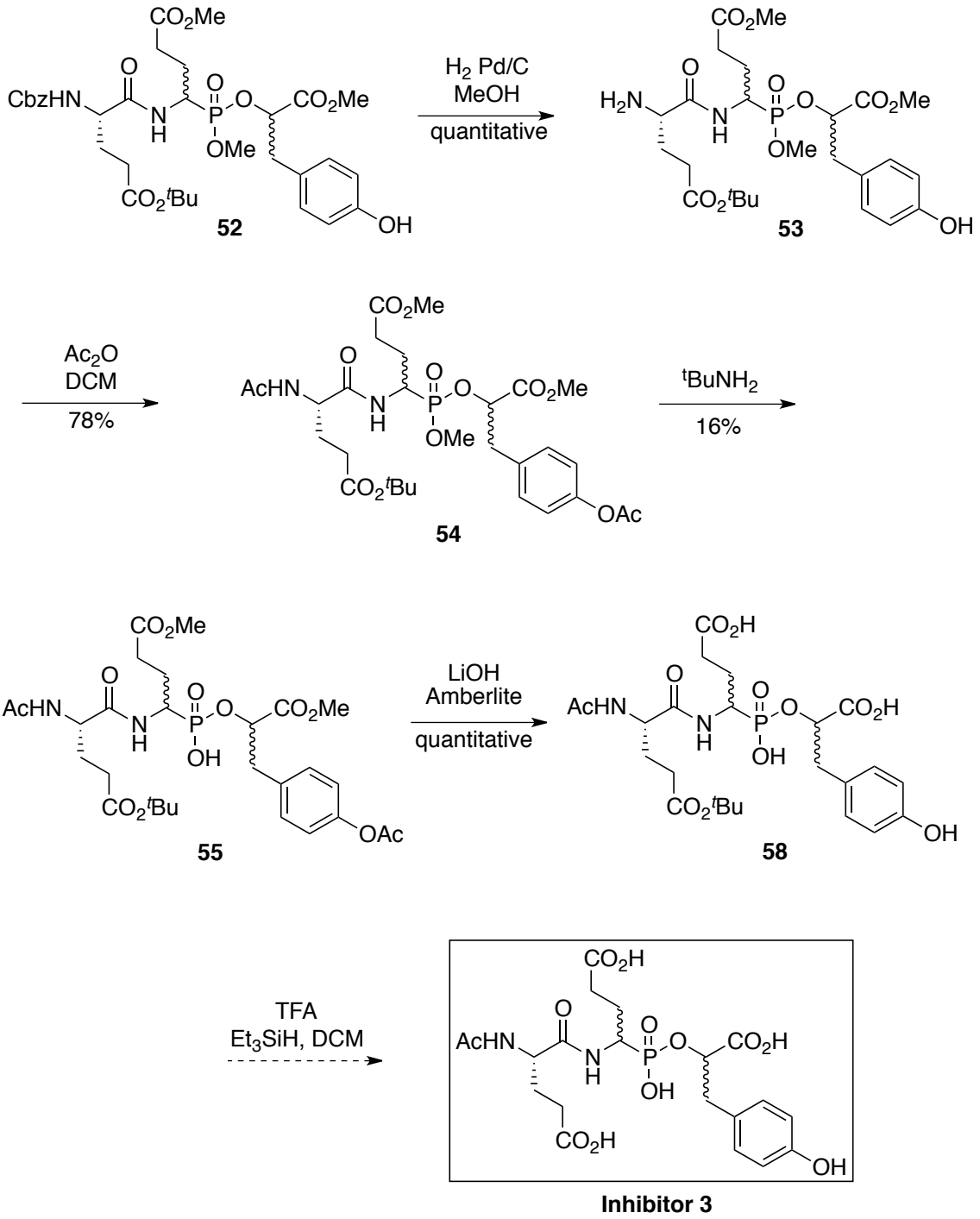

Figure 3.15 Deprotection of inhibitor 3.

Unlike inhibitor **2**, an intramolecular cyclization reaction was not a principle concern at this step, because the adjacent methyl ester had been replaced with a *tert*-butyl

ester. The resulting free amine of **53** was capped with an acetyl group in order to mimic the continuation of the α-tubulin peptide chain. Treatment with excess acetic anhydride in dichloromethane resulted in the diacetylated product **54**, where the free amine and the phenol were both acetylated. Compound **54** was purified by silica gel flash column chromatography in 78% yield.

As seen in the synthesis of inhibitor **2**, the deprotection of the phosphonate methyl ester was accomplished by nucleophilic displacement of the phosphonate anion from the methyl group. At this step in the synthesis, the principle concern is the hydrolysis of the tyrosine residue, to form compound **57**. Compound **54** was heated to reflux in *tert*-butylamine for 12 hours. The reaction progress was followed by mass spectrometry analysis. Even though anhydrous conditions were employed, a mixture of compounds **55**, **56** and **57** was seen (Figure 3.16).

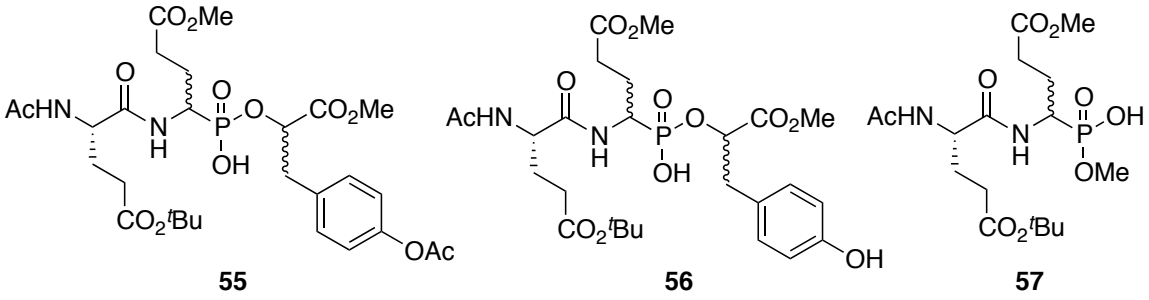

Figure 3.16 Structure of compounds 55, 56 and 57.

Purification of the mixture by silica gel flash column chromatography resulted in isolation of compound **55** in 16% yield. Compounds **56** and **57** coeluted and were never successfully separated.

The methyl esters were hydrolyzed by reaction of compound **55** in aqueous lithium hydroxide. The reaction was monitored by TLC analysis and after 4 hours at

room temperature the reaction was acidified with Amberlite 120-H resin (H^+ form) and compound **58** was carried on without further purification. It should be noted that some racemization of the L-Glu residue could have occurred under these reaction conditions. No attempt was made to quantify this possibility.

Removal of the final protecting group, the *tert*-butyl ester, was attempted by reaction with trifluoroacetic acid in the presence of triethylsilane. The reaction, monitored by mass spectrometry and ^{1}H NMR spectroscopy, never went to completion. Various methods of purification were used in an attempt to purify inhibitor **3**: silica gel flash column chromatography, preparative TLC and a column of AG-1X8 resin (formate form). Unfortunately, inhibitor **3** was never successfully isolated; the compound was either lost or decomposed during purification.

Due to complications in the final deprotection step and in the final purification, the synthesis of inhibitor **3** was not completed. Instead of revising the synthetic design of inhibitor **3** to exclude *tert*-butyl ester groups, research efforts were directed towards the synthesis of inhibitor **4**.

3.4 Synthesis of Inhibitor 4

Inhibitor **4** is a pentapeptide inhibitor where the structure is based on the amino acid sequence of the α-tubulin peptide tail. It consists of a Glu-Gly-Glu-Glu-Tyr peptide chain, with a phosphonic acid replacing the amide bond between the glutamic acid and tyrosine residues (Figure 3.17).

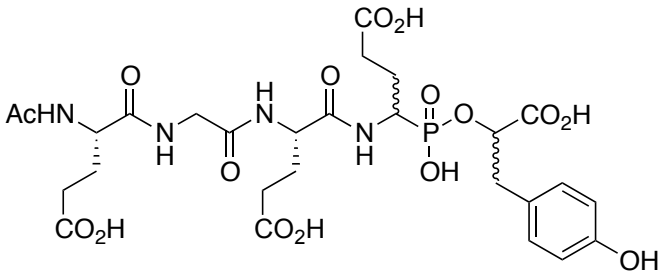

Figure 3.17 The structure of inhibitor 4.

We decided to synthesize the pentapeptide inhibitor (EGEEY) over the tetrapeptide inhibitor (GEEY) because it contained an additional glutamic acid residue that may provide key active site interactions. As discussed previously, the crystal structure of TTL revealed a strip of positively charged residues that extend down the length of the enzyme. The α-tubulin peptide tail (VDSVEGEGEEEGEEY) contains many negatively charged glutamic acid residues that interact with this strip of positively charged surface residues. It was hypothesized that the increased number of glutamic acid residues in inhibitor **4** would increase its interaction with the TTL enzyme and improve inhibition.

Typically, peptide chains are elongated by the sequential addition of single amino acid residues to the parent dipeptide. This linear synthetic method was employed in the synthesis of inhibitor **3**. Because of the low overall synthetic yield in the synthesis of compound **41** (Glu-P(O)-Tyr), a convergent synthetic approach was employed in the synthesis of inhibitor **4**; compound **41** was coupled to the Glu-Gly-Glu tripeptide (Figure 3.18). The synthesis of inhibitor **4** can be divided into two sections: the synthesis of the protected Glu-Gly-Glu tripeptide (**Section 3.4.1**), and synthesis of the phosphonic acid containing pentapeptide (**Section 3.4.2**). As with inhibitors **1** and **2**, it will initially be prepared as a mixture of diastereomers about the "Phe" and "Glu" centers. If potent

inhibition is observed further studies will focus on isolating/synthesizing individual stereoisomers.

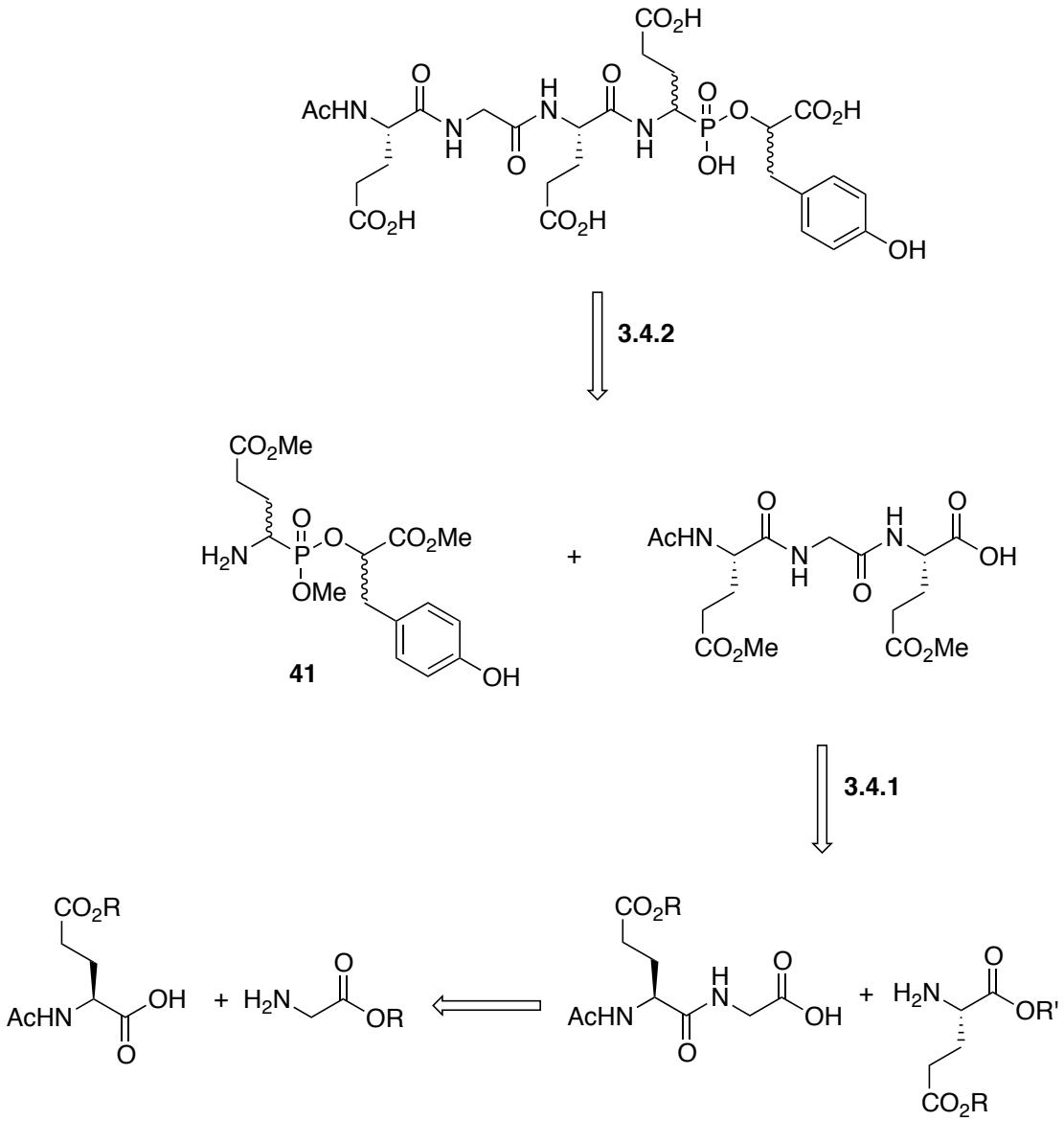

Figure 3.18 Retrosynthesis of inhibitor 4.

3.4.1 Synthesis of the Glu-Gly-Glu Tripeptide

The Glu-Gly-Glu tripeptide was synthesized in the N-to-C terminal direction by the sequential addition of one amino acid. The N-terminal glutamic acid required

protection at the α-amino group and the γ-carboxylic acid. Keeping consistent with the other inhibitors in the series (inhibitors **1**-**3**), the N-terminal amine was protected with an acetyl group to mimic the continuation of the peptide chain. Ideally, the γ-carboxylate would be protected as a methyl ester, however a *tert*-butyl ester protected glutamic acid was used because it was commercially available. This protected glutamic acid was coupled to the next amino acid in the series, a glycine. The glycine required protection at the α-carboxylic acid. A methyl ester was chosen because selective removal of this group over the glutamic acid γ-*t*-butyl ester was required. The methyl ester of glycine (compound **60**) was formed by reaction of glycine with thionyl chloride in methanol, which was isolated in 98% yield (Figure 3.19). Compound **61** was coupled to **60** in a DCC mediated reaction to form the protected dipeptide Glu-Gly (**62**), which was isolated in 99% yield. In order to prepare the dipeptide **62** for coupling to the next glutamic acid residue, the α-methyl ester was hydrolyzed to the free carboxylic acid by reaction with lithium hydroxide. Compound **63** was isolated in 95% yield (Figure 3.19). It should be noted that some racemization could have occurred under these conditions. No attempt was made to test whether this had happened.

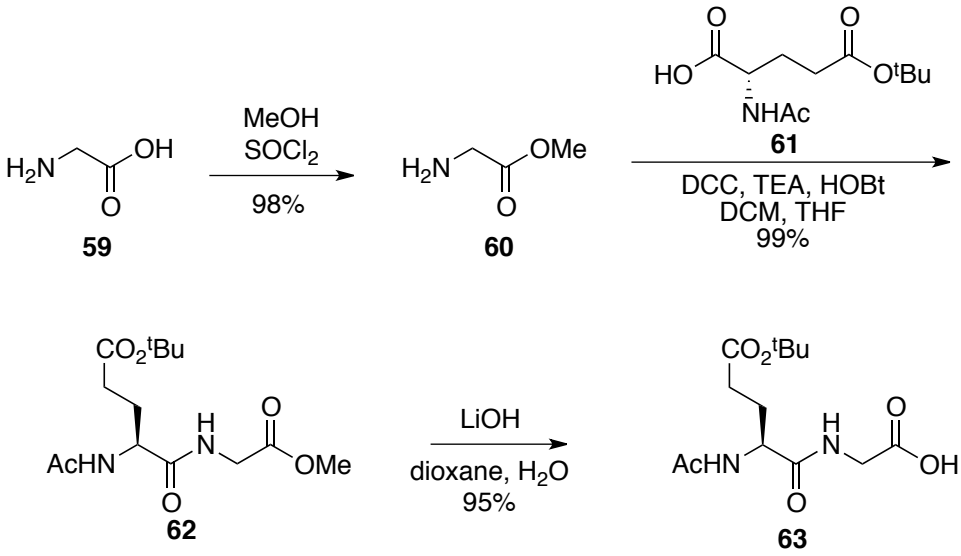

Figure 3.19 Synthesis of a protected Glu-Gly dipeptide.

The Glu-Gly dipeptide was coupled to the next amino acid in the series, the C-terminal glutamic acid. This glutamic acid required protection at the α- and γ-carboxylic acids. The commercially available Fmoc-Glu(O^{t}Bu)-OH (compound **64**) was used. First, the α-carboxylic acid was protected as a benzyl ester. Using a benzyl ester protecting group allows for selective removal of this group over the γ-*tert*-butyl esters. The α-benzyl ester glutamic acid was formed in a DCC mediated coupling between **64** and benzyl alcohol. Fmoc-Glu(O^{t}Bu)-OBn (compound **65**) was purified by silica gel flash column chromatography in 52% yield. The free amine was made by removing the Fmoc with 20% piperidine in DMF, followed by purification using silica gel flash column chromatography to produce **66** in 84% yield (Figure 3.20).

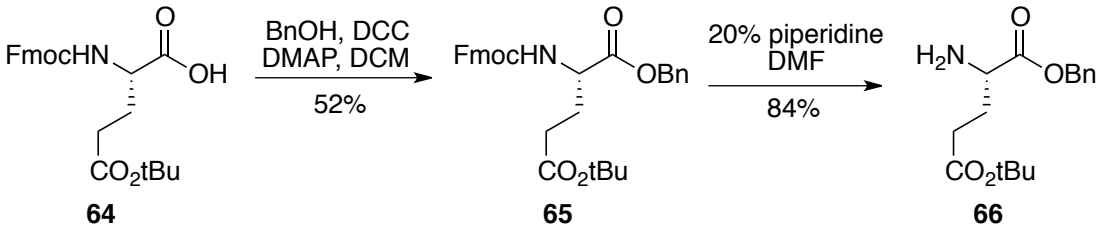

Figure 3.20 Synthesis of a protected glutamic acid residue.

Compound **66** was coupled to the dipeptide **63** through DCC mediated coupling to produce the protected tripeptide **67** in 81% yield (Figure 3.21). The synthesis of inhibitor **3** was not completed due to complications caused by complete cleavage of the *tert*-butyl ester, which hindered final purification. Because of this, the synthesis of inhibitor **4** was designed to include only methyl ester protecting groups, therefore reducing the number of deprotection steps and purifications. The commercially available γ-carboxylic acid glutamic acids used in the tripeptide synthesis were only available as *tert*-butyl esters. Therefore, at this stage in the tripeptide synthesis all the γ-*tert*-butyl esters were removed by treatment with trifluoroacetic acid and triethylsilane. The free γ-carboxylic acids were then protected as methyl esters by reaction with trimethylsilyl diazomethane in dichloromethane and methanol. Purification by silica gel column chromatography resulted in compound **69** in 69% yield. The free α-carboxylic acid is needed in order to couple this tripeptide to the phosphonic acid **41**. Therefore, the benzyl group was removed by treatment with palladium on carbon under a hydrogen atmosphere to produce compound **70** in quantitative yield (Figure 3.21). Compound **70** was synthesized from glycine in seven steps, in an overall yield of 50%.

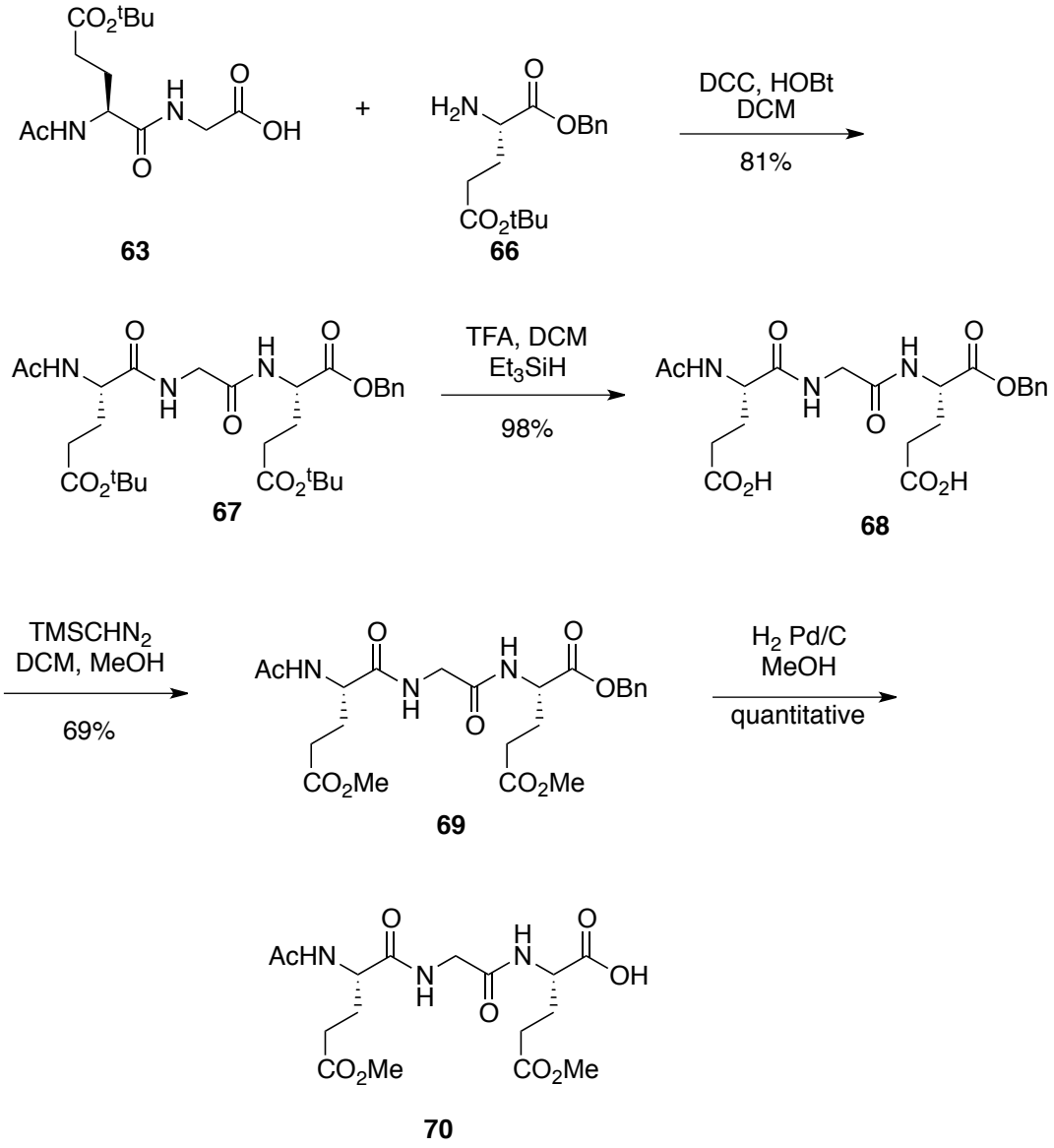

Figure 3.21 Synthesis of a protected Glu-Gly-Glu tripeptide.

3.4.2 Formation of the Phosphonic Acid Containing Pentapeptide

Previous attempts at coupling a glutamic acid residue to the phosphonate **41** resulted in intramolecular cyclization when base and carbodiimide reagents were present. In order to avoid this side reaction, an excess of the highly activated NHS glutamic acid ester was used. In order to employ this method in the synthesis of inhibitor **4**, an excess

of the tripeptide **70** (1.7 equivalents) was activated as the NHS ester and mixed with compound **41**.

The first attempt involved reaction of compound **70** and NHS with the carbodiimide EDC. However, after 24 hours analysis by mass spectrometry only revealed starting materials. The coupling reagent was changed to DCC, which resulted in the formation of the NHS activated tripeptide **71** (Figure 3.22). At this step, purification without decomposition is difficult; therefore, compound **71** was used directly without further purification.

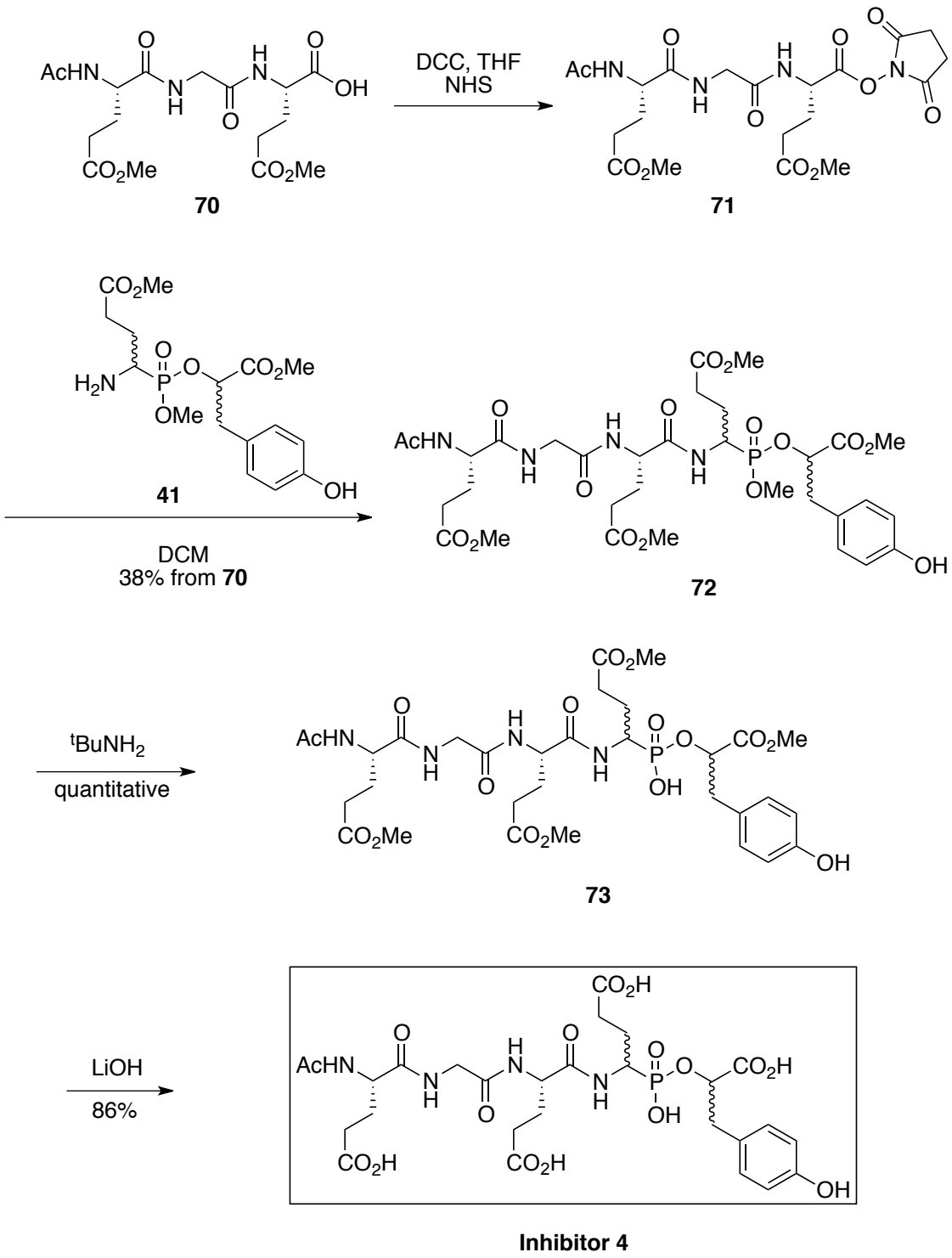

Figure 3.22 Synthesis of inhibitor 4.

After formation, the NHS ester tripeptide **71** was immediately mixed with compound **41** and stirred at room temperature for 12 hours. Analysis by mass spectrometry revealed the formation of product. After purification by silica gel chromatography, the phosphonate pentapeptide, **72**, was isolated in 38% yield.

The final two steps in the synthesis of inhibitor **4** involve the deprotection of the phosphonate methyl ester and the carboxylate methyl esters. In the synthesis of inhibitors **2** and **3**, nucleophilic displacement of the phosphonate anion from the methyl group by reaction with *tert*-butyl amine was used to deprotect the phosphonate ester. This method was successful in selectively displacing only the methyl group in the synthesis of inhibitor **2**. However, in the synthesis of inhibitor **3** this deprotection method resulted in a mixture of products: displacement of the methyl group and displacement of the tyrosine group. This method was used to remove the phosphonate methyl ester in compound **72**. In an effort to selectively displace only the methyl group, special care was taken to ensure conditions were anhydrous. After 12 hours at 45 °C, analysis by mass spectrometry confirmed that only the methyl group had been displaced, resulting in compound **73**.

As in the synthesis of inhibitors **2** and **3**, the methyl ester protecting groups were hydrolyzed by reaction in aqueous lithium hydroxide. Compound **73** was subjected to a 0.5 M solution of lithium hydroxide, and after 2 hours at room temperature the crude reaction mixture was acidified with Amberlite 120-H (H^+ form) resin and filtered. It should be noted that this treatment could result in epimerization of L-Glu residues. No attempts were made to quantify this possibility. The first attempts at purifying inhibitor **4** invovled size exclusion chromatrography. Crude reaction mixture was passed through a column of Biogel P2, eluting with water and monitoring the eluent by UV-vis

spectroscopy. NMR analysis of UV active fractions did not reveal product. The next method of purification investigated was anion exchange chromatography. Crude reaction mixture was passed through a column of AG-1X8 resin (formate form) and eluted with various concentrations of formic acid. NMR analysis of the 5M and 6M formic acid fractions confirmed the presence of inhibitor **4**. After treatment with a weakly anionic resin (sodium form), the pentasodium salt was isolated in 86% yield. Inhibitor **4** was synthesized in 23 synthetic steps with a longest linear sequence of 13 steps and an overall yield of 3%. The final NMR spectra for inhibitor **4** can be found in the Appendix, Figures A.39 and A.40.

3.5 Inhibition Studies with Inhibitor 4

Inhibition studies with inhibitor **4** were completed by our collaborators in the Roll-Mecak lab at the Cell Biology and Biophysics Unit, National Institute of Neurological Disorders in Maryland, USA. The potency of inhibitor **4** was assayed with bovine brain tubulin as the substrate. Reactions were assembled at room temperature in MES buffer at pH 6.9 containing KCl, $MgCl_2$, DTT, ATP, Try (2% [^{3}H]-Tyr) and tubulin. The reactions were initiated by the addition of TTL (from *X. tropicalis*) and a variable concentration of inhibitor **4** (0. 0.2, 0.5, 1 and 5 mM), and reactions were incubated for 0-120 minutes. The tyrosinated tubulin was separated from free tyrosine and measured by scintillation counting (CPM).

The molar amount of tyrosine incorporated into tubulin was calibrated for a known specific activity of [^{3}H]-tyrosine. This quantity was compared to the amount of [^{3}H]-Tyr-tubulin formed when no inhibitor was present to give a percent activity (Table

3.1). The resulting activities of TTL were plotted against the concentration of inhibitor **4** (Figure 3.23).

[Inh. **4**]	**0.0** mM	**0.2** mM	**0.5** mM	**1.0** mM	**5.0** mM
Activity (%)	100	109	99	66	3

Table 3.1 Activity of TTL at various concentrations of inhibitor 4 with tubulin as substrate.

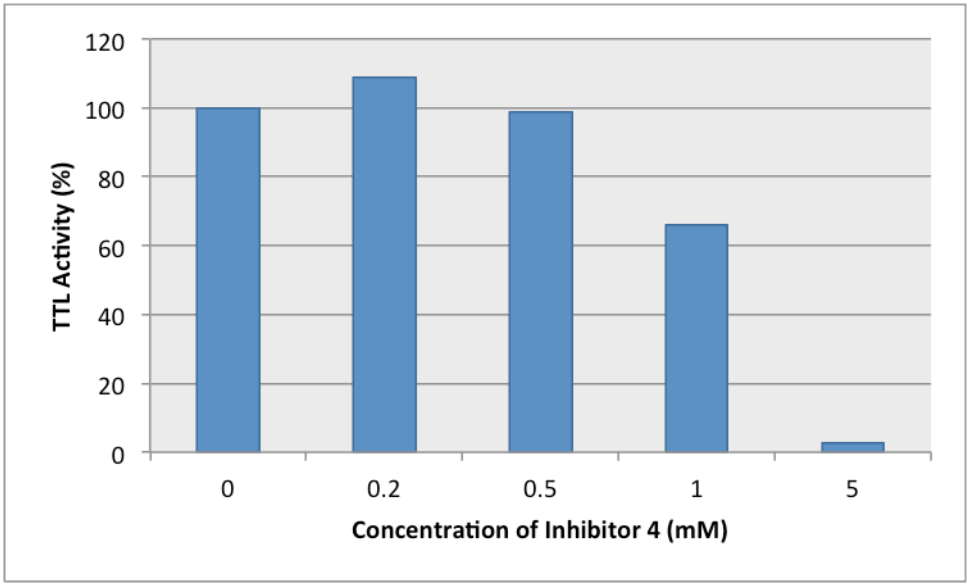

Figure 3.23 TTL activity vs. concentration of inhibitor 4 with tubulin as substrate.

The activity of TTL was also plotted against the log of inhibitor **4** concentration in units of μM. From this data, an IC_{50} value of 1.17 mM was extrapolated (Figure 3.24).

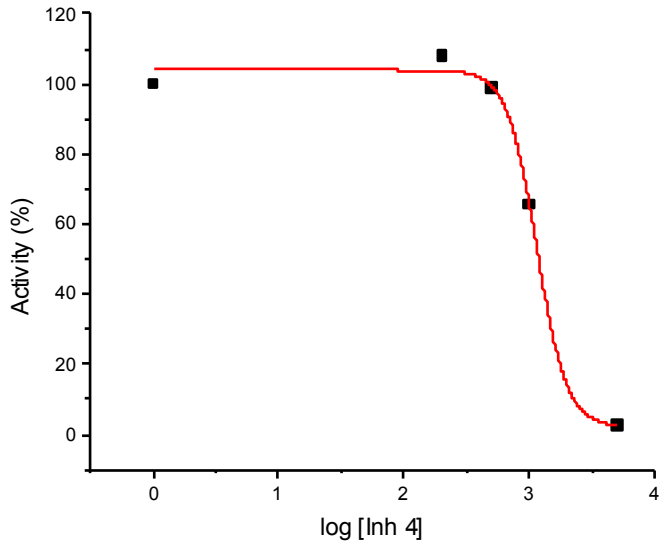

Figure 3.24 Tubulin as substrate: TTL activity vs log of inhibitor 4 concentration.

The activity of inhibitor **4** was next assayed with the C-terminal α-tubulin tail peptide as substrate. The 14-mer synthetic peptide (VDSVEGEGEEEGEE) was dissolved in MES buffer at pH 6.9 containing KCl, $MgCl_2$, DTT, ATP, and Tyr. The reaction was initiated by the addition of TTL and a variable concentration of inhibitor **4** (0.0, 0.1, 0.3, 0.5, 0.75, and 1.0 mM). After 0-120 minutes at room temperature, aliquots were subjected to HPLC using a reversed phase analytical column. The more hydrophobic product (VDSVEGEGEEEGEEY) is separated from the starting material peptide substrate and the quantities of both substrate and product peptides were estimated form the areas of the corresponding peaks on the UV detection absorbance spectrum.

The activity of TTL on the synthetic C-terminal α-tubulin tail peptide at various concentrations of inhibitor **4** was determined by comparison of product peak area when no inhibitor was present (0.0 mM) to the product peak area when inhibitor **4** was present (Table 3.2). These activities were plotted against inhibitor **4** concentration (Figure 3.25).

[Inh. **4**]	**0.0** mM	**0.1** mM	**0.3** mM	**0.5** mM	**0.75** mM	**1.0** mM
Activity (%)	100	86	80	58	59	36

Table 3.2 Activity of TTL at various concentrations of inhibitor 4, with peptide tail as substrate.

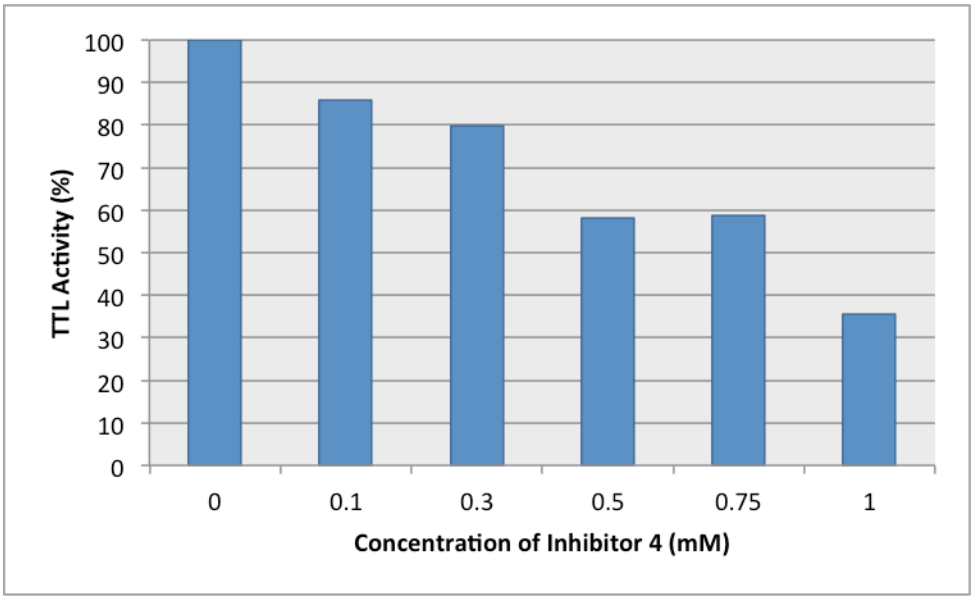

Figure 3.25 TTL activity vs. concentration of inhibitor 4.

The activity of TTL was also plotted against the log of inhibitor **4** concentration in units of μM. From this data, an IC_{50} value of 0.76 mM was extrapolated (Figure 3.26).

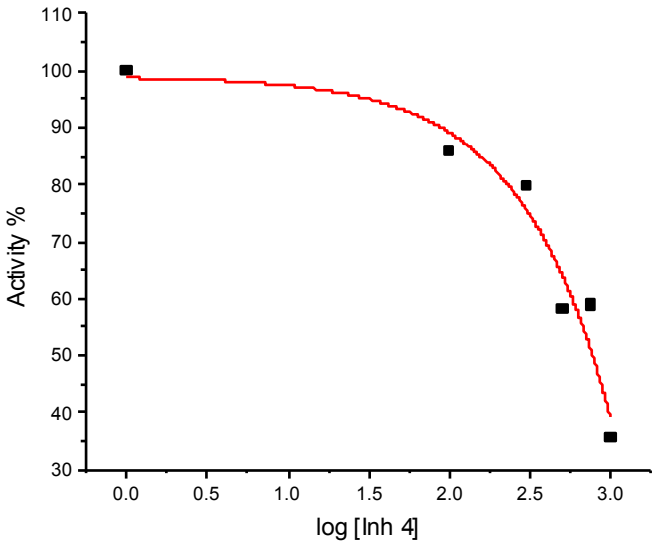

Figure 3.26 Peptide as substrate: TTL activity vs log of inhibitor 4 concentration.

The activity of inhibitor **4** against the C-terminal α-tubulin tail peptide was repeated using a similar assay method. However, this time inhibitor **4** was pre-incubated with TTL and ATP at room temperature for one hour, followed by addition to the reaction mixture (Table 3.3). The resulting activities of TTL were plotted against pre-incubated inhibitor **4** concentration (Figure 3.27).

[Inh. **4**]	**0.0** mM	**0.1** mM	**0.5** mM	**1.0** mM
Activity (%)	100	89	56	35

Table 3.3 Activity of TTL at various concentrations of inhibitor 4 with pre-incubation.

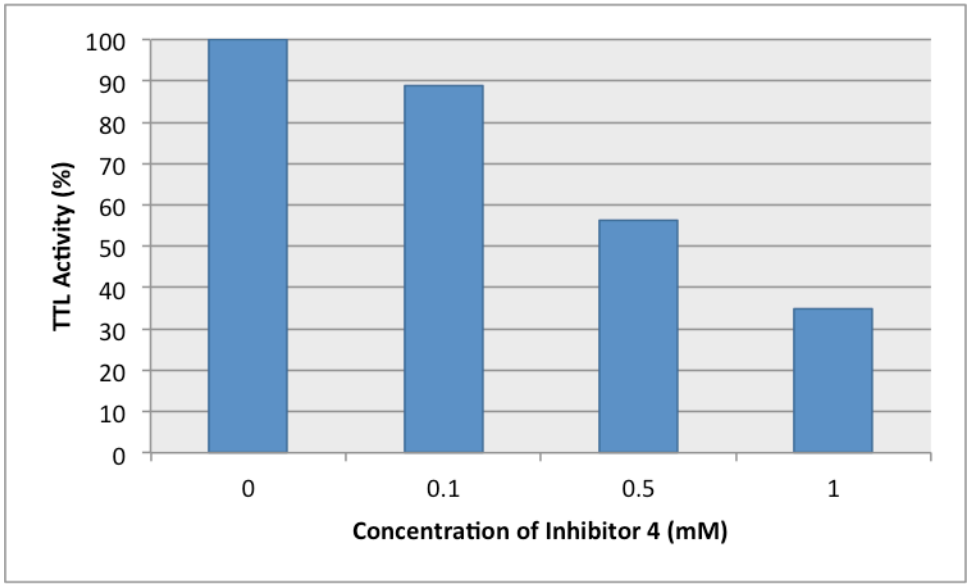

Figure 3.27 TTL activity vs. concentration of inhibitor 4 with pre-incubation.

The activity of TTL was also plotted against the log of pre-incubated inhibitor **4** concentration in units of μM. From this data, an IC_{50} value of 0.56 mM was extrapolated (Figure 3.28).

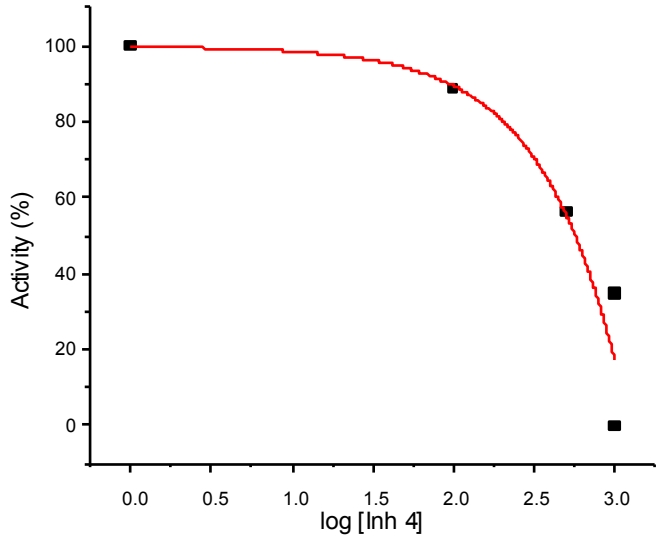

Figure 3.28 Pre-incubated with peptide tail: TTL activity vs log of inhibitor 4 concentration.

The IC_{50} values for inhibitor **4**, while not indicative of a strong inhibitor, are an improvement from inhibitor **2**, where a 50% reduction in TTL activity was not observed even at high inhibitor concentration. Increasing the length of the inhibitor peptide chain successfully increased the interactions between enzyme and inhibitor leading to measurable inhibition. Compared to inhibitor **2**, inhibitor **4** contains an increased number of glutamic acid residues. The improvement in inhibition between inhibitor **2** and inhibitor **4** supports the idea that interaction between substrate and the conserved strip of positively charged TTL surface residues is occurring and is important for enzyme activity.

Rüdiger (1994) demonstrated that while a C-terminal α-tubulin peptide chain acts as a substrate for TTL, it does so at a 50-fold lower efficiency than α/β-tubulin. This statement is confirmed by the increase in TTL inhibition when inhibitor **4** was assayed

against the C-terminal α-tubulin peptide tail instead of tubulin. This result also indicates that there are additional binding interactions between tubulin and the non-tail folded portion of TTL. Rüdiger (1994) also demonstrated that the tetradecapeptide was the optimal length for a peptide substrate. The fact that inhibitor **4**, a pentapeptide substrate, is active against the tetradecapeptide supports the idea that the phosphonic acid improves binding; if it didn't improve binding, no inhibition would be seen.

Pre-incubation of Inhibitor **4** with TTL and ATP is performed to determine if the inhibitor is being phosphorylated. When the inhibitor is phosphorylated it mimics the tetrahedral intermediate in the reaction mechanism even more so. This leads to an increase in interaction between the enzyme and inhibitor. In some cases, phosphorylation of the inhibitor results in irreversible inhibition. Because only a modest increase in TTL inhibition was seen when inhibitor **4** was pre-incubated with TTL and ATP, it can be concluded that inhibitor **4** is not being phosphorylated. These studies would need to be repeated before any conclusive statements could be made.

3.6 Future Work

Future work on the inhibition of TTL will focus on the synthesis of elongated phosphonic acid inhibitors. A significant increase in inhibition was seen between the dipeptide and the pentapeptide phosphonic acid inhibitors. This increase in inhibition was due to the increased number of glutamic acid residues in the pentapeptide inhibitor available to interact with the strip of positively charged surface residues on TTL. Because of this important interaction between enzyme and inhibitor, the next logical inhibitor to synthesize and test would be the heptapeptide phosphonic acid analogue, Glu-Glu-Glu-Gly-Glu-Glu-P(O)-Tyr. This inhibitor would be synthesized by procedures

similar to those used in the synthesis of inhibitor **4**. First, the pentapeptide Glu-Glu-Glu-Gly-Glu would be synthesized by classical solution phase methods; one amino acid would be added sequentially from N to C terminus. The N-terminal glutamic acid would be capped with an acetyl and the γ-carboxylic acids would be protected with methyl esters. The α-carboxylic acid of the C-terminal glutamic acid would be activated as an NHS ester and coupled to the phosphonate dipeptide (compound **41**) to produce the protected heptapeptide phosphonate. The phosphonate and methyl esters would be deprotected by methods used in the synthesis of inhibitors **2** and **4**. The activity of TTL, in the presence of this inhibitor, would be assayed against both tubulin and a synthetic α-tubulin peptide sequence.

The final step in studying the inhibition of TTL by a phosphonic acid based inhibitor, would be to synthesize the pentadecapeptide phosphonic acid analogue inhibitor, VDSVEGEGEEEGEE-P(O)-Y. This was the optimal length of peptide shown to serve as a substrate for TTL activity (Rüdiger, 1994). This pentadecapeptide inhibitor would be synthesized by a convergent synthesis, similar to what was used in the synthesis of inhibitor **4**; the tridecapeptide, VDSVEGEGEEEGE, would be coupled to the phosphonate dipeptide (compound **41**) to yield the pentadecapeptide.

The synthesis of the tridecapeptide would be best accomplished by the use of solid-phase peptide synthetic methods. It is not reasonable to construct the entire peptide using solid-phase peptide synthesis (SPPS), because the SPPS reagents would hydrolyze the phosphonate dipeptide (compound **41**). Using a polystyrene resin, the sequence would be assembled linearly from C- to N-terminus. The α-amine of each amino acid would be protected as a Boc and the glutamic acids, serine, and aspartic acid side chains

would be protected with a benzyl group. After the thirteen amino acid sequence is assembled, the N-terminal Boc would be removed and capped with an acetyl group, and the benzyl-protected peptide chain would be cleaved from the resin by a dicyclohexyl-18-crown-6 ether complex of potassium cyanide in DMF (Tam, 1977).

Activation of the C-terminal carboxylic acid to the NHS ester, followed by coupling to compound **41**, would result in the fully protected pentadecapeptide. The benzyl protecting groups could be removed by either hydrogenolysis or strong acid, and the phosphonate and methyl ester would be removed by methods used in the synthesis of inhibitors **2** and **4**. The activity of TTL, in the presence of this large inhibitor, would be assayed against both tubulin and a synthetic α-tubulin peptide sequence.

Future work on the inhibition of TTL will also focus on the synthesis of phosphonamidate inhibitors. Even though the phosphonamidate is less stable than the phosphonate or phosphinate, it has been shown to be a potent inhibitor. A phosphonamidate inhibitor of thermolysin was shown to be 1000 times more potent than the phosphonate analogue (Bartlett, 1987). Synthesis of the phosphonamide dipeptide, Glu-P-Tyr, would be accomplished similarly to the synthesis of the phosphonate dipeptide; a protected tyrosine would replace the protected 4-hydroxyphenyllactic acid (Figure 3.29). The dipeptide phosphonamidate can then be elongated by the addition of peptide fragments of variable lengths.

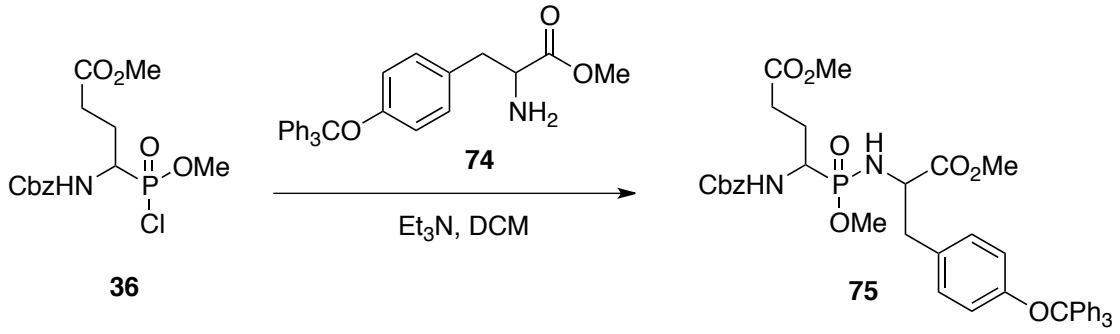

Figure 3.29 Synthesis of the phosphonamidate dipeptide Glu-P-Tyr.

Revisiting the synthesis of a phosphinic acid-containing inhibitor would also be important in the study of TTL inhibition. Not only is the phosphinate moiety more stable than the phosphonate or phosphonamide, but D-alanine:D-alanine ligase, an enzyme similar to TTL, has been shown to be more strongly inhibited by a phosphinic acid-containing inhibitor. The best strategy for completing the synthesis of a phosphinic acid-containing inhibitor would be to revisit the strategy of masking the glutamic acid side chain carboxylate with an alkene. When this work was done previously, there were complications with isolating the coupled product and reproducing the coupling reaction. A possible reason for the lack of reproducibility is due to low-purity starting marterials. Careful purification of compound **29** would be accomplished and the coupling reaction would be attempted again.

3.7 Summary

This chapter details the design and synthesis of inhibitors **3** and **4**. The synthesis of inhibitor **3** involved the elongation of inhibitor **2** to a tripeptide phosphonic acid analogue by standard peptide bond formation procedures. A protected glutamic acid, activated as an NHS ester was coupled to the phosphonate dipeptide Tyr-P(O)-Glu

(compound **41**). To avoid an intramolecular cyclization of compound **41**, no base was used. The remaining deprotection steps were completed in a similar fashion to the deprotection of inhibitor **2**. Unique to inhibitor **3** was the presence of a *tert*-butyl ester protecting group. Attempts at removing the *tert*-butyl ester and purifying the final inhibitor were unsuccessful.

A convergent synthetic approach was undertaken in the synthesis of inhibitor **4**. First, the Glu-Gly-Glu tripeptide was synthesized by standard peptide bond synthetic procedures. The tripeptide was then coupled to the phosphonate dipeptide Tyr-P(O)-Glu (compound **41**). The resulting pentapeptide was then deprotected in a manner similar to that of inhibitors **2** and **3**. Because of the difficulties in removing the *tert*-butyl ester, only methyl esters were used. The total synthesis of inhibitor **4** was completed and sent to our collaborators in the Roll-Mecak lab. The inhibition of TTL in the presence of inhibitor **4** was measured with both tubulin and a C-terminal α-tubulin peptide tail as substrate. Weak inhibition of TTL with inhibitor **4** was seen against both substrates. An improvement in inhibition was seen against the C-terminal α-tubulin peptide tail over tubulin. Inhibitor **4** represents the first rationally designed inhibitor of tubulin tyrosine ligase.

3.8 Experimental Procedures

3.8.1 Materials and General Methods

All reagents were purchased from Alfa Aesar, BaChem or Aldrich and were used without further purification unless otherwise noted. Silica gel chromatography was performed using Silica Gel SiliaFlash (230-400 mesh, Silicycle). The solvents

triethylamine, dichloromethane and methanol were distilled over CaH_2 under inert atmosphere.

^1H NMR spectra were recorded on either a Bruker AV300 or Bruker AV400 spectrometer at field strengths of 300 or 400 MHz. Proton-decoupled ^{31}P NMR spectra were recorded on either a Bruker AV300 or Bruker AV400 spectrometer at field strengths of 121.5 or 162 MHz. Mass spectrometry was performed by electrospray ionization (ESI-MS) using an Esquire LC mass spectrometer. Neutral compounds were detected as positive ions, and negatively charged compounds were detected as negative ions.

3.8.2 Experimental Procedures in the Synthesis of Inhibitor 3

3.8.2.1 NH_2-Glu(OMe)-OH (47)

Anhydrous methanol (50 mL), under argon atmosphere, was cooled to 0 °C and thionyl chloride (2.5 mL, 35 mmol) was added dropwise via syringe over 10 min. L-Glutamic acid **46** (3.7 g, 25 mmol) was added in portions and the reaction was stirred at rt for 3 h. The reaction mixture was cooled to -10 °C and diethyl ether (100 mL) was slowly added. The resulting solid was filtered, washed with diethyl ether, and dried under vacuum to yield **47** as the hydrochloride salt (4.04 g, 82%). ^1H NMR data was identical to that previously reported in the literature (El Marini, 1992).

3.8.2.2 NHAc-Glu(OMe)-OH (48)

Sodium bicarbonate (3.2 g) was slowly added to a solution of **47** (3.7 g, 18.7 mmol) in water (140 mL) at 0 °C. Acetic anhydride (3.5 mL, 37.4 mmol) was added dropwise via syringe over 10 min. The reaction was warmed to rt and stirred for 12 h.

The reaction mixture was acidified to pH = 3 with 2 M hydrochloric acid and transferred to a continuous liquid extractor and extracted for 18 h with ethyl acetate. The organic layer was dried with $MgSO_4$, filtered and concentrated under vacuum to yield **48** (3.16 g, 83%) as a white solid, which was used without further purification. ^{1}H NMR (300 MHz, D_2O) δ 4.33 (dd, 1H, *J* = 5.1, 9.2 Hz), 3.63 (s, 3H), 2.44 (t, 2H, *J* = 7.4 Hz), 2.21-2.10 (m, 1H), 1.99-1.89 (m, 1H), 1.96 (s, 3H).

3.8.2.3 Cbz-Glu($CO_2{}^t$Bu)-Glu(CO_2Me)-PO(OMe)-O-Tyr-CO_2Me (52)

A solution of Z-Glu(O^{t}Bu)-OSu, **51**, (0.71 g, 1.64 mmol) in anhydrous dichloromethane (10 mL) was added to compound **41** under argon atmosphere. After stirring at rt for 12 h, the formation of product was confirmed by TLC (EtOAc) and mass spectrometry analysis. The reaction mixture was concentrated under vacuum and the crude residue was purified by silica gel flash column chromatography (EtOAc) to yield **52** (0.25 g, 43%) (a mixture of eight diastereomers). ^{1}H NMR (300 MHz, $CDCl_3$) δ 7.32 (m, 5H), 7.16-6.96 (m, 2H), 6.89-6.68 (d, 2H), 5.08 (s, 2H), 5.02-4.91 (m 1H), 4.61-4.03 (m, 1H), 4.37-4.18 (m, 1H), 3.76 (m, 3H), 3.64 (m, 3H), 3.62 (m, 3H), 3.37-3.09 (m, 2H), 2.50-1.69 (m, 4 × 2H), 1.42 (s, 9H); ^{31}P NMR (121.5 MHz, $CDCl_3$) δ 26.23, 25.91, 25.47, 24.61; ESI-MS *m/z* 731.4 $[M - Na]^+$.

3.8.2.4 NH_2-Glu($CO_2{}^t$Bu)-Glu(CO_2Me)-PO(OMe)-O-Tyr-CO_2Me (53)

Compound **52** (0.27 g, 0.39 mmol) was dissolved in 20 mL of anhydrous MeOH and 10% Pd/C (20.5 mg, 5 mol %) was added. The reaction mixture was placed under vacuum and then blanketed with H_2 (760 mmHg). This sequence was repeated twice to ensure a complete hydrogen atmosphere. The reaction mixture was stirred for 4 h; reaction progress was monitored by ESI-MS. The reaction mixture was filtered through

Celite and the filtrate was concentrated and dried under high vacuum for 1 h. Crude **53** was used immediately without further purification. ESI-MS *m/z* 575.5 $[M - H]^+$.

3.8.2.5 AcHN-Glu($CO_2{}^t$Bu)-Glu(CO_2Me)-PO(OMe)-O-Tyr-CO_2Me (54)

A solution of compound **53** (0.39 mmol) in anhydrous dichloromethane (30 mL) under argon atmosphere was charged with acetic anhydride (1.45 mL, 15.4 mmol). After 12 h at rt, the reaction was concentrated under vacuum. The resulting crude residue was purified by flash column chromatography (1:1 EtOAc/pet ether followed by 9:1 EtOAc/MeOH) to yield **54** (0.20 g, 78%) (a mixture of eight diastereomers). ^{1}H NMR (400 MHz, $CDCl_3$) δ 7.26-7.21 (m, 2H), 7.06-7.0 (m, 2H), 5.19-5.01 (m, 1H), 4.56-4.42 (m, 1H), 4.42-4.25 (m, 1H), 3.86-3.72 (m, 6H), 3.67-3.63 (m, 3H), 3.27-3.12 (m, 2H), 2.42-1.86 (m, 4 × 2H), 2.26 (m, 6H), 1.43 (s, 9H); ^{31}P NMR (162 MHz, $CDCl_3$) δ 26.12, 25.96, 25.30, 25.15; ESI-MS *m/z* 681.4 $[M - Na]^+$.

3.8.2.6 AcHN-Glu($CO_2{}^t$Bu)-Glu(CO_2Me)-PO(OH)-O-Tyr-CO_2Me (55)

Compound **54** (0.20 g, 0.30 mmol) was dissolved in freshly distilled *tert*-butylamine (20 mL). A flame-dried condenser was attached and the reaction mixture was heated to reflux for 24 h. The reaction mixture was concentrated under vacuum and purified by silica gel flash chromatography (8:2 DCM/MeOH) to yield **55** (32 mg, 16%) (a mixture of four diastereomers). ^{1}H NMR (400 MHz, CD_3OD) δ 7.27 (d, 2H, J = 8.6 Hz), 7.00 (d, 2H, J = 8.4), 4.39-4.25 (m, 1H), 4.17-3.99 (m, 1H), 3.64 (s, 6H), 3.17-2.92 (m, 2H), 2.40-2.29 (m, 2 × 2H), 2.25 (s, 3H), 2.21-2.06 (m, 2 × 1H), 1.99 (s, 3H), 1.92-1.76 (m, 2 × 1H), 1.43 (s, 9H); ^{31}P NMR (162 MHz, CD_3OD) δ 17.50 (br); ESI-MS *m/z* 643.5 $[M - H]^-$.

3.8.2.7 AcHN-Glu($CO_2{}^tBu$)-Glu(CO_2H)-PO(OH)-O-Tyr-CO_2H (58)

Compound **55** (32 mg, 0.05 mmol) was dissolved in water (5 mL). A 0.5 M solution of $LiOH_{aq}$ was added until the pH of the solution reached 13 (≈ 0.5 mL). After 2 h the reaction mixture was acidified to pH = 6 with Amberlite 120-H (H^+ form) resin. The reaction mixture was filtered, concentrated and dried under high vacuum to yield **58** (a mixture of four diastereomers) in quantitative yield, which was used without further purification. ^{1}H NMR (400 MHz, CD_3OD) δ 7.12-7.02 (m, 2H), 6.73-6.68 (m, 2H), 4.44-4.22 (m, 2 × 1H), 3.18-3.00 (m, 2H), 2.44-2.23 (m, 2 × 2H), 2.14-2.01 (m, 2 × 1H) 2.00-1.96 (m, 3H), 1.92-1.76 (m, 2 ×1H) 1.45-1.43 (m, 9H); ^{31}P NMR (162 MHz, CD_3OD) δ 22.51, 22.19; ESI-MS *m/z* 573.3 $[M - H]^-$.

3.8.3 Experimental Procedures in the Synthesis of Inhibitor 4

3.8.3.1 Methyl 2-Aminoacetate (60)

Anhydrous methanol (20 mL), under argon atmosphere, was cooled to 0 °C and thionyl chloride (3.75 mL, 51.6 mmol) was added dropwise via syringe over 10 min. Glycine (3.15 g, 42 mmol) was added in portions and the reaction was heated to reflux for 12 h. The reaction mixture was cooled to rt and solid crashed out. Methanol (20 mL) was added and the solution was concentrated to dryness, this was repeated in triplicate. The resulting solid was washed diethyl ether (3 × 50 mL), and dried under vacuum to yield **60** as the hydrochloride salt (5.2 g, 99%). ^{1}H NMR (300 MHz, D_2O) δ 3.92 (s, 2H), 3.82 (s, 3H).

3.8.3.2 AcHN-Glu(O^{t}Bu)-Gly(OMe) (62)

AcHN-Glu(O^{t}Bu)-OH, **61**, (1.2 g, 5 mmol) was dissolved in THF (50 mL) and cooled to 0 °C. DCC (1.13 g, 5.5 mmol) and HOBt (0.67 g, 5 mmol) were added to the solution. After 10 min, a solution of compound **60** (0.75 g, 6 mmol) in triethylamine (1 mL. 7.2 mmol) and dichloromethane (30 mL) was added. The reaction was stirred for 16 h at rt under argon atmosphere. The resulting heterogenous solution was filtered through Celite and the filtrate was concentrated under vacuum. The resulting residue was purified by silica gel chromatography (1:1 hexane/EtOAc then 9:1 EtOAc/MeOH) to yield compound **62** (1.56 g, 99%) as a white solid. ^{1}H NMR (400 MHz, $CDCl_3$) δ 7.03 (bt, 1H), 6.59 (bt, 1H), 4.53-4.46 (m, 1H), 4.04 (dd, 2H, J = 11.3, 5.5), 3.76 (s, 3H), 2.53-2.32 (m, 2H), 2.13-1.93 (m, 2H), 2.02 (s, 3H), 1.46 (s, 9H); ESI-MS *m/z* 339.4 $[M - Na]^+$.

3.8.3.3 AcHN-Glu(O^{t}Bu)-Gly(OH) (63)

Compound **62** (1.83 g, 5.8 mmol) was dissolved in 1:1 water/dioxane (100 mL). A 2 M solution of $LiOH_{aq}$ was added until the pH of the solution reached 13 (≈ 15 mL). After 1 h the reaction mixture was acidified to pH = 6 with Amberlite 120-H (H^+ form) resin. The reaction mixture was filtered, concentrated and dried under high vacuum to yield **63** in 95% yield which was used without further purification. ^{1}H NMR (400 MHz, CD_3OD) δ 4.46-4.39 (m, 1H), 3.97-3.84 (m, 2H), 2.45-2.32 (m, 2H), 2.17-1.82 (m, 2H), 2.00 (s, 3H), 1.45 (s, 9H); ESI-MS *m/z* 325.3 $[M - Na]^+$.

3.8.3.4 Fmoc-Glu(O^{t}Bu)-OBn (65)

Fmoc-Glu(O^{t}Bu)-OH, **64**, (2.12 g, 5.0 mmol) was dissolved in DCM (100 mL) and cooled to 0 °C. DCC (1.13 g, 5.5 mmol) and DMAP (0.06 g, 0.5 mmol) were added to the solution. After 10 min, benzyl alcohol (0.78 mL, 7.5 mmol) was slowly added.

The reaction was stirred for 3 h at rt under argon atmosphere. The resulting heterogenous solution was filtered through Celite and the filtrate was concentrated under vacuum. The resulting residue was purified by silica gel flash column chromatography (4:1 hexane/EtOAc) to yield compound **65** (1.33 g, 52%) as a white solid. ^{1}H NMR (400 MHz, $CDCl_3$) δ 7.77 (d, 2H, *J* = 7.5 Hz), 7.60 (d, 2H, *J* = 7.2 Hz), 7.44-7.28 (m, 9H), 5.49 (d, 1H, *J* = 8.2 Hz), 5.20 (s, 2H), 4.48-4.39 (m, 2H), 4.39-4.33 (m, 1H), 4.22 (t, 1H, *J* = 7.06), 2.39-2.12 (m, 2H), 2.09-1.93 (m, 1H), 1.64-1.52 (m, 1H), 1.44 (s, 9H); ESI-MS *m/z* 538.4 $[M - Na]^+$.

3.8.3.5 NH_2-Glu(O^tBu)-OBn (66)

Compound **66** (1.33g, 2.5 mmol) was dissolved in DMF (30 mL) and a 20% solution of piperidine in DMF (30 mL) was added. After stirring at rt for 1 h, the reaction mixture was concentrated under vacuum. The resulting reaction mixture was purified by silica gel flash column chromatography (4:1 hexane:EtOAc) to yield compound **66** (0.61 g, 84%). ^{1}H NMR (400 MHz, $CDCl_3$) δ 7.37 (m, 5H), 5.17 (s, 2H), 3.61 (dd, 1H, *J* = 5.3, 8.0 Hz), 2.37 (t, 2H, *J* = 7.3 Hz), 2.14-1.83 (m, 2H), 1.43 (s, 9H); ESI-MS *m/z* 294.4 $[M - H]^+$.

3.8.3.6 AcHN-Glu(O^tBu)-Gly- Glu(O^tBu)-OBn (67)

Compound **63** (0.3 g, 1 mmol) was dissolved in DMF (20 mL) and cooled to 0 °C. DCC (0.22 g, 1.05 mmol) and HOBt (0.14 g, 1.0 mmol) were added to the solution. After 10 min, a solution of compound **66** (0.33 g, 1.1 mmol) in DMF (15 mL) was added. The reaction was stirred for 24 h at rt under argon atmosphere. The resulting heterogenous solution was filtered through Celite and the filtrate was concentrated under vacuum. The resulting residue was purified by silica gel chromatography (4:1

hexane/EtOAc then 1:1 hexane/EtOAc) to yield compound **67** (0.47 g, 81%) as a white solid. The ^{1}H NMR spectrum contained unidentified peak in the 1-3 ppm region indicating the compound was not pure. ^{1}H NMR (400 MHz, $CDCl_3$) δ 7.35 (m, 5H), 5.17 (s, 2H), 4.67-4.60 (m, 1H), 4.41-4.34 (m, 1H), 4.14-4.04 (m, 2H), 2.53-1.92 (m, 4 × 2H), 2.01 (s, 3H), 1.48 (s, 9H), 1.43 (s, 9H); ESI-MS *m/z* 600.4 $[M - Na]^+$.

3.8.3.7 AcHN-Glu(OH)-Gly-Glu(OH)-OBn (68)

Compound **67** (0.47 g, 0.81 mmol) was dissolved in anhydrous DCM and put under argon atmosphere. Trifluoroacetic acid (10.53 mmol, 0.81 mL) and triethylsilane (2.02 mmol, 0.32 mL) were added and the reaction was stirred at rt for 16 h. The reaction mixture was concentrated under vacuum and the resulting solid was triturated with diethyl ether. The resulting white solid was vacuum dried to yield compound **68** (0.41 g, 98%), which was used without further purification. ^{1}H NMR (400 MHz, CD_3OD) δ 7.37 (m, 5H), 5.17 (s, 2H), 4.53 (dd, 1H *J* = 9.4, 4.9), 4.28 (dd, 1H, *J* = 8.2, 6.1), 4.00-3.80 (m, 2H), 2.42 (t, 2H, *J* = 7.1 Hz), 2.36 (t, 2H, *J* = 7.9 Hz) 2.23-2.06 (m, 2 × 1H), 2.06-1.89 (m, 2 × 1H), 1.98 (s, 3H); ESI-MS *m/z* 488.3 $[M - Na]^+$.

3.8.3.8 AcHN-Glu(OMe)-Gly-Glu(OMe)-OBn (69)

Compound **68** (1.6 mmol) was dissolved in anhydrous MeOH:DCM (50 mL, 1:4) and put under argon atmosphere. A 2 M solution of trimethylsilyldiazomethane in hexanes (2 mL) was added via syringe until a yellow homogenous solution persisted. The reaction was stirred for an additional 20 min and concentrated under vacuum. The crude reaction mixture was purified by silica gel flash column chromatography (EtOAc then 9:1 EtOAc/MeOH) to yield compound **69** (1.1 mmol, 69%). ^{1}H NMR (400 MHz, $CDCl_3$) δ 7.57 (bt, 1H, *J* = 5.78 Hz), 7.47 (bt, 1H, *J* = 7.9 Hz), 7.33 (m, 5H), 7.07 (bt,

1H), 5.14 (s, 2H), 4.68-4.59 (m, 1H), 4.51-4.44 (m, 1H), 4.11-3.86 (m, 2H), 3.65 (s, 3H), 3.63 (s, 3H), 2.53-1.99 (m, 4 × 2H), 1.97 (s, 3H); ESI-MS *m/z* 516.3 $[M - Na]^+$.

3.8.3.9 AcHN-Glu(OMe)-Gly-Glu(OMe)-OH (70)

Compound **69** (0.53 g, 1.1 mmol) was dissolved in 10 mL of anhydrous MeOH and 10% Pd/C (60.5 mg, 5 mol %) was added. The reaction mixture was placed under vacuum and then blanketed with H_2 (760 mmHg). This sequence was repeated twice to ensure a complete hydrogen atmosphere. The reaction mixture was stirred for 4 h at rt; reaction progress was monitored by ESI-MS. The reaction mixture was filtered through Celite and the filtrate was concentrated and dried under high vacuum for 1 h. Crude **70** was used immediately without further purification. ^{1}H NMR (400 MHz, CD_3OD) δ 4.46 (dd, 1H *J* = 9.3, 4.7), 4.28 (dd, 1H, *J* = 8.2, 5.9), 3.99-3.76 (m, 2H), 3.67 (s, 3H), 3.66 (s, 3H), 2.49-2.37 (m, 2 × 2H), 2.28-2.06 (m, 2 × 1H), 2.06-1.88 (2 × 1H), 1.98 (s, 3H); ESI-MS *m/z* 426.3 $[M - Na]^+$.

3.8.3.10 AcHN-Glu(OMe)-Gly-Glu(OMe)-NHS (71)

Compound **70** (0.24 g, 0.6 mmol) was dissolved in DMF (20 mL) and cooled to 0 °C. DCC (0.14 g, 0.66 mmol) was added to the solution. After 10 min, NHS (0.08 g, 0.66 mmol) was added. The reaction was stirred for 2 h at rt under argon atmosphere. The resulting heterogenous solution was filtered through Celite and the filtrate was concentrated under vacuum to yield compound **71**, which was used without further purification. ESI-MS *m/z* 523.3 $[M - Na]^+$.

3.8.3.11 AcHN-Glu(OMe)-Gly-Glu(OMe)-Glu(OMe)-PO(OMe)-O-Tyr(OMe) (72)

To a solution of compound **71** (0.6 mmol) in THF (10 mL) and DCM (3 mL) was added a solution of compound **41** (0.35 mmol) in DCM (7 mL). The yellow heterogenous mixture was stirred for 12 h at rt. The reaction mixture was concentrated under vacuum and the resulting residue was purified by silica gel flash column chromatography (gradient of 4:1 hexane/EtOAc to 8:2 EtOAc/MeOH) to yield compound **72** (0.10 g, 38%) (a mixture of eight diastereomers). The ^{1}H NMR spectrum contained unidentified peak in the 8-8.5 ppm region indicating the compound was not pure. ^{1}H NMR (400 MHz, CD_3OD) δ 7.10 (d, 2H, J = 8.2), 6.75 (d, 2H, J = 7.9), 5.10-5.02 (m, 1H), 4.60-4.48 (m, 1H), 4.45-4.25 (m, 2H), 3.95-3.81 (m, 1 × 2H), 3.82-3.79 (m, 3H), 3.67 (s, 12H), 3.22-2.93 (m, 2H), 2.50-2.35 (m, 3 × 2H), 2.21-2.04 (m, 3 × 1H), 2.04-1.89 (m, 3 × 1H), 2.01 (m, 3H); ^{31}P NMR (162 MHz, CD_3OD) δ 26.17, 26.03, 25.98, 25.64; ESI-MS *m/z* 797.6 $[M - Na]^+$.

3.8.3.12 AcHN-Glu(OMe)-Gly-Glu(OMe)-Glu(OMe)-PO(OH)-O-Tyr(OMe) (73)

Compound **72** (38.8 mg, 0.05 mmol) was dissolved in freshly distilled *tert*-butylamine (8 mL). A flame-dried condenser was attached and the reaction mixture was heated to reflux for 24 h. The reaction mixture was concentrated under vacuum to yield **73** (a mixture of four diastereomers), which was used without further purifcation. The compound was not completely pure and contained peaks attributable to *tert*-butylamine. ESI-MS *m/z* 759.3 $[M - H]^-$ and m/z 834.5 $[M - {}^{t}BuNH_4]^+$.

3.8.3.13 AcHN-Glu(OH)-Gly-Glu(OH)-Glu(OH)-PO(OH)-O-Tyr(OH) (Inhibitor 4)

Compound **73** (26 mg, 0.03 mmol) was dissolved in water (5 mL). A 0.5 M solution of $LiOH_{aq}$ was added until the pH of the solution reached 13 (≈ 2 mL). After 2 h at rt the reaction mixture was acidified to pH = 3 with Amberlite 120-H (H^+ form) resin. The mixture was filtered and concentrated under vacuum. The crude product was dissolved in H_2O (0.5 mL) and loaded onto a 1 mL column of AG-1X8 ion exchange resin (formate form). The column was washed successively with H_2O (10 mL), 1 M formic acid (20 mL), 5 M formic acid (20 mL) and 6 M formic acid (20 mL). The 5 and 6 M fractions were reduced under vacuum and buffer exchanged with H_2O to remove any residual formic acid in the mixture. The product was dissolved in H_2O (3 mL) and stirred with IRC 7481 weak cation exchange resin (sodium form) until the pH of the solution reached 7.0. The solution was then filtered, frozen, and lyophilized to give inhibitor **4** (a mixture of four diastereomers) as the pentasodium salt (21 mg, 86%). ^{1}H NMR (400 MHz, CD_3OD) δ 7.09 (d, 2H, J = 8.5), 6.70 (d, 2H, J = 8.2), 5.01-4.91 (m, 1H) 4.46-4.19 (m, 3 × 1H), 3.96-3.75 (m, 2H), 3.18-2.97 (m, 2H), 2.47-2.19 (m, 3 × 2H), 2.17-2.03 (m, 3 × 1H), 1.99 (s, 3H), 1.97-1.73 (m, 3 × 1H); ^{31}P NMR (162 MHz, CD_3OD) δ 21.88, 21.59; ESI-MS *m/z* 703.3 $[M - H]^-$

3.8.4 Experimental Procedures in the Inhibition Studies of Inhibitor 2

The following experimental procedures were completed by our collaborators in the Roll-Mecak lab at the Cell Biology and Biophysics unit, National Institute of Neurological Disorders in Maryland, USA.

3.8.4.1 Protein Expression and Purification

X. tropicalis tubulin tyrosine ligase was expressed and purified by the same procedure described in section **2.7.4.1**.

3.8.4.2 TTL Activity Assay Against Inhibitor 4 with Tubulin as Substrate

Tyrosination of bovine brain tubulin (Cytoskeleton) by TTL was assayed against variable concentrations of inhibitor **4** (0, 0.2, 0.5, 1.0. and 5 mM). Reactions conditions were the same as was reported in section **2.7.4.2**.

3.8.4.3 TTL Activity Assay Against Inhibitor 4 with Peptide as Substrate

Tyrosination of a C-terminal α-tubulin tail peptide (VDSVEGEGEEEGEE) was assayed against variable concentrations of inhibitor **4** (0, 0.1, 0.3, 0.5, 0.75 and 1.0 mM). Reactions conditions were the same as was reported in section **2.7.4.3**.

References

Abell, L. M.; Villafranca, J. J. *Biochemistry* **1991,** *30,* 6135-6141.

Abrunhosa-Thomas, I.; Sellers, C. E.; Montchamp, J-L. *J. Org. Chem.* **2007,** 7*2,* 2851-2856.

Arce, C. A.; Hallak, M. E.; Rodriguez, J. A.; Barra, H. S.; Caputto, R.; *J. Neurochem.* **1978,** *31,* 205-210.

Arce, C. A.; Rodriguez, J. A.; Barra, H. S.; Caputto, R.; *Eur. J. Biochem.* **1975,** *59,* 145-149.

Argaraña, C. E.; Barra, H. S.; Caputto, R. *J. Neurochem.* **1980,** *34,* 114-118.

Argaraña, C. E.; Barra, H. S.; Caputto, R. *Mol. Cell. Biochem.* **1978,** *19,* 17-21.

Barra, H. S.; Rodriquez, J. A.; Arce, C. A.; Caputto, R. *Biochem. Biophys. Res. Commun.* **1974,** *60,* 1384-1390.

Barra, H. S.; Rodriquez, J. A.; Arce, C. A.; Caputto, R. *J. Neurochem.* **1973,** *20,* 97-108.

Bartlett, P. A.; Hunt, J. T.; Adams, J. L; Gehret, J. E. *Bioorg. Chem.* **1978,** *7,* 421-436.

Bartlett, P. A.; Johnson, W. S. *Tetrahedron Lett.* **1970,** *46,* 4459-4462.

Bartlett, P. A.; Marlowe, C. K. *Science* **1987,** *235,* 569-571.

Bartley, D. M.; Coward, J. K. *J. Org. Chem.* **2005,** *70,* 6757-6774.

Baylis, E. K.; Campbell, C. D.; Dingwall, J. G. *J. Chem. Soc. Perkin. Trans. I* **1984,** 2845-2853.

Bhattacharya, A. K.; Thyagarajan, G. *Chem. Rev.* **1981,** *81,* 415-430.

Bulinski, J. C.; Gundersen, G. G. *BioEssays* **1991,** *13,* 285-293.

Byun, H-S.; Reddy, K. C.; Bittman, R. *Tetrahedron* **1994,** *35,* 1371-1374.

Caldwell, C. G.; Sahoo, S. P.; Polo, S. A.; Eversole, R. R.; Lanza, T. J.; Mills, S. G.; Niedzwiecki, L. M.; Izquierdo-Martin, M.; Chang, B. C.; Harrison, R. K.; Kuo, D. W.; Lin, T.-Y.; Stein, R. L.; Durette, P. L.; Hagmann, W. K. *Bioorg. Med. Chem.* **1996,** *6,* 323-328.

Chen. W.; Zhang, D. *Nat. Cell Biol.* **2004,** *6,* 227-231.

Chu, C-W.; Hou, F.; Zhang, J.; Phu, L. Loktev, A. V.; Kirkpatrick, D. S.; Jackson, P. K.; Zhao, Y.; Zou, H. *Mol. Biol. Cell.* **2011,** *22,* 448-456.

Colanduoni, J. S.; Villafranca, J. J. *Bioorg. Chem.* **1986,** *14,* 163-169.

Cox, R. J.; Wang, P. S. H. *J. Chem. Soc., Perkin Trans. 1* **2001,** 2006-2008.

Cristau, H-J.; Coulombeau, A.; Genevois-Borella, A.; Sanchez, F.; Pirat, J-L. *J. Organomet. Chem.* **2002,** *643-644,* 381-391.

Cullis, P. M.; Harger, M. J. P. *J. Chem. Soc. Perkin. Trans. 2* **2002,** 1538-1543.

Dal Piaz, F.; Vassallo, A.; Lepore, L.; Tosco, A.; Bader, A.; De Tommasi, N. *J. Med. Chem.* **2009,** *52,* 3814-3828.

Deanin, G. G.; Gordon, M. W. *Biochem Biophys. Res. Commun.* **1976,** *71,* 676-683.

Deans, N. L.; Allison, R. D.; Purich, D. L. *Biochem. J.* **1992,** *286,* 243-251.

Desai, A.; Mitchison, T. J. *Annu. Rev. Cell Dev. Biol.* **1997,** *13,* 83-117.

Diemer, V.; Chaumeil, H.; Defoin, A.; Fort, A.; Boeglin, A.; Carre, C. *Eur. J. Org. Chem.* **2006,** 2727-2738.

Downing, K. H. *Annu. Rev. Cell Dev. Biol.* **2000,** *16,* 89-111.

Dráber, P.; Dráberová, E. Microtubules. In *Cytoskeloton and Human Disease,* Kavallaris, M. Ed.; Springer: New York, 2012; 29-53.

Duncan, K.; Walsh, C. T. *Biochemistry* **1988,** *27,* 3709-3714.

Dunn, S.; Morrison, E. E.; Liverpool, T. B.; Molina-Paris, C.; Cross, R. A.; Alonso, M. C.; Peckham, M. *J. Cell. Sci.* **2008,** *121,* 1085-1095.

Edde, B.; Rossier, J.; Le Caer, J.-P.; Desbruyeres, E.; Gros, F. *Science* **1990,** *247,* 83-85.

El Marini, A.; Roumestant, M. L.; Viallefont, P.; Razafindramboa, D.; Bonato, M.; Follet, M. *Synthesis* **1992,** *11*, 1104-1108.

Elliot, W. H.; Gale, E. F. *Nature* **1948,** *161,* 129-130.

Ellsworth, B. A.; Tom, N. J.; Bartlett, P. A. *Chem. Biol.* **1996,** *3,* 37-44.

Erck, C.; Peris, L.; Andrieux, A.; Meissirel, C.; Gruber, A. D.; Vernet, M.; Schweitzer, A.; Saoudi, Y.; Pointu, H.; Bosc, C.; Salin, P. A.; Job, D.; Wehland, J. *Proc. Nat. Acad. Sci.* **2005,** *102,* 7853-7858.

Fan, C.; Moews, P. C.; Walsh, C. T.; Knox, J. R. *Science* **1994,** *266,* 439-443.

Fawaz, M. V.; Topper, N.; Firestine S. M. *Bioorg. Chem.* **2011,** *39,* 185-191.

Fookes, C. J. R.; Gallagher, M. J.; Honegger, H. *J. Chem. Soc. Chem. Commun.* **1978,** 324.

Frey, P. A.; Hegeman, A. D. Acyl Group Transfer: Proteases and Esterases. *Enzymatic Reaction Mechanism*; Oxford University Press: New York, NY, 2007; 297-332.

Frieden, C. *J. Biol. Chem.* **1959,** *234,* 2891-2896.

Gaertig, J.; Cruz, M. A.; Bowen, J.; Gu, L.; Pennock, D. G.; Gorovsky, M. A. *J. Cell. Biol.* **1995,** *129,* 1301-1310.

Gallagher, M. J.; Ranasinghe, M. G.; Jenkins, I. D. *Phosphorus, Sulfur, and Silicon* **1996,** *115,* 255-259.

Gannett, P. M.; Nagel, D. L.; Reilly, P. J.; Lawson, T.; Sharpe, J.; Toth, B. *J. Org. Chem.* **1988,** *53,* 1064-1071.

Garnham, C. P.; Roll-Mecak, A. *Cytoskeleton* **2012,** *69,* 442-463.

Gegnas, L. D.; Waddell, S. T.; Chabin, R. M.; Reddy, S.; Wong, K. K. *Bioorg. Med. Chem. Lett.* **1998,** *8,* 1643-48.

Georgiadis, D.; Matziari, M.; Vassiliou, S.; Dive, V.; Yiotakis, A. *Tetrahedron* **1999,** *55,* 14635-14648.

Götz, F.; Bannerman, T.; Schleifer, K. -H. The Genera *Staphylococcus* and *Macrococcus*. In The Prokaryotes: A Handbook on the Biology of Bacteria, Third Edition; Dworkin, M.; Falkow, S.; Rosenberg, E.; Schleifer, K. -H.; Stackebrandt, E.; Springer Science: Singapore, 2006; 4, 30-32.

Gray, M. D. M.; Smith, D. J. H. *Tetrahedron Lett.* **1980,** *21,* 859-860.

Grobelny, D.; Goli, U. B.; Galardy, R. E. *Biochemistry* **1989,** *28,* 4948-4951.

Gunderson, G. G.; Kalnoski, M. H.; Bulinski, J. C. *Cell* **1984,** *38,* 779-789.

Hallak, M. E.; Rodrigues, J. A.; Barra, H. S.; Caputto, R. *FEBS Lett.* **1977,** *73,* 147-150.

Hammond, J. W.; Cai, D.; Verhey, K. J. *Curr. Opin. Cell Biol.* **2008,** *20,* 71-76.

Han, S.-Y.; Kin, Y.-A. *Tetrahedron* **2004,** *60,* 2447-2467.

Hanson, J. E.; Kaplan, A. P.; Bartlett, P. A. *Biochemistry* **1989,** *28,* 6294-6305.

Healy, V. L.; Lessard, I. A. D.; Roper, D. I.; Knox, J. R.; Walsh, C. T. *Chem. Biol.* **2000,** *7,* R109-R119.

Hermanson, G. T. Introduction to Bioconjugation. *Bioconjugate Techniques*, Third Edition; Academic Press, 2013; 233-234.

Hirschmann, R.; Yager, K. M.; Tayler, C. M.; Witherington, J.; Sprengeler, P. A.; Phillips, B. W.; Moore, W.; Smith, A. B. *J. Am. Chem. Soc.* **1997,** *119,* 8177-8190.

Howard, J.; Hyman, A. A. *Nature* **2003,** *422,* 753-758.

Ikegami, K.; Heier, R. L.; Taruishi, M.; Takagi, H.; Mukai, M.; Shimma, S.; Taira, S.; Hatanaka, K.; Morone, N.; Yao, I.; Campbell, P. K.; Yuasa, S.; Janke, C.; MacGregor, G. R.; Setou, M. *Proc. Nat. Acad. Sci. U.S.A.* **2007,** *104,* 3213-3218.

Jacobsen, N. E.; Bartlett, P. A. *J. Am. Chem. Soc.* **1981,** *103,* 654-657.

Job, D.; Valiron, O.; Oakly, B. *Curr. Opin. Cell Biol.* **2003,** *15,* 111-117.

Jordan, M. A.; Wilson, L. *Nat. Rev. Cancer* **2004,** *4,* 253-265.

Kalinina, E.; Biswas, R.; Berezniuk, I.; Hermoso, A.; Aviles, F. X.; Fricker, L. D. *FASEB J.* **2007,** *21,* 836-850.

Kam, C-M.; Nishino, N.; Powers, J. C. *Biochemistry* **1979,** *18,* 3032-3038.

Kaplan, A. P.; Bartlett, P. A. *Biochemistry* **1991,** *30,* 8165-8170.

Karanewsky, D. S.; Badia, M. C. *Tetrahedron Lett.* **1986,** *27,* 1751-1754.

Karanewsky, D. S.; Badia, M. C.; Cushman, D. W.; DeForrest, J. M.; Dejneka, T.; Loots, M. J.; Perri, M. G.; Petrillo, E. W.; Powell, J. R. *J. Med. Chem.* **1988,** *31,* 204-212.

Kashiwaya, K.; Nakagawa, H.; Hosokawa, M.; Mochizuki, Y.; Ueda, K.; Piao, L. Chung, S.; Hamamoto, R.; Eguchi, H.; Ohigashi, H.; Ishikawa, O.; Janke, C.; Shinomura, Y.; Nakamura, Y. *Cancer Res.* **2010,** *70,* 4024-4033.

Khomutov, R. M.; Osipova, T. I. *Bull. Acad. Sci. USSR Div. Chem. Sci.* **1978,** *27,* 1722.

Klotz, I. M.; Morrison, R. T. *J. Am. Chem. Soc.* **1947,** *69,* 473.

Kormendi, V.; Szyk A.; Piszczek, G.; Roll-Mecak, A. *J. Biol. Chem.* **2012,** *287,* 41569-41575.

Kreis, T. E. *EMBO J.* **1987,** *6,* 2597-2606.

Kubo, K.; Ohyama, S-I.; Shimizu, T.; Takami, A.; Muroka, H.; Nishitoba, T.; Shinichiro, Y.; Kobayashi, Y.; Linama, N.; Isoe, T. *Bioorg. Med. Chem.* **2003,** *11,* 5117-5134.

Kumar, M.; Flavin, M. *J. Biol. Chem.* **1981,** *256,* 7678-7686.

Lacoste, A.; Chollet-Gravey, A.; Vo-Quang, L.; Vo-Quang, Y.; Le Goffic, F. *Eur. J. Med. Chem.* **1991,** *26,* 255-260.

Lafanechère, L.; Courtay-Cahen, C.; Kawakami, T.; Jacrot, M.; Rüdiger M.; Wehland, J.; Job, D.; Margolis, R. L. *J. Cell Sci.* **1998,** *111,* 171-181.

Leason, M.; Cunliffe, D.; Parkin, D.; Lea, P. J.; Miflin, B. J. *Phytochemistry* **1982,** *21,* 855-857.

Liao, G.; Gundersen, G. G. *J. Cell Biol.* **1998,** *273,* 9797-9803.

Linfield, W. M.; Jungermann, E.; Guttmann, A. T. *J. Org. Chem.* **1961,** *26,* 4088-4092.

Liu, X.; Hu, E.; Tian, X.; Mazur, A.; Ebetino, F. H. *J Organomet. Chem.* **2002,** *646,* 212-222.

Malachowski, W. P.; Coward, J. K. *J. Org. Chem.* **1994,** *59,* 7625-7634.

McCleery, P. P.; Tuck, B. *J. Chem. Soc. Perkin. Trans. I* **1989,** 1319-1329.

McDermott, A. E.; Creuzet, F.; Griffin, R. G. *Biochemistry* **1990,** *29,* 5767-5775.
Meek, T. D.; Villafranca, J. J. *Biochemistry* **1980,** *19*, 5513-5519.

Mialhe, A.; Lafanechère, L.; Treilleux, I.; Peloux, N.; Dumontet, C.; Brémond, A.; Panh, M.; Payan, R.; Wehland, J.; Margolis, R.; Job, D. *Cancer Res*. **2001,** *61,* 5024-5027.

Michaelis, A.; Kaehne, R. *Chem. Ber.* **1898,** *31,* 1048-1055.

Mullins, L. S.; Zawadzke, L. E.; Walsh, C. T.; Raushel, F. M. *J. Biol. Chem.* **1990,** *265,* 8993-8998.

Murofushi, H. *J. Biochem.* **1980,** *87,* 979-984.

Ohashi, A.; Satake, A.; Kobuke, Y. *Bull Chem. Soc. Jpn.* **2004,** *77,* 365-374.

Okada, Y. *Curr. Org. Chem.* **2001,** *5,* 1-43.

Parsons, W. H.; Patchett, A. A.; Bull, H. G.; Schoen, W. R.; Taub, D.; Davidson, J.; Combs, P. L.; Springer, J. P.; Gadebusch, H.; Weissberger, B.; Valiant, M. E.; Mellin, T. N.; Busch, R. D.; *J. Med. Chem.* **1988,** *31,* 1772-1778.

Pathak, N.; Austin, C. A.; Drummond, I. A. *J. Biol. Chem.* **2011,** *286,* 11685-11695.

Peris, L.; Thery, M.; Fauré, J.; Saoudi, Y.; Lafanechère, L.; Chilton, J. K.; Gordon-Weeks, P.; Caligart, N.; Bornenes, M.; Wordeman, L.; Wehland, J.; Andrieux, A.; Job, D. *J. Cell Biol.* **2006,** *174,* 839-849.

Preston, S. F.; Deanin, G. G.; Hanson, R. K.; Gordon, M. W. *J. Mol. Evol.* **1979,** *13,* 233-244.

Rabinowitz, R. *J. Am. Chem. Soc.* **1960,** *82,* 4562-4567.

Raudnitz, H. *Chem. Ber.* **1927,** *60B*, 743-748.

Raybin, D.; Flavin, M. *Biochemistry* **1977a,** *16,* 2189-2194.

Raybin, D.; Flavin, M. *Biochem Biophys. Res. Commun.* **1975,** *65,* 1088-1095.

Raybin, D.; Flavin, M. *J. Cell. Biol.* **1977b,** *73,* 492-504.

Redeker, V.; Levilliers, N.; Schmitter, J. M.; Le Caer, J-P.; Rossier, J.; Adoutte, A. *Science* **1994,** *266,* 1688-1690.

Ronzio, R. A.; Meister, A. *Proc. Natl. Acad. Sci. U.S.A.* **1968,** *59,* 164-170.

Ronzio, R. A.; Rowe, W. B.; Meister, A. *Bichemistry* **1969,** *8,* 1066-1075.

Rüdiger, M. Wehland, J.; Weber, K. *Eur. J. Biochem.* **1994,** *220,* 309-320.

Sampson, N. S.; Bartlett, P. A. *J. Org. Chem.* **1988,** *53,* 4500-4503.

Schmidt, H. *Chem. Ber.* **1948,** *81,* 477-483.

Sefkow, M.; Kaatz, H. *Tetrahedron Lett.* **1999,** *40,* 6561-6562.

Shi, Y.; Walsh, C. T. *Biochemistry* **1995,** *34,* 2768-2776.

Suda, H.; Aogagi, T.; Takeuchi, T.; Umezawa, H. *J. Antibiot.* **1973,** *26,* 621-623.

Sueki, S.; Kuninobu, Y. *Org. Lett.* **2013,** *15,* 1544-1547.

Szyk, A.; Deaconescu, A. M.; Piszczek, G.; Roll-Mecak, A. *Nat. Struct. Mol. Biol.* **2011,** *18,* 1250-1259.

Tam, J. P.; Cunningham-Rundles, W. F.; Erickson, B. W.; Merrifield, R. B. *Tetrahedron Lett.* **1977,** *46,* 4001-4004.

Tanner, M. E.; Vaganay, S.; van Heijenoort, J.; Blanot, D. *J. Org. Chem.* **1996,** *61,* 1756-1760.

Thorsett, E. D.; Harris, E.E.; Peterson, E. R.; Greenlee, W. J.; Patchett, A. A.; Ulm, E. H.; Vassil, T. C. *Proc. Natl. Acad. Sci. U.S.A.* **1982,** *79,* 2176-2180.

Thottathil, J. K.; Przybyla, C. A.; Moniot, J. L. *Tetrahedron Lett.* **1984a,** *25,* 4737-4740.

Thottathil, J. K.; Ryono, D. E.; Przybyla, C. A.; Moniot, J. L.; Neubeck, R. *Tetrahedron Lett.* **1984b,** *25,* 4741-4744.

Turk, B. *Nat. Rev. Drug Discov.* **2006,** *5,* 785-799.

Umewaza, S.; tatsuta, K.; Izawa, O.; Tschiya, T. *Tetrahedron Lett.* **1972,** *13,* 97-100.

Valiaeva, N.; Bartley, D.; Konno, T.; Coward, J. K. *J. Org. Chem.* **2001,** *66,* 5146-5154.

Verhey, K. J.; Gaertig, J. *Cell Cycle* **2007,** *6,* 2152-2160.

Villieras, J.; Rambaud, M. *Org. Synth.* **1988,** *66,* 220.

Vinczer, P. *Acta. Chimica Hungarica* **1990,** *127,* 581-585.

Wade, R. H. *Mol. Biotechnol.* **2009,** *43,* 177-191.

Wasteneys, G. O.; Lechner, B. Microtubules. In *Cellular Membrane Domains,* Nabi, I. R. Ed.; Wiley-Blackwell: Hoboken, NJ, 2011; 229-243.

Weaver, L. H.; Kester, W. R.; Matthews, B. W. *J. Mol. Biol.* **1977,** *114,* 119-132.

Webster, D. R.; Oxford, M. G. *J. Cell Biochem.* **1996,** *60,* 424-436.

Webster, D. R.; Wehland, J.; Weber, K.; Borisy, G. G. *J. Cell Biol.* **1990,** *111,* 113-122.

Wehland, J.; Schröder, H. C.; Weber, K. *Methods Enzymol.* **1986,** *134,* 170-179.

Weisenberg, R. C.; Borisy, G. G.; Taylor, E. W. *Biochemistry* **1968,** *7,* 4466-4479.

Westermann, S.; Weber, K. *Nat. Rev. Mol. Cell. Biol.* **2003,** *4,* 938-947.

Wiese, C.; Zheng, Y. *J. Cell. Sci.* **2006,** *119,* 4143-4153.
Yang, J. S.; Chun, K.; Park, J. E.; Cho, M.; Seo, J.; Song, D.; Yoon, H.; Park, C-H.; Joe,

B-Y.; Choi, J-H.; Kim, M-H.; Han, G. *Bioorg. Med. Chem.* **2010,** *18,* 8618-8629.

Zeiss, H. *Tetrahedron* **1992,** *38,* 8263-8270.

Zeng, B.; Wong, K. K.; Pompliano, D. L.; Reddy, S.; Tanner, M. E. *J. Org. Chem.* **1998,** *63,* 10081-10086.

Zhu, Z.; Mazzola, R.; Sinning, L.; McKittrick, B.; Niu, X.; Lundell, D; Sun, J.; Orth, P.; Guo, Z.; Madison, V.; Ingram, R.; Bever, B. M. *J. Med. Chem.* **2008,** *51,* 725-736.

Appendix: NMR of Selected Compounds

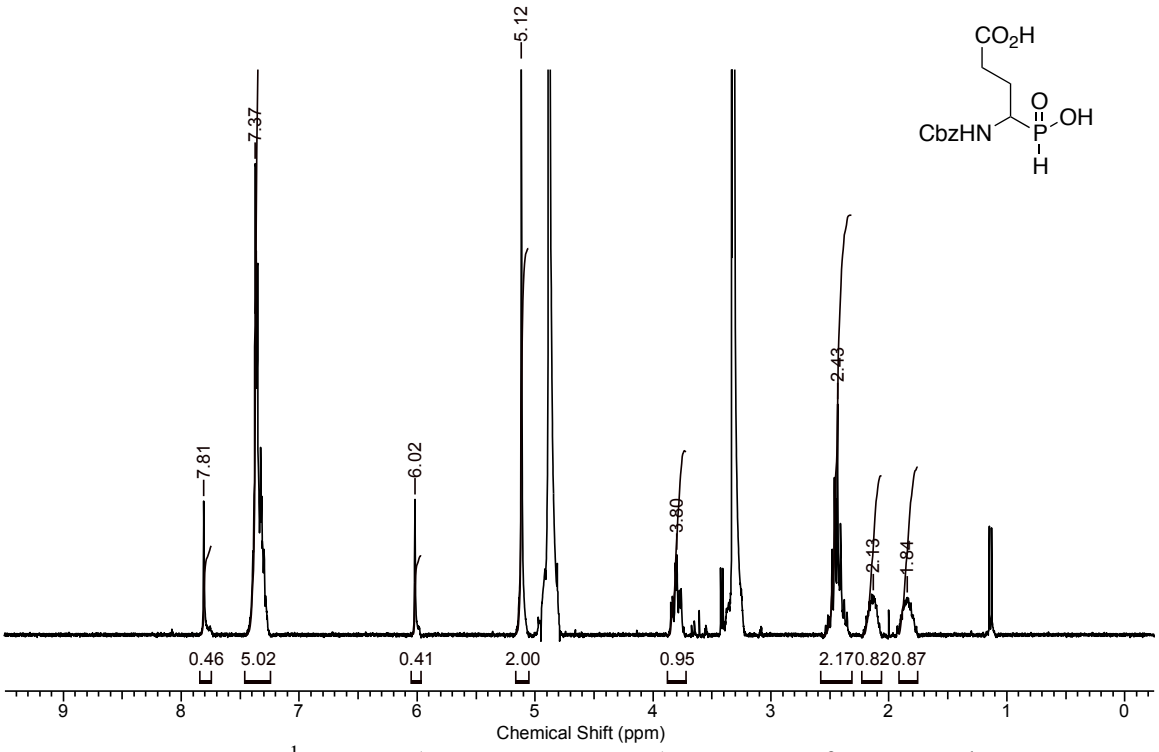

Figure A.1 ^{1}H NMR (300 MHz, CD_3OD) spectrum of compound **10**.

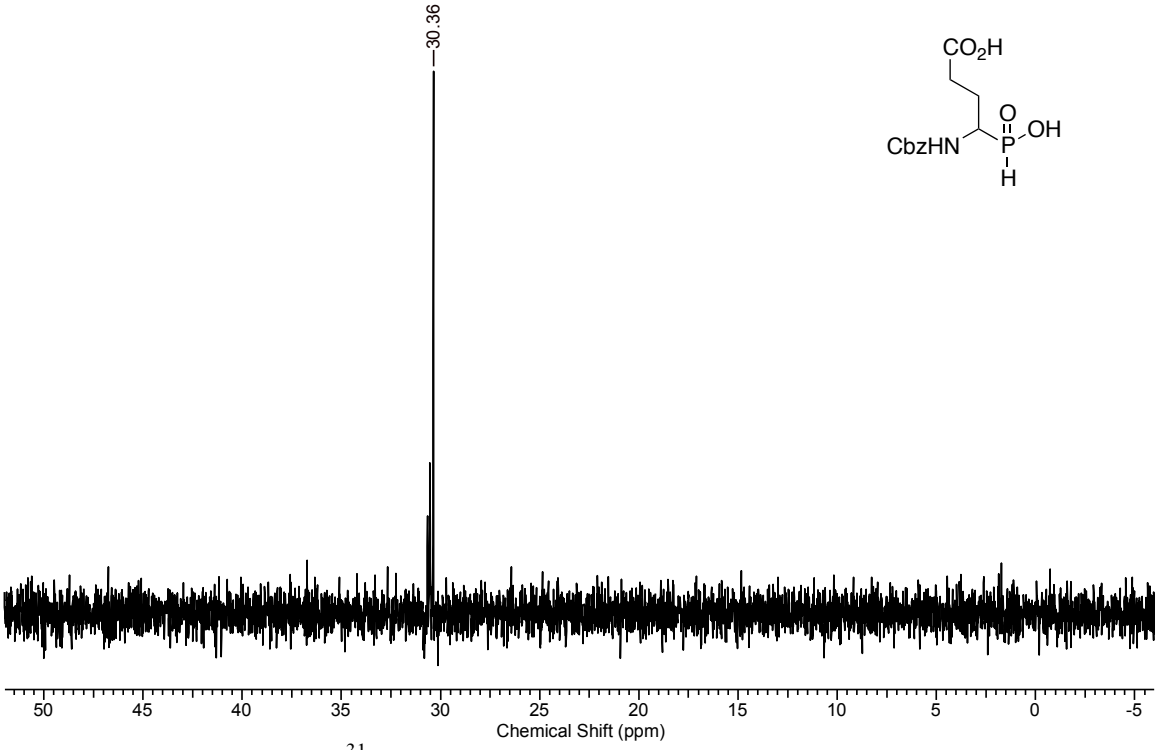

Figure A.2 ^{31}P NMR (121.5 MHz, CD_3OD) spectrum of **10**.

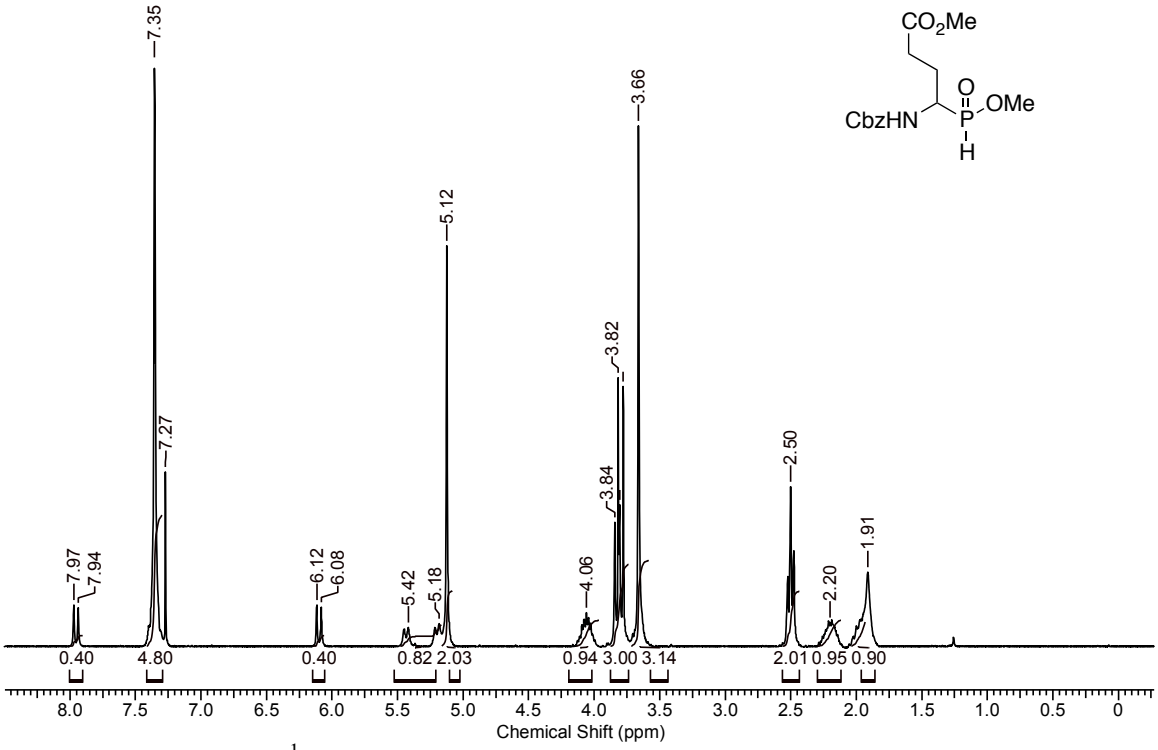

Figure A.3 ^{1}H NMR (300 MHz, CD_3OD) spectrum of compound **11**.

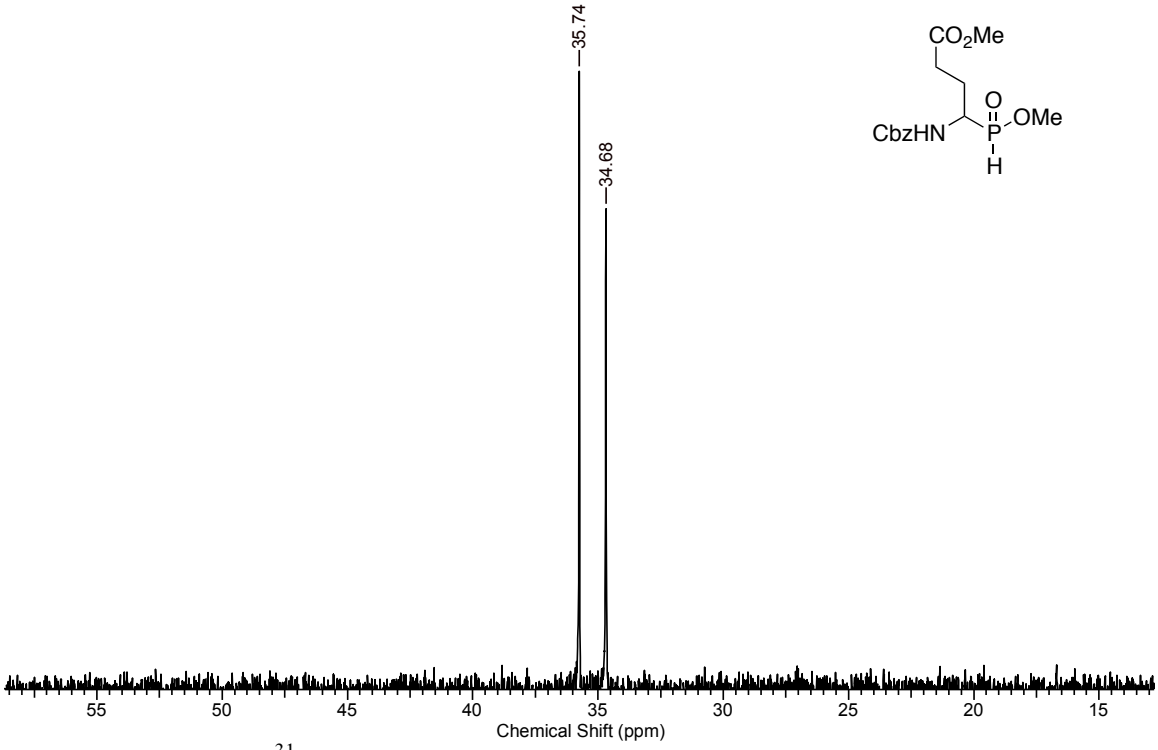

Figure A.4 ^{31}P NMR (121.5 MHz, CD_3OD) spectrum of compound **11**.

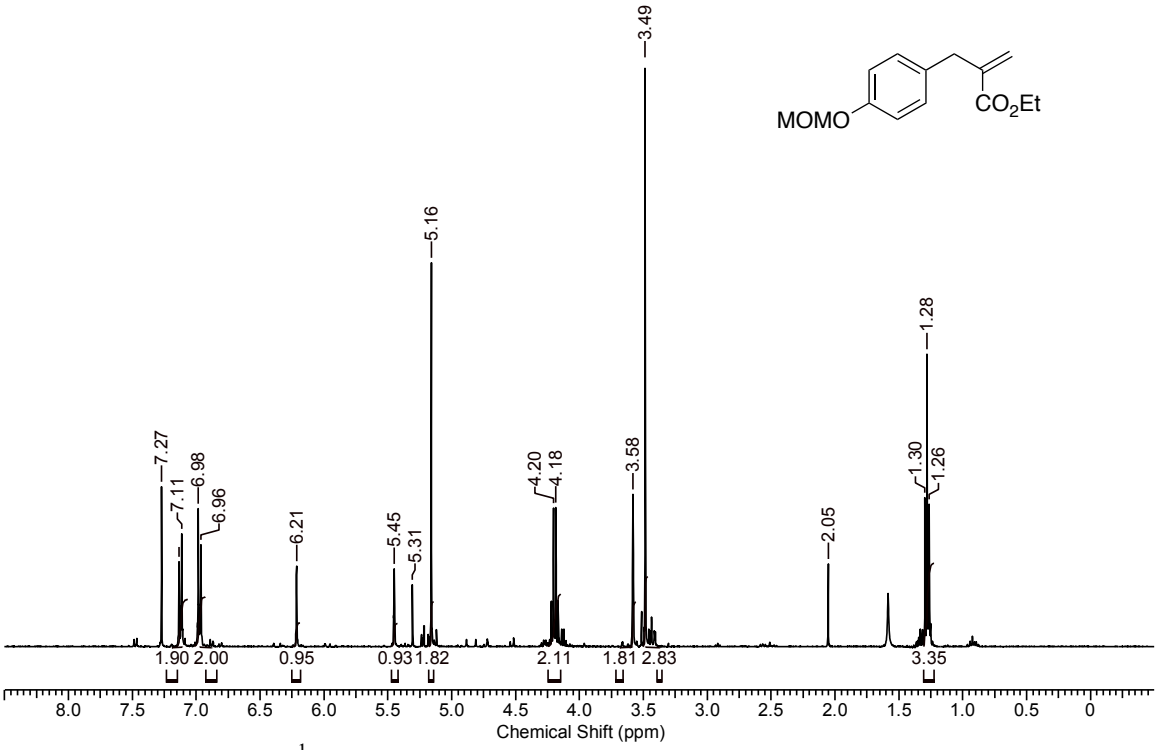

Figure A.5 ^{1}H NMR (300 MHz, $CDCl_3$) spectrum of compound **17**.

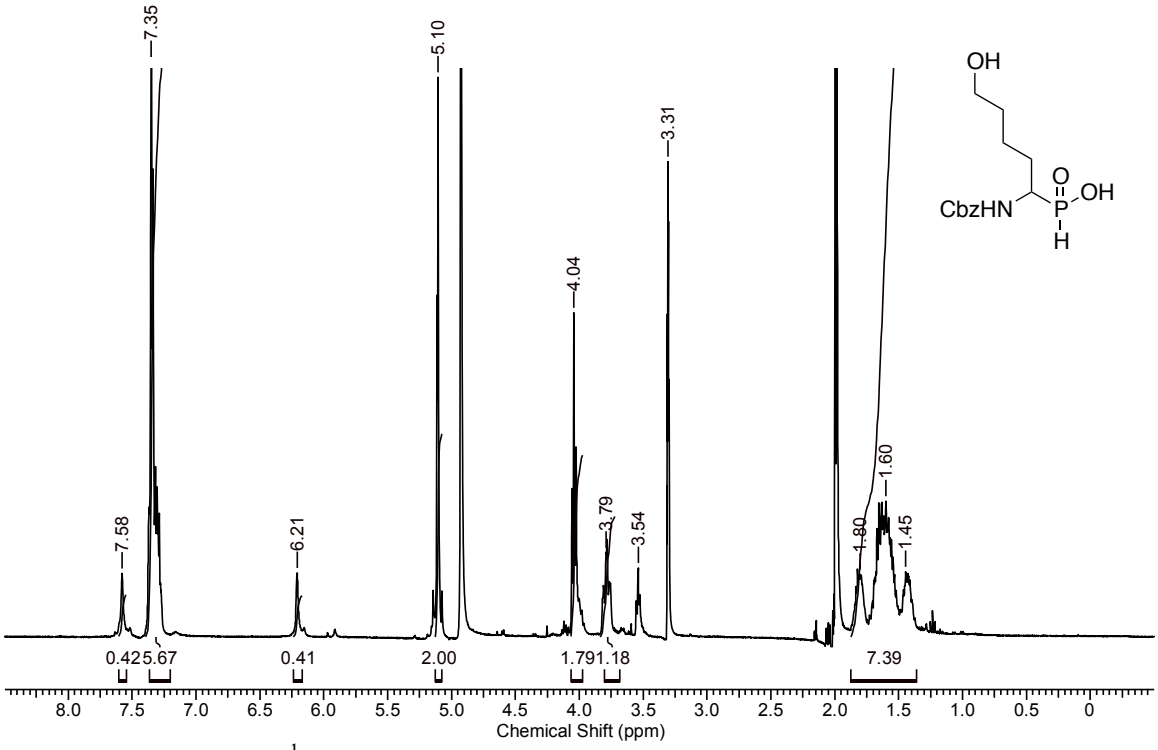

Figure A.6 ^{1}H NMR (400 MHz, CD_3OD) spectrum of compound **28**.

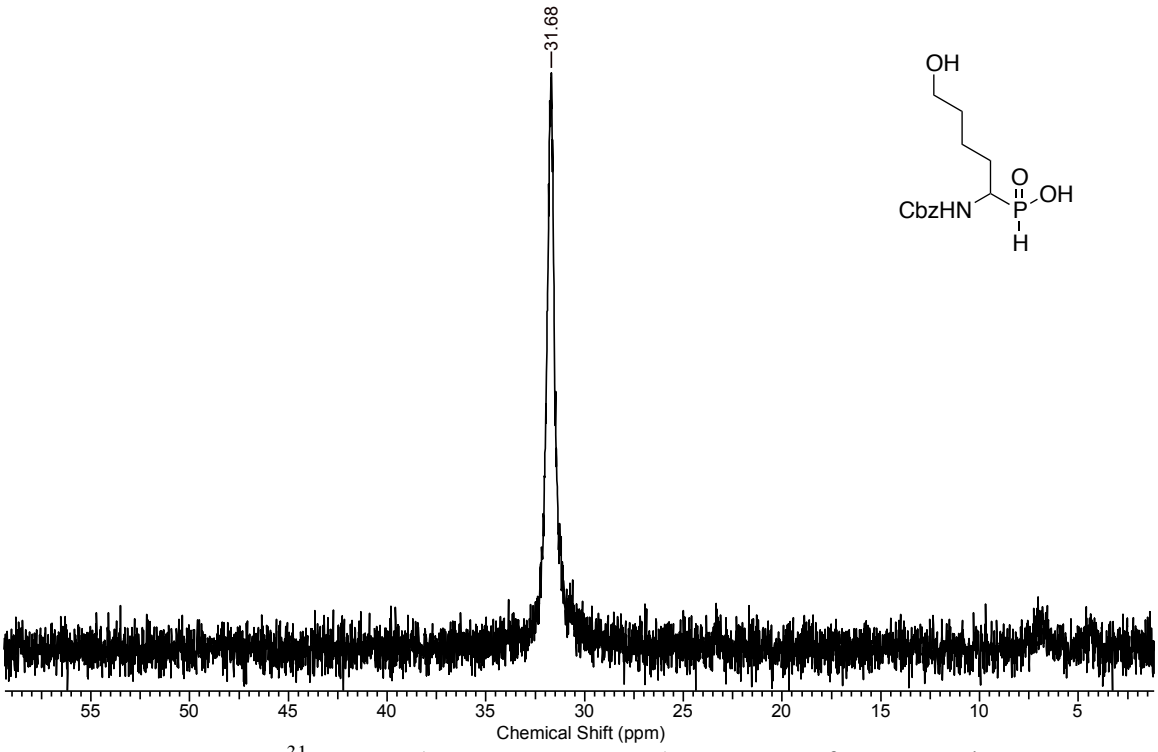

Figure A.7 ^{31}P NMR (162 MHz, CD_3OD) spectrum of compound **28**.

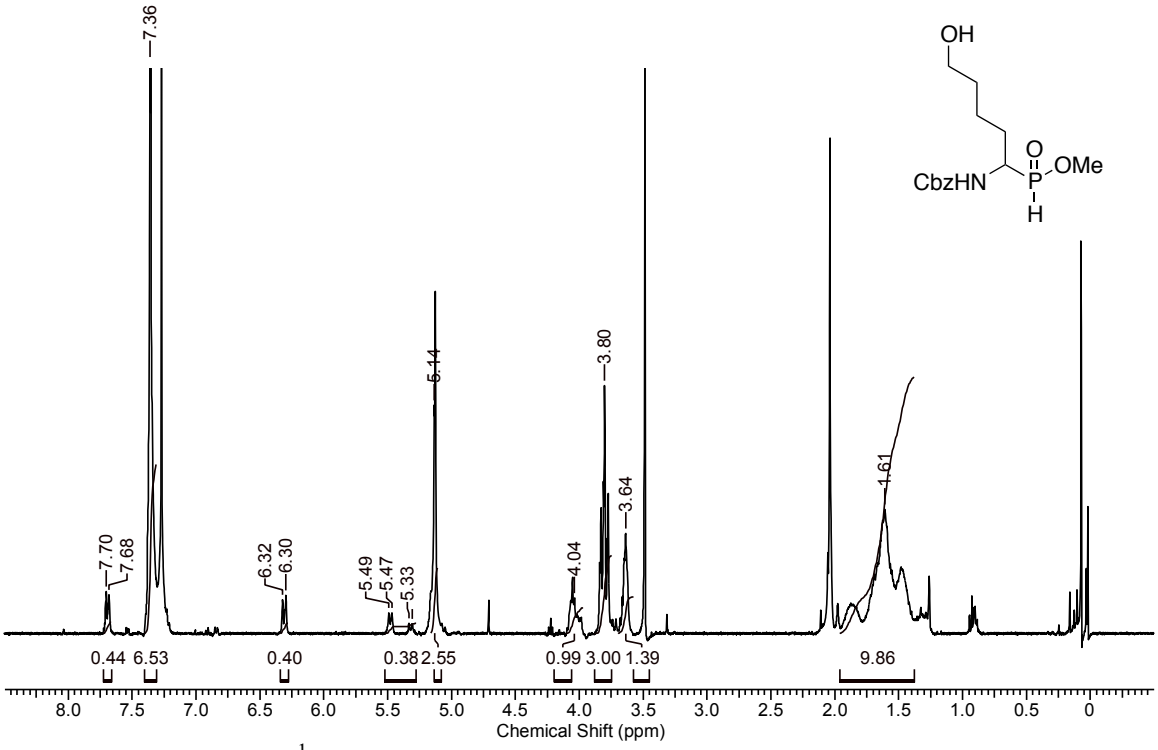

Figure A.8 ^{1}H NMR (400 MHz, $CDCl_3$) spectrum of compound **29**.

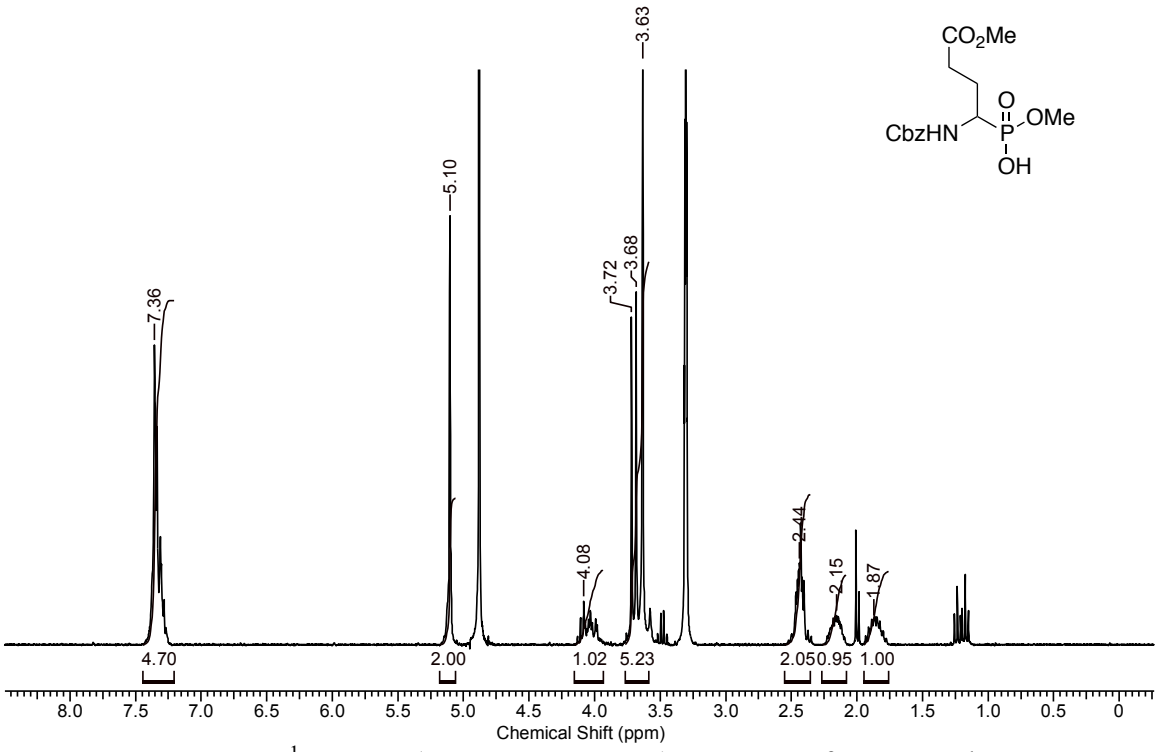

Figure A.9 ^{1}H NMR (300 MHz, CD_3OD) spectrum of compound **35**.

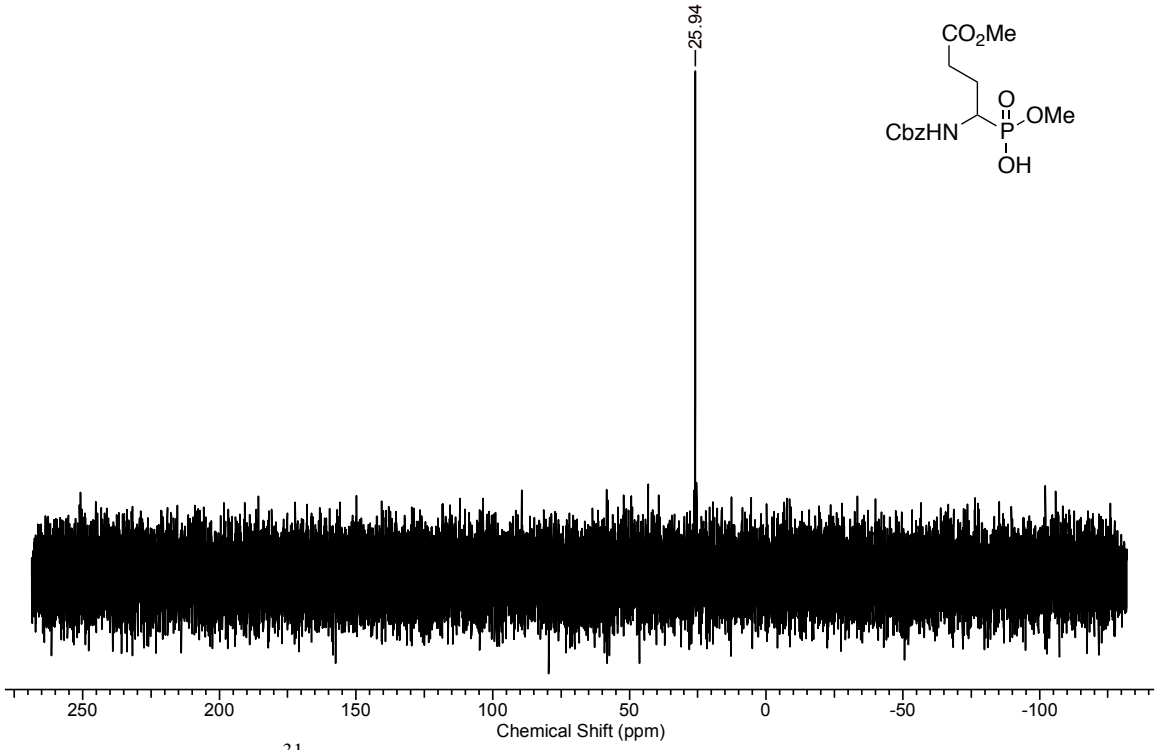

Figure A.10 ^{31}P NMR (121.5 MHz, CD_3OD) spectrum of compound **35**.

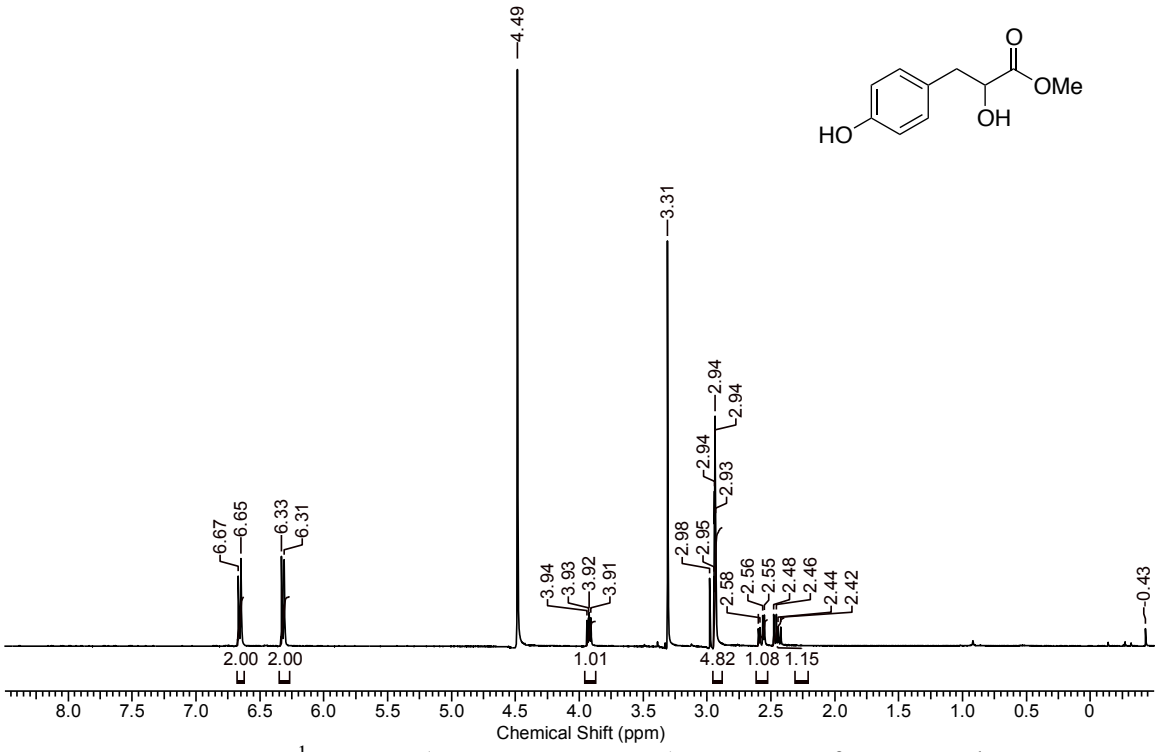

Figure A.11 ^{1}H NMR (300 MHz, CD_3OD) spectrum of compound **38**.

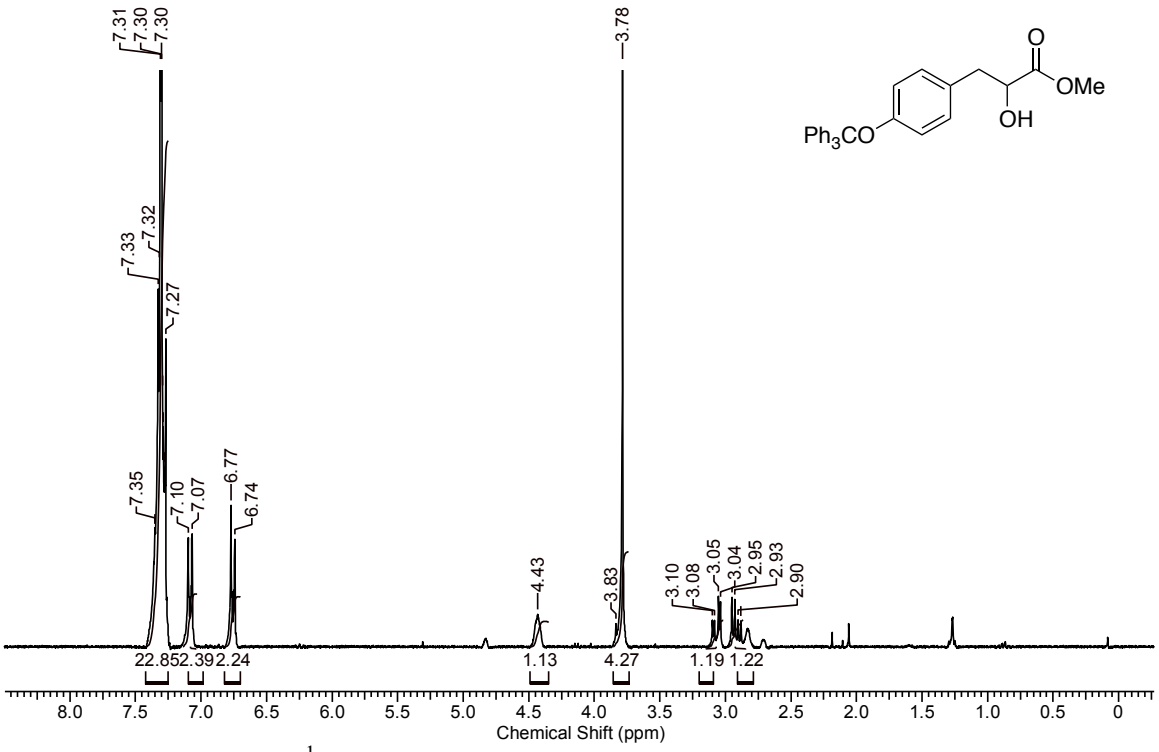

Figure A.12 ^{1}H NMR (400 MHz, $CDCl_3$) spectrum of compound **39**.

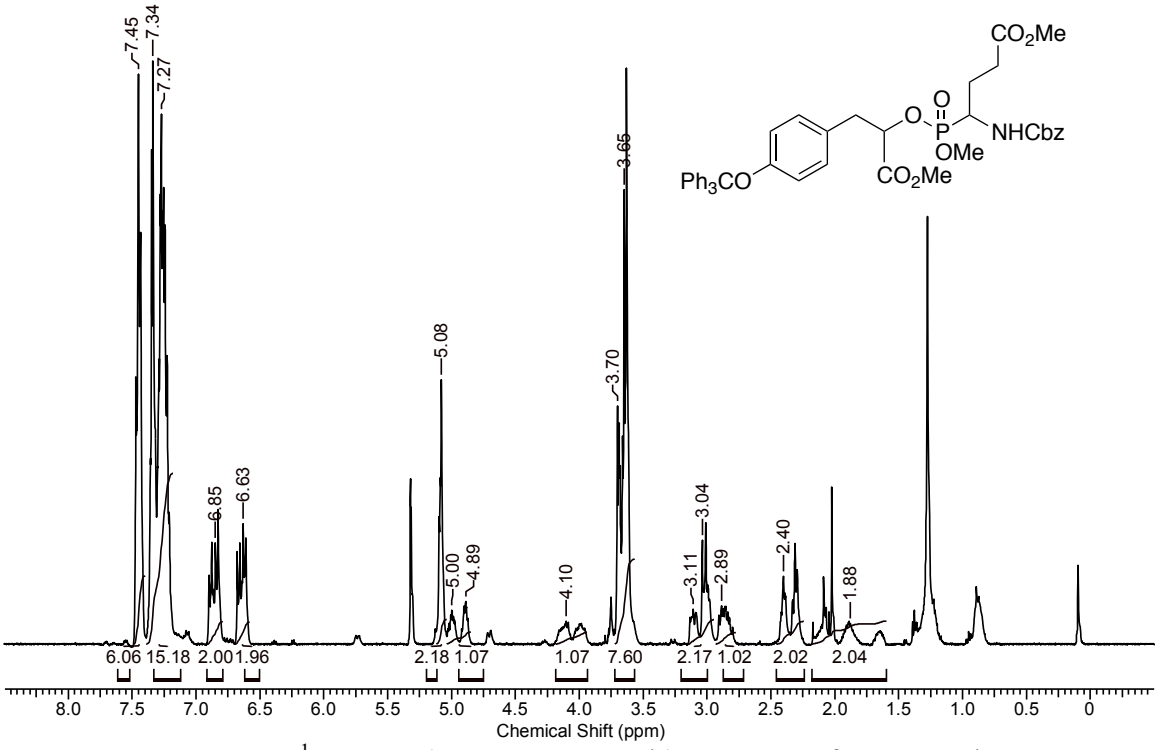

Figure A.13 ^{1}H NMR (400 MHz, CD_2Cl_2) spectrum of compound **40**.

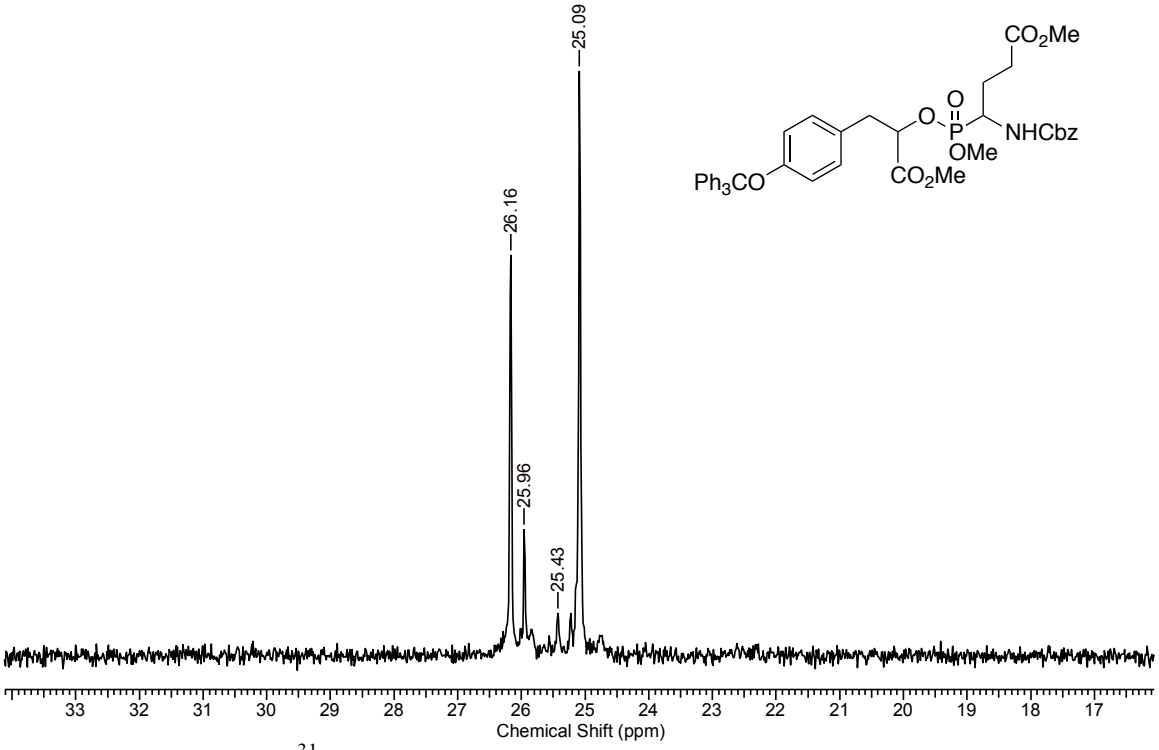

Figure A.14 ^{31}P NMR (400 MHz, CD_2Cl_2) spectrum of compound **40**.

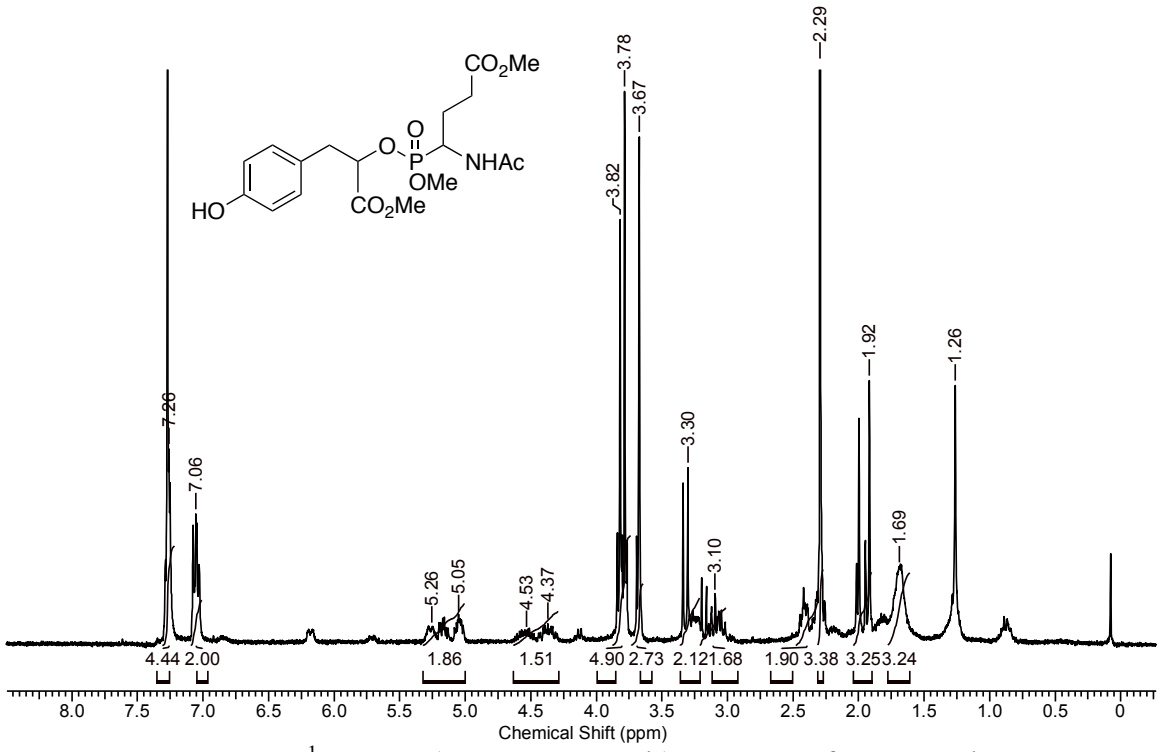

Figure A.15 ^{1}H NMR (400 MHz, $CDCl_3$) spectrum of compound **43**.

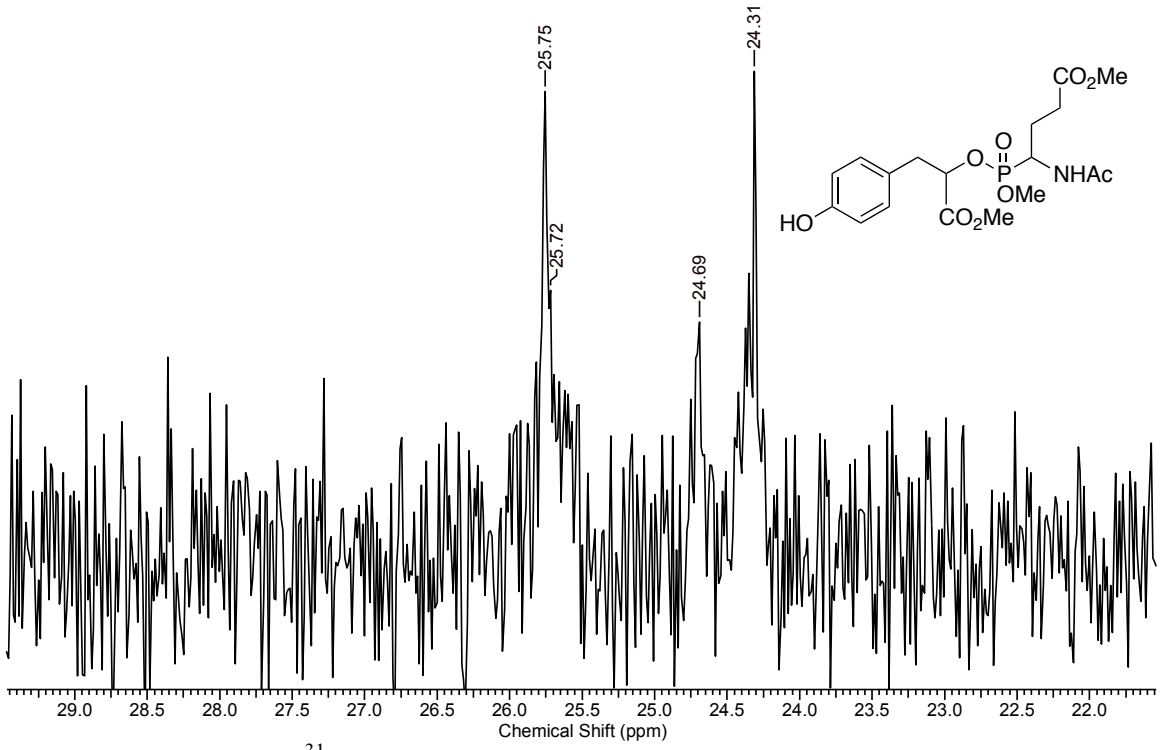

Figure A.16 ^{31}P NMR (162 MHz, $CDCl_3$) spectrum of compound **43**.

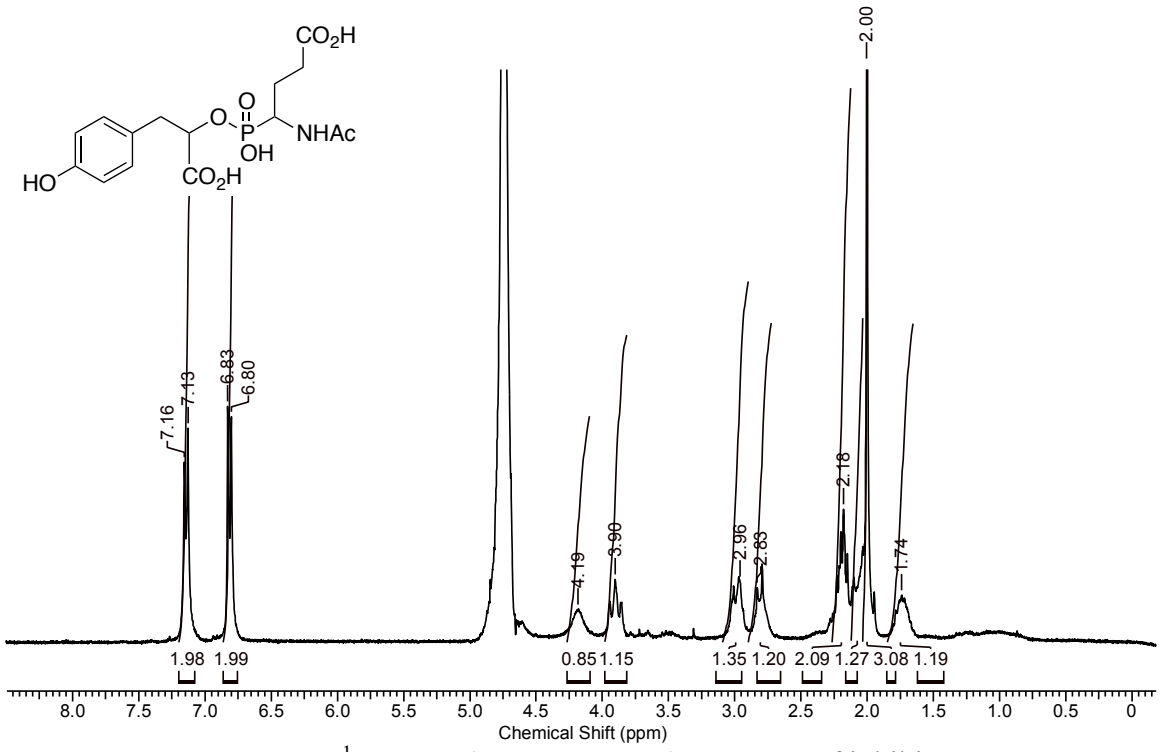

Figure A.17 ^{1}H NMR (400 MHz, D_2O) spectrum of inhibitor **2**.

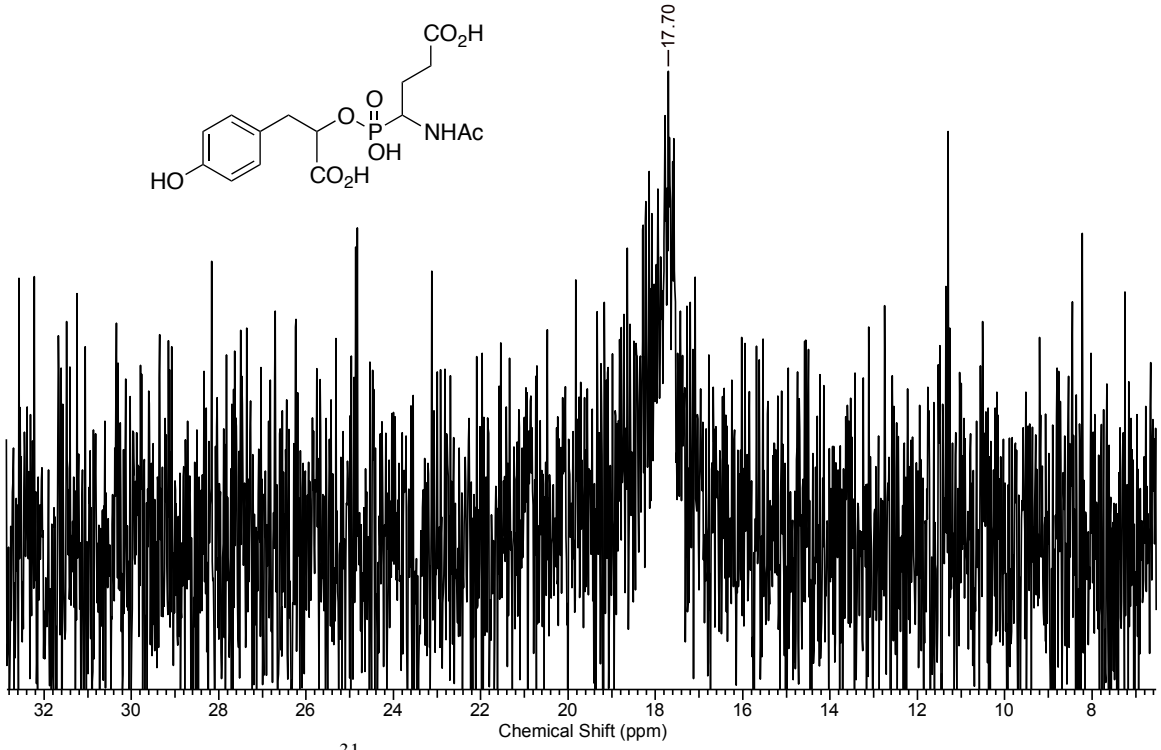

Figure A.18 ^{31}P NMR (162 MHz, D_2O) spectrum of inhibitor **2**.

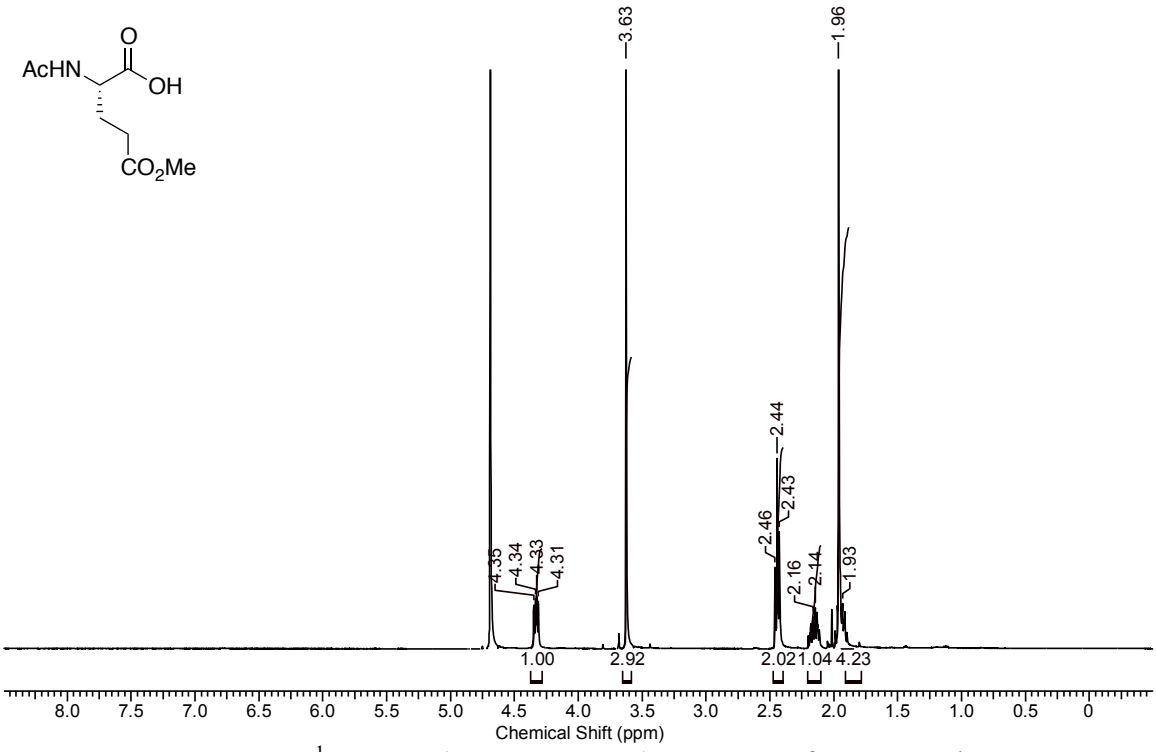

Figure A.19 ^{1}H NMR (300 MHz, D_2O) spectrum of Compound **48**.

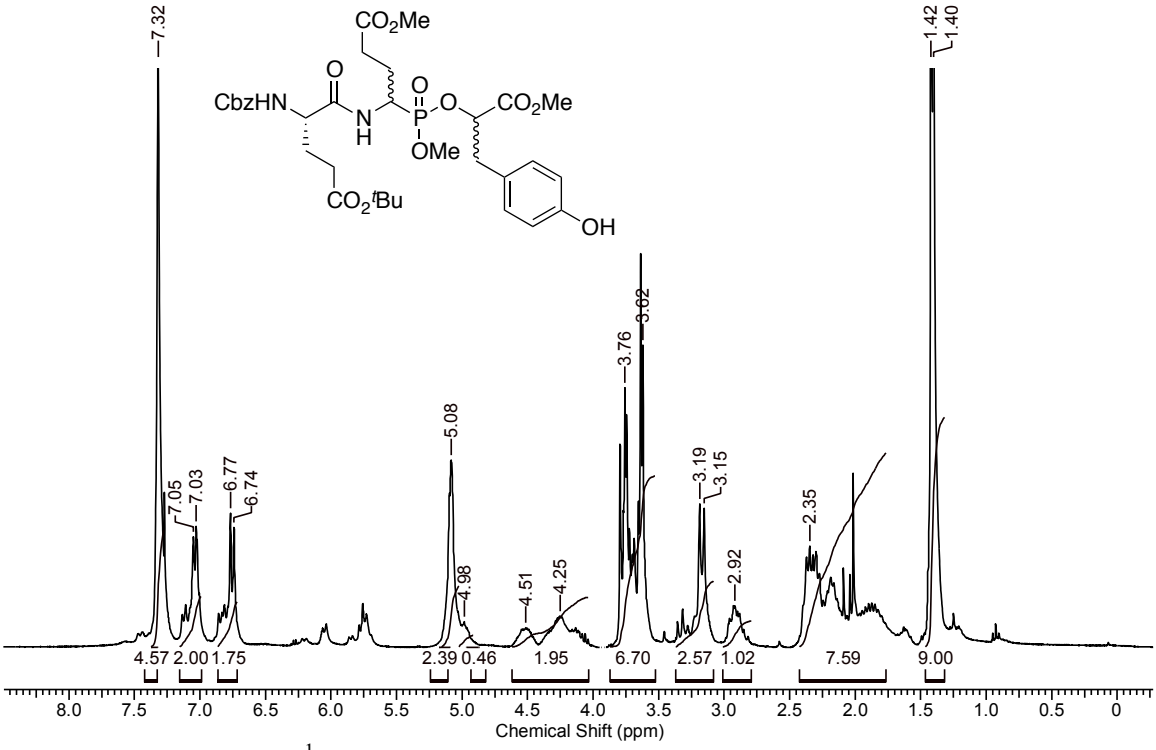

Figure A.20 ^{1}H NMR (300 MHz, $CDCl_3$) spectrum of compound **52**.

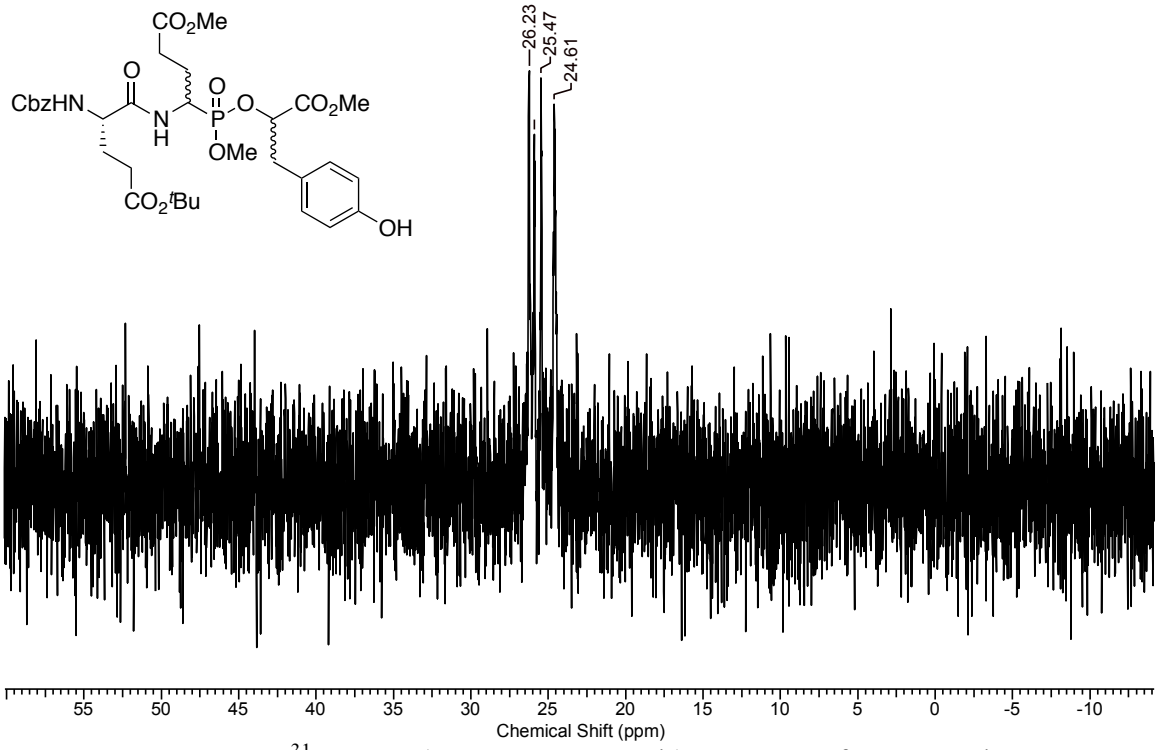

Figure A.21 ^{31}P NMR (121.5 MHz, $CDCl_3$) spectrum of compound **52**.

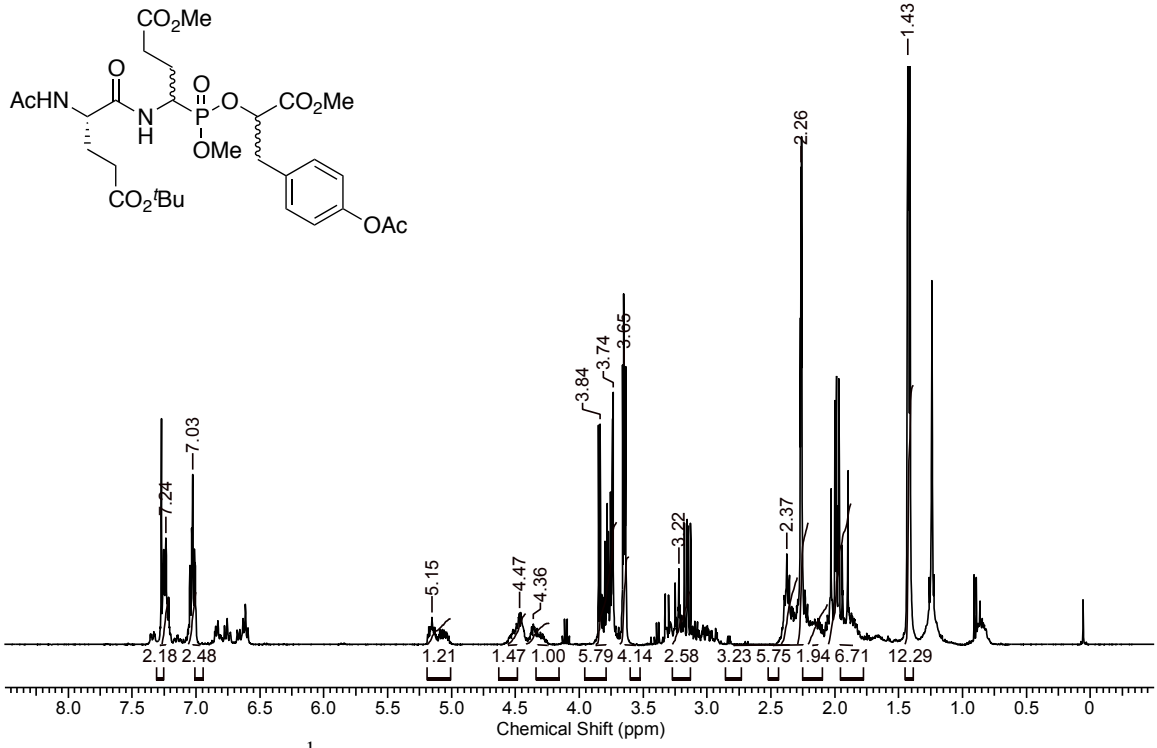

Figure A.22 ^{1}H NMR (400 MHz, $CDCl_3$) spectrum of compound **54**.

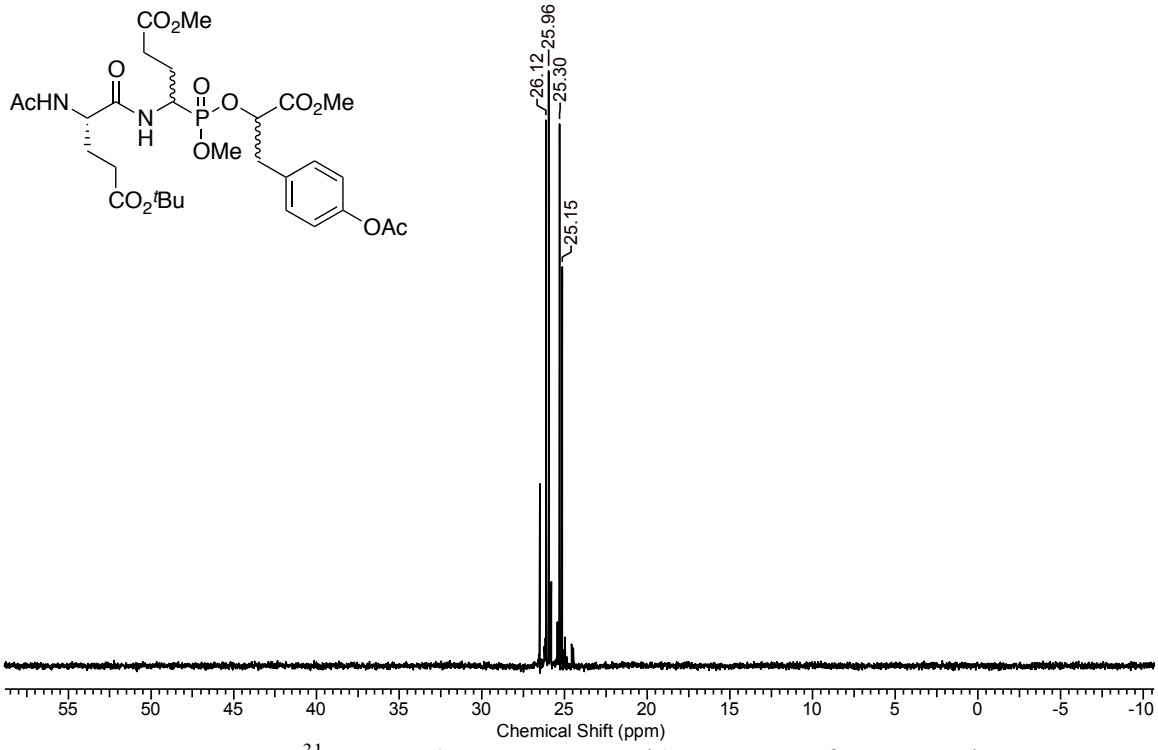

Figure A.23 ^{31}P NMR (161 MHz, $CDCl_3$) spectrum of compound **54**.

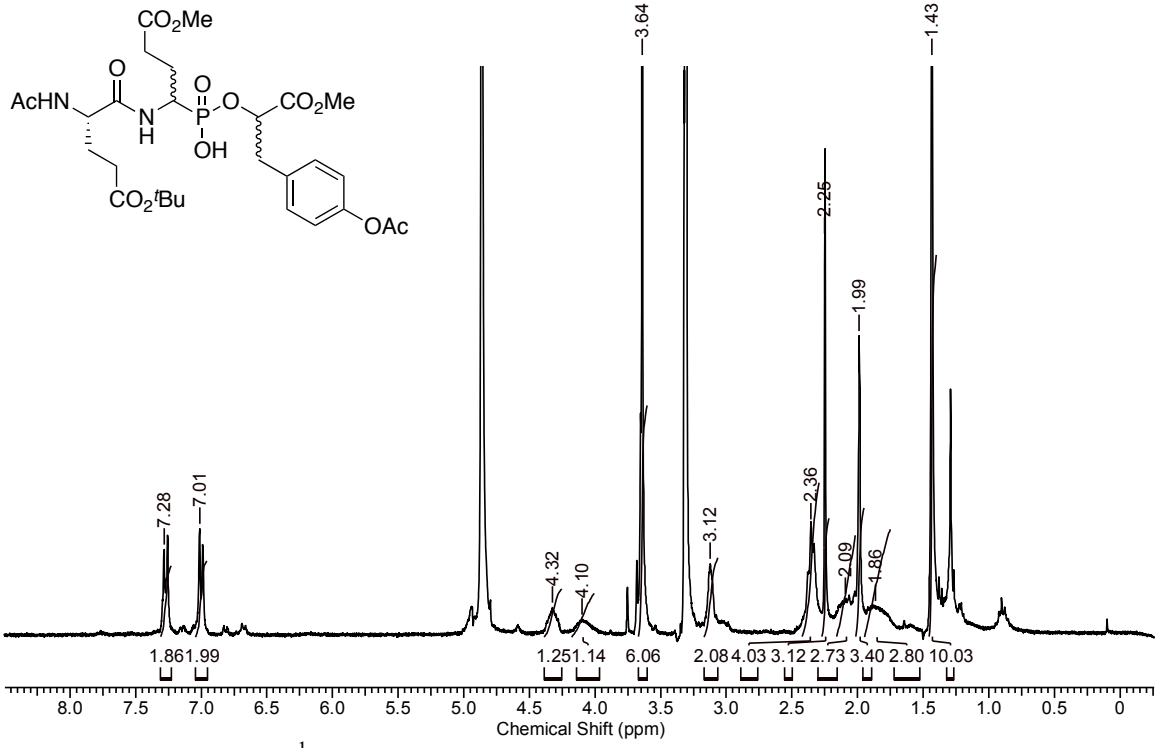

Figure A.24 ^{1}H NMR (400 MHz, CD_3OD) spectrum of compound **55**.

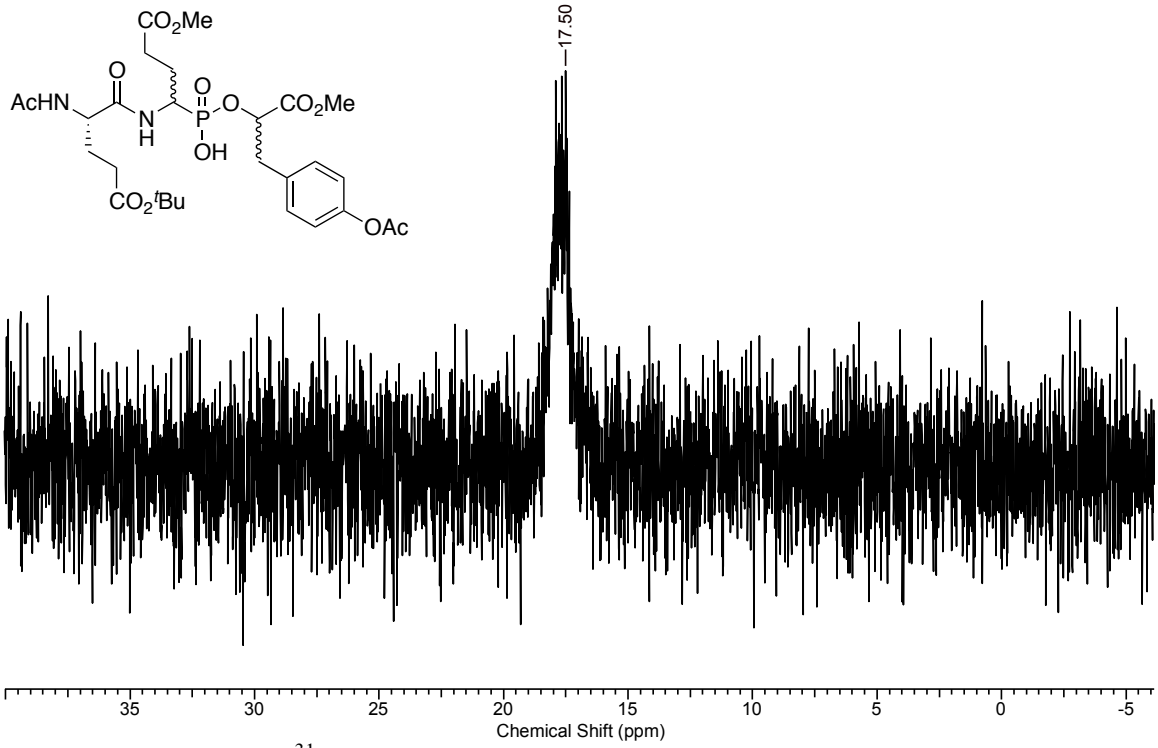

Figure A.25 ^{31}P NMR (162 MHz, CD_3OD) spectrum of compound **55**.

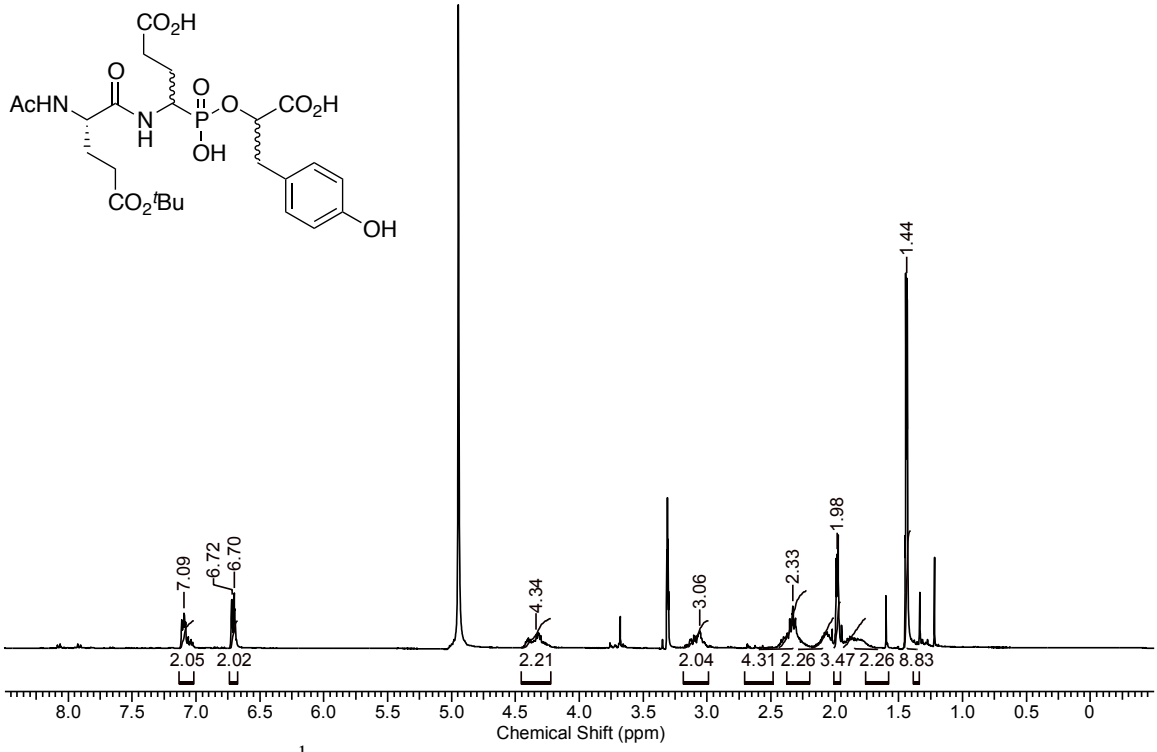

Figure A.26 ^{1}H NMR (400 MHz, CD_3OD) spectrum of compound **58.**

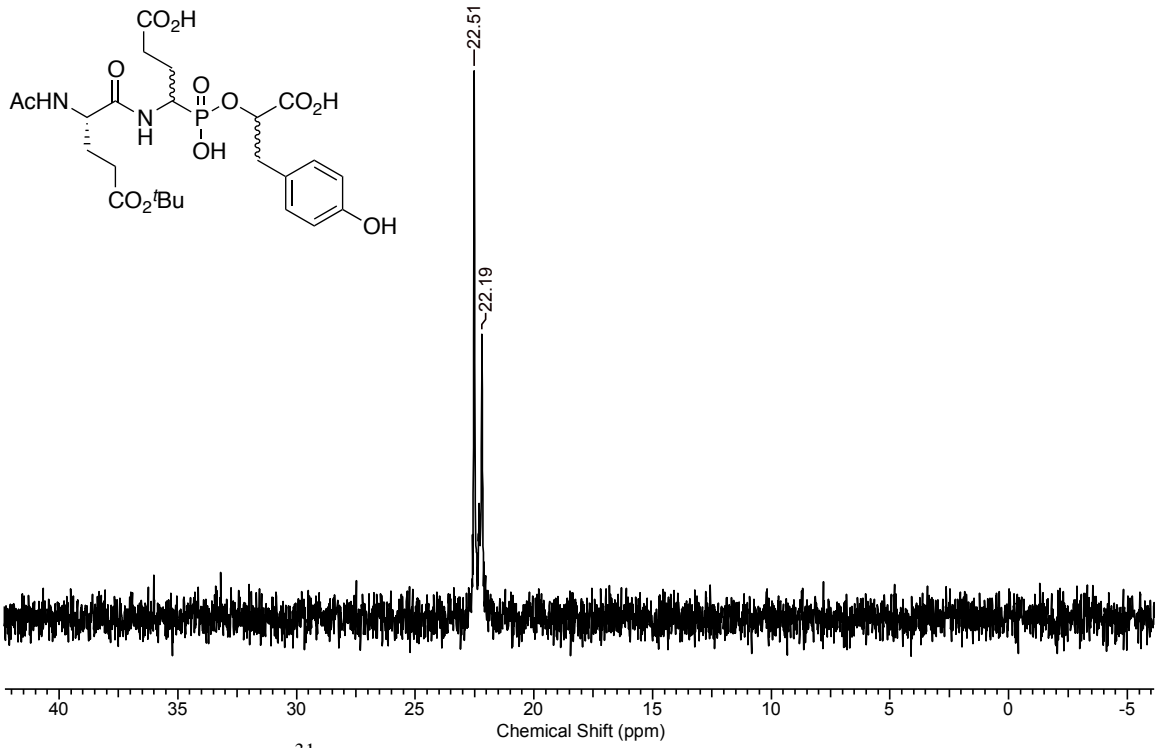

Figure A.27 ^{31}P NMR (162 MHz, CD_3OD) spectrum of compound **58**.

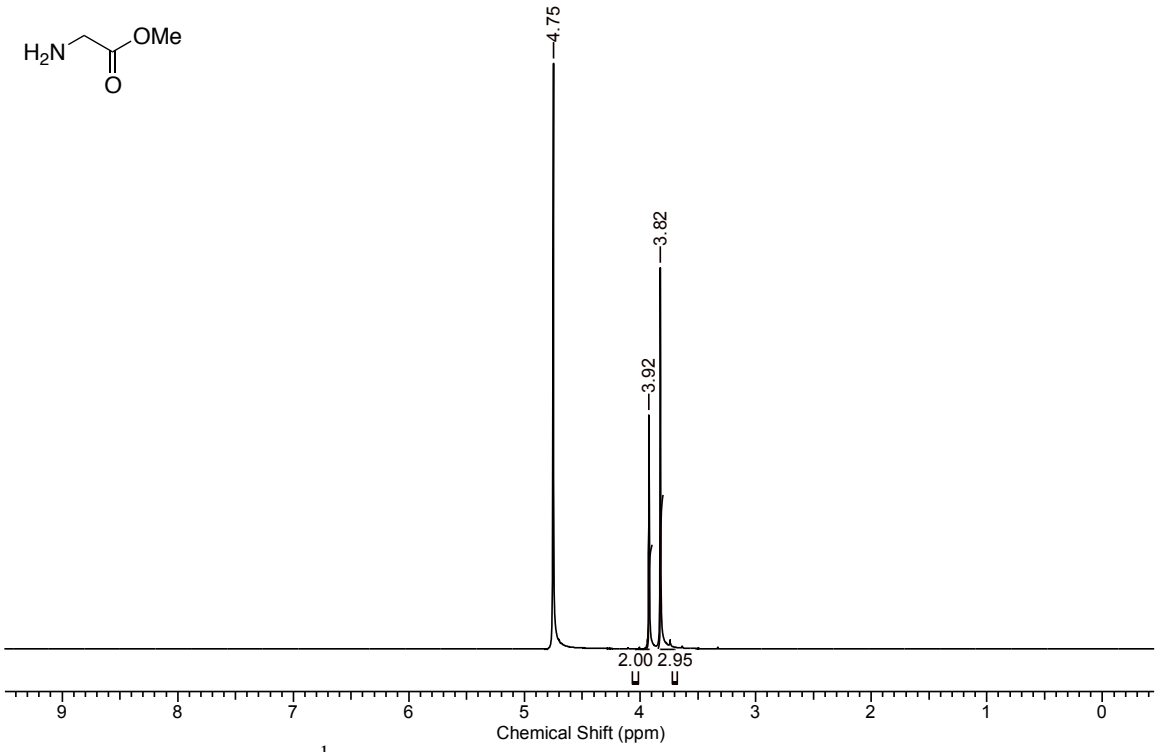

Figure A.28 ^{1}H NMR (300 MHz, D_2O) spectrum of compound **60**.

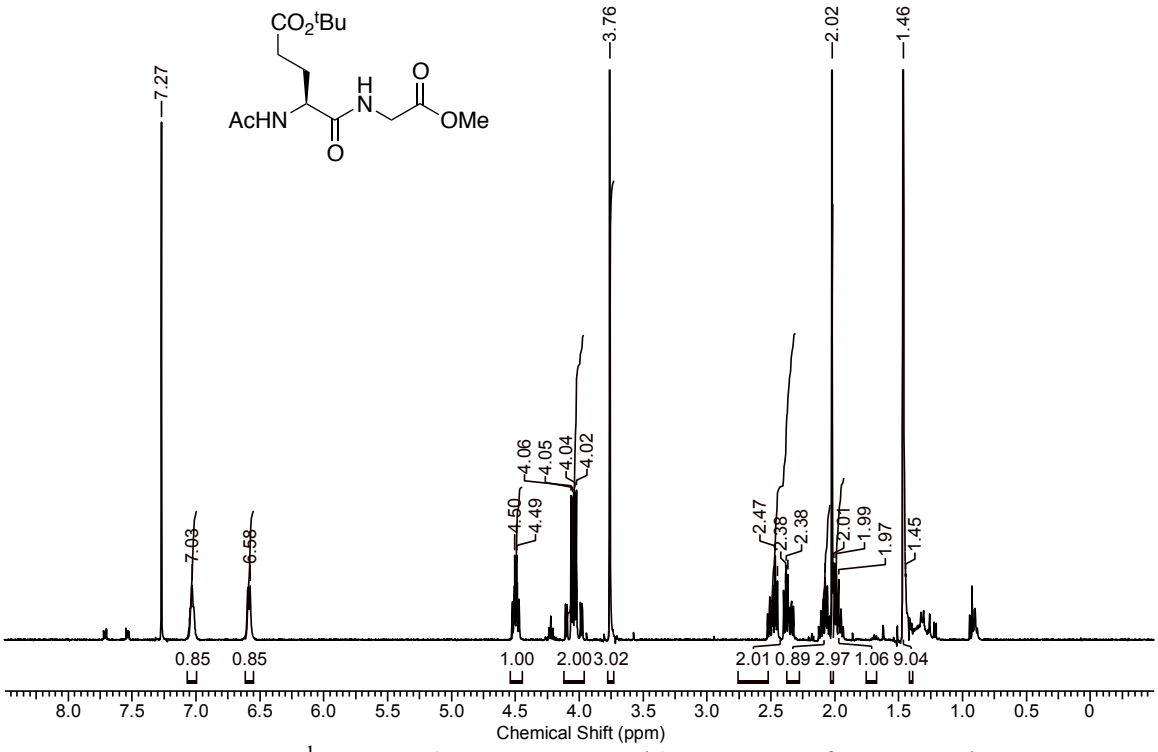

Figure A.29 ^{1}H NMR (400 MHz, $CDCl_3$) spectrum of compound **62**.

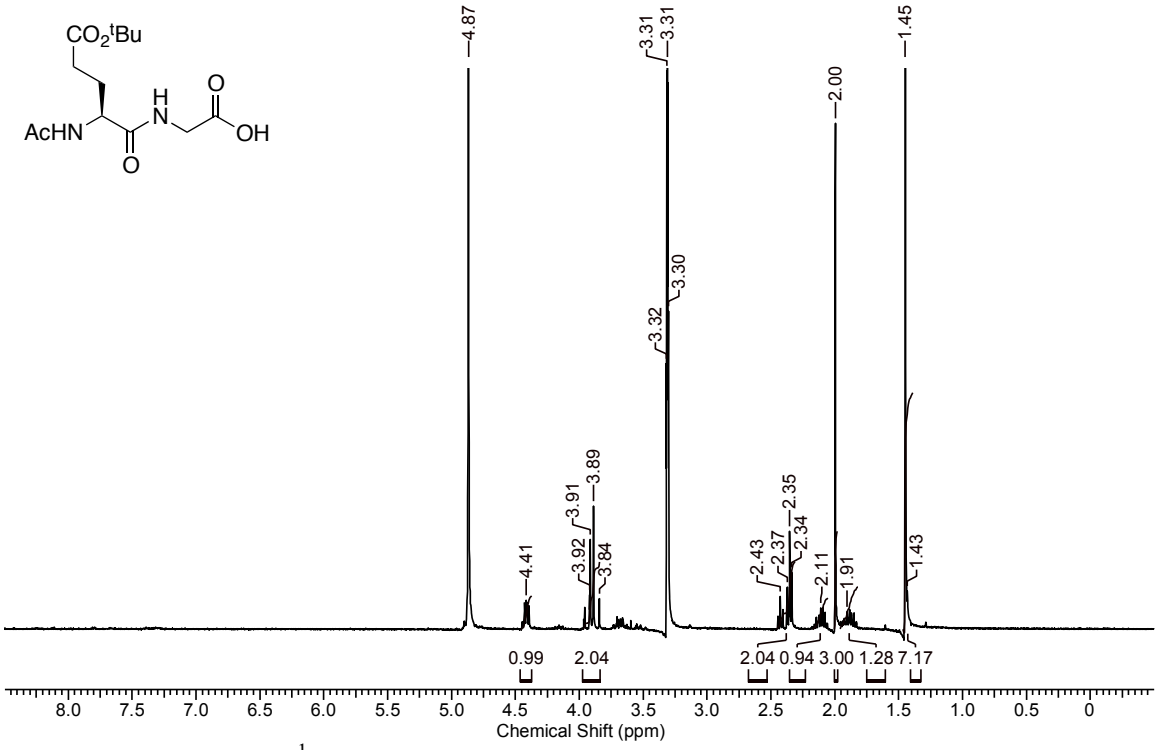

Figure A.30 ^{1}H NMR (400 MHz, CD_3OD) spectrum of compound **63**.

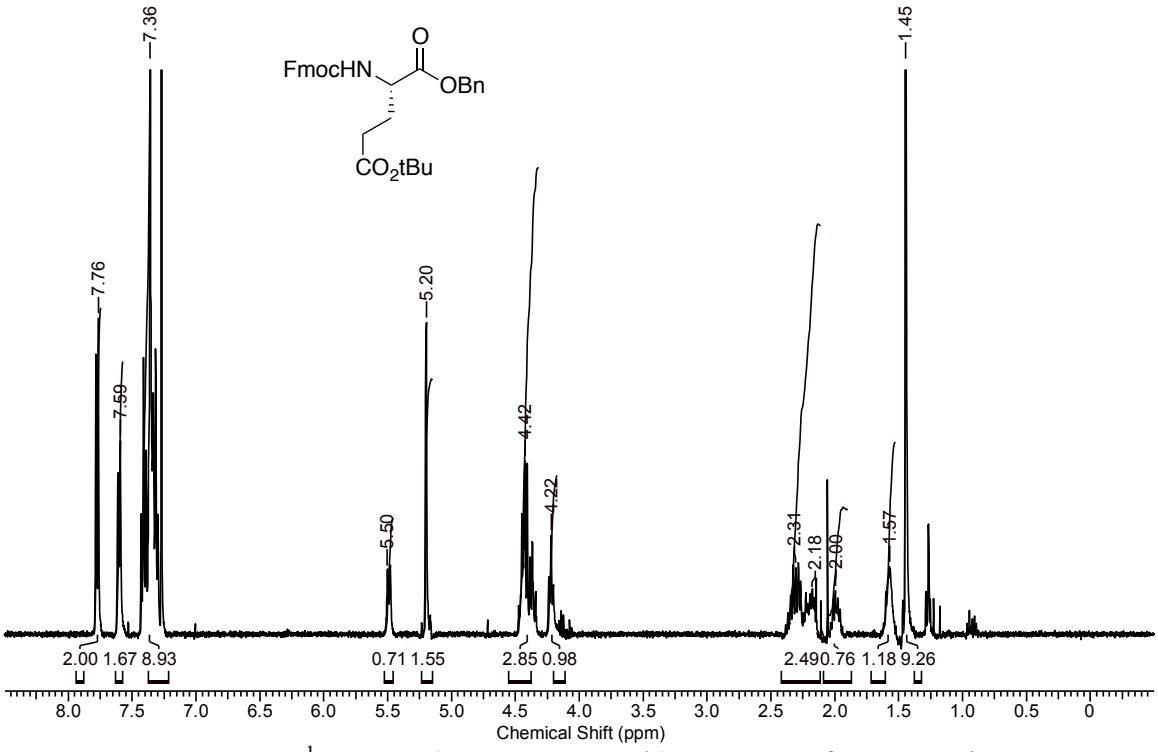

Figure A.31 ^{1}H NMR (400 MHz, $CDCl_3$) spectrum of compound **65**.

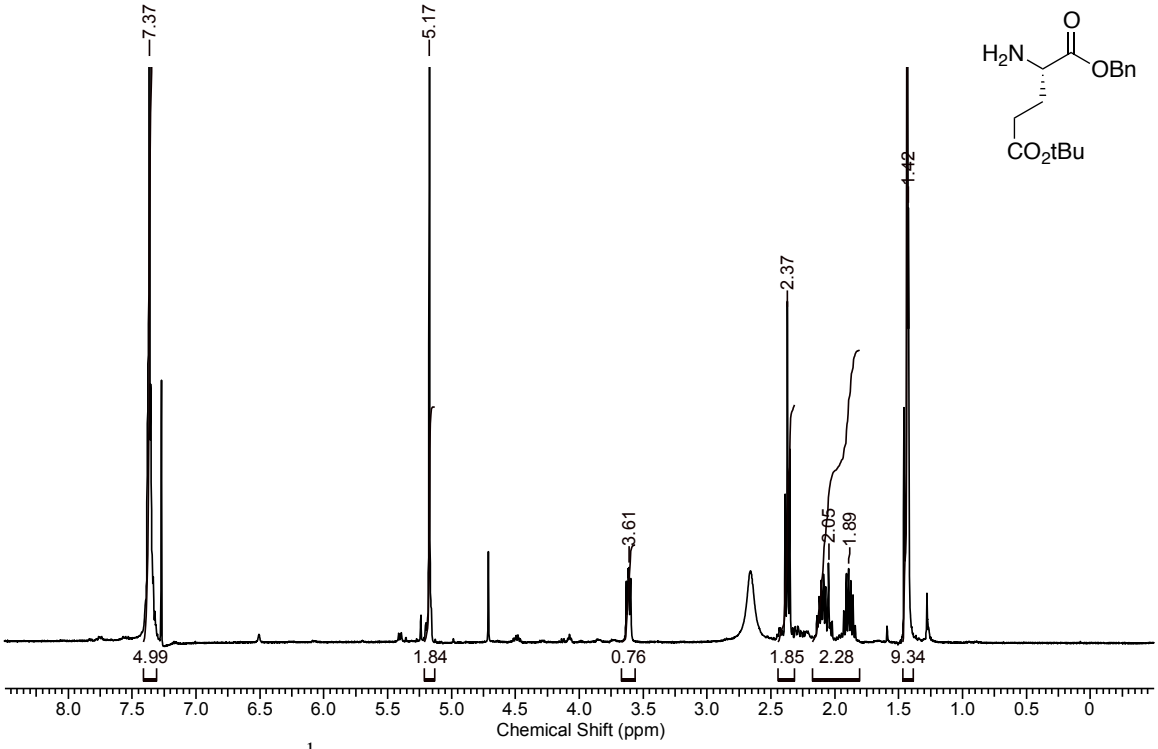

Figure A.32 ^{1}H NMR (400 MHz, $CDCl_3$) spectrum of compound **66**.

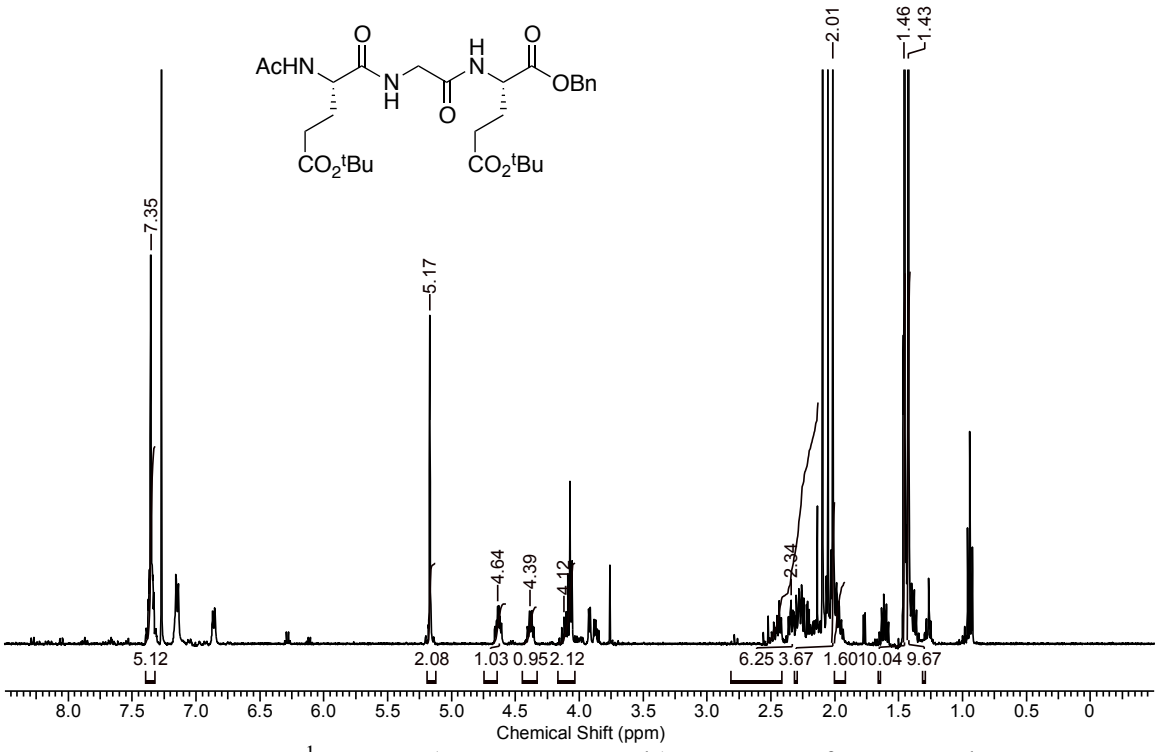

Figure A.33 ^{1}H NMR (400 MHz, $CDCl_3$) spectrum of compound **67**.

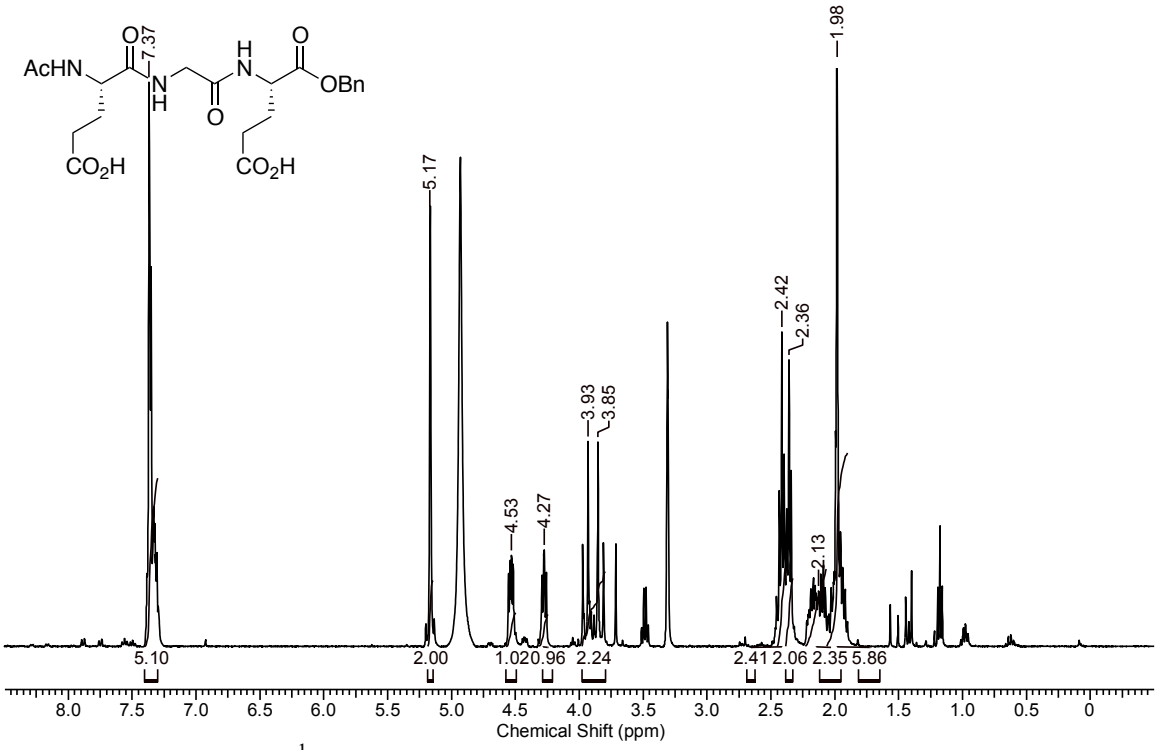

Figure A.34 ^{1}H NMR (400 MHz, CD_3OD) spectrum of compound **68**.

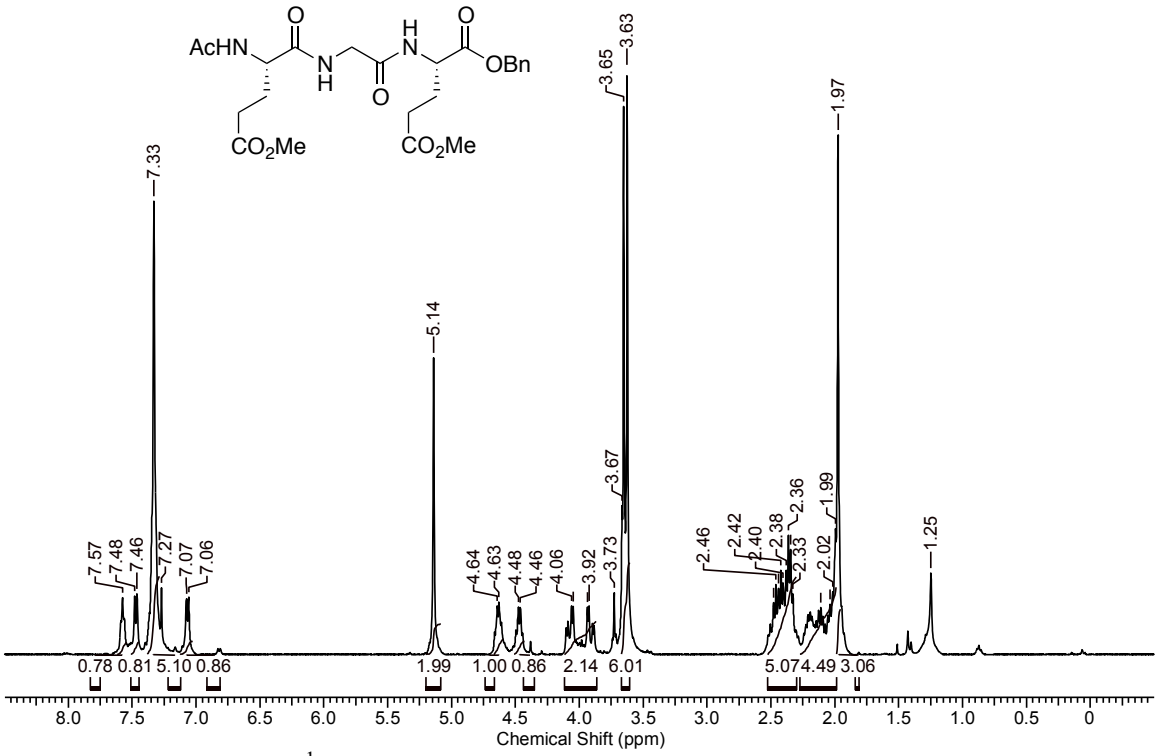

Figure A.35 ^{1}H NMR (400 MHz, $CDCl_3$) spectrum of compound **69**.

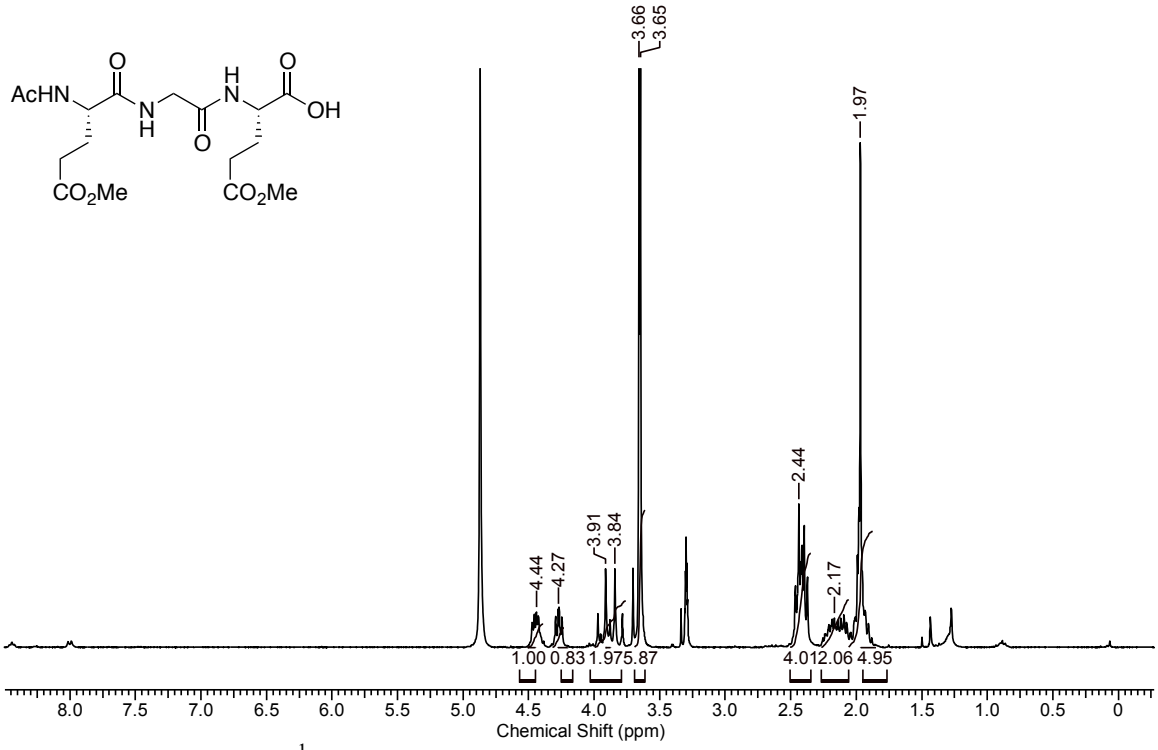

Figure A.36 ^{1}H NMR (400 MHz, CD_3OD) spectrum of compound **70**.

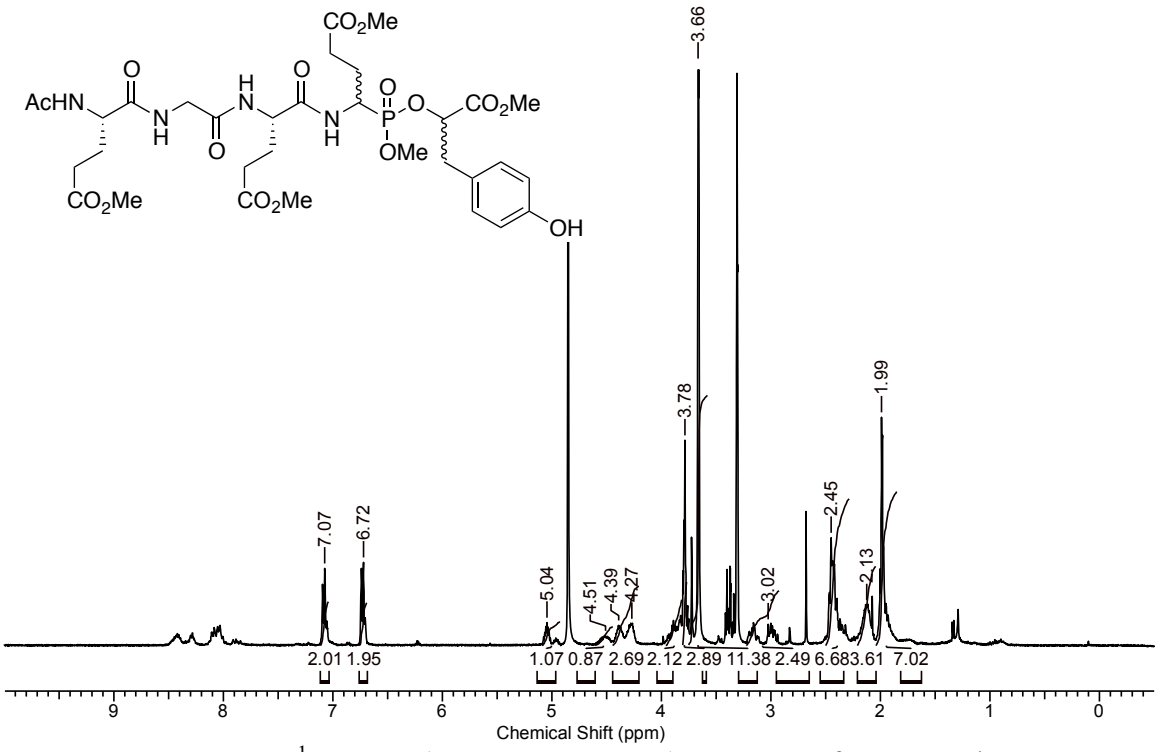

Figure A.37 ^{1}H NMR (400 MHz, CD_3OD) spectrum of compound **72**.

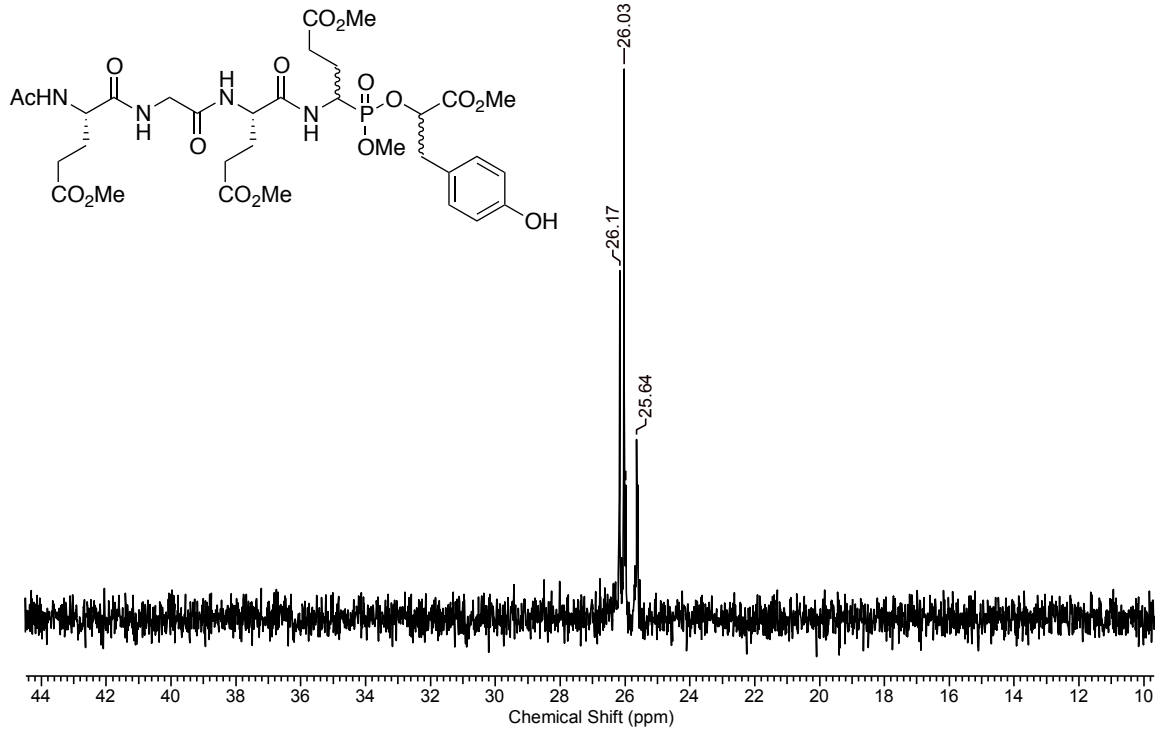

Figure A.38 ^{31}P NMR (162 MHz, CD_3OD) spectrum of compound **72**.

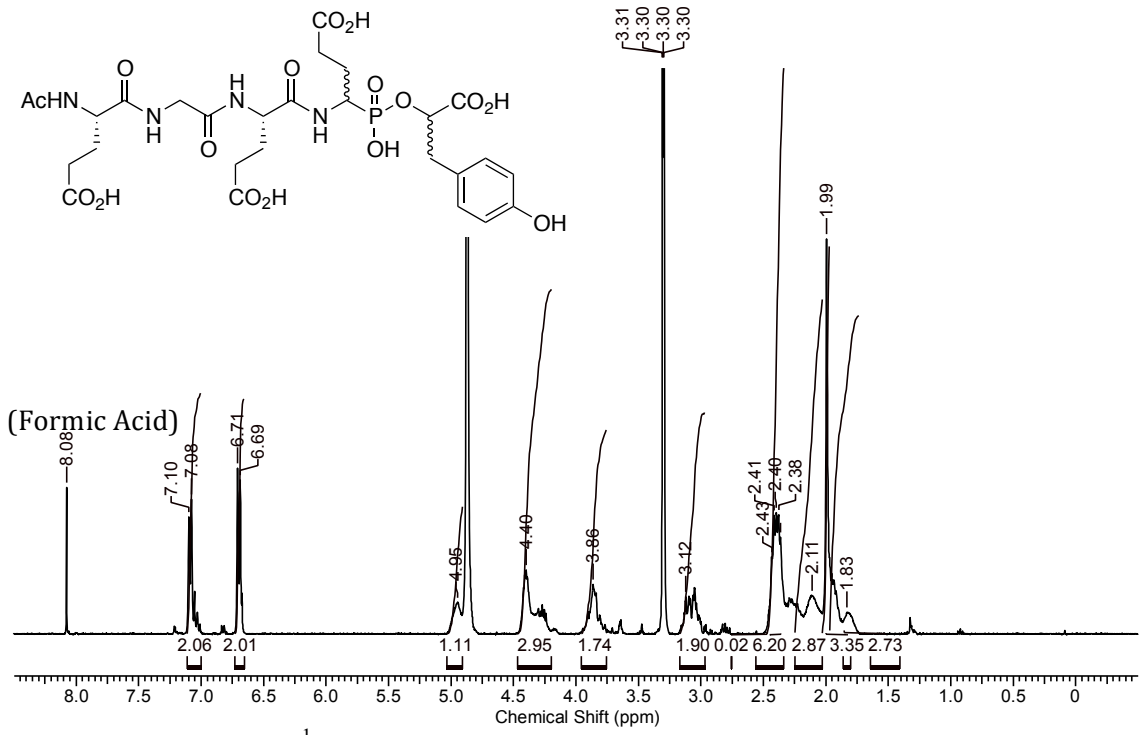

Figure A.39 ^{1}H NMR (400 MHz, CD_3OD) spectrum of inhibitor **4**.

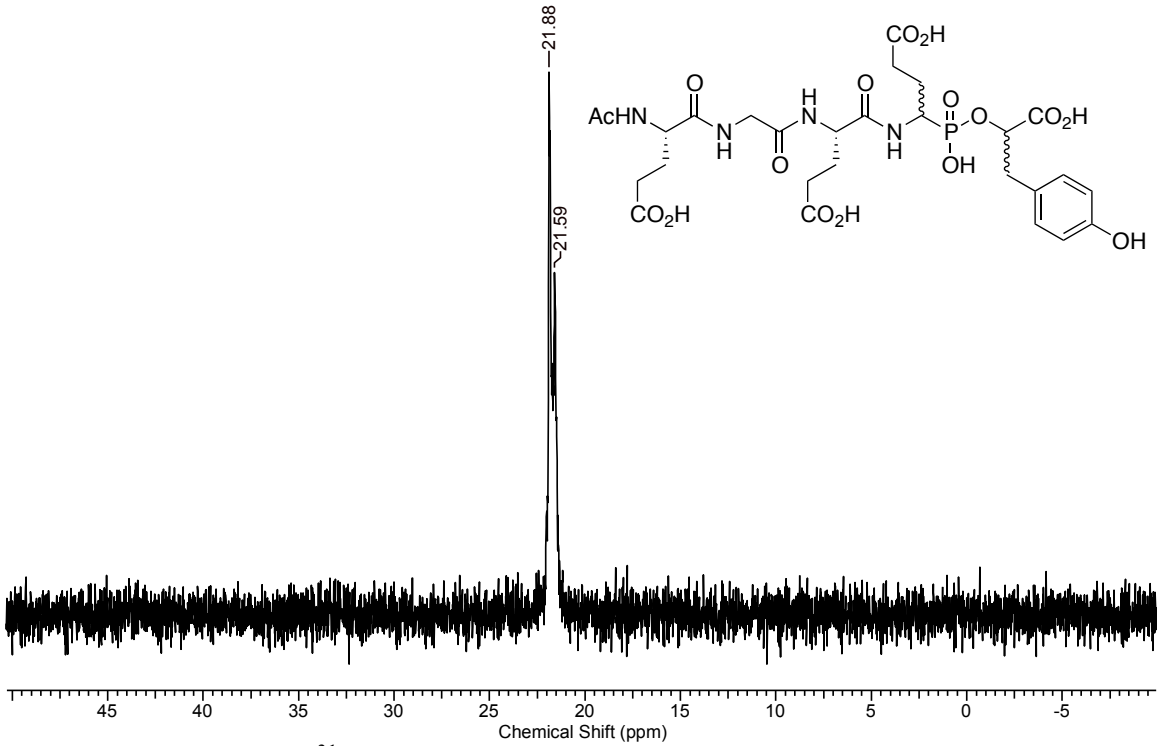

Figure A.40 ^{31}P NMR (162 MHz, CD_3OD) spectrum of inhibitor **4**.